BERICHTE
aus dem Fachbereich Geowissenschaften
der Universität Bremen

Nr. 125

Wolff, T.

MIXED LAYER CHARACTERISTICS IN THE EQUATORIAL ATLANTIC DURING THE LATE QUATERNARY AS DEDUCED FROM PLANKTONIC FORAMINIFERA.

Berichte, Fachbereich Geowissenschaften, Universität Bremen, Nr. 125,
132 Seiten, Bremen 1998

ISSN 0931-0800

Die "Berichte aus dem Fachbereich Geowissenschaften" werden in unregelmäßigen Abständen vom Fachbereich 5, Universität Bremen, herausgegeben.

Sie dienen der Veröffentlichung von Forschungsarbeiten, Doktorarbeiten und wissenschaftlichen Beiträgen, die im Fachbereich angefertigt wurden.

Die Berichte können bei:

Frau Gisela Boelen

Sonderforschungsbereich 261

Universität Bremen

Postfach 330 440

D 28334 BREMEN

Telefon: (49) 421 218-4124

Fax: (49) 421 218-3116

angefordert werden.

Zitat:

Wolff, T.

Mixed layer characteristics in the equatorial Atlantic during the late Quaternary as deduced from planktonic foraminifera.

Berichte, Fachbereich Geowissenschaften, Universität Bremen, Nr. 125, 132 Seiten, Bremen, 1998.

ISSN 0931-0800

Mixed layer characteristics in the equatorial Atlantic during the late Quaternary as deduced from planktonic foraminifera.

Dissertation zur Erlangung des Doktorgrades am Fachbereich Geowissenschaften der Universität Bremen

vorgelegt von
Tobias Wolff
Bremen 1998

Danksagung

Für die Vergabe dieser Arbeit sowie die Betreuung und vielfältige Unterstützung bei deren Ausführung möchte ich mich ganz herzlich bei Prof. Dr. Gerold Wefer bedanken.
Dr. Jürgen Pätzold stand mir während meiner Arbeit stets betreuend zur Seite und hat mir viele Anregungen bei der Einarbeitung in die Paläosalinitäts-Problematik gegeben. Dafür möchte ich mich hier ausdrücklich bedanken.
Priv. Doz. Dr. Andreas Mackensen danke ich für die Übernahme des Zweitgutachtens.

Dr. Stefan Mulitza gilt mein besonderer Dank. Der ständige Gedankenaustausch in zahllosen Diskussionen und die intensive Zusammenarbeit hat viele wertvolle Anregungen für diese Arbeit geliefert. Für eine sehr gute Zusammenarbeit möchte ich auch Dr. Björn Grieger, Dr. Andre Paul, Dr. Carsten Rühlemann, Dr. Anke Dürkoop, Dr. Hans-Stefan Niebler, Helge Arz und Walter Hale danken.
Wertvolle fachliche Diskussionen gab es mit Prof. Dr. Klaus Herterich, Dr. Peter Müller, Dr. Torsten Bickert, Dr. Ralph Schneider und Jens Klump. Allen sei hiermit gedankt.

Die für diese Arbeit benötigten Isotopenmessungen wurden von Dr. Monika Segl und Birgit Meyer-Schack durchgeführt. Dr. Gerrit Meinecke stellte mir Foraminiferenzählungen zur Verfügung. Bei Problemen mit Computern und Druckern standen mir Götz Ruhland, Dr. Volker Ratmeyer und Dr. Gerrit Meinecke zur Seite. Zur angenehmen Atmosphäre am Arbeitsplatz trugen Dr. Martin Cepek, Dörte Budziak und Bob Davenport bei. Ihnen allen möchte ich hiermit danken.

Die gesamte Arbeitsgruppe Meeresgeologie trug zur angenehmen Arbeitsatmosphäre bei und ermöglichte einen intensiven, wissenschaftlichen Austausch. Auch mit Mitgliedern der Arbeitsgruppen Paläomodellierung und Paläozeanographie gab es wichtige, fachliche und nicht-fachliche Gespräche.

Meine Eltern haben mich stets in vielfältiger Weise unterstützt, wofür ich Ihnen herzlich danke.

Die finanzielle Unterstützung erfolgte durch die Deutsche Forschungsgemeinschaft im Rahmen des Sonderforschungsbereichs 261 "Der Südatlantik im Spätquartär".

Contents

Zusammenfassung

In dieser Arbeit werden Deckschichtparameter im äquatorialen Atlantik während des Spätquartärs rekonstruiert. Dazu werden relative Häufigkeiten planktischer Foraminiferenarten sowie das Sauerstoff-Isotopenverhältnis flachlebender planktischer Foraminiferen verwendet.

Zunächst werden unterschiedliche Methoden zur Rekonstruktion von Paläosalzgehalten der Oberflächenwassermassen im tropischen Atlantik vor allem im Hinblick auf die jeweiligen Fehler untersucht. Die Methoden wurden an Oberflächendatensätzen getestet und daraufhin auf Sedimente des tropischen Kerns GeoB 1523-1 auf dem Ceara-Rücken angewendet.
Die Qualität der Paläosalzgehaltsberechnungen anhand des Sauerstoff-Isotopenverhältnisses planktischer Foraminiferen wird durch Ungenauigkeiten in der unabhängigen Temperaturschätzung sowie durch die für die Vergangenheit angenommene Beziehung zwischen der Sauerstoff-Isotopenzusammensetzung des Meerwassers und dem Salzgehalt eingeschränkt. In Abhängigkeit von der Steigung der regional gültigen, linearen Beziehung liegt der Fehler im errechneten Salzgehalt zwischen 0.5 und 1.2 ‰. In den tropischen Ozeanen sind die Fehler am größten, so daß die Ergebnisse solcher Paläosalzgehaltsberechnungen hier als vorwiegend qualitativ bezeichnet werden müssen.
Zwei weitere Methoden zur Rekonstruktion von Paläosalzgehalten wurden untersucht. Beide Methoden verwenden relative Häufigkeiten planktischer Foraminiferenarten. Erstmalig wurde dabei ein künstliches, neuronales Netzwerk zur Paläosalzgehaltsrekonstruktion eingesetzt. Dessen Ergebnisse wurden mit denen einer Modern Analog Technique verglichen. Mit beiden Methoden werden bei der Anwendung auf Oberflächensedimente die tatsächlich gemessenen Salzgehalte zufriedenstellend reproduziert. Die Anwendung auf spätquartäre Sedimentkerne läßt jedoch an der Zuverlässigkeit dieser Methoden zweifeln. Die Ergebnisse können durch die im heutigen Ozean gemessene Beziehung zwischen Salzgehalt und Temperatur erklärt werden und deuten darauf hin, daß die Foraminiferen-Vergesellschaftungen überwiegend durch Temperatur und nicht durch den Salzgehalt bestimmt werden.

Ein weiteres Thema dieser Arbeit ist die Auswirkung der Temperatursensitivität planktischer Foraminiferen auf ihr Sauerstoff-Isotopenverhältnis. Jede Art ist durch eine typische Optimumtemperatur und Temperatursensitivität gekennzeichnet. Anhand von holozänen Oberflächensedimenten konnte gezeigt werden, daß *Globigerinoides sacculifer* und *Globigerinoides ruber* (rosa) Optimumtemperaturen von 22 °C bzw. 27 °C aufweisen. *G. sacculifer* zeigt dabei eine geringe, *G. ruber* (rosa) eine hohe Temperatursensitivität. Die Temperatursensitivitäten können Amplitude und Zeitlichkeit von Zeitserien des Sauerstoff-Isotopenverhältnisses beeinflussen. Außerdem konnte gezeigt werden, daß Jahresmitteltemperatur, Saisonalität und das Sauerstoff-Isotopenverhältnis des Meerwassers für eine Lokation bestimmt werden können, wenn Optimumtemperatur und Temperatursensitivität von mindestens drei Arten planktischer Foraminiferen bekannt sind.

Anhand von 30 Schwerelotkernen und 43 Oberflächenproben wurden Änderungen in der Sauerstoff-Isotopenzusammensetzung der planktischen Foraminifere *G. sacculifer* zwischen dem letzten glazialen Maximum und heute im zentralen und westlichen äquatorialen Atlantik regional zusammengestellt. Dabei zeigte sich, daß diese Änderungen im westlichen äquatorialen Atlantik 2 ‰ überschreiten, was einer Abkühlung von 4 °C entsprechen würde. Im Gegensatz dazu wurden Temperaturänderungen zwischen dem letzten glazialen Maximum und heute in dieser Region von CLIMAP nur mit etwa 1 °C angegeben. Die Diskrepanz kann zum Teil durch Änderungen im hydrologischen Kreislauf erklärt werden. Dabei ist von reduzierten Niederschlagsmengen und einer Anreicherung der schwereren Sauerstoffisotope ^{18}O im Niederschlag auszugehen. Die verbleibende Diskrepanz zu CLIMAP wird als stärkere, eiszeitliche Abkühlung interpretiert. Sie beläuft sich demnach im westlichen äquatorialen Atlantik auf 2-3°C.

Forschungsergebnisse der letzten Jahre haben gezeigt, daß Vergesellschaftungen planktischer Foraminiferen in den Tropen in stärkerem Maße von der Mächtigkeit der Deckschicht als von der Wassertemperatur abhängig sind. Diese Erkenntnis wird hier genutzt, um mit Hilfe einer Modern Analog Technique Thermoklinentiefen in drei Sedimentkernen aus dem äquatorialen Atlantik zu rekonstruieren. Die Ergebnisse können durch das vorherrschende Windsystem erklärt werden. Während der Glaziale vertieft sich die Thermokline im westlichen tropischen Atlantik und verflacht im Osten. Der äquatoriale Thermoklinengradient zeigt ein Maximum, was auf eine Verstärkung der Südost-Passate zurückzuführen ist. In den Interglazialen nehmen die Südost-Passate ab und der Thermoklinengradient geht zurück. Im östlichen Kern GeoB 1105-4 wird das Thermoklinensignal durch den Einfluß des afrikanischen Monsunsystems bestimmt. Die Zeitserien des äquatorialen Thermoklinengradienten und des westlichen Kerns GeoB 2204-2 scheinen durch meridionale Temperaturgradienten im Südatlantik bestimmt zu werden.

Ein weiterer Themenkomplex dieser Arbeit ist der Versuch, Sauerstoff-Isotopen in ein allgemeines Zirkulationsmodell des Ozeans einzubauen. Die Definition der Randbedingung für die Sauerstoff-Isotope an der Meeresoberfläche geschieht mittels regional gültiger Beziehungen zwischen dem Sauerstoff-Isotopenverhältnis des Meerwassers und dem Salzgehalt. Die Isotope werden dann in einem Modellauf für den heutigen Ozean transportiert und die Ergebnisse mit vertikalen, gemessenen Sauerstoff-Isotopenprofilen verglichen. Die Übereinstimmung ist recht gut, Abweichungen im Zusammenhang mit dem antarktischen Zwischen- und Bodenwasser deuten auf Probleme des Zirkulationsmodells hin. Außerdem wurden zur Überprüfung der Ergebnisse theoretische Sauerstoff-Isotopenzusammensetzungen benthischer Foraminiferen berechnet. Hierzu wurden die simulierten Sauerstoff-Isotopenverhältnisse des Meerwassers sowie die simulierten Temperaturen an verschiedenen Kernlokationen verwendet. Die errechneten Werte wurden mit Literaturdaten der Sauerstoff-Isotopenzusammensetzung benthischer Foraminiferen verglichen. Die Abweichungen sind systematisch und können auf ein typisches Problem vieler Ozeanmodelle zurückgeführt werden: Die simulierten Temperaturfelder der tieferen Wassermassen zeigen häufig überhöhte Werte.

Chapter 1

Introduction

Summary

The oxygen isotope composition and the relative abundances of planktonic foraminifera are used to reconstruct mixed layer characteristics in the tropical Atlantic in late Quaternary deep sea sediments.

Methods for the reconstruction of paleosalinities in the tropical Atlantic are investigated and evaluated in terms of their respective uncertainties. The methods are used in conjunction with surface sediments and the results are compared to present day salinities. Furthermore, they are applied to core GeoB 1523-1 in the western equatorial Atlantic.

The quality of the salinity estimates derived from the oxygen isotope signature of planktonic foraminifera is constrained by the accuracy of the independent temperature estimate. Errors in the reconstructed salinities range between 0.5 and 1.2 ‰ depending on the slope of the regional oxygen-isotope salinity relationship. The findings suggest that sea surface salinity estimates from oxygen isotopes are still rather qualitative for tropical oceans.

Additionally, two methods are investigated both of which employ foraminiferal abundance data. An Artifical Neural Network is used for the first time in order to reconstruct paleosalinities. Results are compared with those of a Modern Analog Technique. Both methods give reasonable salinity estimates for surface sediments, but application to downcore sediments yields unrealistic results and shows that the reconstructions are controlled by today's salinity-temperature relationship.

The effect of the temperature sensitivities of planktonic foraminifera on the oxygen isotope record is also addressed in this thesis. Holocene surface sediments from the tropical and subtropical North and South Atlantic are used to infer optimum temperatures and temperature sensitivities of *Globigerinoides sacculifer* and *Globigerinoides ruber* (pink). *G. ruber* (pink) and *G. sacculifer* have optimum temperatures around 27°C and 22°C, respectively. *G. sacculifer* is only moderately temperature sensitive in contrast to *G. ruber* (pink) which tolerates a small range of temperatures only. It is shown that the temperature sensitivities may influence the amplitude and the timing of oxygen isotope time series of planktonic foraminifera. Knowing the specific temperature ranges and sensitivities of three foraminiferal species, average temperature, seasonality and the oxygen isotopic composition of sea water at a particular location can be deduced.

Glacial-to-modern changes in the oxygen isotopic composition of *G. sacculifer* are mapped in the central and western tropical Atlantic on the basis of data from 30 gravity cores and 43 surface sediment samples. It is shown that in the western region (Ceara Rise) the glacial-interglacial differences exceed 2 ‰. If interpreted in terms of temperature changes only (4°C), these data conflict with temperature estimates on the basis of planktonic foraminiferal census counts by CLIMAP (1°C). The discrepancy is partly attributed to increased salinities and increased ^{18}O-content of precipitation. The remaining signal is explained in terms of stronger glacial cooling. The results suggest a lowering of sea surface temperatures in the western equatorial Atlantic during the last glacial maximum (~18 000 years before present) of 2-3 °C as opposed to the estimates by CLIMAP (1°C).

Besides sea surface salinity and temperature reconstructions the question of glacial-interglacial fluctuations in thermocline depth in the tropical Atlantic is addressed. On the basis of recent research results, which suggest a dominant control of mixed layer depth on the relative abundances of planktonic foraminiferal species, a Modern Analog Technique is used to determine past changes in thermocline depth in core GeoB 1105-4 from the eastern equatorial Atlantic and in cores GeoB 2204-2 and GeoB 1523-1 from the western equatorial Atlantic. The results show a strong dependency of thermocline depth on the late Quaternary equatorial wind system. During glacials the thermocline deepens in the west and shallows in the east due to enhanced zonal SE-trade winds. Interglacials are charcterized by a relatively shallow thermocline in the west and a relatively deep thermocline at the location of core GeoB 1105-4. In the east a predominant control of the monsoon system on the thermocline depth is obvious. In the west the thermocline depth appears to be dominated by the strength of the SE-trade winds which, in turn, are driven by subtropical-tropical temperature gradients in the southern hemisphere. The tropical Atlantic east-to-west thermocline gradient is also dominated by the SE-trade wind system.

In addition, this thesis reports on the effort to incorporate oxygen isotopes into a general ocean circulation model as a passive tracer. A set of regional oxygen-isotope salinity relationships are used in conjunction with monthly data of sea surface salinity in order to define a boundary condition for the oxygen isotopes at the sea surface. The model run is performed for the present day situation and the model output is then compared with measured vertical oxygen isotope profiles. Along cross sections in the Atlantic and Pacific and in terms of regional means the measured oxygen isotopic composition of sea water is reasonably well reproduced by the model. Some model deficiencies with respect to the simulation of Antarctic intermediate and bottom waters can be depicted. Additionally, theoretical oxygen isotope compositions of benthic foraminiferal calcite tests are calculated using the simulated temperature and the simulated oxygen isotopic composition of sea water. These are then compared with the oxygen isotope record of benthic foraminifera at various core sites. The disagreement between measured and calculated oxygen isotope compositions of benthic foraminifera reflects the warm bias of the ocean model.

Main objectives

The increase in atmospheric greenhouse gas concentrations during the past two centuries is considered to be largely anthropogenic. It demands predictions of future climate change in order to be able to assess the consequences for our civilization (Houghton et al., 1995). Recently, it has been speculated by many authors that future climatic changes might be more rapid than previously thought (Broecker, 1997; Rahmstorf, 1997; Stocker and Schmittner, 1997). A better knowledge of the climate system at present and in the past will improve the efforts to precisely predict changes in the future (Stocker, 1998).

The world's oceans are a substantial element of the climate system. They cover 71 % of the earth's surface and contain 97.3 % of the earth's water. Water has a specific heat capacity five times larger than air. Therefore, the oceans play an important role in storing heat and ocean currents contribute to delivering heat from low to high latitudes. The oceanic portion of the heat transport may be as large as 40 % of the total (Washington and Parkinson, 1986) while the atmosphere contributes the remainder. The equatorial and South Atlantic surface circulation plays a key role within the global climate system (Berger and Wefer, 1996; Wefer et al., 1996). Heat is transported from the South Atlantic across the equator into the North Atlantic. In this context the role of the equatorial Atlantic in the past is of particular interest for paleoceanographic studies. In order to solve the problem of glacial heat transport it is necessary to reconstruct in detail past changes in this part of the ocean-atmosphere system. Which tools do we have to determine past states of the ocean-climate system?

One way is to look at the geological record. Deep sea sediments have been extensively used to reconstruct ocean and climate history. Parameters like e.g. sea surface temperatures, productivity, nutrient concentration or pCO_2-levels can be infered from proxy indicators. The spatial and temporal data sets of the reconstructed parameters may then be directly interpreted in terms of ocean circulation or climate change. This approach is employed in the majority of paleoceanographic research.

A second possibility is to use parameters derived from proxies in conjunction with numerical models. Since the ocean-climate system is highly complex and is determined by many feedback mechanisms, general circulation models are promising tools to predict what might be our future climate and may help to understand the present and past circulation. To test the models, atmospheric and ocean circulation can be simulated for certain times in the past and the results can be compared with proxy data. Also, models can generate fields of climatic parameters that are not documented in the geological record (Herterich et al., 1998). However, as long as ocean-only or atmosphere-only models are used, boundary conditions based on spatial paleoceanographic parameters derived from proxies have to be prescribed at the ocean-atmosphere interface. For ocean models, sea surface temperature (SST) fields, sea surface salinity (SSS) fields, and wind stress fields are required as boundary conditions. For example, CLIMAP (1981) SST are often used in general circulation model runs for the last glacial maximum (e.g. Lautenschlager et al., 1992). The output of these models is then interpreted in terms of circulation patterns and may be compared with other parameters derived from proxies.

A third approach to learn about past climate and ocean circulation is to incorporate proxies directly into numerical models as passive tracers. For example, oxygen isotopes may be transported or the carbon cycle may be included in atmospheric or ocean general circulation models (e.g. Meier-Reimer and Bacastow, 1990; Jouzel et al., 1994). On the one hand the output of these models may help to understand observed patterns of the proxy. On the other hand it can be used to test the circulation models.

With these approaches in mind, this thesis focuses on the reconstruction of late Quaternary mixed layer characteristics in the equatorial Atlantic from foraminiferal proxy data. The proxies used here are the oxygen isotope ratio in calcite tests of planktonic foraminifera and the relative abundances of planktonic foraminiferal species. In general, the research presented in this thesis centres on questions about late Quaternary
- changes in the evaporation-precipitation regime and SSS,
- changes in SST,
- variations in the surface wind fields and their influence on the surface layer of the ocean.
A focus within the late Quaternary is the last glacial maximum (~18 thousand years before present). Additionally, work is done to improve the methods used for the reconstructions.

Like temperature, salinity is regularily measured on ocean expeditions throughout the world. Global data sets contain annual, seasonal and monthly compilations of this parameter (e.g. Levitus et al., 1994). Information about paleosalinities, however, is still sparse (Herterich et al., 1998). The lack of data is in contrast to the benefits that could be derived from paleosalinity estimates. As an important oceanographic parameter it may be used to learn about past ocean circulation patterns and the hydrological cycle. The sea surface salinity is directly related to the evaporation-precipitation balance (E-P). Thus, paleosalinities contain valuable paleoclimatic information about, e.g., changes in precipitation rates. Paleosalinity estimates with high precisions would also be extremely useful for modelling studies, because they could serve as boundary conditions in ocean general circulation models (Lorenz et al., 1996; Herterich et al., 1998). So far, in most ocean model runs freshwater fluxes from atmospheric general circulation models are used instead.

Recently, efforts have been made to determine past sea surface salinities (SSS) from the oxygen isotope record of planktonic foraminifera (Duplessy et al., 1991; Rostek et al., 1993; Maslin et al., 1995; Wang et al., 1995). Spatial SSS reconstructions have been performed for the last glacial maximum (LGM) in the high latitude North and South Atlantic (Duplessy et al., 1991; Duplessy et al., 1996). In the tropical Atlantic, glacial-interglacial changes in SSS have been estimated in two cores (Dürkoop et al., 1997) but spatial data on particular time slices are not available yet. However, the reliability of paleosalinity estimates from oxygen isotopes has been questioned recently (Rohling and Bigg, 1998). In chapter 2 of this thesis, potential methods for paleosalinity reconstructions in the tropical Atlantic are investigated and evaluated with respect to their precision. Besides the oxygen-isotope method, a Modern Analog Technique and an Artificial Neural Network are investigated. Both methods employ foraminiferal abundance data to calculate past SSS.

More frequently than for paleosalinity estimations the oxygen isotope record of planktonic foraminifera is used to determine past SST. However, different species of planktonic foraminifera prefer different temperature conditions and show different sensitivities to temperature (Mix, 1987). In chapter 3, it is examined how the temperature sensitivity of planktonic foraminifera affects the oxygen isotope record.

Temperature sensitivities of planktonic foraminiferal species are the basis for temperature reconstructions using species counts. Transfer functions relate the relative abundances of planktonic foraminiferal species in surface sediment samples to SST. When applied to core data, paleotemperatures can be calculated (e.g. Imbrie and Kipp, 1971; Hutson, 1980). A prominent example is the CLIMAP (1976, 1981) SST data set for the LGM which is frequently used as boundary condition in general circulation models of the ocean and the atmosphere. The CLIMAP data set is characterized by a moderate glacial cooling of the tropical oceans in the range of 0-2 °C which was doubted by other authors soon after publication (Webster and Streeten, 1978; Rind and Peteet, 1985). Based on glacial snowline depressions in tropical mountains, pollen data, and model results, they argued that a stronger cooling in the order of 5-6 °C is more realistic. Recently, a vast amount of articles was published covering this topic (see references in Broecker (1996) and the section on tropical SST in this chapter). The oxygen isotope record of planktonic foraminifera is ambiguous concerning this topic. Broecker (1986) saw his data in line with CLIMAP SST while Curry and Oppo (1997) interpret their data from a western equatorial Atlantic core in terms of a minimum of 4°C cooling during the LGM. In chapter 4 the oxygen isotope record of the planktonic foraminifer *G. sacculifer* is summarized regarding glacial-to-modern changes in the central and western equatorial Atlantic and is evaluated with respect to changes in the evaporation-precipitation regime and the debate about glacial cooling in the tropics.

Besides the question about the magnitude of glacial cooling in the tropics, the equatorial Atlantic wind system is an important topic discussed within the scientific community. Wind stress exerted at the sea surface causes horizontal and vertical motion of surface waters. It is responsible for surface currents, upwelling, and vertical mixing. Therefore, it also modifies the distribution of parameters like SST and SSS.

In a number of studies it has been shown that the Atlantic trade wind system and the African monsoon system have changed in a glacial-interglacial rhythm. The strength of the monsoon is believed to be determined by boreal summer insolation in low latitudes (Prell and Kutzbach, 1987; DeMenocal and Rind, 1993) with a maximum in monsoonal circulation at times of maximum summer insolation over northern Africa. Enhanced solar heating of the continental landmass leads to the development of a pronounced low pressure cell over Africa which causes strong southerly monsoonal winds. The SE-trade winds and their zonal component are thought to be at their maximum strength during glacials (CLIMAP, 1981; Mix et al., 1986; McIntyre et al., 1989) although there are model results that suggest a weakening (Lautenschlager and Herterich, 1990). Evidence from the central and eastern equatorial Atlantic suggests increased upwelling and shallowing of the thermocline during glacials (Mix et al., 1986; Ravelo et al., 1990; Schneider et al., 1995; Rühlemann et al., 1998) in response to weakened monsoons and enhanced zonality of the SE-trade winds. Meanwhile, in the western

equatorial Atlantic the thermocline might have been deeper as speculated by some authors (Ravelo et al., 1990; Curry and Lohmann, 1990; Rühlemann et al., 1998). In chapter 5 of this thesis the depth of the thermocline in the eastern and the western equatorial Atlantic is reconstructed using the relative abundances of planktonic foraminifera in three gravity cores .

One of the most widely used proxies in paleoceanography is the oxygen isotope ratio of carbonate tests of foraminifera, corals, and other calcite/aragonite producing biota (Wefer and Berger, 1991). The oxygen isotope composition in carbonate tests depends on the oxygen isotope composition of sea water and on the temperature of the ambient water mass. In order to calculate temperatures from the oxygen isotope record, the oxygen isotopic composition of sea water has to be known. Therefore, it is necessary to understand the mechanisms determining the oxygen isotope distribution in the oceans. It is intriguing to incorporate oxygen isotopes in general circulation models. For atmospheric models this has been done during the last decade (e.g. Joussaume et al., 1984; Jouzel et al., 1987; Hoffmann, 1995). Chapter 6 of this thesis reports on an attempt to incorporate oxygen isotopes in an ocean general circulation model (the Geophysical Fluid Dynamics Laboratory Modular Ocean Model - MOM). The oxygen isotopes are included by defining a sea surface boundary condition on the basis of regional oxygen-isotope salinity relationships.

Global ocean circulation

At present, the circulation in the world oceans is characterized by the global conveyor belt system as described by Gordon (1986) and Broecker et al. (1985). In the North Atlantic the Gulf stream transports warm and saline water northwards into the northern North Atlantic, where it is cooled by evaporation (Gordon, 1986). Due to its high salinity it attains a density sufficient for sinking and forms the North Atlantic Deep Water (NADW). The NADW flows to the south and is exported to the Indian and Pacific Oceans by the Antarctic Circumpolar Current. There, the deep water masses eventually return to the surface. The conveyor belt is closed by the surface circulation flowing from the Pacific through the Indonesian Seas into the Indian Ocean feeding the Agulhas current. At the southern tip of Africa the Agulhas current partly retroflects back toward the Indian Ocean while another portion leaks into the Atlanic. This relatively warm water is fed into the Benguela Current, which transports water northwards into the equatorial Atlantic. In the western equatorial Atlantic it crosses the equator and flows into the western North Atlantic where it joins the warm gulf stream. Recently it has been shown that this model of the global thermohaline circulation is highly simplified and does not account for the complexity of the circulation patterns (Lutjeharms, 1996; Macdonald and Wunsch, 1996; Schlitzer, 1996). However, the conveyor belt model is still useful for describing the main features of the global thermohaline circulation especially with respect to the warm-water sphere.

The South Atlantic ocean circulation and hydrography

In general, meridional heat transport is characterized by the poleward redistribution of thermal energy originally received from the sun. The South Atlantic is highly unusual because heat is delivered from subtropical latitudes through the South Atlantic across the equator (Gordon, 1986; Peterson and Stramma, 1991; Berger and Wefer, 1996) and into the North Atlantic. Therefore, the South Atlantic plays a key role in redistributing heat in a global climatic framework.

The surface circulation in the South Atlantic is dominated by the South Atlantic subtropical gyre (Fig. 1). At the southern end of Africa the South Atlantic Current incorporates Agulhas eddies (warm Indian Ocean water) and forms the Benguela current which constitutes the eastern boundary current of the subtropical gyre. At 30 °S the northward directed Benguela current leaves the coast and joins the South Equatorial Current (SEC) which crosses the South Atlantic towards the Northwest. The strength of the SEC varies with the seasons and is

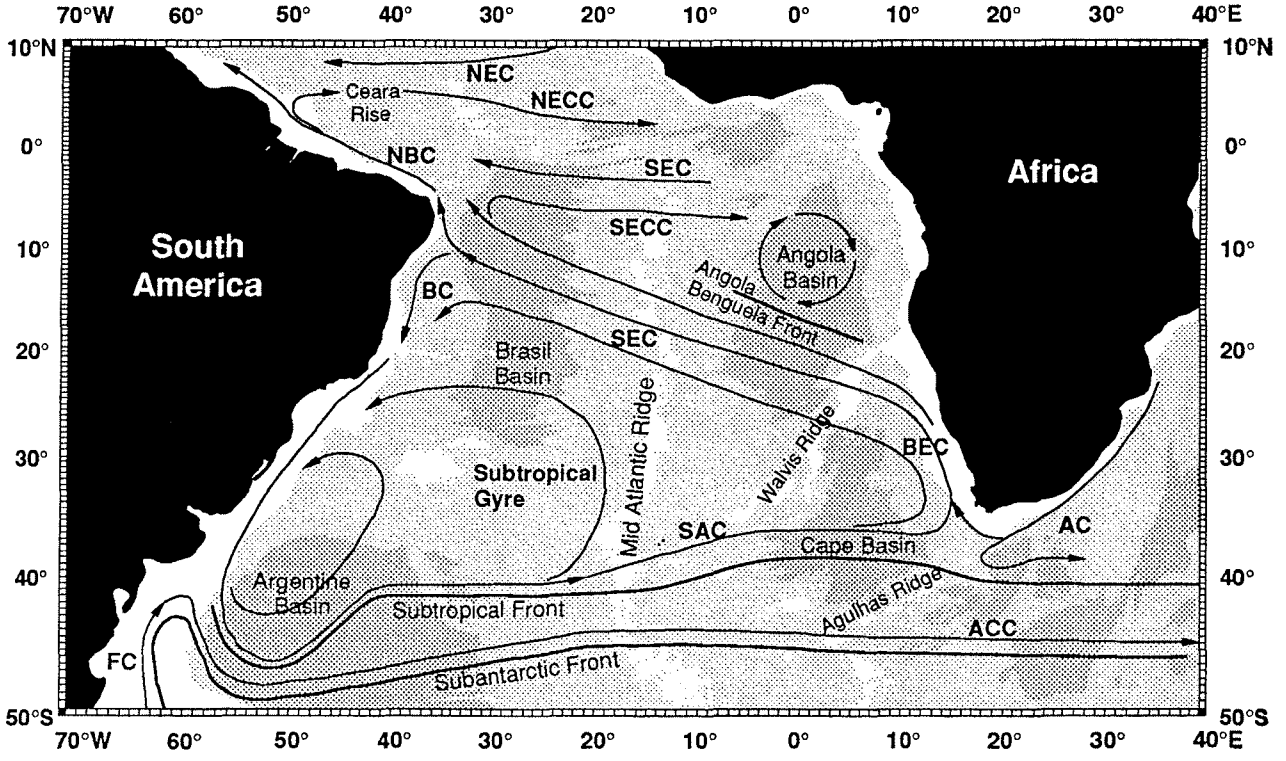

Figure 1: South Atlantic surface ocean circulation. AC: Agulhas Current; ACC: Antarctic Circumpolar Current; BC: Brazil Current; BEC Benguela Current; FC: Falkland Current; NBC: North Brazil Current; NEC: North Equatorial Current; NECC: North Equatorial Counter Current; SAC: South Atlantic Current; SEC: South Equatorial Current; SECC: South Equatorial Counter Current (after Peterson and Stramma, 1991, and Tomczak and Godfrey, 1994, modified).

strongest during boreal summer when the southern trade winds are at a maximum. At 10°S the SEC meets the South American coast and bifurcates. Most of the water enters the North Brazil Current (NBC), the remaining water flows south and feeds the Brazil Current as the western boundary current of the subtropical gyre. The NBC is responsible for the cross-equatorial water and heat transport. Part of the NBC water, however, is retroflected at 5°N to form the North Equatorial Counter Current which is highly seasonal and at a maximum during boreal summer (Condie, 1991). The eastern equatorial Atlantic is characterized by the northern limb of the SEC, the South Equatorial Counter Current and the small Angola cyclonic gyre.

Besides the import of warm surface water from the Indian and Pacific Ocean via the Agulhas Current, the cold water route (Gordon, 1986) is of importance for the South Atlantic water budget. A significant amount of cold water is entering the South Atlantic through the Drake Passage (Rintoul, 1991) and is transfered northward as surface or intermediate water (Macdonald and Wunsch, 1996). Both elements, the warm water route around the southern tip of Africa and the cold water route through Drake Passage, are required to balance the export of Atlantic deep waters to other ocean basins. The relative importance of the warm and cold water routes, however, are still debated within the scientific community (Gordon, 1986; Rintoul, 1991; Macdonald and Wunsch, 1996; Schlitzer, 1996).

In Fig. 2 annual mean sea surface salinities (SSS) and sea surface temperatures (SST) in the equatorial and South Atlantic as taken from Levitus et al. (1994) and Levitus and Boyer (1994) are shown. The SST map demonstrates the asymmetric temperature distribution due to northward advection of cold water in the east and southward advection of warm water in the west. Upwelling zones at the African coast are characterized by low temperatures. The SSS map shows a general influence of the evaporation-precipitation regime which is governed by atmospheric Hadley circulation. The highest salinities are observed in the subtropics where precipitation is low, whereas lower salinities are recorded in the central tropics where precipitation is high. At river mouths salinities are strongly reduced due to continental runoff.

Tropical sea surface temperatures at the last glacial maximum

One of the most controversial disputes in paleoceanography is the ongoing debate about the magnitude of glacial cooling in the tropics. This debate was one of the motivations for the research presented in chapter 4. Furthermore, the question about glacial SST influences many aspects of the tropical Atlantic climate and ocean circulation at the last glacial maximum (LGM). Therefore, the discussion about this issue shall be summarized here.

In 1976 and 1981 the CLIMAP group published their view of the glacial world and presented their well known maps of sea surface temperatures, sea ice extent and continental ice shields (CLIMAP, 1976, 1981) for the LGM. On the basis of foramimiferal census counts (and data from radiolaria and coccolithophoridae) they estimated that tropical SST were only slightly lower than they are today. In the subtropics of the Pacific they even found evidence for a glacial warming. In Fig. 3 glacial-to-modern changes in August and February SST in the tropical and South Atlantic according to CLIMAP (1994) are presented.

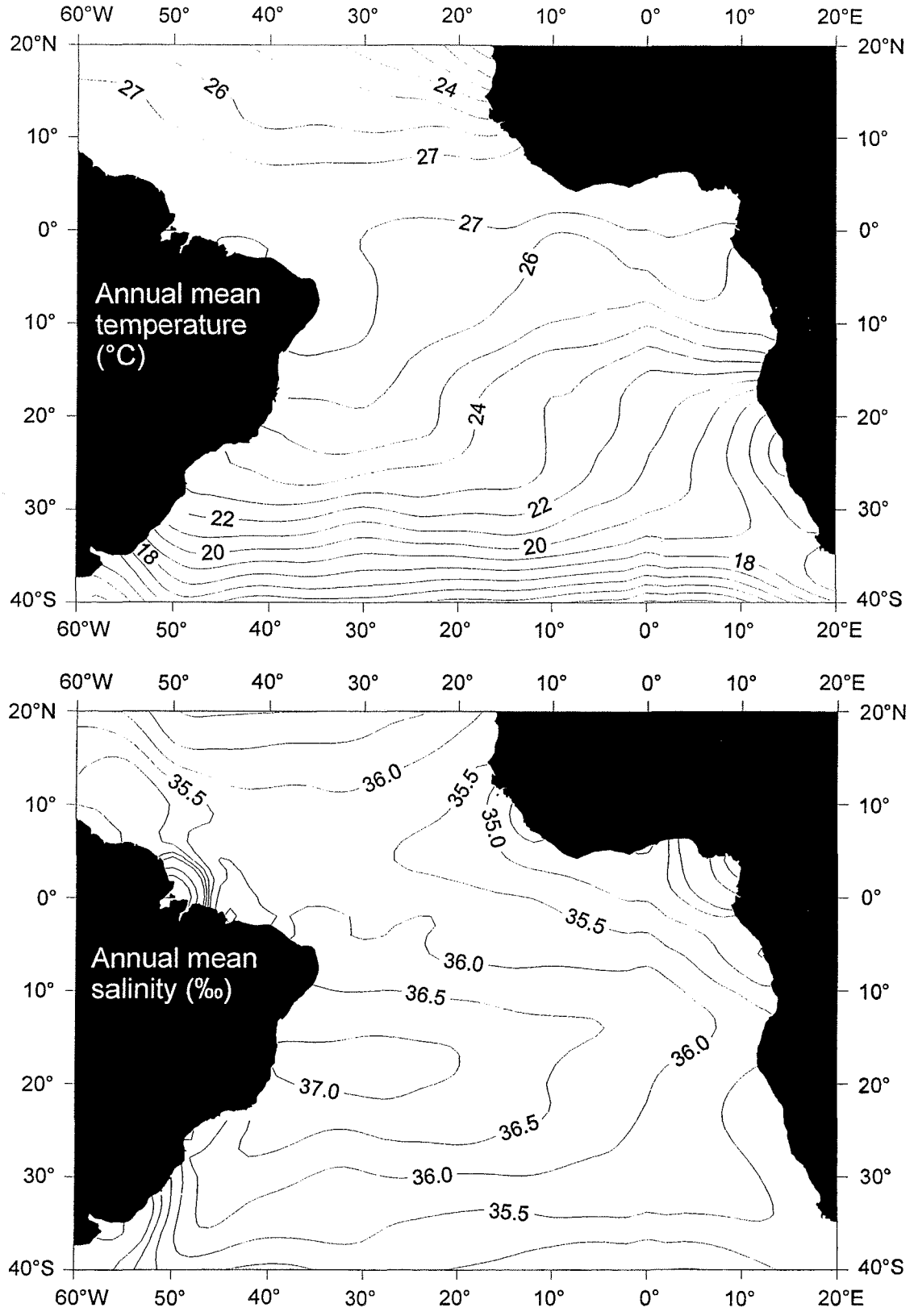

Figure 2: Annual mean temperatures (upper panel, in °C) and annual mean salinities (lower panel, in ‰) as deduced from the World Ocean Atlas 1994 (Levitus et al., 1994; Levitus and Boyer, 1994).

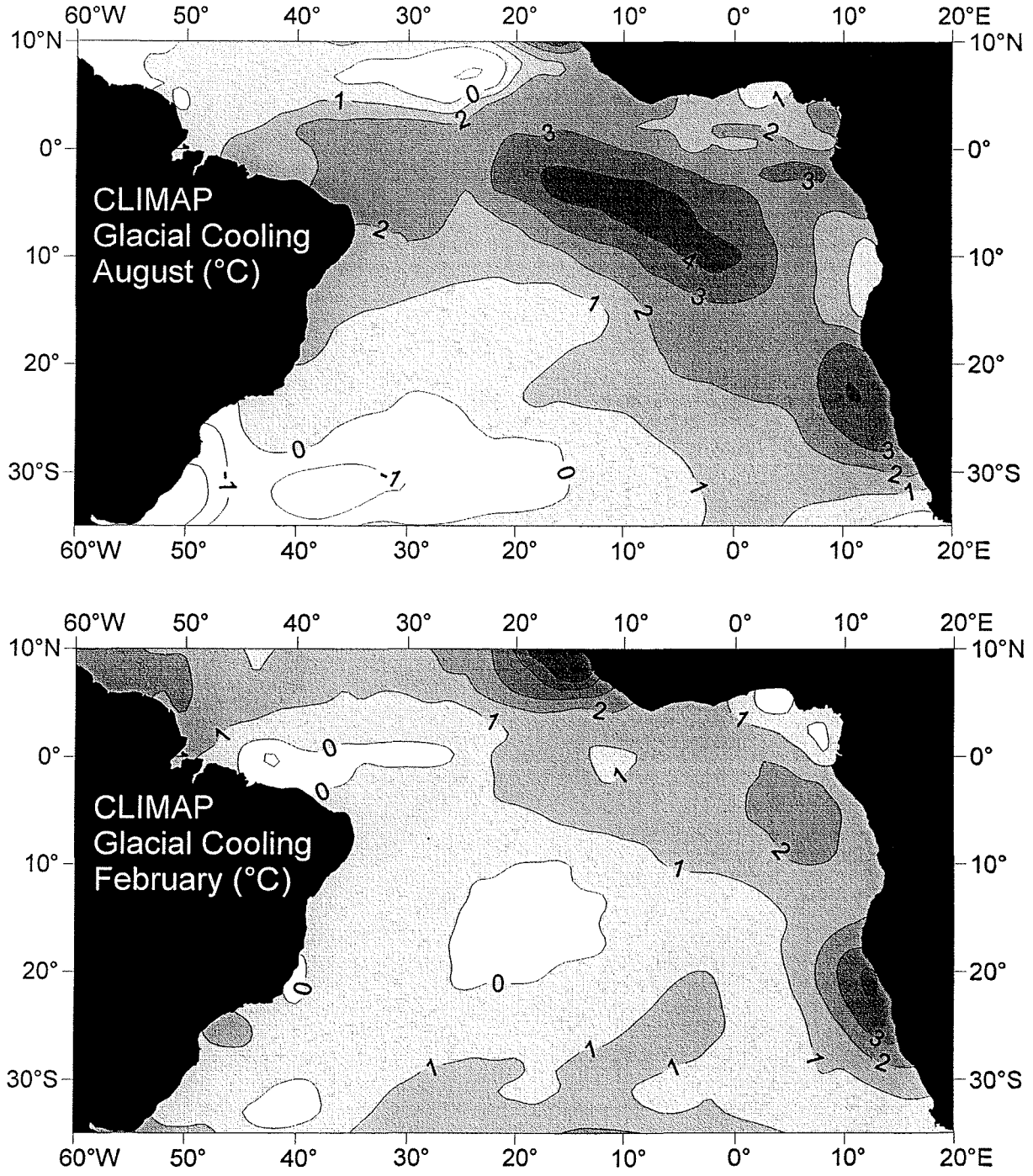

Figure 3: Glacial cooling according to CLIMAP (1994). Upper panel: Modern minus glacial August sea surface temperatures; Lower panel: Modern minus glacial February sea surface temperatures.

Soon after the CLIMAP results were published, the discrepancy between their SST estimates and evidence from glacial snowline depressions in tropical mountains, pollen data, and model results was pointed out (Webster and Streeten, 1978; Rind and Peteet, 1985).

During the last decade numerous articles addressing the question about tropical cooling at the LGM were published.

Most continental data suggest strong glacial cooling in the tropics. Besides the above-mentioned lowered snow lines and pollen data, the terrestrial evidence stems from noble gas concentrations in ground water (Stute et al., 1995) and the glacial-to-modern ^{18}O shift in tropical ice cores (Thompson et al., 1995, 1997). These data imply temperatures at sea level 5-6 °C cooler than today.

The marine record is ambiguous. While the foraminiferal assemblage based estimates of CLIMAP were confirmed by alkenone data (Rostek et al., 1993; Sikes and Keigwin, 1994) and oxygen isotopes in planktonic foraminifera (Broecker, 1986; Stott and Tang, 1996), evidence from pore fluids in deep sea sediments (Schrag et al., 1996) and new results from planktonic foraminiferal ^{18}O in the equatorial Atlantic (Curry and Oppo, 1997; Sikes and Keigwin, 1994) point towards stronger cooling of about 4-5°C. Sr/Ca-thermometry and the oxygen isotope composition of Barbados corals (Guilderson et al., 1994) also suggest glacial temperatures lowered by 4-6 °C, but the temperature changes based on Sr/Ca-ratios of corals may be overestimated due to a glacial effect in the Sr budget of the ocean (Stoll et al., 1997).

Numerical model results are not consistent either. When CLIMAP boundary conditions are used in atmospheric general circulation models, they are not able to simulate substantial cooling (e.g., in tropical mountains) to match the terrestrial record (Rind and Peteet, 1985; Anderson and Webb, 1994). However, recent results from a coupled ocean-atmosphere model (Broccoli and Marciniak, 1996) achieved SST comparable with CLIMAP. The coupled model of Ganopolski et al. (1998) demonstrated that cooling over land might have been consistent with terrestrial data while SST were moderately lowered (3.3 °C in the tropical Atlantic).

Methods and materials

The methods and materials used in this thesis are described in detail in the respective sections of the manuscripts. Relative abundances and the oxygen isotopic composition of planktonic foraminifera are used here. Foraminiferal census counts were performed by coauthors of the manuscripts or were published elsewhere and cited in the respective sections. Oxygen isotope data of sediment cores used in chapter 4 are listed in Appendix B. Secondary data, i.e., paleotemperature, paleosalinity and thermocline depth estimates based on the Modern Analog Technique or Artifical Neural Networks are listed in Appendices A and C.

Accepted and submitted manuscripts:

The objectives of this thesis as described above were addressed in five manuscripts which are published, in press, in revision or to be submitted to international journals. The following manuscripts are presented in chapters 2-6:

(1)
T. Wolff, B. Grieger, W. Hale, A. Dürkoop, S. Mulitza, J. Pätzold, G. Wefer
On the reconstruction of paleosalinities, in: G. Fischer and G. Wefer (eds): Proxies in paleoceanography: Examples from the South Atlantic, Springer, Berlin, in press.

(2)
S. Mulitza, T. Wolff, J. Pätzold, W. Hale, G. Wefer
Temperature sensitivity of planktic foraminifera and its influence on the oxygen isotope record, Marine Micropaleontology 33 (1998), 223-240

(3)
T. Wolff, S. Mulitza, H. Arz, J. Pätzold, G. Wefer
Oxygen isotopes versus CLIMAP (18 ka) temperatures - A comparison from the tropical Atlantic, Geology 26 (1998), 675-678.

(4)
T. Wolff, S. Mulitza, C. Rühlemann, G. Wefer
The tropical Atlantic thermocline seesaw: surface water response to the South Atlantic trade wind system during the late Quaternary, submitted to Paleoceanography.

(5)
A. Paul, S. Mulitza, J. Pätzold, T. Wolff
Simulation of oxygen isotopes in a global ocean model, in: G. Fischer and G. Wefer (eds): Proxies in paleoceanography: Examples from the South Atlantic, Springer, Berlin, in press.

References:

Anderson, D. M., and R. S. Webb (1994). Ice-age tropics revisited. *Nature 367*, 23-24.

Berger, W. H., and G. Wefer (1996). Central themes of South Atlantic circulation. In G. Wefer, W. H. Berger, G. Siedler, and D. J. Webb (Eds.), *The South Atlantic: Present and past circulation*, pp. 1-11. Berlin Heidelberg: Springer.

Broccoli, A. J., and E. P. Marciniak (1996). Comparing simulated glacial climate and paleodata: A reexamination. *Paleoceanography 11*, 3-14.

Broecker, W. S., D. M. Peteet, and D. Rind (1985). Does the ocean-atmosphere system have more than one stable mode of operation? *Nature 315*, 21-26.

Broecker, W. S. (1986). Oxygen isotope constraints on surface ocean temperatures. *Quaternary Research 26*, 2-14.

Broecker, W. S. (1996). Glacial Climate in the Tropics. *Science 272*, 1902-1904.

Broecker, W. S. (1997). Will our ride into the greenhouse future be a smooth one? *GSA Today 7*, 1-7.

CLIMAP, P. M. (1976). The Surface of the Ice-Age Earth. *Science 191*, 1131-1137.

CLIMAP, P. M. (1981). Seasonal reconstructions of the Earth's surface at the last glacial maximum. *GSA Map and Chart Ser. MC-36*, 1-18.

CLIMAP, P. M. (1994). Climap 18k Database. *IGBP PAGES/World Data Center-A for Paleoclimatology Data Contribution Series 94-001.*

Condie, S. A. (1991). Separation and recirculation of the North Brazil Current. *Journal of Marine Research 49*, 1-19.

Curry, W. B., and G. P. Lohmann (1990). Reconstructing past particle fluxes in the tropical Atlantic Ocean. *Paleoceanography 5*, 487-506.

Curry, W. B., and D. W. Oppo (1997). Synchronous, high-frequency oscillations in the tropical sea surface temperatures and North Atlantic Deep Water production during the last glacial cycle. *Paleoceanography 12*, 1-14.

DeMenocal, P. B., and D. Rind (1993). Sensitivity of Asian and African climate to variations in seasonal insolation, glacial ice cover, sea surface temperature and Asian orography. *Journal of Geophysical Research 98*, 7265-7287.

Duplessy, J. C., L. Labeyrie, A. Juillet-Leclerc, F. Maitre, J. Duprat, and M. Sarnthein (1991). Surface salinity reconstruction of the North Atlantic Ocean during the last glacial maximum. *Oceanologica Acta 14*, 311-324.

Duplessy, J. C., L. Labeyrie, M. Paterne, S. Hovine, T. Fichefet, J. Duprat, and M. Labracherie (1996). High Lattitude Water Sources During the Last Glacial Maximum and the Intensity of the Global Oceanic Circulation. In G. Wefer, W. H. Berger, G. Siedler, and D. J. Webb (Eds.), *The South Atlantic - Present and Past Circulation*, pp. 445-460. Berlin: Springer.

Dürkoop, A., W. Hale, S. Mulitza, J. Pätzold, and G. Wefer (1997). Late Quaternary variations of sea surface salinity and temperature in the western tropical Atlantic: Evidence from $\delta^{18}O$ of *Globigerinoides sacculifer. Paleoceanography 12*, 764-772.

Ganopolski, A., S. Rahmstorf, V. Petoukhov, and M. Claussen (1998). Simulation of modern and glacial climates with a coupled global model of intermediate complexity. *Nature 391*, 351-356.

Gordon, A. L. (1986). Interocean exchange of thermocline water. *Journal of Geophysical Research 91*, 5037-5046.

Guilderson, T. P., R. G. Fairbanks, and J. L. Rubenstone (1994). Tropical temperature variations since 20 000 years ago: Modulating interhemispheric climate change. *Science 263*, 663-665.

Herterich, K., S. Determann, B. Grieger, I. Hansen, P. Helbig, S. Lorenz, A. Manschke, M. Matthies, A. Paul, R. Schlotte, and U. Wyputta (1998). Reconstructing and Modelling the Last Glacial Maximum: Beyond CLIMAP. In G. Wefer, and G. Fischer (Eds.), *Proxies in Paleoceanography - Examples from the South Atlantic*, Berlin: Springer, in press.

Hoffmann, G. (1995). *Stabile Wasserisotope im allgemeinen Zirkulationsmodell ECHAM.* Max-Planck-Institut für Meteorologie, Examensarbeit 27.

Houghton, J. T., G. J. Jenkins, and J. J. Ephaums, Eds. (1990). *Climate change - the IPPC scientific assessment.* Cambridge, Cambridge University Press.

Hutson, W. H. (1980). The Agulhas Current during the late Pleistocene: Analysis of Modern Faunal Analogs. *Science 207*, 64-66.

Imbrie, J., and N. G. Kipp (1971). A new micropaleontological method for quantitative paleoclimatology: application to a Late Pleistocene Carribean core. In K. K. Turekian (Ed.), *Late Cenocoic glacial ages*, pp. 71-181. New Haven: Yale University Press.

Joussaume, S., J. Jouzel, and R. Sadourny (1984). A general circulation model of water isotope cycles in the atmosphere. *Nature 311*, 24-29.

Jouzel, J., G. L. Russell, R. J. Suozzo, R. D. Koster, J. W. C. White, and W. S. Broecker (1987). Simulations of the HDO and $H_2{}^{18}O$ atmospheric cycles using the NASA GISS General Circulation Model: The seasonal cycle for present-day conditions. *Journal of Geophysical Research 92*, 14739-14760.

Jouzel, J., R. D. Koster, S. R. J., and G. L. Russell (1994). Stable water isotope behaviour during the last glacial maximum: A general circulation model analysis. *Journal of Geophysical Research 99*, 25791-25801.

Lautenschlager, M., and K. Herterich (1990). Atmospheric response to ice age conditions: climatology near the earth's surface. *Journal of Geophysical Research 95*, 22547-22557.

Lautenschlager, M., U. Mikolajewicz, E. Maier-Reimer, and C. Heinze (1992). Application of ocean models for the interpretation of AGCM experiments on the climate of the last glacial maximum. *Paleoceanography 7*, 769-782.

Levitus, S., and T. P. Boyer (1994). World Ocean Atlas 1994, Volume 4: Temperature. *NOAA Atlas NESDIS 4*, 117 pp.

Levitus, S., R. Burgett, and T. P. Boyer (1994). World Ocean Atlas 1994, Volume 3: Salinity. *NOAA Atlas NESDIS 3*, 99 pp.

Lorenz, S., B. Grieger, P. Helbig, and K. Herterich (1996). Investigating the sensitivity of the Atmospheric General Circulation Model ECHAM 3 to paleoclimatic boundary conditions. *Geologische Rundschau 85*, 513-524.

Lutjeharms, J. R. E. (1996). The exchange of water between the South Indian and South Atlantic Oceans. In G. Wefer, W. H. Berger, G. Siedler, and D. J. Webb (Eds.), *The South Atlantic - Present and Past Circulation*, pp. 125-162. Berlin: Springer.

MacDonald, A. M., and C. Wunsch (1996). An estimate of global ocean circulation and heat fluxes. *Nature 382*, 436-439.

Maier-Reimer, E., and R. Bacastow (1990). Modelling of geochemical tracers in the ocean. In M. E. Schlesinger (Ed.), *Climate-Ocean Interaction*, pp. 233-267. Dordrecht: Kluwer Academ. Publ.

Maslin, M. A., N. J. Shackleton, and U. Pflaumann (1995). Surface water temperature, salinity, and density changes in the northeast Atlantic during the last 45,000 years: Heinrich events, deep water formation, and climatic rebounds. *Paleoceanography 10*, 527-544.

McIntyre, A., W. F. Ruddiman, K. Karlin, and A. C. Mix (1989). Surface water response of the equatorial Atlantic ocean to orbital forcing. *Paleoceanography 4*, 19-55.

Mix, A. C., W. F. Ruddiman, and A. McIntyre (1986). Late Quaternary paleoceanography of the tropical Atlantic, 1: Spatial variability of annual mean sea-surface temperatures, 0-20,000 years B.P. *Paleoceanography 1*, 43-66.

Mix, A. C. (1987). The oxygen-isotope record of glaciation. In W. F. Ruddiman, and H. E. J. Wright (Eds.), *North America and adjacent oceans during the last deglaciation*, pp. 111-135. Boulder, Colorado: Geological Society of America.

Peterson, R. G., and L. Stramma (1991). Upper-level circulation in the South Atlantic Ocean. *Progress in Oceanography 26*, 1-73.

Prell, W. L., and J. L. Kutzbach (1987). Monsoon variability over the past 150,000 years. *Journal of Geophysical Research 92*, 8411-8425.

Rahmstorf, S. (1997). Risk of sea-change in the Atlantic. *Nature 388*, 825-826.

Ravelo, A. C., R. G. Fairbanks, and S. G. H. Philander (1990). Reconstructing tropical Atlantic hydrography using planktonic foraminifera and an ocean model. *Paleoceanography 5*, 409-431.

Rind, D., and D. Peteet (1985). Terrestrial conditions at the last glacial maximum and CLIMAP sea-surface temperature estimates: Are they consistent? *Quaternary Research 24*, 1-22.

Rintoul, S. R. (1991). South Atlantic interbasin exchange. *Journal of Geophysical Research 96*, 2675-2692.

Rohling, E. J., and G. R. Bigg (1998). Paleosalinity and $\delta^{18}O$: A critical assessment. *Journal of Geophysical Research 103*, 1307-1318.

Rostek, F., G. Ruhland, F. C. Bassinot, P. J. Müller, L. D. Labeyrie, Y. Lancelot, and E. Bard (1993). Reconstructing sea surface temperature and salinity using $\delta^{18}O$ and alkenone records. *Nature 364*, 319-321.

Rühlemann, C., P. J. Müller, and R. R. Schneider (1998). Organic carbon and carbonate as paleoproductivity proxies: Examples from high and low productivity areas of the tropical Atlantic. In: G. Fischer and G. Wefer (Eds): *Proxies in paleoceanography: Examples from the South Atlantic*, Berlin: Springer, in press.

Schlitzer, R. (1996). Mass and heat transports in the South Atlantic derived from historical hydrographic data. In G. Wefer, W. H. Berger, G. Siedler, and D. J. Webb (Eds.), *The South Atlantic - Present and Past Circulation*, pp. 305-323. Berlin: Springer.

Schneider, R. R., P. J. Müller, and G. Ruhland (1995). Late Quaternary surface circulation in the east equatorial Atlantic: Evidence from alkenone sea surface temperatures. *Paleoceanography 10*, 197-219.

Schrag, D. P., G. Hampt, and D. W. Murray (1996). Pore fluid constraints on the temperature and oxygen isotopic composition of the glacial ocean. *Science 272*, 1930-1932.

Sikes, E. L., and L. D. Keigwin (1994). Equatorial Atlantic sea surface temperature for the last 30 ky: A comparison of U^{k}_{37}, $\delta^{18}O$, and foraminiferal assemblage temperature estimates based analysis on controls of foraminiferal estimates. *Paleoceanography 9*, 31-46.

Stocker, T. F. (1998). A glimpse of the glacial. *Nature 391*, 338-339.

Stocker, T. F., and A. Schmittner (1997). Influence of CO2 emission rates on the stability of the thermohaline circulation. *Nature 388*, 862-865.

Stoll, H. M., D. P. Schrag, and S. C. Clemens (1997). Effect of sea-level cycles on the Sr budget of the ocean. *Eos Transactions AGU 78*, 387.

Stott, L. D., and C. M. Tang (1996). Reassessment of foraminiferal-based tropical sea surface $\delta^{18}O$ paleotemperatures. *Paleoceanography 11*, 37-56.

Stute, M., M. Forster, H. Frischkorn, A. Serejo, J. F. Clark, P. Schlosser, W. S. Broecker, and G. Bonani (1995). Cooling of Tropical Brazil (5°C) During the Last Glacial Maximum. *Science 269*, 379-383.

Thompson, L. G., E. Mosley-Thompson, M. E. Davis, P.-N. Lin, K. A. Henderson, J. Cole-Dai, J. F. Bolzan, and K.-B. Liu (1995). Late Glacial Stage and Holocene Tropical Ice Core Records from Huascarán, Peru. *Science 269*, 46-50.

Thompson, L. G., T. Yao, M. E. Davis, K. A. Henderson, E. Mosley-Thompson, P.-N. Lin, J. Beer, H.-A. Synal, J. Cole-Dai, and J. F. Bolzan (1997). Tropical climate instability: The last glacial cycle from a Qinghai-Tibetan ice core. *Science 276*, 1821-1825.

Tomczak, M., and J. S. Godfrey (1994). *Regional oceanography: An introduction.* New York: Pergamon.

Wang, L., M. Sarnthein, J. C. Duplessy, H. Erlenkeuser, S. Jung, and U. Pflaumann (1995). Paleo sea surface salinities in the low-latitude Atlantic: The $\delta^{18}O$ record of Globigerinoides ruber (white). *Paleoceanography 10*, 749-761.

Washington, W. M., and C. L. Parkinson (1986). *An Introduction to Three-Dimensional Climate Modelling*. Mill Valley: University Science Books.

Webster, P. J., and N. A. Streeten (1978). Late Quaternary ice age climates of tropical Australasia: Interpretations and Reconstructions. *Quaternary Research 10*, 279-309.

Wefer, G., and W. H. Berger (1991). Isotope paleontology: growth and composition of extant calcareous species. *Marine Geology 100*, 207-248.

Wefer, G., W. H. Berger, T. Bickert, B. Donner, G. Fischer, S. Kemle-von Mücke, G. Meinecke, P. J. Müller, S. Mulitza, H. S. Niebler, J. Pätzold, H. Schmidt, R. R. Schneider, and M. Segl (1996). Late Quaternary Surface Circulation of the South Atlantic: The Stable Isotope Record and Implications for Heat Transport and Productivity. In G. Wefer, W. H. Berger, G. Siedler, and D. J. Webb (Eds.), *The South Atlantic - Present and Past Circulation*, pp. 461-502. Berlin: Springer.

Chapter 2

On the reconstruction of paleosalinities

Tobias Wolff
Björn Grieger
Walter Hale
Anke Dürkoop
Stefan Mulitza
Jürgen Pätzold
Gerold Wefer

in: G. Fischer and G. Wefer (eds): Proxies in paleoceanography: Examples from the South Atlantic, Springer, Berlin, in press.

On the reconstruction of paleosalinities

T.Wolff[1], B. Grieger[1], W. Hale[2], A. Dürkoop[1], S. Mulitza[1], J. Pätzold[1] and G. Wefer[1]*

[1]Universität Bremen, Fachbereich Geowissenschaften, Klagenfurter Straße, D-28359 Bremen, Germany
[2]ODP Bremen Core Repository, Konsul-Schmidt Str.30, D-28217 Bremen, Germany
**corresponding author (e-mail): twolff@uni-bremen.de*

Abstract: Methods potentially useful for paleosalinity reconstructions are summarized and applied to surface sediments and two cores from the Atlantic. The first approach is based on the oxygen isotope ratio in calcite tests of planktonic foraminifera in conjunction with an independent sea-surface temperature estimate. A two-step procedure from foraminiferal $\delta^{18}O$ to the isotopic composition of sea-water and from there to an estimate of paleosalinity is proposed. The quality of the estimation of $\delta^{18}O$ for sea-water depends heavily on the reliability of the independent temperature method. The final salinities are obtained through an assumed $\delta^{18}O$-salinity relationship for sea-water. Propagation of errors yields large deviations, especially in the tropics where slopes of the $\delta^{18}O$-salinity relationship are low. An uncertainty in temperature of ±1°C leads to errors in the salinity reconstruction of ±0.5 to ±1.2 ‰. Downcore application at a site in the western equatorial Atlantic indicates salinity increases of roughly 2.5 ‰ in the glacials, but also demonstrates sensitivity of the results to the temperature estimates and the $\delta^{18}O$-salinity relationship. Two additional methods of paleosalinity estimation were investigated both of which employ foraminiferal abundance data. An Artificial Neural Network was used for the first time to reconstruct paleosalinities. The obtained results were then compared to results from a Modern Analog Technique. Application to surface sediments yields comparable results for both methods, with standard deviations between 0.49 and 0.63 ‰. Salinity calculations performed on downcore data in the tropical and subtropical South Atlantic indicate that the results are controlled by today's temperature-salinity relationship. This leads to the conclusion that paleosalinity reconstructions from species composition of foraminiferal assemblages are unrealistic, because of a predominant response of the fauna to temperature.

Introduction

Temperature and salinity determine the density of a water mass, thus, they are important keys to the thermohaline circulation and as boundary conditions they are of special interest for modelling purposes (Washington and Parkinson 1986). The formation of deep water is extremely sensitive to salinity (Broecker and Denton 1989) and so, therefore, are general circulation models of the ocean (Lautenschlager et al. 1992). These models are executed with Newtonian or flux boundary conditions. For sea-surface temperatures (SSTs), Newtonian boundary conditions are usually employed, i.e. direct SST estimates (e.g. from CLIMAP 1976, CLIMAP 1981) are taken. Paleosalinities have to be roughly estimated, otherwise flux boundary conditions are used instead. This implicates that salinities are replaced by freshwater fluxes taken from atmospheric model outputs. To improve ocean modelling, paleosalinity „measurements" with high accuracies are needed.

No direct methods exist so far. In other words, there is no geological parameter that can be related directly to paleosalinity in the open ocean. Instead, salinities are estimated by performing a number of successive computations on compound proxies, each of which requires approximations.

From FISCHER G, WEFER G (eds) 1998, *Use of Proxies in Paleoceanography: Examples from the South Atlantic.* Springer-Verlag Berlin Heidelberg, pp xxx-xxx.

One method encountered in recent publications (Duplessy et al. 1991; Rostek et al. 1993) is based on the oxygen isotopic composition of calcite shells of planktonic foraminifera, which depends on the temperature and isotopic composition of the ambient water mass. The isotopic composition of the water is again empirically related to salinity. The most severe problems with the oxygen-isotope method result from uncertainties in the isotope-salinity relationship and uncertainties in the estimated temperature.

Other methods are based on the ecological preferences of foraminiferal assemblages, relating relative abundances of planktonic foraminiferal species to oceanographic parameters. The most critical point here is the isolation of one desired parameter (salinity) which does not account for complex dependency of the assemblages on various other factors such as temperature, nutrients, seasonality and thermocline structure, any one of which may be of greater significance in determining the overall faunal composition.

The aim of this paper is to summarize recent approaches for paleosalinity reconstruction and to evaluate the pros and cons, flaws and perspectives of the various methods. This will be pursued by investigation of core-top and downcore data for each method.

Salinity reconstructions using oxygen isotopes

The paleotemperature equation

Several attempts have been made in the last decade to estimate paleosalinities from the oxygen isotope compositions of calcite tests of planktonic foraminifera (Fillon and Williams 1984; Broecker 1989; Spero and Williams 1990; Broecker 1990; Sikes and Keigwin 1996). Recently, more quantitative approaches were made to reconstruct paleosalinities downcore (Duplessy et al. 1992; Rostek et al. 1993; Maslin et al. 1995; Wang et al. 1995; Kallel et al. 1997) and on the time slice of the last glacial maximum (Duplessy et al. 1991, 1996).

The oxygen isotope composition recorded in the tests of planktonic foraminifera is determined mainly by the temperature and the isotopic composition of the water mass in which they calcify. To a lesser extent it also depends on the carbonate ion concentration as shown by Spero et al. (1997). This effect will be neglected here.

The $^{18}O/^{16}O$-ratio of the precipitated calcite is greater than the $^{18}O/^{16}O$-ratio of the sea-water. This difference decreases with increasing temperatures of the water at the time of calcite precipitation (Berger and Gardner 1975). Thus, measuring the isotopic composition of planktonic foraminifera and estimating the isotopic composition of the ambient sea-water enables us to compute temperatures for this water mass. This method has been used to reconstruct sea-surface temperatures since Emiliani applied it to Pleistocene sediments in 1955 (e.g. Emiliani 1955; Vincent and Shackleton 1980; Van Campo et al. 1990; Keigwin 1996). The approach is based on the theoretically and empirically derived equation (Urey 1947; Epstein et al. 1953):

$$T = 16.5 - 4.3\left(\delta^{18}O_c - \delta^{18}O_w\right) + 0.14\left(\delta^{18}O_c - \delta^{18}O_w\right)^2 \quad (1)$$

where T is the temperature in °C, $\delta^{18}O_C$ is the isotopic composition of the calcite test in ‰ relative to the PDB standard and $\delta^{18}O_W$ is the isotopic composition of the ambient sea-water in ‰ (PDB). Fig. 1 illustrates the dependency of $\Delta\delta^{18}O$ ($\delta^{18}O_C$-$\delta^{18}O_W$) on the temperature as determined in culture studies by Erez and Luz (1983).

Reconstructing the oxygen isotope composition of sea-water

Returning to equation (1), however, it is obvious that if the water temperature is known from an independent method the oxygen-isotope ratio of sea-water can easily be calculated from $\delta^{18}O$ measurements of foraminiferal tests. Solving equation (1) for $\delta^{18}O_W$ gives

$$\delta^{18}O_w = \delta^{18}O_c - 21.9 + \sqrt{310.6 + 10 \cdot T} \quad (2)$$

Computing the oxygen-isotope ratio of sea-water can be regarded as the first step towards sa-

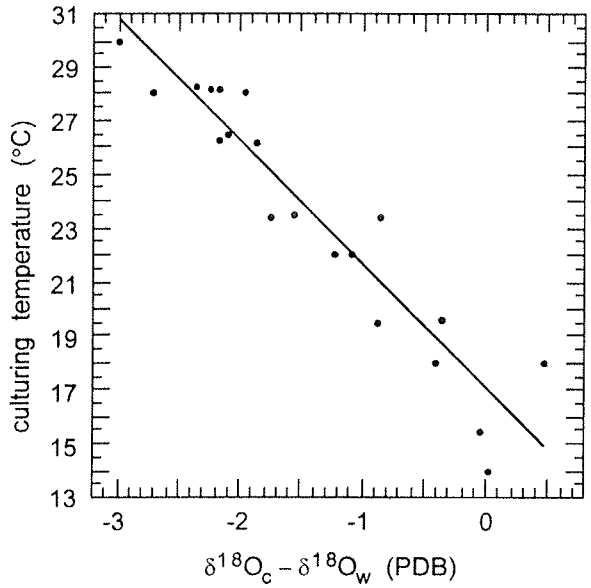

Fig. 1. Dependency of $\delta^{18}O_C$ -$\delta^{18}O_W$ on temperature as determined in culturing experiments by Erz and Luz (1983).

linity reconstructions and may be used as a quality control parameter. This was done for the first time by Fillon and Williams (1984). Mix and Ruddiman (1985) tried to remove the temperature effect from the isotope curves of two tropical Atlantic cores. They stated that a convincing interpretation of their $\delta^{18}O_W$ data was difficult, because after correcting for temperature the two downcore records were more dissimilar than before. Duplessy et al. (1991) reconstructed summer sea-surface water $\delta^{18}O$ and salinities for the last glacial maximum in the North Atlantic, while Rostek et al. (1993), Wang et al. (1995) and Maslin et al. (1995) proceeded directly towards salinity estimations.

One problem inherent to using the $\delta^{18}O$ of planktonic foraminifera arises from the deviation of the isotope record of a selected species from an „ideal" species, for which equation (1) holds. In reality, plots of isotopic temperature vs. measured temperature for core-top data sets are not identical to the expected straight line with a slope equal to one. Preference of a species for a particular temperature results in higher fluxes during times of their „optimum temperature", meaning that downcore $\delta^{18}O_C$ do not necessarily represent the same time of the year (e.g. Williams et al. 1979; Deuser et al. 1981; Curry et al. 1983; Mix 1987; Mulitza et al. 1998). Furthermore, vertical migration of some planktonic foraminifera causes deviations of computed temperatures from sea surface conditions (e.g. Emiliani 1971).

Additionally the so-called „vital effects" (Deuser and Ross 1989) must be taken into consideration. That is, some species of planktonic foraminifera do not calcify in thermodynamic equilibrium with the ambient sea-water (on which equation (1) is based).

These problems are usually addressed by performing core-top calibrations for each selected species of the form

$$T_{iso} = kT + m \qquad (3)$$

where T_{iso} is the calculated isotopic temperature, T is the actual temperature, k and m are the coefficients of the regression line used for calibration.

Thus equation (2) has to be modified to

$$\delta^{18}O_w = \delta^{18}O_c - 219 + \sqrt{3106 + 10\cdot(kT+m)} \qquad (4)$$

As an example Duplessy et al. (1991) performed two calibrations for *N. pachyderma* and *G. bulloides* to cover a wide range of temperatures encountered in the North and South Atlantic. Wang et al. (1995) calibrated *G. ruber* (white) for salinity reconstructions in the eastern tropical Atlantic.

For the purpose of paleosalinity reconstructions the final $\delta^{18}O_W$ has to be converted from PDB standard to V-SMOW standard by adding 0.27 ‰ (Hut 1987).

From sea-water $\delta^{18}O$ to paleosalinities

There is a relationship between $\delta^{18}O$ of sea-water and its salinity (Craig and Gordon 1965), which can be written as:

$$\delta^{18}O_w = a \cdot S + b \qquad (5)$$

where b is the $\delta^{18}O$ of a freshwater end member, S is the salinity and a is the slope of the $\delta^{18}O_W$ -

salinity relationship. When global data are used a regression line with a = 0.5 and b = -17 can be inferred (Broecker 1986). However, different regions in the oceans are governed by different equations (Berger and Gardner 1975; Fairbanks et al. 1992). While the slope of the $\delta^{18}O_w$-salinity relationship approaches 1.0 towards the polar regions (Vetshtein et al. 1974, Fairbanks et al. 1992), it becomes smaller towards the equator. Fairbanks computed a slope of 0.19 for the western equatorial Atlantic. In the eastern equatorial Atlantic it is as low as 0.08.

Why is there a relationship between $\delta^{18}O$ of sea-water and salinity? Both the $^{18}O/^{16}O$ ratio and salinity are controlled by the evaporation-precipitation regime. Excess of evaporation over precipitation drives both salinity and $\delta^{18}O_w$ up, because salt is left behind during evaporation and oxygen isotopes are fractionated with water vapor being depleted in $\delta^{18}O$ relative to sea-water.

But, while the salt content of water vapor is constant and essentially equal to zero, the $\delta^{18}O$ of water vapor can vary considerably depending on its origin and its residence time in the atmosphere. While evaporating and precipitating waters have quite similar isotopic signatures in the tropics, precipitation in higher latitude is increasingly depleted in ^{18}O due to further fractionation (Craig and Gordon 1965; Wefer and Berger 1991). This is the reason why the slope of the straight line in equation (5) increases at higher latitudes.

Various other influences complicate the system, e.g., fractionation during evaporation and during formation of rainfall is influenced by windspeed and temperature, respectively (Merlivat and Jouzel 1979). In fact, the relation between isotope enrichment and salinity increase is characterized by non-linearity (Ferronsky and Brezgunov 1989).

In a regional context, however, isotopic signatures of precipitation and evaporation remain rather constant in the long-term annual mean. A linear $\delta^{18}O_w$-salinity relationship as is expressed in equation (5) can be assumed (Epstein and Mayeda 1953). This straight line represents a continuum between dry and moist conditions in a given region.

To reconstruct absolute salinity values from sea-water $\delta^{18}O$, a $\delta^{18}O_w$-salinity relationship has to be adopted and, if we ignore regional changes in the evaporation-precipitation regime, modifications have to be performed accounting for global effects due to water storage in the continental ice-caps. These corrections reflecting past variations of both the $\delta^{18}O$ of sea-water and salinity can either be made as individual computational steps or can be included in equation (5). We prefer the second strategy because it allows the formulation of a paleo-$\delta^{18}O_w$ salinity relationship which is useful in the view of numerical models that include the transport of $\delta^{18}O$ in both atmosphere (Hoffmann 1995) and ocean (Paul et al., this volume). Also, it allows the evaluation of the hydrological cycle at a certain time in the past (Wolff et al. in press).

Rewriting equation (5) gives:

$$\delta^{18}O_w = a \cdot (S - S_g) + b + d_g \qquad (6)$$

where d_g is the correction for $\delta^{18}O$ of sea-water and S_g is the correction term for globally changing salinities. Fig. 2 graphically illustrates the shift of the $\delta^{18}O_w$-salinity relationship neglecting changes in the slope of the straight line.

Solving equation (6) for salinity yields:

$$S = \frac{\delta^{18}O_w - b}{a} - \frac{d_g}{a} + S_g \qquad (7)$$

How do we compute the correction terms d_g and S_g? Maximum global glacial-interglacial changes in $\delta^{18}O_w$ and S have been estimated as 1.2 ‰ (see Wefer et al. 1996) and 1.1 ‰ (Rostek et al. 1993), respectively .The correction terms d_g can be approximated from a global $\delta^{18}O_w$ time series, e.g. from the SPECMAP stack or the curve given by Labeyrie et al. (1987) which have to be adjusted to a maximum glacial-interglacial $\Delta\delta^{18}O_w$ of 1.2 ‰. A global $\delta^{18}O_w$-curve based on Labeyrie et al. (1987) and Vogelsang (1990) for the last 360 kyrs is shown in Fig. 9D. The correction term for salinity S_g can be obtained in the same way by normalizing the global curve to 1.1 ‰. Another approach is to relate S_g to changes in sea level relative to the modern should a sea level curve be available (Rostek et al. 1993).

Application to core-top data

We computed salinities for a global data set of core-top isotopic measurements. Data have been collected from the literature (references are summarized in Table 1). The data set comprises 777 measurements from high to low latitudes in all major oceans with a large number of samples in the Atlantic and Indian Oceans, and only a few in the Pacific. Isotopic data from four shallow-dwelling planktonic foraminifera *G. ruber*, *G. sacculifer*, *G. bulloides* and *N. pachyderma* have been used. The data were not selected according to the size fractions of analyzed foraminifera or the number of individuals measured in one sample. Distinctions between *G. ruber* (white) and *G. ruber* (pink) were not made here.

In the first step, $\delta^{18}O$ of sea-water was calculated by inserting annual mean temperatures for all sample locations in equation (2). Temperatures were taken from the World Ocean Atlas 1994 (Levitus and Boyer 1994). Calibrations according to equation (3) were not applied. In the second step, annual mean salinities were computed by inserting the SMOW-corrected sea-water $\delta^{18}O$ into equation (7). A global $\delta^{18}O_w$-salinity relationship was used (a = 0.5, b = 17), corrections for ice effects are, of course, not necessary for the modern ocean.

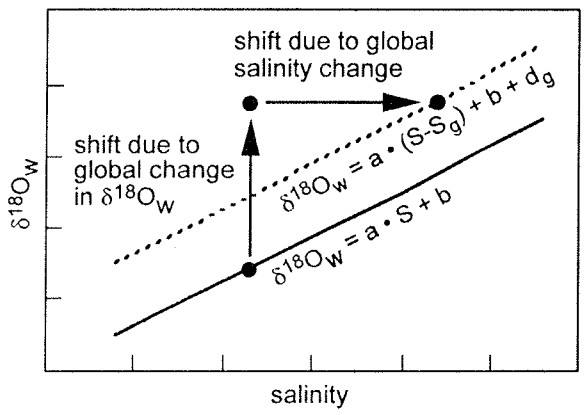

Fig. 2. Shift of the $\delta^{18}O$-salinity relationship due to global increase in $\delta^{18}O_w$ and salinity, not accounting for additional local shifts or changes in the slope of the straight line.

Application to downcore data

The oxygen isotope method of paleosalinity reconstruction has also been applied to a gravity core in the western equatorial Atlantic. Core site GeoB 1523 is located in the Intertropical Convergence Zone (ITCZ) off Brazil (3°50 N, 41°37 W, water depth: 3292 m). The core was taken on RV METEOR cruise M 16/2 (Schulz et al. 1991).

Isotopic measurements (Dürkoop et al. 1997) were made on the surface dwelling planktonic foraminifer *Globigerinoides sacculifer* (without saclike chamber). Paleosalinities were estimated for samples at 10 cm intervals to coincide with the available paleotemperature estimations. Temperatures were calculated by Modern Analogue Technique (MAT) using relative abundances of planktonic foraminifera. Temperatures were estimated twice using slightly different MAT techniques, but from the same faunal abundance data. For the first run, temperatures (Hale and Pflaumann, this volume) calculated by the SIMMAX technique (Pflaumann et al. 1996) were used. For comparison, temperatures derived from MacMAT were then used to calculate a second paleosalinity curve (the procedure for temperature estimation is the same as the computation of salinities by MacMAT and is described in detail below). In both cases, MAT summer temperature estimates were taken. Calibration terms as indicated in equation (3) were not used. Duplessy (1981) described deviations of the $\delta^{18}O_c$ of *G. sacculifer* obtained from nets compared to calculated equilibrium sea surface conditions, but he also stated that surface sediment samples gave results close to the equilibrium line, probably due to gametogenic calcification. Thus, proceeding without additional calibration is justified. Paleosalinities were then computed using a $\delta^{18}O_w$-salinity relationship for the entire Atlantic excluding the polar regions derived from GEOSECS data (1987) with a and b in equation (5) being 0.48 and -16.3, respectively. Based on measurements in the surficial water layer of the Brazil Basin, Pierre et al. (1991) reported a very similar slope of the $\delta^{18}O_w$-salinity relationship of 0.5. For reasons of comparison, calculations were repeated with a $\delta^{18}O_w$-salinity relationship for today's tropical Atlantic based on GEOSECS measurements between 30°S and

Species	Region	Reference
bul, pal	N. Atl., South. Oc.	Duplessy et al. 1991
rub	Indic	Duplessy 1982
rub, sac	Equ. Atl., South. Atl.	Mulitza 1994
bul, pal, sac, rub	South. Oc.	Niebler 1995
sac	Indic	Vincent and Shackleton 1980
pal	South. Oc.	Charles and Fairbanks 1990
sac	NW. Atl.	Showers and Margolis 1985
sac, rub	N. Atl.	Durazzi 1981
rub, sacc	Indic	Williams and Healy-Williams 1980
rub, sacc	Pacific	Savin and Douglas 1973
sac	global	Hecht and Savin 1972
pal	South. Oc.	Melles 1991
sac	Pacific	Wu and Berger 1989
bul, pal	South. Oc.	Grobe et al. 1990

bul=*G.bulloides*; pal=*N.pachyderma* (sin.); rub=*G.ruber*; sac=*G.sacculifer*

Table 1. Species, regions and references of the core-top data compiled from the literature and used in conjunction with the oxygen isotope method.

30°N. The equation obtained (a = 0.182, b = -5.6) is close to an equation given by Fairbanks et al. (1992) for the western equatorial Atlantic. Corrections for the global ice effect were made for d_g and S_g from equation (6) by normalizing a global $\delta^{18}O$ curve (Labeyrie et al. 1987 and Vogelsang 1990) to a maximum $\Delta\delta^{18}O_w$ of 1.2 ‰ and a maximum ΔS of 1.1 ‰, respectively.

Salinity reconstructions using relative abundances of planktonic foraminifera

Several authors have calculated past sea-surface salinities using relative abundance data of foraminifera (Imbrie and Kipp 1971; Kipp 1976; Hutson 1980; Cullen 1981) or coccolithophores (Giraudeau 1992) in deep-sea sediments. Since salinity is correlated with temperature in the modern ocean (Sverdrup et al. 1942), this approach has often been criticized (Berger 1981; Vincent and Berger 1981; Duplessy et al. 1991). Because temperature is the dominant factor in determining foraminiferal assemblage compositions, it is argued that the salinity estimate is not independent of the temperature signal. Thus, applying the methods to downcore data would give unrealistic results because the temperature-salinity relationship cannot be regarded as constant in time.

On the other hand, laboratory experiments (Bijma et al. 1990) and field studies (Cullen 1981; Naidu 1993) show that foraminiferal species are, to a certain degree, sensitive to salinity . Foraminiferal assemblages are influenced by a number of factors including temperature, salinity, productivity and seasonality. As a consequence, relative abundances of planktonic foraminifera should contain information about each of these environmental parameters.

There are various approaches for dealing with foraminiferal count data. Three of them should be mentioned here, two of them in greater detail.

All methods are based on the actualistic principle: Foraminiferal assemblages were determined by surface hydrography in the past as they are today. We can therefore estimate paleoenvironmental parameters by comparing downcore assemblages with modern ones. For the latter, properties of the ambient water masses are knowns.

Transfer functions

Imbrie and Kipp (1971) were the first to reconstruct salinities using transfer functions. This well-known method is based on Q-mode factor analysis which reduces the total number of different species to a smaller number of independent foraminiferal assemblages in the core-top reference data set. The next step involves a multiple linear regression which relates these assemblages to modern sea-surface salinities. The regression equation is then used to compute salinities for fossil data. This approach has been extensively used for sea-surface temperature estimation and is described in detail elsewhere (e.g. Imbrie and Kipp 1971; Kipp 1976; Hutson and Prell 1980; Pflaumann 1985; Niebler 1995).

Modern Analog Technique

Another method which has been used in the past to reconstruct paleosalinities (and paleotemperatures) is the Modern Analog Technique (MAT) as desribed by Hutson (1980). He was the first to use this method for paleotemperature and paleosalinity reconstruction on a core in the southwest Indian Ocean. Prell (1985) recalculated sea surface temperatures for the last glacial maximum on the basis of foraminiferal counts provided by the CLIMAP group (1981). Overpeck et al. (1985) used modern analogs for the interpretation of fossil pollen data. Recent workers have achieved differing results with their MAT methods for temperature estimation. While Pflaumann et al. (1996) see the potential of their SIMMAX above other methods (for temperature estimation), Le (1993) received unstable SST estimates which he claimed were due to the failure of his dissimilarity coefficient. We used a MAT to compute salinities directly for core-top and downcore data, and also to calculate downcore temperatures used for paleosalinity reconstructions with the oxygen isotope method described above.

Compared to transfer functions, MAT is relatively simple in terms of its computational procedure. The relative abundances of planktonic foraminifera of each sample are compared to the counts of all samples in the modern reference data set. The unknown environmental parameters are then computed by averaging the parameters linked to the most similar samples of the reference data set, the „modern analogs". The computational procedure is as follows:

Vectors are created containing the counts of all species as components. All vectors are normalized (to unity lengths). Then a similarity index (or dissimilarity index) is calculated between each sample of the reference data set and the sample data set (see Overpeck et al. 1985, for a good overview of dissimilarity coefficients). We used the program MacMAT developed by R. Sieger (Alfred Wegener Institut, Bremerhaven). This program uses a similarity index that is equal to the cosine of the angle between the two vectors of which foraminiferal relative abundances shall be compared. A similarity index of one results from a comparison of identical assemblages whereas an index of zero means no similarity at all. The similarity index is calculated as

$$Si_{j,k} = \frac{\sum_{i=1}^{n} P_{i,k} \cdot R_{i,j}}{\sqrt{\sum_{i=1}^{n} P_{i,k}^2 \cdot \sum_{i=1}^{n} R_{i,j}^2}} \qquad (8)$$

where $Si_{j,k}$ is the similarity index, n is the number of species, i is the counting index of species, j is the counting index of reference samples, k is the counting index of subject samples, P is the relative abundance in the core sample, and R is the relative abundance in the reference sample.

In the second step, the most similar samples of the reference data set are taken to calculate the salinity of the sample with unknown environmental parameters. We used the five most similar samples, because this number gave the best results (as will be shown later). The final value is computed by weighting the salinities of the five „modern analogs" according to their similarity indices and then averaging them:

$$S_k = \frac{\sum_{j=1}^{n_s} Si_{j,k} \cdot S_j}{\sum_{j=1}^{n_s} Si_{j,k}} \quad (9)$$

with S_k denoting the estimated salinity of the sample, n_s the number of most similar samples and S_j the salinity of the reference sample.

We employed MAT for paleosalinity reconstruction in conjunction with data from core-tops and two cores of the central and south Atlantic. To test the method, we first applied it to the CLIMAP (1981) core-top data set (356 samples). The data set was downloaded from SPECMAP Archive No1 from the NOAA ftp server. 42 species counts were included (only abundances of *G. ruber* total, *G. sacculifer* total and *G. menardii* complex were excluded to avoid redundancy).

The entire data set was split into two subsets. This was done by consecutively numbering the core-tops and then selecting an even-numbered and an odd-numbered set. The first half was used as a reference data set, whilst the second was used as the sample data set, for which annual mean salinities were computed. The results were compared to the actual sea surface salinities (annual means) derived from Levitus (1982). In a second step, the reference and sample data sets were exchanged and computations were performed for the first half.

The MAT was optimized by calculating salinities using 2 to 10 most similar reference samples (Fig. 3). Five samples were considered optimal for salinity determination.

Annual mean paleosalinities were calculated for core GeoB 1523-1 located in the ITCZ. Thirty-five species of planktonic foraminifera were distinguished in the core samples (see Hale and Pflaumann, this volume). The entire CLIMAP core-top data set was reduced accordingly and used as the reference data set.

Paleosalinities were also reconstructed for core RC 12-294 (Imbrie et al. 1989). This core was chosen in order to test the method on a core in the mid-latitudes, where the above mentioned linear

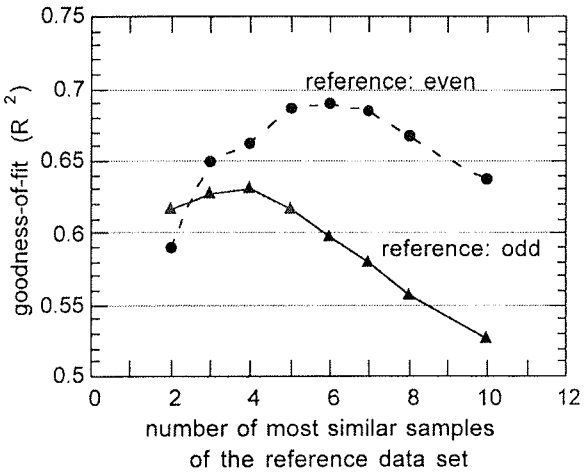

Fig. 3. Optimization of MacMAT: Goodness-of-fit of regression between calculated and observed salinities (Levitus 1982) vs. the number of most similar samples of the reference data set used for estimation. Using 4 or 6 most similar samples gave best results taking the odd or even data set as reference, respectively. As a consequence 5 most similar samples are used for further calculations.

relationship between temperature and salinity is strongest. The core site is located in the central South Atlantic at the southern margin of the subtropical gyre (37°15.6S, 10°5.8W). Foraminiferal counts were obtained from SPECMAP Archive No1 from the NOAA ftp server. The data set was reduced to 35 species for consistency with Core GeoB 1523-1. Again, the CLIMAP core-top data set served as reference data set.

Before we proceed to the results, we will introduce a new method of paleosalinity reconstruction which also employs faunal relative abundance data: Artificial Neural Networks. We do so, because the procedure parallels MAT somewhat, so that results of the two methods are easy to compare.

Artificial Neural Networks

The idea to use artificial neural networks (ANN) (Widrow and Lehr 1990) for paleosalinity reconstruction originated from the following considerations:

1. Foraminiferal assemblages are influenced by salinity as well as temperature and other factors.
2. The salinity-assemblage relationship might be characterized by non-linearity.

Artificial neural networks are able to detect patterns other than linear dependency in contrast to, e.g., transfer functions.

The optimization of an appropriately structured neural network with the backpropagation learning algorithm (Rumelhart et al. 1986) is comparable to fitting a parameterized function by error minimization using steepest descent methods. The neural network approach provides a large class of nonlinear model functions accompanied by a matching optimization procedure.

In a layered feed-forward network (an example is shown in Fig. 4), the output of neuron i in layer k is given by

$$y_i^{(k)} = f_{out}^{(ki)}\left(\sum_{j=0}^{N_{k-1}} W_{ij}^{(k)} y_j^{(k-1)}\right) \qquad (10)$$

where N_{K-1} is the number of neurons in layer k-1, $W_{ij}^{(k)}$ is the weight for input j and $f_{out}^{(ki)}$ is the output function of neuron i in layer k. In the present case a two-layered network is used, where the input layer (k=0) is not counted. There are two layers of neurons (k=1,2), the first of which is called the hidden layer. The output functions used are $f_{out}^{(1i)}$ =tanh, and $f_{out}^{(2i)}$=identity. $y_j^{(0)}$ denotes the input vector. The so-called dummy inputs are $y_0^{(k)}=1$

Given a training set of input vectors accompanied by desired output vectors (in our case the output is just a single value, i.e. the salinity), the neural network can be optimized by backpropagation of the output errors through the whole network to adjust all weights, see e.g. Rumelhart et al. (1986). Initially, the network weights are set to small random values. Then an input vector representing the relative abundances of a foraminiferal assemblage is chosen (randomly or in cyclic order) from the training set and presented to the network. The desired output value y (salinity), is used to adjust the weights of the network with the backpropagation algorithm. This is repeated until convergence is achieved.

If the number of species to be considered is fixed (42 or 35 in our case), the two-layered and fully connected neural network model is completely described by the number of hidden neurons N_1. By increasing N_1 the number of free parameters is increased and the model can be fitted to a given data set with an arbitrary small error. But the results become useless when the model reproduces the stochastic component of the data (compare Barnett and Hasselmann 1979), i.e., the results are poor for new input vectors which were not incorporated in the training data.

To determine the optimum number of hidden neurons, we trained various networks using the 42 species counted in 356 CLIMAP core-tops from the Atlantic. As in MAT, only one half of the data

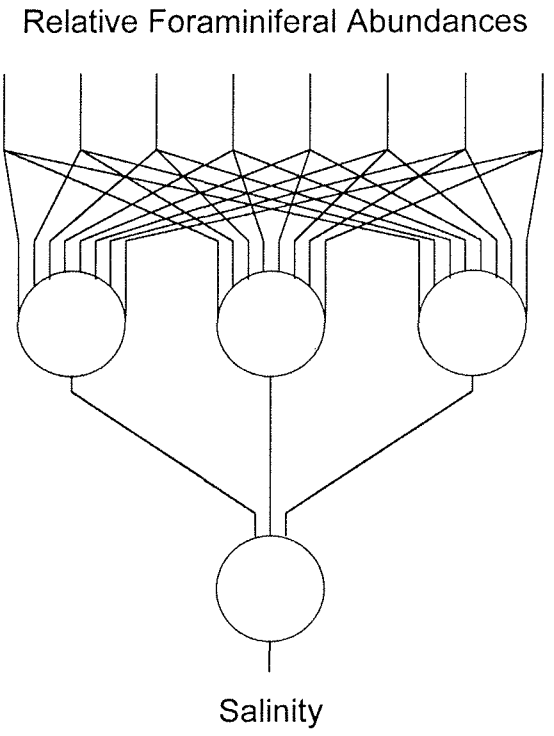

Fig. 4. Schematic structure of an example neural network. Input (top) are the relative abundances of the species in a foraminiferal assemblage (while eight are shown, we used 35 and 42), output (bottom) is the corresponding sea surface salinity. The number of neurons in the hidden layer (three in the example shown) determines the complexity of the mapping function.

was used and the correlation of the network output with the other independent half was checked. The results are shown in Fig. 5. Using either the odd or the even half of the data to train the model, we obtained a maximum goodness-of-fit for the complementary data set with two or three hidden neurons, respectively. Larger networks with four or more hidden neurons consequently have too many free parameters and reproduce in part the stochastic component of the data. For the application to downcore data, which is described below, we trained a network with three hidden neurons using the complete set of core-tops, but only the 35 species which were also counted in the downcore samples. This approach is illustrated and compared with MAT in Fig. 6.

A general problem of the backpropagation training of neural networks is the large computation expense. We required about a hundred thousand presentations of the reference data before convergence was achieved. The number of necessary training cycles increases dramatically with the size of the network. Some computation time could be saved if the steepest descent strategy which we use is replaced by a line-search algorithm. Nevertheless, if no special neurocomputer is available, the expenditure is much larger than for other methods, such as transfer functions or MAT.

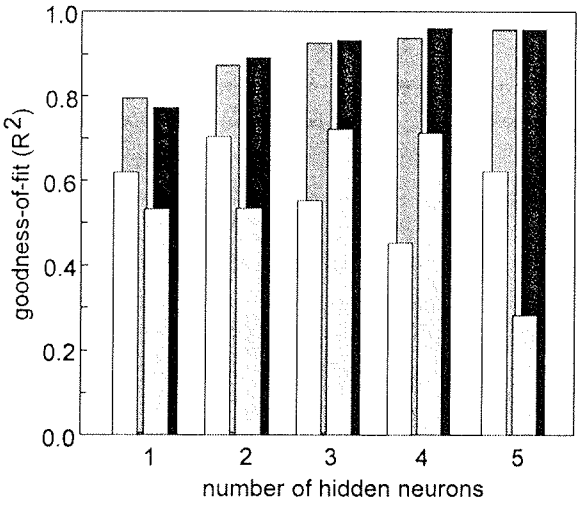

Fig. 5. Goodness-of-fit of regression between the salinities estimated with the neural network model and given by Levitus (1982) as a function of the number of hidden neurons. Foreground bars show the R^2 for the unused half of the data, background bars show the R^2 for the reference half itself. White and dark gray bars correspond to training with the odd half of the data, light gray and black to training with the even half.

Results

Core-top results

Results from the oxygen isotope method applied to core-tops are shown in Fig. 7 in a plot of the calculated salinities vs. annual mean salinities from Levitus et al. (1994). A linear regression has been performed. The goodness-of-fit (R^2) of the regression line is 0.59, and the standard deviation of the calculated salinities from the annual means is 1.22 ‰, which is considerably greater than those obtained by MAT and ANN. Fig. 8 illustrates the results obtained for the CLIMAP core-top data set by MAT and ANN as described above. The MAT and ANN methods produce comparable results. While the ANN shows a better goodness-of-fit than MAT for the even data set as reference, MAT gives higher R^2-values for the odd data set. MAT produces lower standard deviations in both cases (0.49 and 0.55 as opposed to 0.54 and 0.63 from ANN), but straight regression lines deviate from the expected curves by producing lower salinity values in the range of 36 to 37 ‰ and higher salinity values in the 34 to 35 ‰ range. The regression lines from the ANN output, on the other hand, lie quite near the 1:1 line.

When limited to intermediate values, however, all methods, the oxygen isotope method, MAT, and ANN show only weak correlations suggesting that the methods are able to distinguish between high, intermediate, and low salinities but do not represent more than a qualitative estimate.

Downcore-Results

The results from application of the various methods to core 1523-1 are shown in Fig. 9. After the correction of the oxygen isotope curve of *G. sacculifer* (Fig. 9A) for the temperature effect (MacMAT summer temperatures of Fig. 9B) the

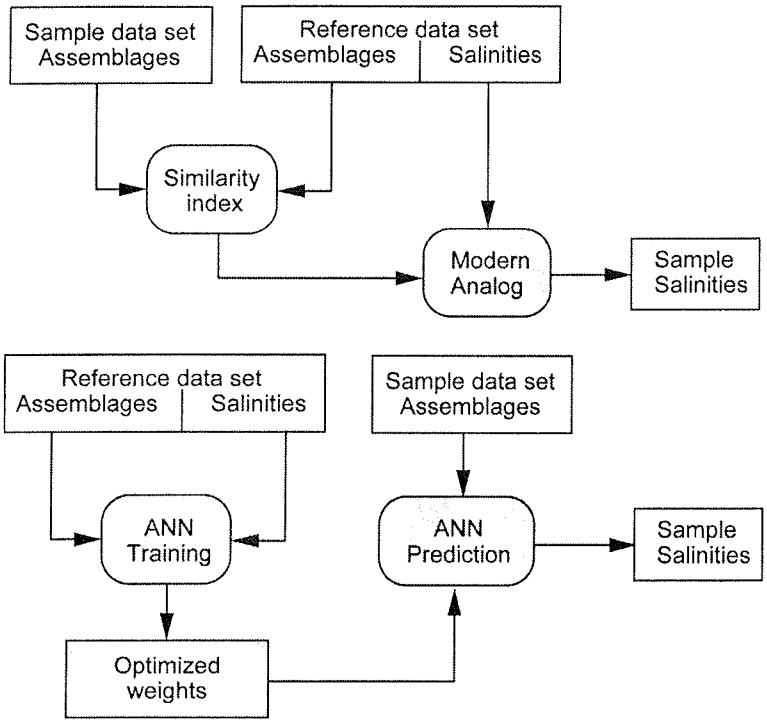

Fig. 6. Comparison of the Modern Analog Technique and the neural network approach. Top: Modern Analog Technique. The similarity of a sample assemblage to all reference assemblages is checked. Then the salinities corresponding to the most similar reference assemblages - the modern analogs - are weighted according to the similarity index and averaged. Bottom: Artificial Neural Networks. The neural network is trained with the assemblages and corresponding salinities of the reference data set. The optimized network weights are then used to estimate salinities from sample assemblages.

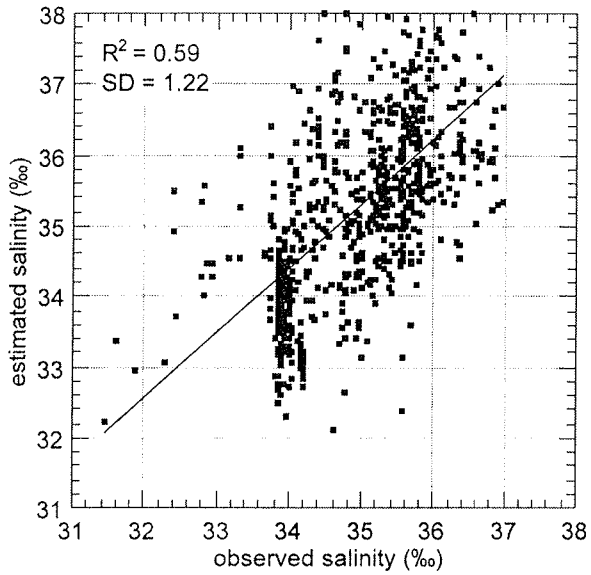

Fig. 7. Salinities obtained by the isotope method vs. annual mean salinities taken from the World Ocean Atlas (Levitus et al. 1994). 777 core-top oxygen isotope values taken from the literature were used. Independent temperatures were taken from WOA (Levitus and Boyer 1994). A regression line close to the expected is also shown. Standard deviation (SD) refers to deviations of estimated from observed salinities.

resulting $\delta^{18}O$ of sea-water (Fig. 9C) still shows pronounced glacial-interglacial changes (of up to 2 ‰). Fig. 9D illustrates the correction term for globally changing $\delta^{18}O_w$ in time as obtained from Labeyrie et al. (1987) and Vogelsang (1990). After inserting the $\delta^{18}O_w$ values in equation (7), paleosalinities are finally obtained as shown in curve „a" of Fig. 9E. Curve „b" is based on exactly the same data, except that the independent temperature estimates were calculated by the SIMMAX MAT (Hale and Pflaumann, this volume). The two downcore salinity estimates show similar glacial-interglacial patterns, with generally higher salinities in curve „b". This is due to very stable temperature estimates by SIMMAX except in stage 6. Additionally, both curves exibit considerable glacial-interglacial changes of about 2.5 ‰. At some points the salinity estimates of the two curves differ by as much as 1.5 ‰, which illustrates the sensitivity of the oxygen isotope method with regard to the used temperature estimate.

When today's $\delta^{18}O_w$-salinity relationship of the tropical western Atlantic is used (Fig. 10), the resulting salinity curve exibits even higher glacial-

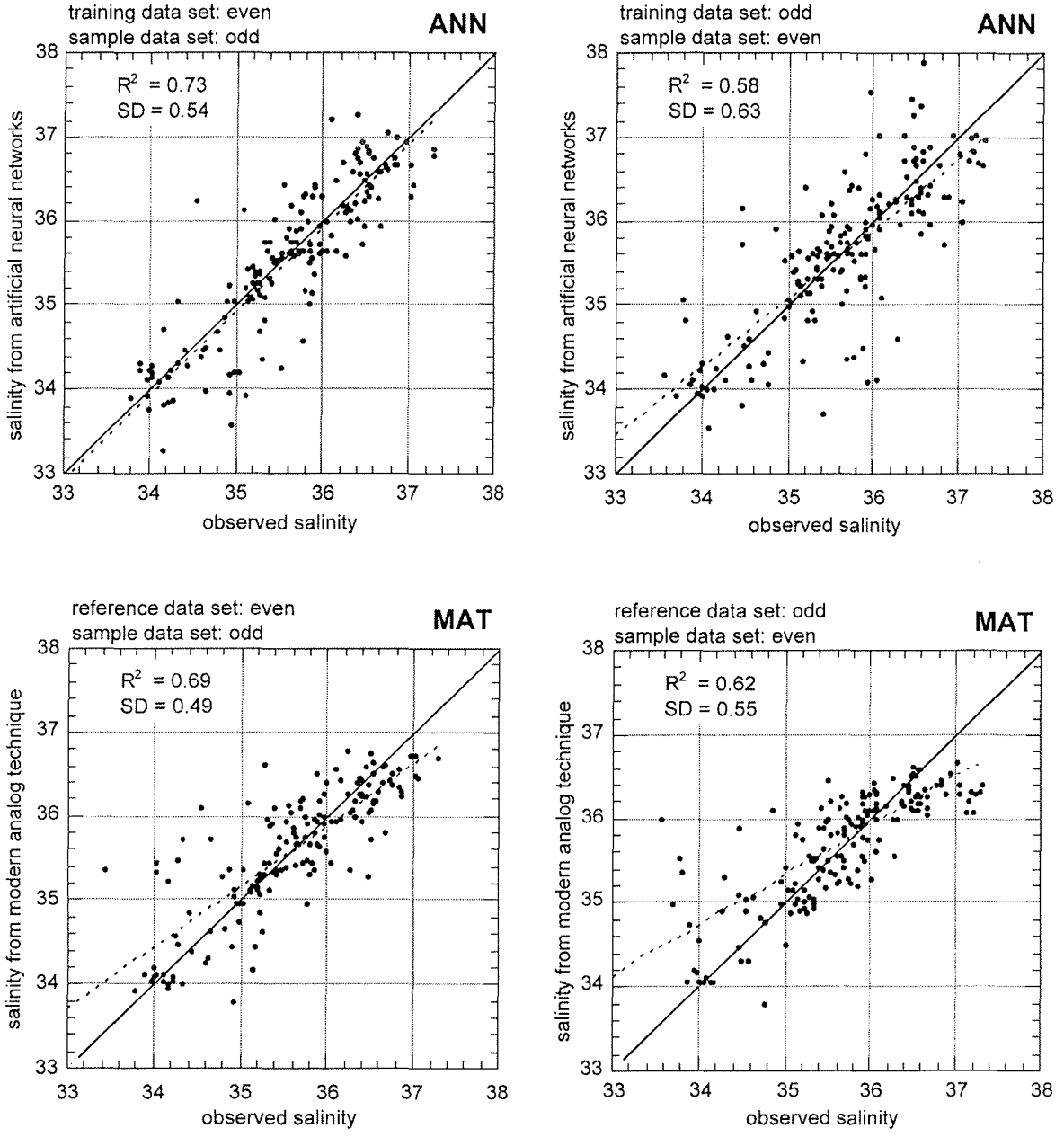

Fig. 8. Salinities obtained by ANN and MAT vs. annual mean salinities taken from Levitus (1982) for each half of the CLIMAP core-top data set. Stipled lines represent bivariate regression lines. Solid lines show expected 1:1 relationships. R^2 is goodness-of-fit of regression line. Standard deviation (SD) refers to deviations of estimated from observed salinities. MAT shows slightly lower standard deviations but straight regression lines deviate considerably from 1:1 relationship.

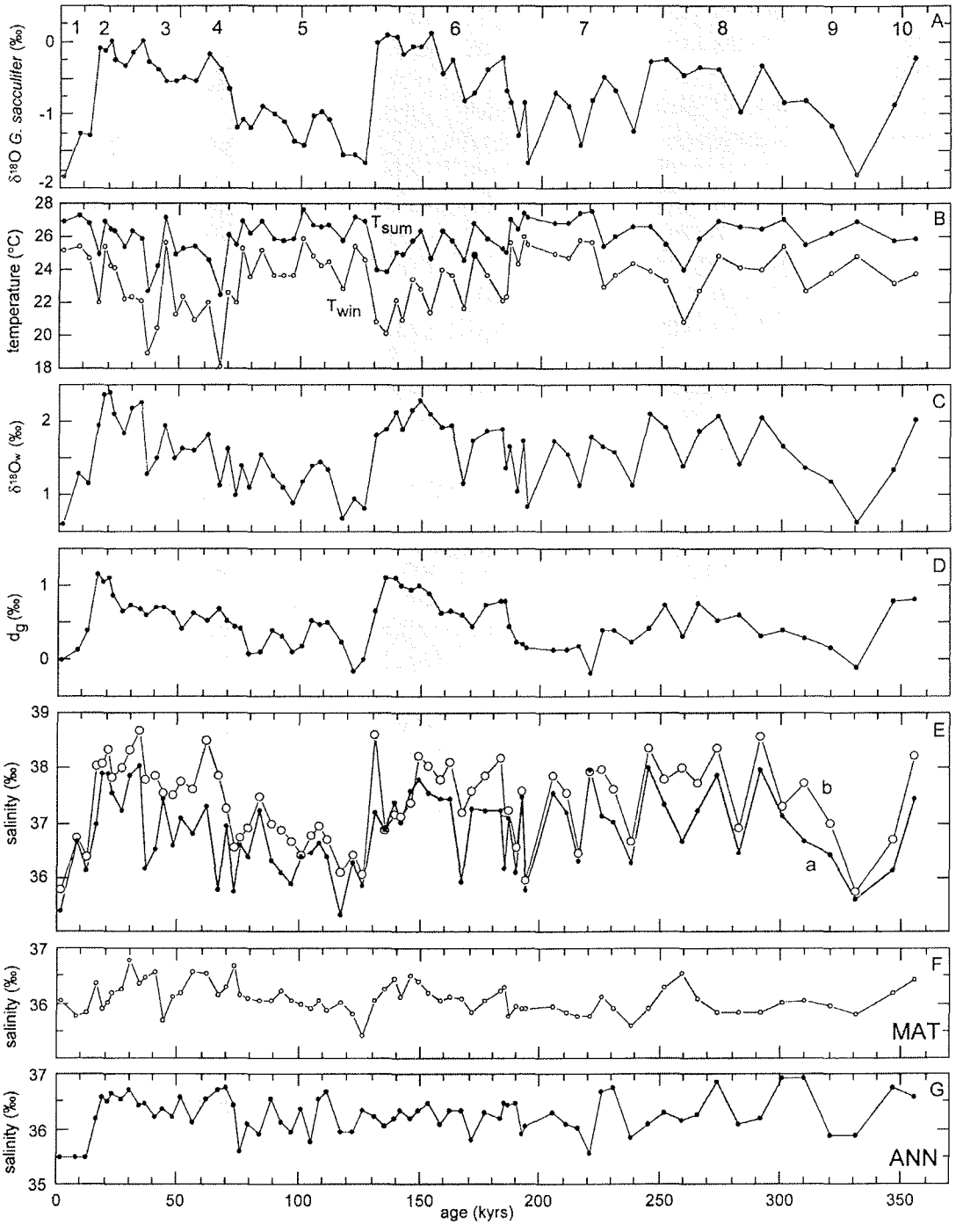

Fig. 9. Results for core GeoB 1523-1 vs. age of the core, isotopic stages are numbered at the top, glacials are indicated by light grey, interglacials by white. **A**: $\delta^{18}O$ for *G. sacculifer*, only every second data point of the original curve (Dürkoop et al. 1997) is shown; **B**: temperature estimates for summer and winter calculated by MacMAT; **C**: $\delta^{18}O$ of sea-water as reconstructed from $\delta^{18}O$ for *G. sacculifer* and MacMAT summer temperatures; **D**: global $\delta^{18}O_W$ curve **E**: Paleosalinity estimates from $\delta^{18}O_W$ (curve a), paleosalinities of curve b employed SIMMAX summer temperature estimates by Hale and Pflaumann (this volume); **F**: Annual mean paleosalinity estimates from MAT; G: Annual mean paleosalinity estimates from ANN.

interglacial changes of up to 6 ‰, illustrating the extreme sensitivity to the assumed $\delta^{18}O_w$-salinity relationship.

Fig. 9F shows the MAT-derived salinities which are qualitatively comparable to the isotope derived curves with low salinities in stages 1, 5, 7 and high salinities in stages 3, 4 and 6. The glacial-interglacial amplitude is about 1 ‰ as compared to at least 2.5 ‰ in the salinity estimates from the oxygen isotope record. ANN-derived salinities (Fig. 9G) also have a low amplitude of about 1.2 ‰ and show trends similar to the isotope-derived salinities in stages 1 through 4. From stage 6 downwards, no distinct features can be recognized. Salinities from MAT show an inverse correlation to MAT temperatures (Fig. 11), especially to winter temperatures (r = -0.66). This observation is discussed later in more detail.

Fig. 12 shows summer SST, winter SST, and salinities calculated by MAT as well as ANN-derived salinities for core RC 12-294. Salinities and temperatures derived from MAT are highly correlated (r = 0.95, Fig. 11) with generally higher temperatures and salinities in the interglacials and lower values in the glacials. Salinities from ANN parallel MAT-derived salinities most of the time with some deviations in stages 6 and 7, and a higher range of estimates.

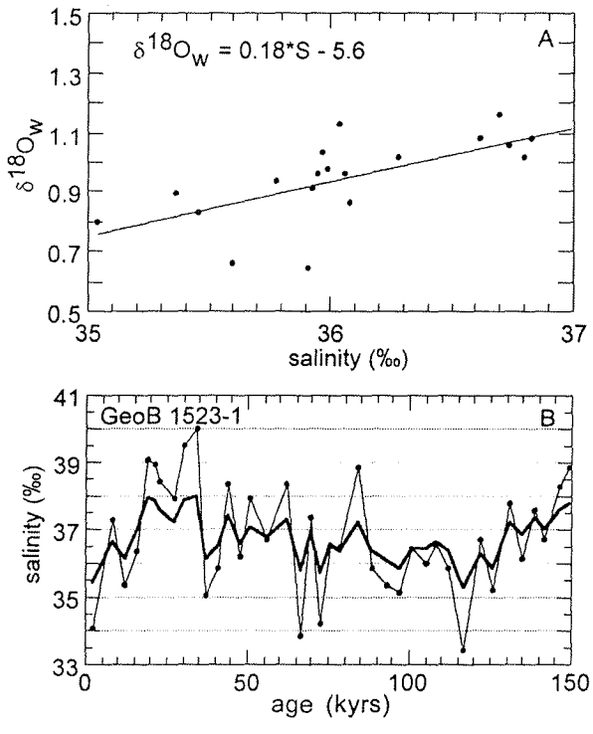

Fig.10. A: $\delta^{18}O$-salinity relationship for the equatorial western Atlantic based on unpublished GEOSECS data (H. Craig); **B:** salinity estimates for GeoB 1523-1 (first 150 kyrs) based on the above $\delta^{18}O$ -salinity relationship (thin line) as opposed to the estimates based on the $\delta^{18}O$ -salinity relationship for the entire Atlantic (thick line). The differences in the two curves illustrate the sensitivity of the isotope method to the slope of the assumed $\delta^{18}O$ -salinity relationship.

Errors associated with the methods and discussion of results

Interpretation of proxy data and their application to modelling studies require some estimation of the validity of the obtained values. Thus error analysis should be performed.

Errors associated with the calculation of paleosalinities using the oxygen isotope method may be introduced at several points:

One of the major factors of potential error is the uncertainty associated with the independent method of paleotemperature estimation. Temperatures can be obtained by calculations based either on foraminiferal count data (Transfer functions, MAT) or on alkenone analysis (Brassell et al. 1986; Prahl and Wakeham 1987).

Imbrie et al. (1973) reported an accuracy of about ±2°C for the 80% confidence interval for their transfer equation F3. Later, other workers obtained standard error values between ±1.4 and ±1°C (Kipp 1976; Hutson and Prell 1980; Prell 1985). Pflaumann et al. (1996) reported standard deviations as low as ±0.9 °C. Their estimation is based on core-top calculation of modern temperatures by a new MAT which employs an unusually large core-top sample data base (SIMMAX). SIMMAX differs from other MATs by a distance weighting procedure in which the selected most similar samples of the reference data set are weighted according to their inverse geographical distance from the subject sample. This approach might optimize the results for core-top calculations,

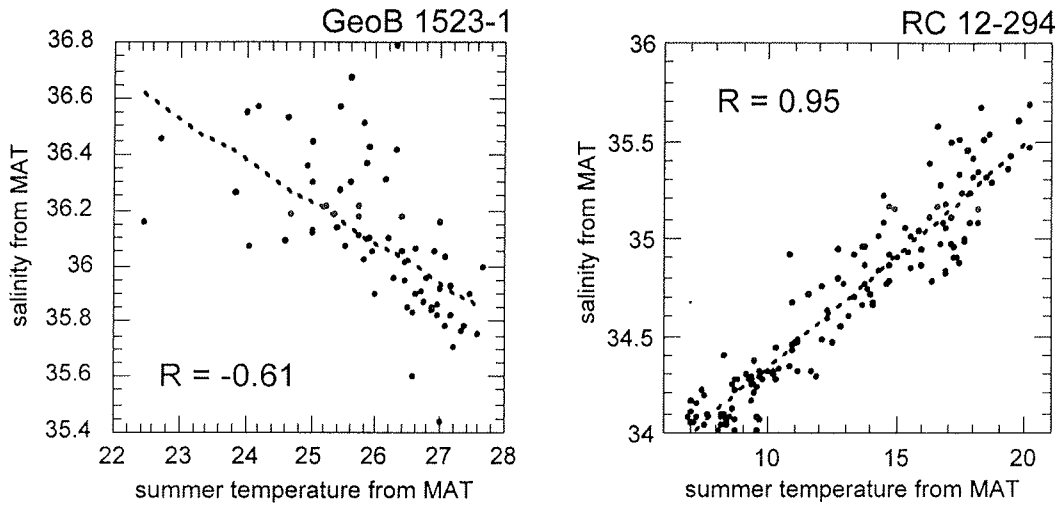

Fig.11. Plot of MAT-derived salinities vs. summer temperatures for cores GeoB 1523-1 and RC 12-294. Note inverse correlation for the tropical core and strong positive correlation for the subtropical core.

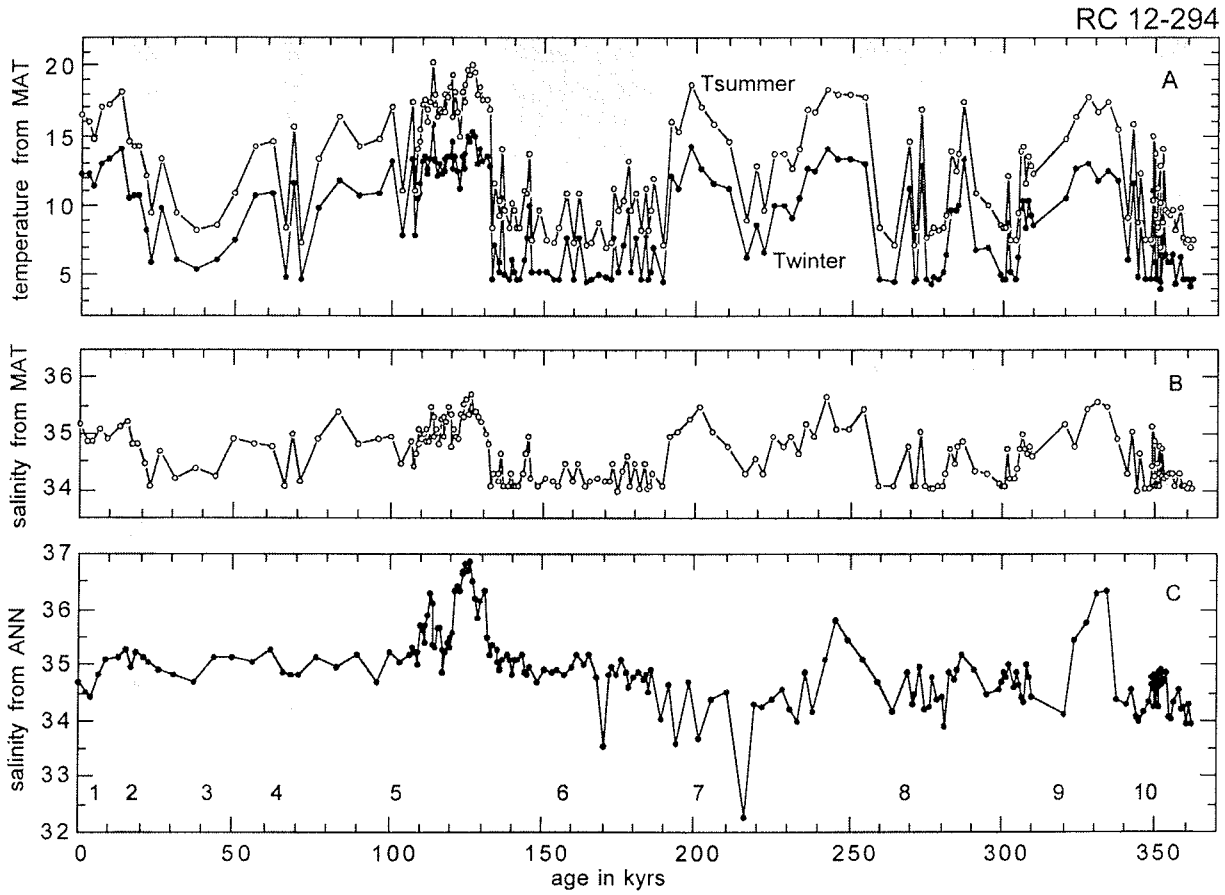

Fig. 12. Results for core RC 12-294 vs. age of the core, isotopic stages are numbered in the bottom, glacials are marked by light grey, interglacials by white. **A**: Summer and winter temperatures as determined by MacMAT; **B**: Annual mean salinities from MAT; **C**: Annual mean salinities from ANN.

but its applicability to paleoenvironments may be questioned. Thus errors of 1°C are considered to be a lower limit to the uncertainty associated with temperature estimates obtained from the species composition of foraminifera assemblages.

Reproducibility associated with the alkenone method is reported by Müller et al. (1994) to be ±0.3°C. This precision is based solely on duplicate and multiple measurements of the same sample and cannot be considered as the total error of the method. Rosell-Melé determined an errror of ±0.7°C (95% significance) for calibrations of core-top sediments not including deviations due to regression (Rosell-Melé et al. 1995). Sikes and Volkman (1993) calculated an error envelope of ± 0.6°C for their calibration. Application of calibrations to independent surface sediments and a subsequent comparison with measured temperatures has not yet been performed. Furthermore, problems may arise from unresolved questions concerning the alkenone production throughout the year. Prahl et al. (1995) found that temperature calculations on alkenones in sediments off the coast of Oregon show best fits with winter SST. Work in the east equatorial South Atlantic (Schneider et al. 1995) indicated that alkenone temperatures represent annual mean values. Thus, the downcore temperatures obtained might represent different times of the annual cycle. An error of 1°C for the alkenone method is assumed here and might be a realistic estimation (P. Müller, personal communication).

Vital effects account for the deviation of the measured foraminiferal $\delta^{18}O$ from the theoretically derived value based on the paleotemperature equation. Literature review shows different vital effects depending on species, material and location, a fact that introduces an additional error to the measured $\delta^{18}O_w$. Further uncertainty might be introduced by the basic problem of isotope analysis of planktonic foraminifera regarding the preference of a particular species for a certain temperature range (Mulitza et al. 1998). The errors associated with vital effects and temperature dependency of foraminifera are neglected here because they cannot be quantified yet. However, preliminary estimations show that they have the potential to add significant uncertainty to the reconstruction of the $\delta^{18}O_w$.

We quantified errors related to the independent temperature estimate and the analytical error of the measuring procedure of the foraminiferal $\delta^{18}O$. Assuming an analytical error of 0.07 ‰ in the determination of $\delta^{18}O_c$, an error of 1°C in the temperature reconstruction and ignoring further possible sources of error gives ± 0.22 ‰ for $\delta^{18}O_w$ at T = 25°C (Table 2). Propagation of errors in equation (7) yields a final error in salinity which depends on the slope of the $\delta^{18}O_w$ -salinity relationship. Error estimates of salinity for different values of „a" are presented in Table 2. It can be seen clearly that the lower the slope of the $\delta^{18}O_w$-salinity relationship is, the higher the associated error for the estimated salinity will become. This result is especially important in the evaluation of the use of isotope studies for paleosalinity reconstruction in the tropics, where slopes of the linear relationship might be as low as 0.08 (Fairbanks et al. 1992). Here, the insertion of $\delta^{18}O_w$ into equation (7) acts as an amplifier of the possible error in temperature. In the case of core GeoB 1523-1, we used a $\delta^{18}O_w$-salinity relationship of the entire modern Atlantic with a slope of 0.48 which resulted in a final error of at least ± 0.5 ‰. An equation derived for today's tropical Atlantic (slope of 0.18) yielded unrealistically high salinities of up to 40 ‰; a lower limit of the error estimates was 1.2 ‰.

T	$\Delta\delta^{18}O$	ΔS	ΔS	ΔS
(°C)	(‰) for ΔT=1°C	(‰) a=0.5	(‰) a=0.3	(‰) a=0.18
0	0.29	0.58	0.97	1.61
5	0.27	0.54	0.90	1.50
10	0.26	0.51	0.85	1.42
15	0.24	0.48	0.81	1.34
20	0.23	0.46	0.77	1.28
25	0.22	0.44	0.74	1.23
28	0.22	0.43	0.72	1.20

Table 2. Error estimates for the oxygen isotope method assuming an error of ±1°C in the temperature estimate for different temperatures and varying slopes (a) of the $\delta^{18}O$-salinity relationship. $\Delta\delta^{18}O$ denotes the error in the $\delta^{18}O$ of sea-water, ΔS denotes the error in the final salinity estimate.

The still large amplitudes in salinities achieved with a $\delta^{18}O_w$-salinity relationship of the entire Atlantic might be explained in two ways. On the one hand there is evidence for drier conditions in the nearby Amazon basin during the last glacial maximum (LGM) (Clapperton 1993) which has been confirmed by atmospheric circulation models (Jouzel et al. 1994; Lorenz et al. 1996). On the other hand, modelling the transport of oxygen isotopes in the atmosphere shows among the highest positive deviations in $\delta^{18}O$ of precipitation at the LGM (Jouzel et al. 1994; Hoffmann 1995), i.e., an additional local shift of the $\delta^{18}O_w$-salinity relationship towards higher $\delta^{18}O$ during glacials (Wolff et al. in press) might be appropriate and would lower the overall paleosalinity amplitudes.

The errors associated with paleosalinities reconstructed by MAT and ANN can easily be expressed in terms of our core-top results. Standard deviations of estimated to measured salinities range between 0.49 and 0.63 ‰. Salinities in the cores GeoB 1523-1 and RC 12-294 show amplitudes around 1 ‰ which approximately equals the global glacial-interglacial salinity change due to the storage of water in the polar ice caps. At first glance this seems to be more promising than salinity estimates obtained from oxygen isotopes, especially in the tropical regions. On the other hand, we saw an inverse correlation between salinity and temperature estimates from MAT at site GeoB 1523 in the ITCZ and a strong positive correlation between the two parameters in core RC 12-294 (Fig. 11). Especially at the latter location we would not expect salinity decreases during glacials because salinities were generally increasing in glacial stages and the core is still located north of a possible meltwater influence (Niebler 1995). The two features shown in Fig. 11 can be explained in terms of today's prevalent temperature-salinity dependency. In general, salinity is positively correlated with temperature, with the exception of the tropical regions near the ITCZ (Fig. 13). Here, increasing temperatures near the ITCZ are accompanied by decreasing salinities which are due to higher precipitation. Thus, salinities reconstructed from MAT are mainly based on the temperature sensitivity of foraminiferal assemblages. That is, the modern analogs found for, e.g., glacial samples „move" along the temperature-salinity relationship toward lower SSTs leading to higher salinities in the tropical core GeoB 1523-1, and to lower salinities in core RC 12-294. Since the temperature-salinity relationship is probably not constant over time and the reference data set does not include temperature-salinity combinations that appear possible for the glacials (no-analog situation: e.g. higher salinities and lower temperatures in the subtropics, see Fig. 13), the results have to be questioned. The same is true for salinities from ANN, because there are no fundamental differences to MAT results in core RC 12-294.

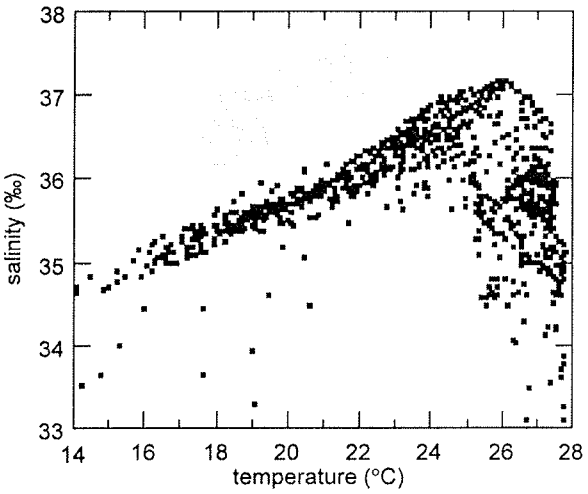

Fig. 13. Annual mean salinities vs. annual mean temperatures for about 1000 locations in the South Atlantic (south of 10°N and north of 40°S) as taken from the World Ocean Atlas (Levitus and Boyer 1994; Levitus et al. 1994). Locations were selected in regular distances. Note the positive correlation between temperature and salinity in the subtropical regions. For temperatures above 26°C salinities decrease with increasing temperatures, which is particularily true for the tropical regions near the ITCZ. Grey field marks combinations of T and S which are possible for glacial conditions, but are not represented in today's Atlantic Ocean.

Conclusions

Salinity reconstruction using oxygen isotope ratios of foraminiferal calcite tests are constrained by uncertainties in the method of temperature determination, the assumed $\delta^{18}O_w$-salinity relationships, and possible vital effects. Knowledge of the ecological preferences of planktonic foraminifera is still incomplete, accounting for additional error. Error analysis shows low signal-to-noise ratios suggesting that paleosalinity reconstructions on the basis of oxygen isotopes are still rather qualitative. Accuracies needed for modelling purposes (± 0.1 ‰, Herterich, personal communication) will be extremely difficult to achieve. Future work is necessary to improve:

1. the accuracy of the independent temperature reconstruction methods,
2. the knowledge of the preferred environmental conditions of planktonic foraminifera and possible vital effects, and
3. the knowledge of the regional $\delta^{18}O_w$-salinity relationships in the present and past and their determining factors.

Work on temperature sensitivities of some planktonic foraminifera and the effect on the oxygen isotope record has shown that isotope analysis of three species has the potential to provide direct estimates of the $\delta^{18}O_w$ without the need for independent temperature methods (Mulitza et al. 1998). Also, modelling might improve our understanding of the $\delta^{18}O_w$-salinity relationship (Herterich, personal communication).

Salinity reconstructions methods using foraminiferal species data do not provide reliable results when they are applied to downcore data, since foraminiferal species abundance patterns seem to be primarily controlled by temperature. Therefore salinity estimates are governed by the present day temperature-salinity relationships.

Future work should focus on the ecological constraints of foraminiferal assemblages. Transfer functions and MAT isolate single environmental parameters and try to reconstruct these disregarding other factors. ANN's have the potential of combining several parameters and may impart a better insight into the dependency of faunal assemblages on the environment's properties as a whole. It may then become possible to improve the determination of temperature, salinity, nutrient concentration, and other paleoceanographically important parameters by using foraminiferal count data.

Acknowledgements

We would like to thank R.Sieger who provided the program MacMAT. We thank B.Meyer-Schack and M.Segl for performing the stable isotope analysis. Reviews by R. Zahn and W.H. Berger significantly improved the manuscript.
This is contribution No. 179 of Sonderforschungsbereich 261 at University of Bremen.

References:

Barnett TP, Hasselmann K (1979) Techniques of linear prediction with application to oceanic and atmospheric fields in the tropical Pacific. Revs Geophys Space Phys 17: 949-968

Berger WH, Gardner JV (1975) On the determination of Pleistocene temperatures from planktonic foraminifera. J Foram Res 5: 102-113

Berger WH (1981) Paleoceanography: the deep-sea record. In: Emiliani C (ed), The Sea, Vol. 7, Wiley-Interscience, New York, pp 1437-1519

Bijma J, Faber WW, Hemleben C (1990) Temperature and salinity limits for growth and survival of some planktonic foraminifers in laboratory cultures. J Foram Res 20: 95-116

Brassell SC, Eglington G, Pflaumann U, Sarnthein M (1986) Molecular stratigraphy: a new tool for climatic assessment. Nature 320: 129 -133

Broecker WS (1986) Oxygen isotope constraints on surface ocean temperatures. Quaternary Res 26: 2-14

Broecker WS (1989) The salinity contrast between the Atlantic and Pacific oceans during glacial time. Paleoceanography 4: 207-212

Broecker WS, Denton GH (1989) The role of ocean-atmoshere reorganisations in glacial cycles. Geochim Cosmochim Acta 53: 2465-2501

Broecker WS (1990) Salinity history of the Northern Atlantic during the last deglaciation. Paleoceanography 5: 459-467

Charles CD, Fairbanks RG (1990) Glacial to interglacial changes in the isotopic gradients of southern ocean surface waters. In: Bleil U, Thiede J (eds) Geological History of the Polar Oceans: Arctic versus Antarctic. Kluwer Academic, Dordrecht, pp 519-538

Clapperton CM (1993) Nature of environmental changes in South America at the last glacial maximum. Paleogeogr, Paleoclimatol, Paleoecol 101: 189-208

CLIMAP Project Members (1976) The Surface of the Ice-Age Earth. Science 191: 1131-1137

CLIMAP Project Members (1981) Seasonal reconstructions of the Earth's surface at the last glacial maximum. GSA Map and Chart Ser MC-36: 1-18

Craig H, Gordon LI (1965) Deuterium and oxygen-18 variations in the ocean and marine atmosphere. In: Tongiorgi E (eds) Stable isotopes in oceanic studies and paleotemperatures, Spoleto, Consiglio Naz Delle Ricerche, Laboratorio di Geol Nuc, Pisa, pp 9-130

Cullen JL (1981) Microfossil evidence for changing salinity patterns in the Bay of Bengal over the last 20,000 years. Palaeogeogr, Palaeoclimatol, Palaeoecol 35: 315-356

Curry WB, Thunell RC, Honjo S (1983) Seasonal changes in the isotopic composition of planktonic foraminifera collected in Panama basin sediment traps. Earth and Plan Sc Lett 64: 33-43

Deuser WG, Ross EH, Hemleben C, Spindler M (1981) Seasonal changes in species composition, numbers, mass, size, and isotopic composition of planktonic foraminifera settling into the deep Sargasso Sea. Palaeogeogr, Palaeoclimatol, Palaeoecol 33: 103-127

Deuser WG, Ross EH (1989) Seasonally abundant planktonic foraminifera of the Sargasso Sea: Succession, deep-water fluxes, isotopic compositions and paleoceanographic implications. J Foram Res 19: 268-293

Duplessy JC (1981) Oxygen-18 enrichment of planktonic foraminifera due to gametogenic calcification below the euphotic zone. Science 213: 1247-1250

Duplessy JC (1982) Glacial to interglacial contrasts in the northern Indian Ocean. Nature 295: 494-498

Duplessy JC, Labeyrie L, Arnold M, Paterne M, Duprat J, van Weering TCE (1992) Changes in surface salinity of the North Atlantic Ocean during the last deglaciation. Nature 358: 485-488

Duplessy JC, Labeyrie L, Juillet-Leclerc A, Maitre F, Duprat J, Sarnthein M (1991) Surface salinity reconstruction of the North Atlantic Ocean during the last glacial maximum. Oceanol Acta 14: 311-324

Duplessy JC, Labeyrie L, Paterne M, Hovine S, Fichefet T, Duprat J, Labracherie M (1996) High Latitude Water Sources During the Last Glacial Maximum and the Intensity of the Global Oceanic Circulation. In: Wefer G, Berger WH, Siedler G, Webb DJ (eds) The South Atlantic - Present and Past Circulation. Springer, Berlin, pp 445-460

Durazzi JT (1981) Stable-isotope studies of planktonic foraminifera in North Atlantic core-tops. Palaeogeogr, Palaeoclimatol, Palaeoecol 33: 157-172

Dürkoop A, Hale W, Mulitza S, Pätzold J, Wefer G (1997) Late Quaternary variations of sea surface salinity and temperature in the western tropical Atlantic: Evidence from $\delta^{18}O$ of *Globigerinoides sacculifer*. Paleoceanography 12: 764-772

Emiliani C (1955) Pleistocene temperatures. J Geol 63: 538-578

Emiliani C (1971) Depth habitats of growth stages of pelagic foraminifera. Science 173: 1122-1124

Epstein S, Buchsbaum R, Lowenstam HA, Urey HC (1953) Revised carbonate-water isotopic temperature scale. Bull Geol Soc Am 64: 1315-1325

Epstein S, Mayeda T (1953) Variation of O-18 content of waters from natural sources. Geochim Cosmochim Acta 4: 213-224

Erez J, Luz B (1983) Experimental paleotemperature equation for planktonic foraminifera. Geochim Cosmochim Acta 47: 1025-1031

Fairbanks RG, Charles CD, Wright JD (1992) Origin of global meltwater pulses. In: Taylor RE (ed) Radiocarbon after four decades. Springer, New York, pp 473-500

Ferronsky VI, Brezgunov VS (1989) Stable isotopes and ocean dynamics. In: Fritz P, Fontes JC (eds) The marine environment. Elsevier, Amsterdam, pp 1-27

Fillon RH, Williams DF (1984) Dynamics of meltwater discharge from Northern hemisphere ice sheets during the last deglaciation. Nature 310: 674-677

GEOSECS Executive Committee (1987) GEOSECS Atlantic, Pacific, and Indian Ocean Expeditions, Shorebased Data and Graphics. In: Ostlund HG, Craig H, Broecker WS, Spencer D (eds) International decade of ocean exploration. National Science Foundation, Washington D.C., pp 1-200

Giraudeau J (1992) Coccolith Paleotemperature and Paleosalinity estimates in the Caribbean Sea for the middle-late Pleistocene (DSDP Leg 68 - Hole 502B). Memorie di Scienze Geologiche 43: 375-387

Grobe H, Mackensen A, Hubberten H-W, Spiess V, Fütterer DK (1990) Stable isotope record and late Quaternary sedimentation rates at the Antarctic continental margin. In: Bleil U, Thiede J (eds) Geological History of the polar Oceans: Arctic versus Antarctic. Kluwer Academic, Dordrecht, pp 539-572

Hecht AD, Savin SM (1972) Phenotypic variation and oxygen isotope ratios in recent planktonic foraminifera. J Foram Res 2: 55-67

Hoffmann G (1995) Stabile Wasserisotope im allgemeinen Zirkulationsmodell ECHAM. Max-Planck-Institut für

Meteorologie, Examensarbeit 27, pp 1-96
Hut G (1987) Stable isotope reference samples for geochemical and hydrological investigations. Consultant Group Meeting IAEA, Report to the Director General, Vienna, pp 1-42
Hutson WH (1980) The Agulhas Current during the late Pleistocene: Analysis of Modern Faunal Analogs. Science 207: 64-66
Hutson WH, Prell WL (1980) A paleoecological transfer function, FI-2, for Indian Ocean planktonic foraminifera. J Paleontol 54: 381-399
Imbrie J, Kipp NG (1971) A new micropaleontological method for quantitative paleoclimatology: application to a Late Pleistocene Caribbean core. In: Turekian KK (ed) Late Cenocoic glacial ages. Yale University Press, New Haven, pp 71-181
Imbrie J, McIntyre A, Mix A (1989) Oceanic response to orbital forcing in the late Quaternary: Observational and experimental strategies. In: Berger A (ed) Climate and Geo- Sciences. Kluwer Academic, Dordrecht, pp 121-164
Imbrie J, van Donk J, Kipp NG (1973) Paleoclimatic investigation of a late Pleistocene Caribean deep-sea core: Comparison of isotopic and faunal methods. Quaternary Res 3: 10-38
Jouzel J, Koster RD, Suozzo RJ, Russell GL (1994) Stable water isotope behaviour during the last glacial maximum: A general circulation model analysis. J Geophy Res 99: 25791-25801
Kallel N, Paterne M, Labeyrie L, Duplessy J, Arnold M (1997) Temperature and salinity records of the Tyrrhenian Sea during the last 18,000 years. Palaeogeogr, Palaeoclimatol, Palaeoecol 135: 97-108
Keigwin LD (1996) The Little Ice Age and Medieval Warm period in the Sargasso Sea. Science 274: 1504-1508
Kipp NG (1976) New transfer function for estimating past sea-surface conditions from sea-bed distribution of planktonic foraminiferal assemblages in the North Atlantic. In: Cline RM, Hays JD (eds) Investigation of late Quaternary Paleoceanography and Paleoclimatology. Geol Soc Am Mem, pp 3-41
Labeyrie LD, Duplessy JC, Blanc PL (1987) Variations in mode of formation and temperature of oceanic deep waters over the past 125,000 years. Nature 327: 477-482
Lautenschlager M, Mikolajewicz U, Maier-Reimer E, Heinze C (1992) Application of ocean models for the interpretation of AGCM experiments on the climate of the last glacial maximum. Paleoceanography 7: 769-782
Le J (1993) Paleotemperature estimation methods: Sensitivity test on two western equatorial Pacific cores. Quat Sc Rev 11: 801-820
Levitus S (1982) Climatological Atlas of the World Ocean. NOAA Professional Paper 13: 1-173
Levitus S, Boyer TP (1994) World Ocean Atlas 1994, Volume 4: Temperature, pp 1-117
Levitus S, Burgett R, Boyer TP (1994) World Ocean Atlas 1994, Volume 3: Salinity, pp 1-99
Lorenz S, Grieger B, Helbig P, Herterich K (1996) Investigating the sensitivity of the Atmospheric General Circulation Model ECHAM 3 to paleoclimatic boundary conditions. Geol Rundschau 85: 513-524.
Maslin MA, Shackleton NJ, Pflaumann U (1995) Surface water temperature, salinity, and density changes in the northeast Atlantic during the last 45,000 years: Heinrich events, deep water formation, and climatic rebounds. Paleoceanography 10: 527-544
Melles M (1991) Paläozeanographie im Spätquartär am Kontinentalrand des südlichen Weddellmeeres, Antarktis. Ber Polarforsch 81, pp 1-190
Merlivat L, Jouzel J (1979) Global climatic interpretation of the deuterium-oxygen-18 relationship for precipitation. J Geophys Res 84: 5029-5033
Mix AC (1987) The oxygen-isotope record of glaciation. In: Ruddiman WF, Wright HEJ (eds) North America and adjacent oceans during the last deglaciation. Geol. Soc. Am., Boulder, Colorado, pp 111-135
Mix AC, Ruddiman WF (1985) Structure and timing of the last deglaciation: Oxygen isotope evidence. Quat Sc Rev 4: 59-108
Mulitza S (1994) Spätquartäre Variationen der oberflächennahen Hydrographie im westlichen äquatorialen Atlantik. Berichte, Fachbereich Geowissenschaften, Univ. Bremen 57, pp 1-97
Mulitza S, Wolff T, Pätzold J, Hale W, Wefer G (1998) Temperature sensitivity of planktonic foraminifera and its influence on the oxygen isotope record. Marine Micropaleontology, 33:223-240
Müller PJ, Schneider R, Ruhland G (1994) Late Quaternary pCO_2 variations in the Angola Current: Evidence from organic carbon $\delta^{13}C$ and alkenone temperatures. In: Zahn R, Pedersen TF, Kaminski MA, Labeyrie L (eds) Carbon cycling in the glacial ocean: Constraints on the ocean's role in global change. Springer, Heidelberg, pp 343-366
Naidu PD (1993) Distribution patterns of recent planktonic foraminifera in surface sediments of the western continental margin of India. Mar Geol 110: 403-418
Niebler HS (1995) Reconstruction of palaeo-environmental parameters using stable isotopes and faunal as-

semblages of planktonic foraminifera in the South Atlantic Ocean. Berichte zur Polarforschung 167, pp 1-198

Overpeck JT, Webb III T, Prentice, IC (1985) Quantitative interpretation of fossil pollen spectra: Dissimilarity coefficients and the method of modern analogs. Quaternary Res 23: 87-108

Pflaumann U (1985) Transfer function '134/6' - a new approach to estimate sea-surface temperatures and salinities of the eastern North Atlantic from the planktonic foraminifers in the sediments. METEOR Forschungs-Ergebnisse C39: 37-71

Pflaumann U, Duprat J, Pujol C, Labeyrie LD (1996) SIMMAX: A modern analog technique to deduce Atlantic sea surface temperatures from planktonic foraminifera in deep-sea sediments. Paleoceanography 11: 15-35

Pierre C, Vergnaud-Grazzini C, Faugeres JC (1991) Oxygen and carbon stable isotope tracers of the water masses in the Central Brazil Basin. Deep Sea Res 38: 597-606

Prahl FG, Pisias N, Sparrow MA, Sabin A (1995) Assessment of sea-surface temperature at 42 °N in the California Current over the last 30,000 years. Paleoceanography 10: 763-773

Prahl FG, Wakeham SG (1987) Calibration of unsaturation patterns in long-chain ketone compositions for paleotemperature assessment. Nature 330: 367-369

Prell WL (1985) The stability of low-latitude sea surface temperatures: An evaluation of the CLIMAP reconstruction with emphasis on the positive SST anomalies. Dep. of Energy, Washington D.C., pp 1-60

Rosell-Melé A, Egington G, Pflaumann U, Sarnthein M (1995) Atlantic core-top calibration of the Uk'_{37} index as a sea-surface paleotemperature indicator. Geochim Cosmochim Acta 59: 3099-3107

Rostek F, Ruhland G, Bassinot FC, Müller PJ, Labeyrie LD, Lancelot Y, Bard E (1993) Reconstructing sea surface temperature and salinity using $\delta^{18}O$ and alkenone records. Nature 364: 319-321

Rumelhart DG, Hinton GE, Williams RJ (1986) Learning representations by back-propagating errors. Nature 323: 533-536

Savin SM, Douglas RG (1973) Stable isotope and magnesium geochemistry of recent planktonic foraminifera from the South Pacific. Geol Soc of Am Bull 84: 2327-2342

Schneider RR, Müller PJ, Ruhland G (1995) Late Quaternary surface circulation in the east equatorial South Atlantic: Evidence from alkenone sea surface temperatures. Paleoceanography 10: 197-219

Schulz HD und Fahrtteilnehmer (1991) Bericht und Ergebnisse der Meteor-Fahrt M16/2, Recife - Belem (28.04 - 21.05.1991). Berichte, Fachbereich Geowissenschaften, Univ Bremen 19, pp 1-149

Showers WJ, Margolis SV (1985) Evidence for a tropical freshwater spike during the last glacial/interglacial transition in the Venezuela Basin: $\delta^{18}O$ and $\delta^{13}C$ of calcareous plankton. Mar Geol 68: 145-165

Sikes EL, Volkman, JK (1993) Calibration of alkenone unsaturation ratios (Uk'_{37}) for paleotemperature estimation in cold polar waters. Geochim Cosmochim Acta 57: 1883-1889

Sikes EL, Keigwin LD (1996) A reexamination of the Northeast Atlantic sea surface temperature and salinity over the last 16 kyr. Paleoceanography 11: 327-342

Spero HJ, Williams DF (1990) Evidence for seasonal low-salinity surface waters in the Gulf of Mexico over the last 16,000 years. Paleoceanography 5: 963-975

Spero HJ, Bijma J, Lea DW, Bemis BE (1997) Effect of sea-water carbonate concentration on foraminiferal carbon and oxygen isotopes. Nature 390: 497-500

Sverdrup HU, Johnson MW, Fleming RH (1942) The oceans: their physics, chemistry and general biology. Prentice-Hall, Englewood Cliffs, pp 1-1087

Urey HC (1947) The thermodynamic properties of isotopic substances. Jour Chem Soc 562-581

Van Campo E, Duplessy JC, Prell WL, Barratt N, Sabatier R (1990) Comparison of terrestrial and marine temperature estimates for the past 135 kyr off southeast Africa: a test for GCM simulations of paleoclimate. Nature 348: 209-212

Vetshteyn VY, Malyuk GA, Rusanov VP (1974) Oxygen-18 distribution in the central arctic basin. Oceanology 14: 514-519

Vincent E, Shackleton NJ (1980) Agulhas Current temperature distribution delineated by oxygen isotope analysis of foraminifera in surface sediments. Cushman Foundation Special Publication 19: 89-95

Vincent E, Berger WH (1981) Planktonic foraminifera and their use in paleoceanography. In: Emiliani C (ed) The Sea. Wiley-Interscience, New York, pp 1025-1119

Vogelsang E (1990) Paläo-Ozeanographie des Europäischen Nordmeeres an Hand stabiler Kohlenstoff- und Sauerstoffisotope. Ber Sonderforschungsbereich 313, Univ Kiel 23, pp 1-136

Wang L, Sarnthein M, Duplessy JC, Erlenkeuser H, Jung S, Pflaumann U (1995) Paleo sea surface salinities in the low-latitude Atlantic: The $\delta^{18}O$ record of *Globigerinoides ruber* (white). Paleoceanography 10: 749-761

Washington WM, Parkinson CL (1986) An Introduction to Three-Dimensional Climate Modelling. University

Science Books, Mill Valley, pp 1-422

Wefer G, Berger WH (1991) Isotope paleontology: growth and composition of extant calcareous species. Mar Geol 100: 207-248

Wefer G, Berger WH, Bickert T, Donner B, Fischer G, Kemle-von Mücke S, Meinecke G, Müller PJ, Mulitza S, Niebler HS, Pätzold J, Schmidt H, Schneider RR, Segl M (1996) Late Quaternary Surface Circulation of the South Atlantic: The Stable Isotope Record and Implications for Heat Transport and Productivity. In: Wefer G, Berger WH, Siedler G, Webb DJ (eds) The South Atlantic - Present and Past Circulation. Springer, Berlin, pp 461-502

Widrow B, Lehr MA (1990) 30 years of adaptive neural networks: Perceptron, madaline, and back-propagation. Proc IEEE 78: 1415-1441

Williams DF, Bé AWH, Fairbanks RG (1979) Seasonal oxygen isotopic variations in living planktonic foraminifera off Bermuda. Science 206: 447-449

Williams DF, Healy-Williams N (1980) Oxygen isotopic-hydrographic relationships among recent planktonic foraminifera from the Indian ocean. Nature 283: 848-852

Wolff T, Mulitza S, Arz H, Pätzold J, Wefer G (1998) Oxygen isotopes versus CLIMAP (18 ka) temperatures: A comparison from the tropical Atlantic. Geology 26: 675-678

Wu G, Berger WH (1989) Planktonic foraminifera: Differential dissolution and the Quaternary stable isotope record in the west equatorial Pacific. Paleoceanography 4: 181-198

Chapter 3

Temperature sensitivity of planktic foraminifera and its influence on the oxygen isotope record

Stefan Mulitza
Tobias Wolff
Jürgen Pätzold
Walter Hale
Gerold Wefer

Marine Micropaleontology 33 (1998), 223-240

ELSEVIER

Marine Micropaleontology 33 (1998) 223–240

MARINE MICROPALEONTOLOGY

Temperature sensitivity of planktic foraminifera and its influence on the oxygen isotope record

Stefan Mulitza *, Tobias Wolff, Jürgen Pätzold, Walter Hale, Gerold Wefer

Universität Bremen, Fachbereich Geowissenschaften, Klagenfurter Strasse, Postfach 330 440, D-28334 Bremen, Germany

Received 24 April 1997; accepted 23 September 1997

Abstract

We used oxygen isotope measurements from Holocene surface sediments to infer optimum temperature and temperature sensitivity of the planktic foraminiferal species *Globigerinoides ruber* (pink) and *Globigerinoides sacculifer*. The (isotopic) optimum temperature of *G. ruber* (pink) is close to 27°C. *G. sacculifer* seems to have optimum vital conditions around 22°C and is less temperature sensitive than *G. ruber* (pink). Our estimations of optimum temperature and temperature sensitivity are in good accordance with laboratory and field investigations. Two simple experiments show that the temperature sensitivity of planktic foraminifera, determined from oxygen isotopes, can influence phase and amplitude of oxygen isotope records, if the temperature distribution at the sea surface changes through time. To use this distortion for paleoceanography, we suggest to derive an 'isotopic transfer function' which allows the calculation of average temperature, temperature variability and the isotopic composition of seawater if the oxygen-isotope differences between at least three species are known.

Keywords: planktic foraminifera; Holocene; Atlantic Ocean; oxygen isotopes

1. Introduction

Planktic foraminifera are one of the most commonly used tools in paleoceanography. This fossil group yields two main types of signal. First, the abundance patterns of planktic foraminiferal species in the sediment can be used to reconstruct paleoenvironmental parameters such as SST with statistical methods (e.g. Imbrie and Kipp, 1971). Second, the oxygen-isotope ratios of these planktic foraminifera serve as a proxy for the isotopic composition and temperature of seawater in which the tests grew (Emiliani, 1954). On the one hand, this dual signal from planktic foraminifera is of advantage, because it theoretically permits removal of the temperature effect from the $\delta^{18}O$ signal which would, in turn, allow an estimation of the isotopic composition of the ambient seawater (e.g. Duplessy et al., 1991). On the other hand, the temperature dependency of the foraminiferal flux bears problems for the interpretation of stable isotopes, if the species used for $\delta^{18}O$ is also temperature sensitive. That is, we do not know exactly which seasonal 'temperature mixture' is represented by the mean $\delta^{18}O$ of a foraminiferal population in the sediment. Mix (1987) has shown in a simple model that the temperature recorded by a temperature-sensitive foraminiferal population

* Corresponding author. Tel: +49-421-2187110. Fax: +49 421 2183116. E-mail: smul@palmod.uni-bremen.de

0377-8398/98/$19.00
PII S0377-8398(97)00040-6

should depend on both the seasonal distribution of temperatures at the sea surface and the temperature sensitivity of the considered species. He stated that "...the recording of $\delta^{18}O$ by a foraminiferal population must be better understood before temperature and ice volume can be isolated". Nevertheless, in the past, some efforts have been undertaken to remove temperature from North Atlantic oxygen-isotope records (Duplessy et al., 1991; Wang et al., 1995). These authors overcome the above mentioned problems with so-called 'core-top calibrations'. Such studies assume that the present relationships between oxygen-isotope composition, ecology, and hydrography were the same in the past and that they can be adjusted to a certain season or temperature range. In this paper, we propose to test whether this assumption is justified with regard to two tropical species. We have compiled a data set of core-top $\delta^{18}O$ values for *G. sacculifer* and *G. ruber* (pink) covering different hydrographic regimes. We will use this data set to evaluate: (1) the influence of the SST distribution and temperature sensitivity on the mean oxygen-isotope temperature recorded by a foraminiferal population in the sediment, (2) the consequences for the late Quaternary isotope record and (3) the possible application for paleoceanography.

2. Mix's model of temperature-dependent flux

The model employed here was described by Mix (1987). It illustrates the influence of the temperature distribution on the mean isotope-temperature signal of a temperature-sensitive foraminiferal population. Fig. 1 shows the basic assumptions of the model. The frequency distribution of temperatures at any site in the ocean is assumed to be normally distributed with a mean temperature (T_m) and some variability expressed by the standard deviation (σ_W), a large σ_W representing a large temperature variability and vice versa. The foraminiferal flux is also assumed to be normally distributed with an optimum temperature (T_{opt}) and a standard deviation (σ_F) which describes the temperature sensitivity of a given species. A high σ_F indicates a large temperature tolerance. The overall flux at a certain temperature [$SF(T)$] is then:

$$SF(T) = F(T) \cdot W(T) \quad (1)$$

$F(T)$ is the frequency of the foraminiferal species

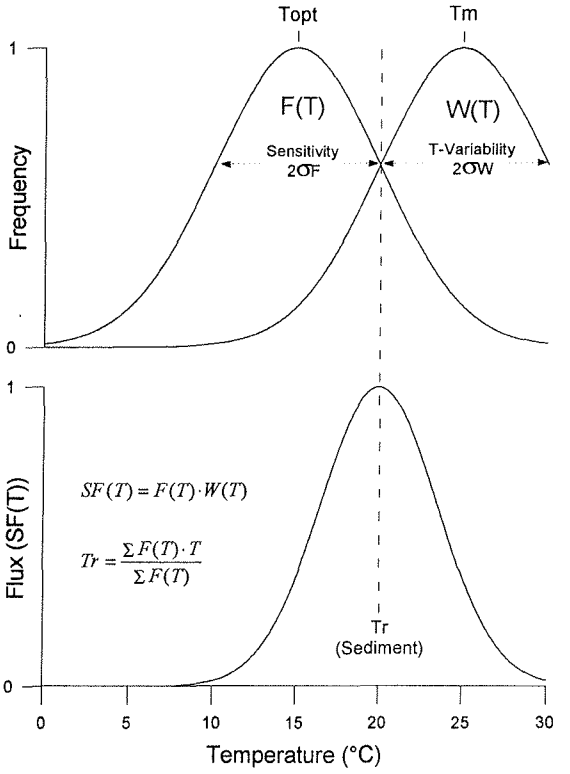

Fig. 1. Model of Mix (1987) showing how the temperature preference [F(T)] of a species and the distribution of temperatures [$W(T)$] determines the recorded temperature, e.g. by oxygen-isotope ratios of a species. The lower panel shows the resulting flux [$SF(T)$] as a function of temperature. The recorded temperature (T_r) is the flux-weighted mean of all temperatures at the site. σ_W is the variability of temperatures and σ_F the temperature sensitivity of the foraminiferal species, expressed as standard deviation.

and $W(T)$ is the frequency of sea surface temperatures. The total flux (F_t) is then:

$$F_t = \int SF(T)\,dt \quad (2)$$

The temperature sensed by the mean population (T_r) is the flux-weighted mean of the temperature distribution:

$$T_r = \frac{1}{F_t} \cdot \left(\int SF(T) \cdot T\,dt \right) \quad (3)$$

With this model, Mix (1987) has elegantly demonstrated how the temperature distribution and individual ecological requirements of a species can influence the temperature recorded in the sediment. For the two normal distributions $F(T)$ and $W(T)$

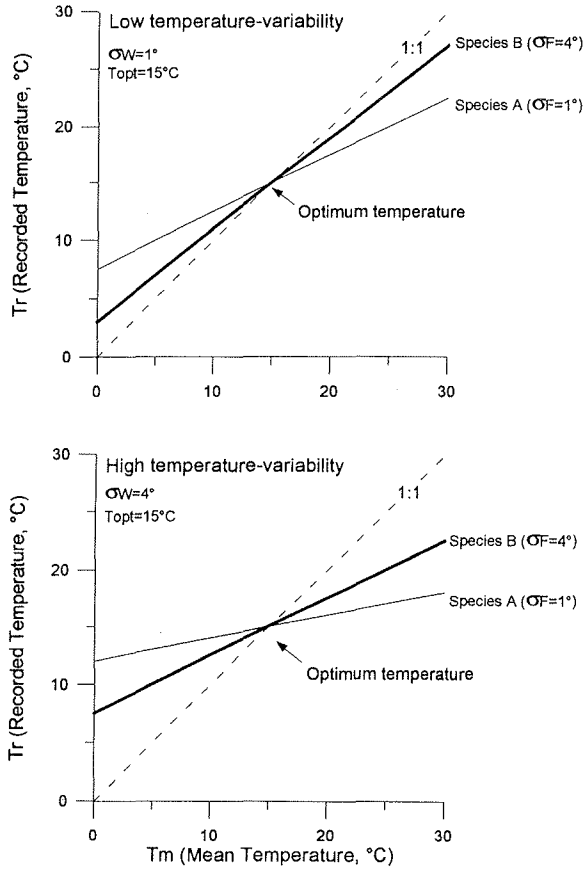

Fig. 2. Outputs from the model shown in Fig. 1, demonstrating the effect of temperature sensitivity and temperature distribution on the recorded temperature of a foraminiferal species. *Species A* is very temperature sensitive. It largely underestimates the change of temperatures. *Species B* is relatively temperature tolerant, recording temperatures close to the annual mean. The upper panel illustrates a situation of low temperature variability (low σ_W). Greater σ_W, as shown in the lower panel, increases the effect of temperature sensitivity.

(Fig. 1), T_r and T_m are linearly related. We can simplify Eq. 3 to:

$$T_r = T_{opt} \cdot \frac{\sigma_W}{\sigma_W + \sigma_F} + T_m \cdot \frac{\sigma_F}{\sigma_W + \sigma_F} \quad (4)$$

Fig. 2 compares model outputs of two theoretical species having the same optimum temperatures but different temperature tolerances. Species A is very temperature-sensitive ($\sigma_F = 1$°C), whereas species B has a comparably large temperature tolerance ($\sigma_F = 4$°C). Assuming a constant temperature variability ($\sigma_W = 1$°C) a temperature change is largely underestimated by species A. This species tends to calcify in the warmer season if the mean temperature is lower than the optimum temperature. By contrast, the flux of species B changes only little with temperature and it records temperatures close to the annual mean. A situation with higher SST variability is simulated in the lower panel ($\sigma_W = 4$°C). The underestimation of the average temperature change is greater because the larger temperature variability allows larger flux close to the optimum temperature.

3. Data and strategy

Is the model of Mix a suitable approximation to reality? If so, we should expect a large influence of the temperature distribution at the sea surface on the temperature recorded in the sediment. As demonstrated in the previous section, both the optimum temperature and the temperature sensitivity influence the flux pattern of planktic foraminifera. Thus, our strategy to estimate temperature sensitivity and optimum temperature should be to compare only samples from stations with similar temperature variabilities (σ_W), but different mean temperatures (T_m). Expressed in terms of Mix's model, this could be regarded as moving the normal distribution of temperatures over the normal distribution of the foraminiferal abundance. If the foraminiferal flux is really temperature dependent, the difference between the mean and the recorded temperature should change with mean temperature. A plot of T_r vs. T_m should theoretically allow the estimation of T_{opt} and σ_F. T_{opt} should be where T_r equals T_m, and σ_F can be calculated via the slope (S) of T_r vs. T_m using the formula:

$$\sigma_F = \sigma_W \cdot \frac{S}{1 - S} \quad (5)$$

This approach, however, contains some inherent difficulties. We do not know the exact temperature variability (σ_W), nor do we know the exact depth habitat of a species for the time period in which a surface sediment sample is deposited. Results from the water column, however, show that the species examined here are predominantly limited to the surface waters. The timing and magnitude of the seasonal mixed-layer temperature cycle is very well represented by oxygen isotope values of

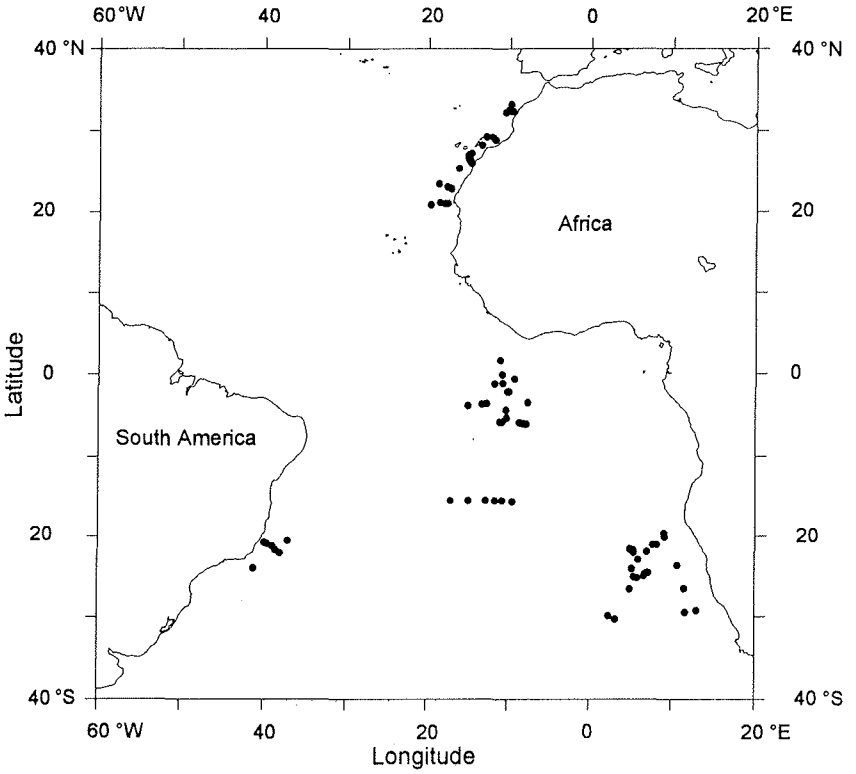

Fig. 3. Locations of surface sediment samples used in this study.

planktic foraminifera from sediment traps and plankton tows (Williams et al., 1981; Deuser and Ross, 1989). Therefore, it is realistic to assume that oxygen isotope values represent a mixture of surface water conditions. The temperature range is known for approximately the last 50 years. We must first assume that this time period is representative of the time period of deposition of our surface sediment samples. The next problem is how to estimate temperature variability from these data. An estimation of the temperature variability can be made based on the maximum seasonal temperature difference. Low seasonality stations should have a low temperature variability and vice versa. Although no two positions in the ocean have exactly the same seasonality, similar stations could be found within a certain range, e.g. ±1°C. We compiled a data set of core-top $\delta^{18}O$ values from subtropical and tropical Atlantic core tops (Fig. 3; Ganssen, 1983; Mulitza, 1994). These stations were sorted according to the seasonality of the overlying surface water based on the maximum seasonal difference of the monthly temperature estimates compiled by Levitus and Boyer (1994). Most stations were found to have a seasonal range between 3.13 and 5.29°C. We included oxygen isotope data from surface samples deposited within this temperature range for testing Mix's model. The isotope data are listed in Tables 1 and 2 together with the hydrographic data used for the calculations. Isotopic temperatures (the 'recorded temperature') have been calculated using the paleotemperature equation (Epstein et al., 1953) as modified by Shackleton (1974):

$$T_r = 16.9 - 4.38 \cdot (\delta_c - \delta_w) + 0.1 \cdot (\delta_c - \delta_w)^2 \quad (6)$$

with δ_c being the foraminiferal isotope value and δ_w being the isotope value of the ambient seawater. δ_w was estimated from salinity using the regression equation illustrated in Fig. 4 (Broecker, 1986; Craig, unpubl. data). There are some hints that the slope of the δ_w/salinity relationship is somewhat lower in the tropics (Craig and Gordon, 1965; Fairbanks et al., 1992). However, calculations using different re-

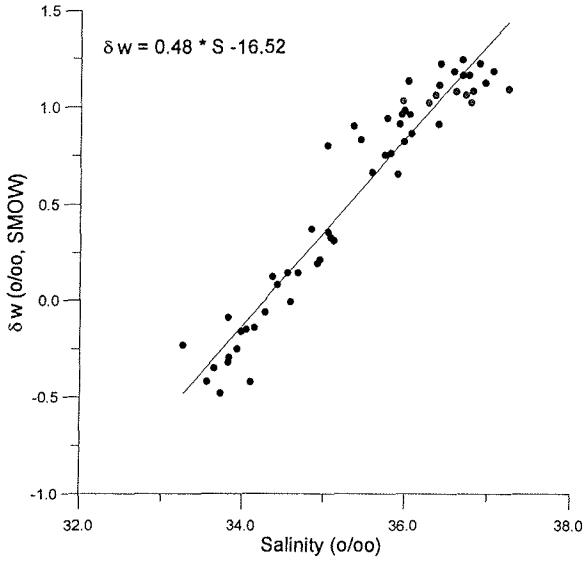

Fig. 4. Relationship between $\delta^{18}O$ of seawater and salinity for Atlantic surface waters (GEOSECS, Craig, unpubl. data). The regression was used to calculate $\delta^{18}O$ of seawater from salinity (Levitus et al., 1994) at the sites examined in this study.

gressions for the tropics and the subtropics did not result in a significant change of the isotope temperature with respect to the equation in Fig. 4. As we do not know the season of calcification or the apparent δ_w, we selected only stations with seasonal variations of δ_w ($\Delta\delta_w$ in Tables 1 and 2, calculated from monthly salinities of Levitus et al., 1994) smaller than ±0.2‰. This ensures an error of less than one degree due to seasonal variations of δ_w for the calculation of isotope temperatures. Fig. 5 shows scatter-plots of calculated isotope temperatures against the annual mean temperatures of Levitus and Boyer (1994). Neither species follows the 1:1 relationship. The isotope temperatures of *G. ruber* (pink) are extremely distorted towards the summer at colder temperatures and scatter around the annual mean at warmer temperatures (Fig. 5B). The values of *G. sacculifer* deviate to the summer at colder temperatures and to the colder season at warmer temperatures (Fig. 5A). The change of temperature in the surface water seems to be underestimated by both species. Our explanation for this pattern points to the temperature sensitivity of the species: in the colder subtropical regions the flux of both species is greatest in summer (warm season) because the

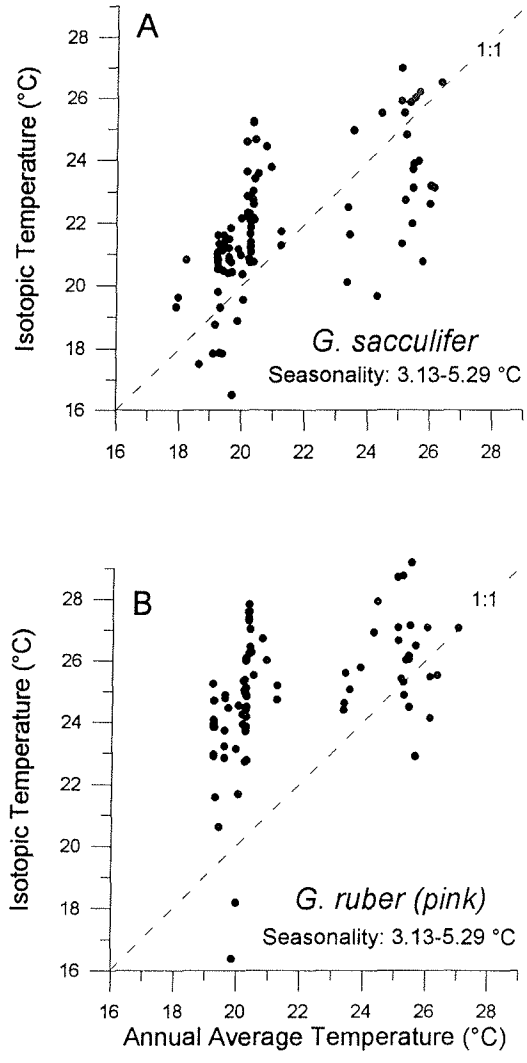

Fig. 5. (A) Calculated isotopic temperatures for *G. sacculifer* vs. annual average temperatures. (B) as (A) for *G. ruber* (pink). We used samples in the seasonality range from 3.13 to 5.29°C.

annual mean temperature is below the optimum temperature of the species. The reverse response occurs in the warm tropical realm: *G. ruber* (pink) scatters around the annual mean (it is close to its 'optimum temperature'), whereas *G. sacculifer* seems to prefer the colder season. Unfortunately, the deviations from the annual mean at a certain temperature are not very uniform. This can be explained by several mechanisms blurring the isotope record in the sediment. First of all, older shells could have been mixed

Table 1
Oxygen-isotope values of *G. sacculifer* from core-top samples and hydrographic data used in this study

Core	Ref.	Lat. (°)	Long. (°)	$\delta^{18}O$ (‰, PDB)	T_{an} (°C)	ΔT (°C)	δ_w (‰, SMOW)	$\Delta\delta_w$ (‰, SMOW)	T_{iso} (°C)
12301-5	G	27.05	−15.05	−0.09	20.24	3.81	1.04	0.09	20.8
12302-3	G	26.00	−14.67	−0.41	20.25	3.66	1.03	0.09	22.2
12303-3	G	26.20	−14.79	−0.39	20.25	3.67	1.03	0.09	22.1
12304-3	G	26.23	−14.81	−0.39	20.25	3.67	1.03	0.09	22.1
12305-2	G	26.29	−14.86	−0.30	20.25	3.67	1.03	0.09	21.7
12306-2	G	26.49	−14.93	−0.20	20.26	3.68	1.04	0.09	21.2
12307-3	G	26.41	−14.96	−0.24	20.26	3.68	1.04	0.09	21.4
12308-2	G	26.65	−15.05	−0.34	20.25	3.78	1.04	0.09	21.9
12309-1	G	26.84	−15.11	−0.21	20.25	3.79	1.04	0.09	21.3
12310-1	G	23.50	−18.72	−0.75	20.90	3.67	1.04	0.04	23.8
12317-1	G	22.86	−17.15	−0.80	20.13	3.26	0.96	0.05	23.6
12322-2	G	22.90	−17.16	−1.00	20.14	3.26	0.96	0.05	24.6
12323-1	G	22.91	−17.19	−0.52	20.15	3.26	0.96	0.05	22.3
12324-1	G	22.92	−17.22	−0.63	20.15	3.26	0.96	0.05	22.9
12327-2	G	23.13	−17.74	−0.75	20.50	3.49	1.00	0.04	23.6
12328-1	G	21.15	−18.57	−1.03	20.75	4.55	0.90	0.07	24.4
13526-4	G	21.00	−17.62	−1.24	20.33	4.69	0.85	0.08	25.2
13527-1	G	20.99	−17.66	−0.72	20.34	4.70	0.85	0.08	22.8
13528-2	G	20.99	−17.68	−1.25	20.34	4.70	0.85	0.08	25.2
13529-1	G	20.99	−17.70	−0.78	20.34	4.70	0.85	0.08	23.0
13530-1	G	21.00	−17.73	−0.69	20.35	4.69	0.85	0.08	22.6
13532-2	G	20.98	−17.88	−0.86	20.38	4.69	0.85	0.08	23.4
13533-1	G	20.99	−18.03	−1.12	20.41	4.67	0.86	0.07	24.7
13534-1	G	21.02	−17.88	−0.58	20.38	4.66	0.85	0.08	22.1
13536-2	G	21.00	−17.58	−0.60	20.33	4.69	0.85	0.08	22.2
15626-1	G	29.22	−12.84	−0.10	19.69	3.95	0.96	0.12	20.4
15627-2	G	29.17	−12.09	−0.36	19.58	3.86	0.93	0.14	21.5
15628-4	G	29.08	−11.98	−0.22	19.58	3.85	0.93	0.14	20.8
15629-1	G	29.06	−11.95	−0.24	19.58	3.85	0.93	0.14	20.9
15630-1	G	29.04	−11.92	−0.22	19.57	3.85	0.93	0.14	20.8
15631-1	G	29.02	−11.90	−0.30	19.58	3.85	0.93	0.14	21.2
15632-1	G	28.91	−11.70	−0.13	19.57	3.84	0.93	0.14	20.4
15634-1	G	28.26	−13.40	−0.20	19.95	3.89	0.98	0.13	21.0
15635-2	G	27.20	−14.66	−0.44	20.22	3.82	1.04	0.10	22.3
15638-2	G	32.21	−10.45	−0.28	19.26	4.80	0.98	0.11	21.3
15639-1	G	32.49	−10.11	−0.12	19.25	4.85	0.98	0.11	20.6
15640-1	G	32.45	−9.96	−0.17	19.24	4.85	0.98	0.11	20.8
15641-2	G	32.43	−9.87	−0.15	19.23	4.87	0.98	0.11	20.7
15642-1	G	32.41	−9.85	−0.34	19.23	4.87	0.98	0.11	21.6
15643-1	G	32.40	−9.82	0.06	19.23	4.87	0.98	0.11	19.8
15644-1	G	32.40	−9.81	−0.17	19.23	4.88	0.98	0.11	20.8
15645-1	G	32.39	−9.80	−0.10	19.23	4.88	0.98	0.11	20.5
15646-1	G	32.38	−9.78	−0.17	19.22	4.88	0.98	0.11	20.8
15647-1	G	32.38	−9.77	−0.22	19.22	4.88	0.98	0.11	21.1
15648-1	G	32.37	−9.65	−0.21	19.21	4.92	0.98	0.11	21.0
15651-4	G	33.19	−9.83	−0.18	19.21	5.24	0.99	0.12	20.9
16012-3	G	25.40	−16.25	−0.09	20.36	3.45	1.05	0.08	20.8
GeoB 1027-2	M	−19.66	9.14	−0.16	19.15	5.27	0.53	0.12	18.8
GeoB 1028-4	M	−20.10	9.18	0.04	19.09	5.21	0.52	0.13	17.8
GeoB 1029-1	M	−21.06	8.23	−0.28	19.30	5.01	0.53	0.14	19.3
GeoB 1030-3	M	−21.08	7.78	0.06	19.39	5.00	0.54	0.14	17.8
GeoB 1031-1	M	−21.89	7.10	−0.82	19.62	4.98	0.55	0.14	21.8

Table 1 (continued)

Core	Ref.	Lat. (°)	Long. (°)	$\delta^{18}O$ (‰, PDB)	T_{an} (°C)	ΔT (°C)	δ_w (‰, SMOW)	$\Delta\delta_w$ (‰, SMOW)	T_{iso} (°C)
GeoB 1032-2	M	−22.91	6.03	−0.64	19.86	5.05	0.58	0.13	21.2
GeoB 1033-2	M	−22.05	5.54	−0.28	20.02	4.98	0.59	0.14	19.5
GeoB 1034-1	M	−21.72	5.43	−0.55	20.21	4.95	0.61	0.14	20.9
GeoB 1035-3	M	−21.60	5.03	−0.59	20.27	4.95	0.61	0.14	21.1
GeoB 1041-1	M	−3.48	−7.59	−1.01	25.18	5.06	0.56	0.36	22.8
GeoB 1048-2	M	20.91	−19.72	−0.32	21.21	4.61	0.93	0.09	21.3
GeoB 1104-5	M	−1.16	−10.71	−0.59	25.76	5.13	0.55	0.41	20.8
GeoB 1108-6	M	−2.17	−9.87	−0.85	25.42	5.22	0.56	0.40	22.0
GeoB 1111-5	M	−5.84	−8.65	−1.57	25.32	4.45	0.67	0.32	25.9
GeoB 1112-3	M	−5.77	−10.75	−1.16	25.60	4.24	0.67	0.27	24.0
GeoB 1113-7	M	−5.75	−11.04	−1.63	25.63	4.22	0.67	0.26	26.2
GeoB 1114-3	M	−5.28	−10.20	−1.18	25.45	4.60	0.63	0.31	23.9
GeoB 1115-4	M	−3.56	−12.58	−1.05	26.01	5.19	0.62	0.34	23.2
GeoB 1117-3	M	−3.82	−14.90	−1.72	26.35	4.53	0.65	0.26	26.5
GeoB 1121-1	M	20.84	−19.74	−0.41	21.22	4.64	0.93	0.09	21.7
GeoB 1203-2	M	−26.55	5.02	−0.44	20.01	5.29	0.61	0.12	20.4
GeoB 1207-2	M	−24.60	6.86	−0.71	19.41	5.13	0.56	0.10	21.4
GeoB 1208-1	M	−24.49	7.11	−0.66	19.38	5.09	0.55	0.11	21.1
GeoB 1209-1	M	−24.51	7.28	0.06	19.31	5.11	0.55	0.11	17.9
GeoB 1216-2	M	−24.93	6.79	−0.51	19.40	5.14	0.56	0.10	20.5
GeoB 1217-1	M	−24.95	6.73	−0.76	19.41	5.14	0.56	0.10	21.6
GeoB 1218-1	M	−25.17	5.92	−0.55	19.66	5.17	0.58	0.10	20.7
GeoB 1220-2	M	−24.03	5.31	−0.84	19.96	5.12	0.60	0.11	22.2
GeoB 1402-7	M	−2.18	−10.07	−1.09	25.44	5.23	0.56	0.40	23.1
GeoB 1403-2	M	−1.20	−11.71	−0.97	26.00	5.18	0.57	0.42	22.6
GeoB 1404-8	M	−0.08	−10.78	−1.16	26.11	4.76	0.49	0.38	23.2
GeoB 1407-8	M	−4.33	−10.25	−1.18	25.42	4.99	0.60	0.32	23.7
GeoB 1413-1	M	−15.68	−9.46	0.04	23.34	4.24	1.03	0.10	20.1
GeoB 1414-2	M	−15.53	−10.73	−0.46	23.36	4.23	1.05	0.10	22.5
GeoB 1415-1	M	−15.53	−11.58	−0.26	23.41	4.11	1.07	0.11	21.6
GeoB 1417-1	M	−15.53	−12.71	−0.95	23.53	4.09	1.09	0.11	25.0
GeoB 1419-1	M	−15.54	−17.07	0.29	24.29	3.13	1.18	0.10	19.7
GeoB 1709-3	M	−23.59	10.76	−0.39	17.90	4.28	0.42	0.13	19.3
GeoB 1715-1	M	−26.48	11.64	−0.45	17.95	4.04	0.43	0.12	19.6
GeoB 1721-4	M	−29.18	13.09	−0.69	18.22	4.38	0.46	0.09	20.8
GeoB 1722-3	M	−29.45	11.75	0.10	18.64	4.55	0.51	0.09	17.5
GeoB 1726-1	M	−30.27	3.26	0.45	19.71	4.89	0.63	0.17	16.5
GeoB 1728-3	M	−29.84	2.41	−0.07	19.86	5.06	0.64	0.19	18.9
GeoB 2102-1	M	−23.98	−41.12	−1.11	24.40	4.19	1.05	0.15	25.5
GeoB 2118-1	M	−22.09	−38.02	−0.99	25.14	4.38	1.17	0.16	25.5
GeoB 2119-2	M	−21.73	−38.55	−0.10	25.08	4.23	1.17	0.15	21.3
GeoB 2124-1	M	−20.96	−39.56	−1.30	25.06	3.98	1.16	0.18	27.0
GeoB 2125-2	M	−20.82	−39.86	−1.08	25.05	3.97	1.16	0.18	25.9
GeoB 2126-1	M	−21.27	−38.93	−0.83	25.21	4.07	1.18	0.18	24.8
GeoB 2130-1	M	−20.62	−37.10	−1.04	25.48	4.19	1.22	0.22	26.0

δ_w values were calculated with the regression equation in Fig. 4 and corrected to PDB by subtracting 0.27‰ (Hut, 1987). Annual temperatures (T_{an}) were interpolated from Levitus and Boyer (1994). Isotope temperatures were calculated with the equation of Shackleton (1974). G = Ganssen (1983); M = Mulitza (1994).

Table 2
As in Table 1 for *G. ruber* pink

Core	Ref.	Lat. (°)	Long. (°)	$\delta^{18}O$ (‰, PDB)	T_{an} (°C)	ΔT (°C)	δ_w (‰, SMOW)	$\Delta\delta_w$ (‰, SMOW)	T_{iso} (°C)
12301-5	G	27.05	−15.05	−0.88	20.24	3.81	1.04	0.09	24.4
12302-3	G	26.00	−14.67	−0.74	20.25	3.66	1.03	0.09	23.7
12303-3	G	26.20	−14.79	−1.24	20.25	3.67	1.03	0.09	26.1
12304-3	G	26.23	−14.81	−1.04	20.25	3.67	1.03	0.09	25.1
12305-2	G	26.29	−14.86	−1.22	20.25	3.67	1.03	0.09	26.0
12306-2	G	26.49	−14.93	−0.98	20.26	3.68	1.04	0.09	24.8
12307-3	G	26.41	−14.96	−0.77	20.26	3.68	1.04	0.09	23.9
12308-2	G	26.65	−15.05	−0.83	20.25	3.78	1.04	0.09	24.2
12309-1	G	26.84	−15.11	−0.90	20.25	3.79	1.04	0.09	24.5
12310-1	G	23.50	−18.72	−1.22	20.90	3.67	1.04	0.04	26.0
12322-2	G	22.90	−17.16	−0.93	20.14	3.26	0.96	0.05	24.3
12323-1	G	22.91	−17.19	−1.16	20.15	3.26	0.96	0.05	25.3
12324-1	G	22.92	−17.22	−0.86	20.15	3.26	0.96	0.05	23.9
12325-4	G	22.99	−17.33	−1.09	20.18	3.28	0.96	0.05	25.0
12326-2	G	23.04	−17.41	−1.16	20.20	3.28	0.97	0.05	25.4
12327-2	G	23.13	−17.74	−1.16	20.50	3.49	1.00	0.04	25.5
12328-1	G	21.15	−18.57	−1.51	20.75	4.55	0.90	0.07	26.7
13526-4	G	21.00	−17.62	−1.79	20.33	4.69	0.85	0.08	27.8
13527-1	G	20.99	−17.66	−1.68	20.34	4.70	0.85	0.08	27.3
13528-2	G	20.99	−17.68	−1.46	20.34	4.70	0.85	0.08	26.2
13529-1	G	20.99	−17.70	−1.70	20.34	4.70	0.85	0.08	27.4
13530-1	G	21.00	−17.73	−1.74	20.35	4.69	0.85	0.08	27.6
13532-2	G	20.98	−17.88	−1.62	20.38	4.69	0.85	0.08	27.0
13533-1	G	20.99	−18.03	−1.46	20.41	4.67	0.86	0.07	26.3
13534-1	G	21.02	−17.88	−1.50	20.38	4.66	0.85	0.08	26.5
13536-2	G	21.00	−17.58	−1.74	20.33	4.69	0.85	0.08	27.6
15626-1	G	29.22	−12.84	−0.97	19.69	3.95	0.96	0.12	24.5
15627-2	G	29.17	−12.09	−1.09	19.58	3.86	0.93	0.14	24.9
15628-4	G	29.08	−11.98	−1.07	19.58	3.85	0.93	0.14	24.8
15629-1	G	29.06	−11.95	−0.74	19.58	3.85	0.93	0.14	23.2
15630-1	G	29.04	−11.92	−0.85	19.57	3.85	0.93	0.14	23.7
15631-1	G	29.02	−11.90	−0.85	19.58	3.85	0.93	0.14	23.7
15632-1	G	28.91	−11.70	−0.66	19.57	3.84	0.93	0.14	22.8
15634-1	G	28.26	−13.40	−0.67	19.95	3.89	0.98	0.13	23.1
15635-2	G	27.20	−14.66	−1.00	20.22	3.82	1.04	0.10	25.0
15638-2	G	32.21	−10.45	−0.82	19.26	4.80	0.98	0.11	23.8
15639-1	G	32.49	−10.11	−1.00	19.25	4.85	0.98	0.11	24.7
15640-1	G	32.45	−9.96	−0.86	19.24	4.85	0.98	0.11	24.0
15641-2	G	32.43	−9.87	−0.82	19.23	4.87	0.98	0.11	23.8
15643-1	G	32.40	−9.82	−0.63	19.23	4.87	0.98	0.11	23.0
15644-1	G	32.40	−9.81	−1.00	19.23	4.88	0.98	0.11	24.7
15645-1	G	32.39	−9.80	−0.84	19.23	4.88	0.98	0.11	23.9
15646-1	G	32.38	−9.78	−0.62	19.22	4.88	0.98	0.11	22.9
15647-1	G	32.38	−9.77	−0.87	19.22	4.88	0.98	0.11	24.1
15651-4	G	33.19	−9.83	−1.11	19.21	5.24	0.99	0.12	25.2
GeoB 1029-1	M	−21.06	8.23	−0.78	19.30	5.01	0.53	0.14	21.6
GeoB 1033-2	M	−22.05	5.54	−0.75	20.02	4.98	0.59	0.14	21.7
GeoB 1034-1	M	−21.72	5.43	−0.96	20.21	4.95	0.61	0.14	22.7
GeoB 1035-3	M	−21.60	5.03	−0.96	20.27	4.95	0.61	0.14	22.8
GeoB 1041-1	M	−3.48	−7.59	−1.58	25.18	5.06	0.56	0.36	25.4
GeoB 1048-2	M	20.91	−19.72	−1.15	21.21	4.61	0.93	0.09	25.2
GeoB 1101-4	M	1.66	−10.98	−2.13	27.00	4.03	0.35	0.29	27.1

Table 2 (continued)

Core	Ref.	Lat. (°)	Long. (°)	$\delta^{18}O$ (‰, PDB)	T_{an} (°C)	ΔT (°C)	δ_w (‰, SMOW)	$\Delta\delta_w$ (‰, SMOW)	T_{iso} (°C)
GeoB 1103-3	M	−0.60	−9.26	−1.11	25.63	4.98	0.49	0.39	22.9
GeoB 1108-6	M	−2.17	−9.87	−1.74	25.42	5.22	0.56	0.40	26.2
GeoB 1109-4	M	−6.01	−7.75	−1.35	25.26	4.61	0.67	0.34	24.9
GeoB 1110-3	M	−5.94	−8.14	−1.44	25.27	4.58	0.67	0.33	25.3
GeoB 1111-5	M	−5.84	−8.65	−1.60	25.32	4.45	0.67	0.32	26.0
GeoB 1113-7	M	−5.75	−11.04	−1.69	25.63	4.22	0.67	0.26	26.5
GeoB 1114-3	M	−5.28	−10.20	−1.87	25.45	4.60	0.63	0.31	27.1
GeoB 1115-4	M	−3.56	−12.58	−1.86	26.01	5.19	0.62	0.34	27.1
GeoB 1116-1	M	−3.62	−13.19	−1.24	26.12	5.04	0.63	0.32	24.1
GeoB 1117-3	M	−3.82	−14.90	−1.51	26.35	4.53	0.65	0.26	25.5
GeoB 1121-3	M	20.84	−19.74	−1.06	21.22	4.64	0.93	0.09	24.7
GeoB 1203-2	M	−26.55	5.02	−1.34	20.01	5.29	0.61	0.12	24.5
GeoB 1204-3	M	−25.05	5.50	0.45	19.85	5.16	0.60	0.11	16.4
GeoB 1207-2	M	−24.60	6.86	−0.55	19.41	5.13	0.56	0.10	20.6
GeoB 1220-2	M	−24.03	5.31	0.04	19.96	5.12	0.60	0.11	18.2
GeoB 1402-7	M	−2.18	−10.07	−1.38	25.44	5.23	0.56	0.40	24.5
GeoB 1404-8	M	−0.08	−10.78	−1.65	26.11	4.76	0.49	0.38	25.5
GeoB 1407-8	M	−4.33	−10.25	−1.67	25.42	4.99	0.60	0.32	26.0
GeoB 1413-1	M	−15.68	−9.46	−0.89	23.34	4.24	1.03	0.10	24.4
GeoB 1414-2	M	−15.53	−10.73	−0.91	23.36	4.23	1.05	0.10	24.6
GeoB 1415-1	M	−15.53	−11.58	−1.11	23.41	4.11	1.07	0.11	25.6
GeoB 1417-1	M	−15.53	−12.71	−0.97	23.53	4.09	1.09	0.11	25.1
GeoB 1418-1	M	−15.53	−14.89	−1.08	23.88	3.53	1.13	0.10	25.8
GeoB 1419-1	M	−15.54	−17.07	−1.27	24.29	3.13	1.18	0.10	26.9
GeoB 2102-1	M	−23.98	−41.12	−1.61	24.40	4.19	1.05	0.15	27.9
GeoB 2119-2	M	−21.73	−38.55	−1.23	25.08	4.23	1.17	0.15	26.7
GeoB 2124-1	M	−20.96	−39.56	−1.32	25.06	3.98	1.16	0.18	27.1
GeoB 2125-2	M	−20.82	−39.86	−1.65	25.05	3.97	1.16	0.18	28.7
GeoB 2126-1	M	−21.27	−38.93	−1.64	25.21	4.07	1.18	0.18	28.7
GeoB 2130-1	M	−20.62	−37.10	−1.69	25.48	4.19	1.22	0.22	29.2

upward by bioturbation in some cases. Secondly, the seasonality was not really constant. Thirdly, the isotopic measurements are associated with an internal error on the order of ±0.1‰. Fourthly, the hydrographic data might also not be representative of the time period of deposition. Finally, and perhaps most important, some of the samples are probably not representative of the average isotope value of the foraminiferal population in the sediment. Schiffelbein and Hills (1984) have shown that 417 tests of *G. sacculifer* must be measured in one sample to get a reproducibility of 0.1‰ with 90% reliability. Less than this number were measured by Ganssen (1983) and Mulitza (1994). We assume, however, that the above mentioned errors are random. Therefore, to get a better estimation for the deviation of T_r from T_m, we averaged all isotope temperatures which were derived from stations with comparable annual mean temperatures within 1°C classes. This procedure should result in a more realistic deviation estimate.

4. Temperature sensitivity and optimum temperature

Fig. 6 shows average isotope temperature versus the average temperature of the respective class. As previously noted, these graphs should enable us to estimate the optimum temperature (T_{opt}) and the temperature sensitivity (σ_F) of the two species. Theoretically, the optimum temperature should be where the deviations from annual mean temperature are zero. This means that the distribution of SST is centered exactly over the flux distribution. The temperature

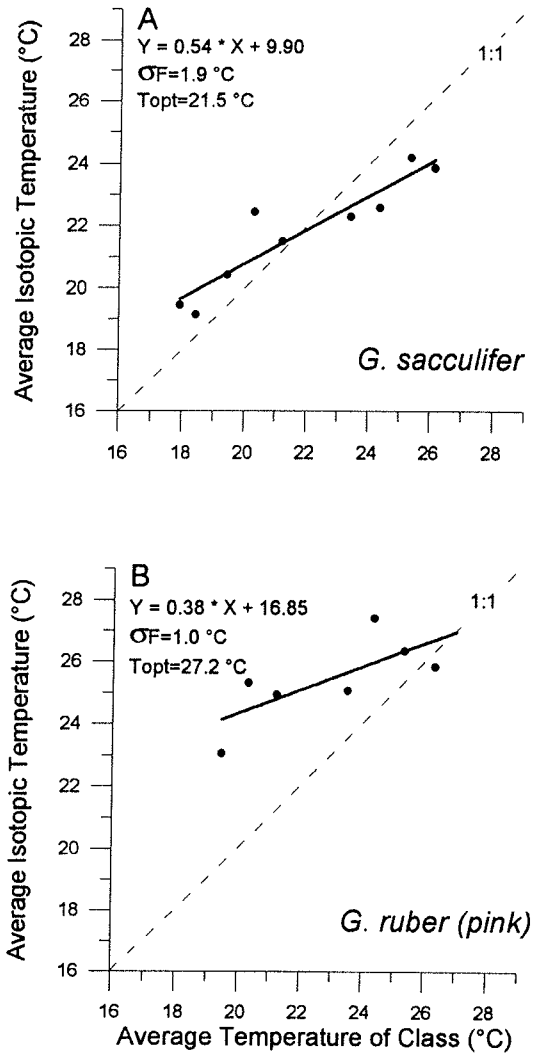

Fig. 6. Isotopic temperatures averaged in one-degree classes of annual mean temperatures of Levitus and Boyer (1994) for the seasonality range between 3.13 to 5.29°C. σ_f and T_{opt} are the temperature sensitivity and optimum temperature calculated from the respective regression equation.

sensitivity is related to the slope (S) as described by Eq. 5. A broad σ_F leads to a steep slope close to the 1:1 line (low temperature sensitivity), whereas a narrow σ_F results in a flat slope (high temperature sensitivity). To estimate S and T_{opt}, we fitted a regression line through the data. The optimum temperature of the two species can be estimated from the regression equations by setting $x = y$. *G. ruber* (pink) seems to be the warmer and the more temperature sensitive of the two species. Its optimum temperature is around 27°C and the slope of the regression is small ($S = 0.38$). *G. sacculifer* has its apparent optimum temperature near 22°C, and it seems to be less temperature sensitive than *G. ruber* (pink) ($S = 0.54$). To calculate σ_F from S with Eq. 5 we need the standard deviation (σ_W) of SSTs of our samples. We determined a value of 1.6°C by calculating the standard deviation of all monthly SSTs for the positions used in this study after subtraction of the respective annual mean. This is only a rough estimate of the true variability because the seasonality (and thus the variability) is not really constant for our samples. However, using the approximated optimum temperature (T_{opt}) and the temperature sensitivity (σ_F), we can now estimate the frequency distributions of the two species (Fig. 7). This will allow us to test our results for T_{opt} and σ_F with independent data.

5. Reliability of the model

Generally, there are a lot of hints towards a temperature sensitivity of planktic foraminifera. Early workers recognized that the distribution pattern of planktic foraminifera in the sediment displays a certain degree of similarity to the latitudinal temperature distribution (e.g. Murray, 1897). Subsequently, it has become obvious that many species, in particular some deep-dwelling foraminifera, are more sensitive to other parameters than temperature, e.g., productivity, oxygen concentration or stratification (Jones, 1967; Mix, 1989; Ravelo, 1991). However, temperature sensitivity is important, to some extent, at least for some shallow dwelling species such as *G. ruber* (pink) and *G. sacculifer*. In culture experiments, Bijma et al. (1990) have shown that vital processes of *G. ruber* (pink) and *G. sacculifer* are influenced by the water temperature in the culture vessel. Fig. 8 shows the percentage of reproduction and chamber formation of the two species versus temperature. Maximum reproduction of *G. ruber* (pink) occurs very close to the optimum temperature inferred from stable isotopes. Our results concerning the temperature sensitivity are also substantiated by the results of Bijma et al. (1990). For *G. sacculifer* gametogenesis changes very little between 20 and 30°C. By contrast, reproduction of *G. ruber* (pink) is considerably reduced below and above the isotopic optimum tem-

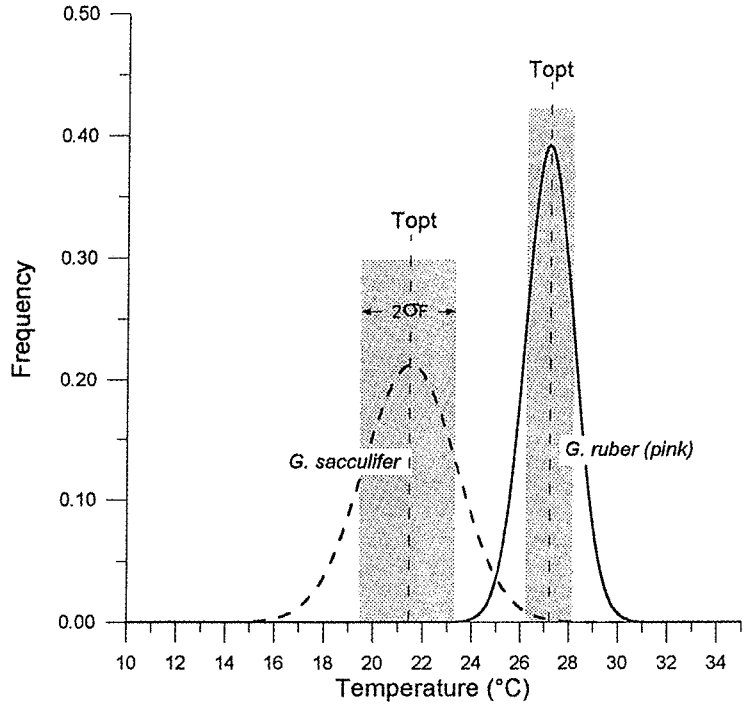

Fig. 7. Theoretical frequency distributions of *G. ruber* (pink) and *G. sacculifer* inferred from the regression equations in Fig. 6.

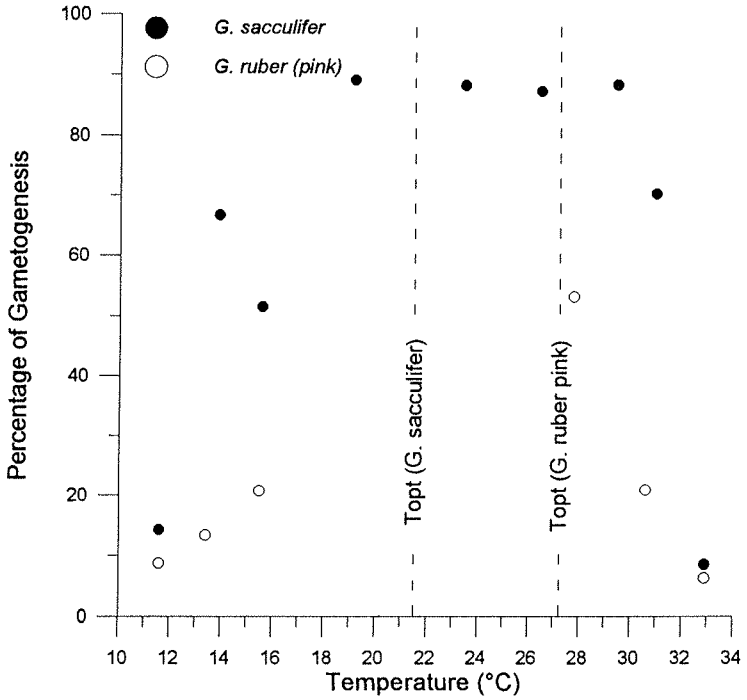

Fig. 8. Comparison of T_{opt} with the results from culture experiments of Bijma et al. (1990). This study shows the response of vital processes of different species to temperature. Percentage of gametogenesis is the percentage of the foraminiferal population in the culture vessel undergoing gametogenesis at a certain temperature.

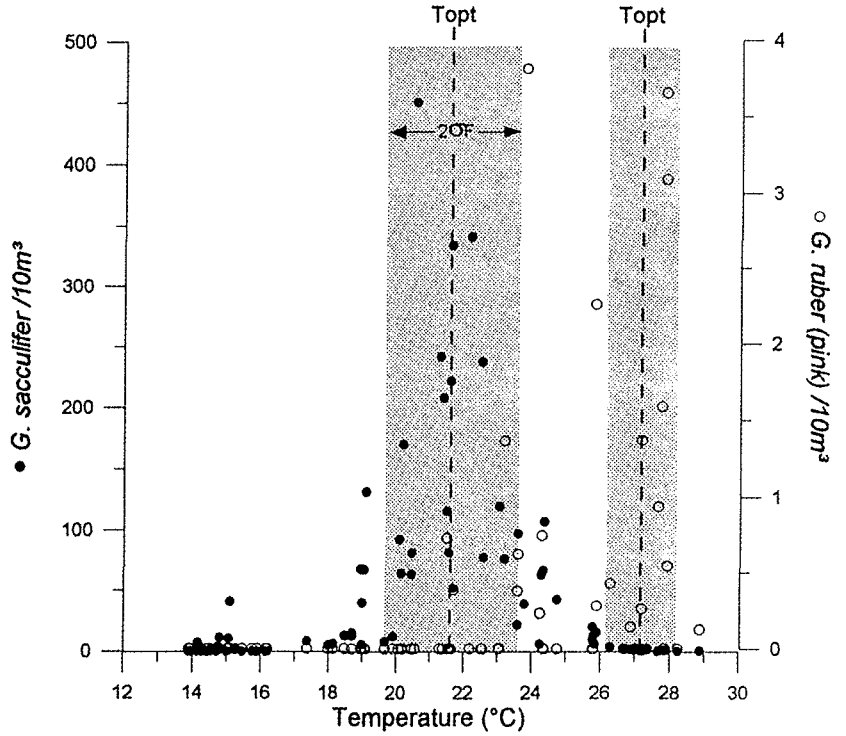

Fig. 9. Comparison of σ_F and T_{opt} with the concentrations of *G. ruber* (pink) and *G. sacculifer* in North Atlantic surface waters (Ottens, 1991). Note the different scales for *G. ruber* (pink) and *G. sacculifer*.

perature. Thus, the vital processes of *G. ruber* (pink) appear to be more strictly limited by temperature variation than those of *G. sacculifer*.

A second indication of the dissimilar responses of *G. ruber* (pink) and *G. sacculifer* populations to temperature comes from the open ocean. Ottens (1991) collected planktic foraminifera from eastern North Atlantic surface waters. The concentrations of *G. ruber* (pink) and *G. sacculifer* are shown in Fig. 9, overlain with our estimated optimum temperatures and temperature sensitivities. The frequency distribution of *G. sacculifer* is very well centered around the isotopic optimum temperature, reaching maximum concentrations close to 22°C. The concentrations of *G. ruber* (pink) are very low in the Ottens (1991) transect reaching maximum numbers of 3 ind./10 m^3. Highest concentrations, however, were found around 27°C, the optimum temperature inferred from oxygen isotopes.

The temperature sensitivity is not so easy to evaluate. A snapshot, like the transect of Ottens (1991), taken over a short time period could also be influenced by processes not directly related to temperature, e.g. the monthly or bimonthly reproduction cycle of the species (Hemleben et al., 1989; Erez et al., 1991). Therefore, to get a better representation of concentration vs. temperature, we averaged all concentrations of Otten's *G. sacculifer* and *G. ruber* data over one-degree temperature classes (Fig. 10). Assuming that the flux of planktic foraminifera to the seafloor is proportional to the concentration in surface water, we can now use the real frequency distribution to calculate the temperatures recorded by the respective foraminiferal species. This provides an independent test for our 'isotopic-temperature-sensitivity estimate'. To be comparable with the surface sediments, we used the same normal temperature distribution as for the oxygen isotope calculations (σ_W = 1.6°C). Fig. 11 shows a comparison of the recorded temperatures derived from oxygen isotopes and the recorded temperatures derived from the Ottens (1991) data. Generally, the slopes of the two lines are in fairly good correspondence with each other for *G. sacculifer*, suggesting that the sensitivity

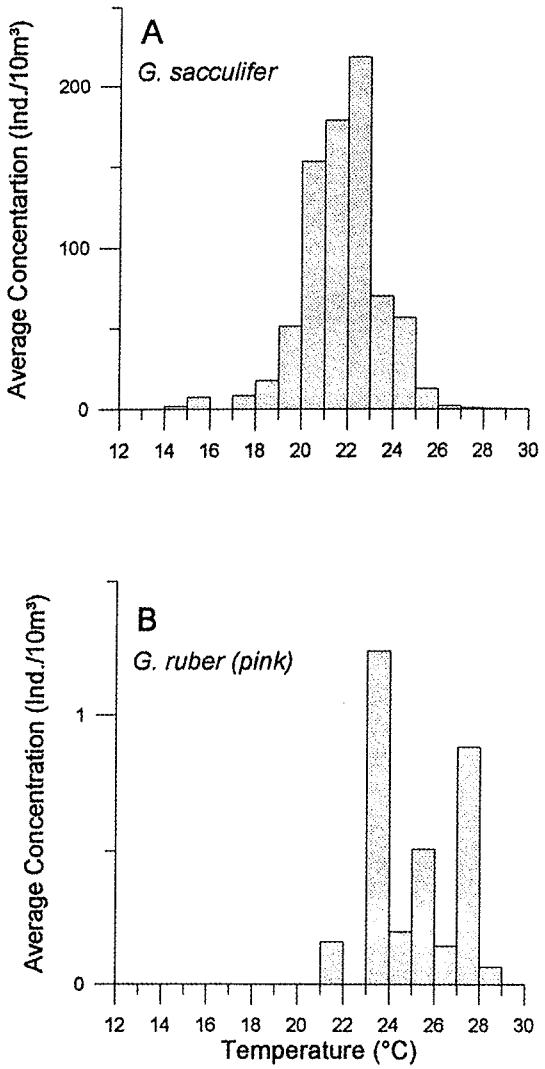

Fig. 10. Concentrations of *G. sacculifer* (A) and *G. ruber* (pink) (B) averaged within one-degree temperature classes. Discrete data are given in Fig. 9 (Ottens, 1991).

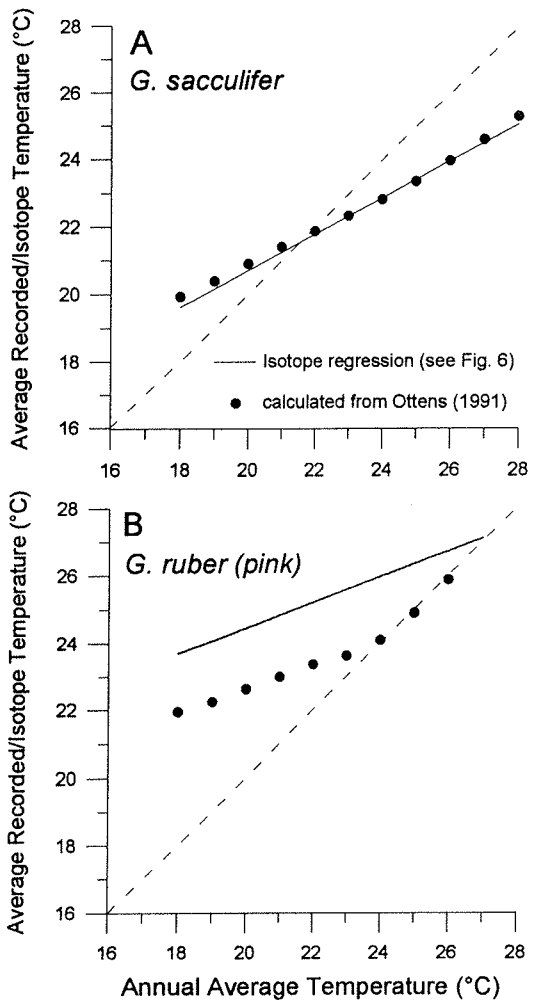

Fig. 11. Comparison of the recorded temperature calculated from the regression in Fig. 6 (line) with the recorded temperature calculated from the real distribution of the species in surface waters (•) from the Ottens (1991) data. We also assumed a normal distribution of temperatures and a σ_W of 1.6°C for the calculation of the recorded temperatures with the Ottens (1991) data.

estimate obtained using Mix's model is in accordance with real data from the water column. It must be noted, however, that some evidence exists that *G. sacculifer* adds a secondary layer of calcite at the end of its life cycle, which makes the final $\delta^{18}O$ value of the shell up to 0.9‰ greater with respect to the initial shell (Duplessy et al., 1981). This secondary calcite should shift the regression line in Fig. 11 towards colder isotope temperatures and our estimation of the optimum temperature would be to low. In this case, however, we need an alternative explanation for the maximum abundance of *G. sacculifer* around 22°C in the data set of Ottens (1991).

An offset of about 1.5°C occurs for the two lines for *G. ruber* (pink). One contributing factor to this could be a vital effect of *G. ruber* (pink). Negative offsets between −0.2 to −0.8‰ have been reported by different authors (Deuser and Ross, 1989, and citations therein). This would cause *G. ruber* (pink) to

show a too-warm optimum temperature. The sensitivity estimate would be unaffected by a constant vital effect. In addition, the large error associated with the low concentrations of *G. ruber* (pink) in the work of Ottens (1991) could bias the estimation of the recorded temperature. However, our data show that the simple model provided by Mix is a good first-order approximation for the real temperature dependency of the flux of *G. ruber* (pink) and *G. sacculifer* to the seafloor, at least over longer time periods.

6. Influence on the isotope-temperature record

Using the estimated optimum temperature and temperature sensitivity, we can now model the influence of the temperature-dependent flux on the isotope temperature recorded in the sediment. We performed two sensitivity tests. For the first test we assumed that the temperature variability (σ_W) oscillates between 0 and 2°C around a mean temperature (T_m) of 25°C (Fig. 12). The recorded temperatures of the two species diverge from the point where temperature variability starts to increase. The reason is that as soon as the temperature range starts to increase both species have the opportunity to develop in the season of their temperature preference, which is the summer for *G. ruber* (pink) and the winter for *G. sacculifer* in this experiment. To show that such a response can actually be observed in the oxygen-isotope record, we compared two cores from regions with different surface-water seasonalities (Fig. 13): GeoB 1523 is from the western equatorial Atlantic, where today's seasonality is small (<1°C), while GeoB 1112 was recovered from the eastern equatorial Atlantic (Wefer et al., 1996) where the seasonal contrast in temperature is as high as 5°C. $\delta^{18}O$ differences of up to 1‰ are clearly illustrated in GeoB 1112. In contrast, Holocene differences in GeoB 1523 are near zero. GeoB 1112 reveals another interesting feature: minima and maxima of the two isotope records are sometimes shifted with respect to each other. We tested whether such a phenomenon could also be due to temperature sensitivity. To this purpose, we conducted a second sensitivity test with temperature variability (σ_W) being phase shifted by 90° relative to temperature. As can be seen in Fig. 14, such a combination causes a phase lag between minima and maxima of the two temperature records. Consequently, we can speculate that the phase of late Quaternary isotope records, which is a mixture of ice volume and recorded temperature, may be influenced by the temperature sensitivity of planktic foraminifera.

7. Towards an isotopic transfer function

As noted previously, on the one hand, the oxygen-isotope record can be distorted by the temperature sensitivity of planktic foraminifera. On the other hand, this distortion provides new opportunities for paleoceanographic reconstructions. The oxygen isotope difference between different planktic foraminiferal species has been suggested as a tool for the estimation of seasonality (Deuser, 1978; Deuser and Ross, 1989). How seasonality can be quantified, however, is still unclear. In this section, we will demonstrate how this may theoretically be achieved. The distribution of surface water temperatures can be described by two parameters, the mean temperature (T_m) and the temperature variability (σ_W). In principle, these variables can be calculated by formulating Eq. 4 for two different temperature-sensitive species [e.g. *G. sacculifer* and *G. ruber* (pink)] and to solve for one variable. This method, however, requires an isotopic (recorded) temperature (T_r), which can be calculated via Eq. 6, if δ_w is known for the time of calcification. Unfortunately, δ_w can not be determined as precisely as necessary for the past to obtain good isotopic temperatures. It is, therefore, more promising to use three species with different temperature sensitivities. Assuming that seasonal variations of δ_w are small, we can calculate the temperature difference of the recorded temperatures (ΔT_r) for the species 1 and 2 (and similarly for species 2 and 3) with the formula:

$$\Delta T_{r(12)} = \frac{\Delta\delta^{18}O_{(12)}}{0.22} \tag{7}$$

Rewriting Eq. 4 for a temperature difference (ΔT_r) between species 1 and 2 (and similarly for species 2 and 3) yields:

$$\Delta T_{r(12)} = T_m\left(\frac{\sigma_{F(1)}}{\sigma_W+\sigma_{F(1)}} - \frac{\sigma_{F(2)}}{\sigma_W+\sigma_{F(2)}}\right) + T_{opt(1)}\frac{\sigma_W}{\sigma_W+\sigma_{F(1)}} - T_{opt(2)}\frac{\sigma_W}{\sigma_W+\sigma_{F(2)}} \tag{8}$$

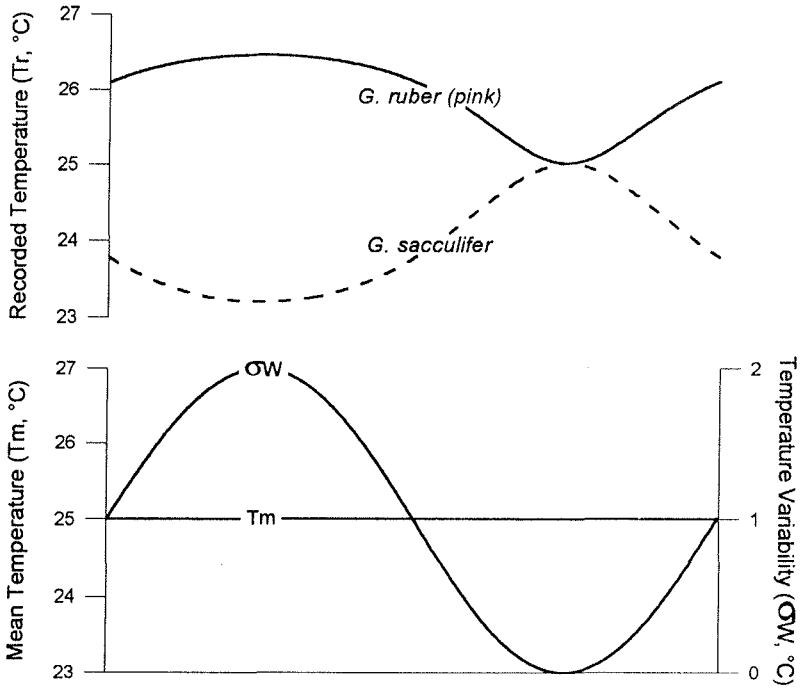

Fig. 12. Sensitivity test for the recorded temperatures of *G. ruber* (pink) and *G. sacculifer*, assuming that σ_W varies between 0 and 20°C around a mean temperature (T_m) of 25°C. Note that the recorded temperatures diverge toward the optimum temperatures of the respective species as soon as temperature variability starts to increase. We assumed the frequency distributions from Fig. 7.

and

$$\Delta T_{r(23)} = T_m \left(\frac{\sigma_{F(2)}}{\sigma_W + \sigma_{F(2)}} - \frac{\sigma_{F(3)}}{\sigma_W + \sigma_{F(3)}} \right) + T_{opt(2)} \frac{\sigma_W}{\sigma_W + \sigma_{F(2)}} - T_{opt(3)} \frac{\sigma_W}{\sigma_W + \sigma_{F(3)}} \quad (9)$$

We can now combine Eqs. 8 and 9 to eliminate T_m and to calculate σ_W:

$$\sigma_W = \left[\Delta T_{r(12)} \cdot \sigma_{F(2)} (\sigma_{F(1)} - \sigma_{F(3)}) - \Delta T_{r(13)} \cdot \sigma_{F(3)} (\sigma_{F(1)} - \sigma_{F(2)}) \right] \times \left[(\Delta T_{opt(12)} - \Delta T_{r(12)})(\sigma_{F(1)} - \sigma_{F(3)}) - (\Delta T_{opt(13)} - \Delta T_{r(13)})(\sigma_{F(1)} - \sigma_{F(2)}) \right]^{-1} \quad (10)$$

Fig. 15 illustrates the method. The possible combinations of T_m and σ_W for one ΔT_r of two species is represented by a single line. The crosspoint of the two lines is the only possible combination of T_m and σ_W for two ΔT_rs derived from the same hydrographic situation.

Now that we can calculate T_m and σ_W, we can also calculate T_r for each individual species with Eq. 4. This, in turn, enables us to calculate the isotopic composition of seawater by solving for δ_w in Eq. 6. Theoretically, the 'three-species approach' described here should work in the ocean as long as temperatures are truly normally distributed. Based on the past 50 years of observations this assumption seems to be unrealistic in some places. Today, especially in regions with high seasonality, temperatures are often bimodally distributed. However, the normal distribution may be a good approximation for a bimodal distribution if the means of the two subpopulations are close to each other.

8. Conclusions

Mix's model was originally designed to illustrate the influence of the temperature distribution at the sea surface on the temperature recorded in the sediment and not for real application. Our results indicate that some observable phenomena can be

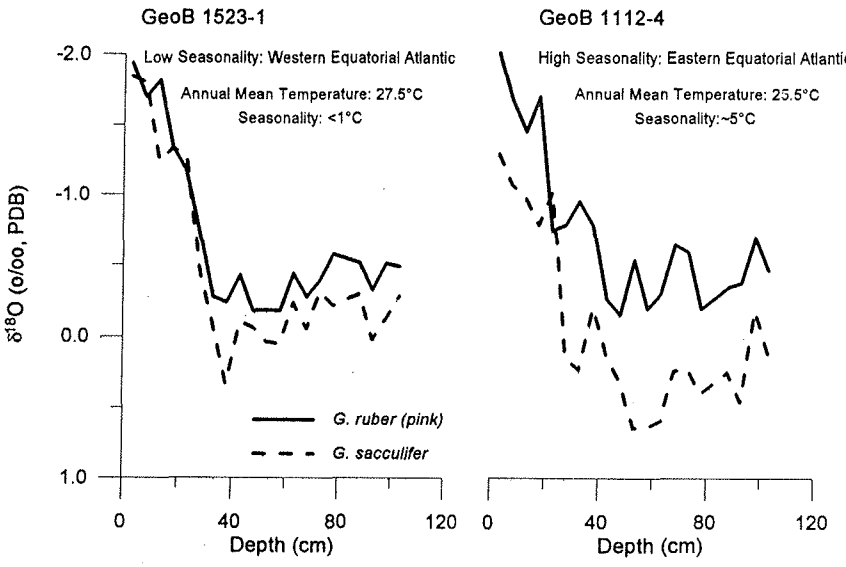

Fig. 13. Comparison of *G. sacculifer* and *G. ruber* (pink) oxygen isotope records from high-seasonality (GeoB 1112-4) and low-seasonality (GeoB 1523-1) sites. Data are from Meinecke (1992) and Wefer et al. (1996).

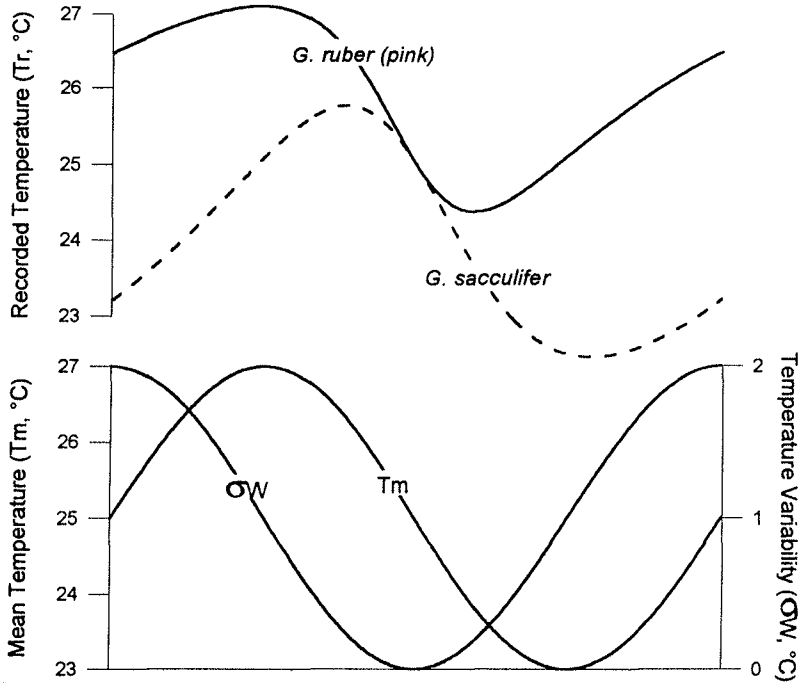

Fig. 14. Same as in Fig. 12 but with σ_W and T_m being phase shifted by 90°.

simulated with this model. Temperature sensitivity and optimum temperature of *G. sacculifer* and *G. ruber* (pink) derived from Holocene sediment surfaces are in accordance with data from the water column and from laboratory studies. We have demonstrated that temperature sensitivity can influence amplitude

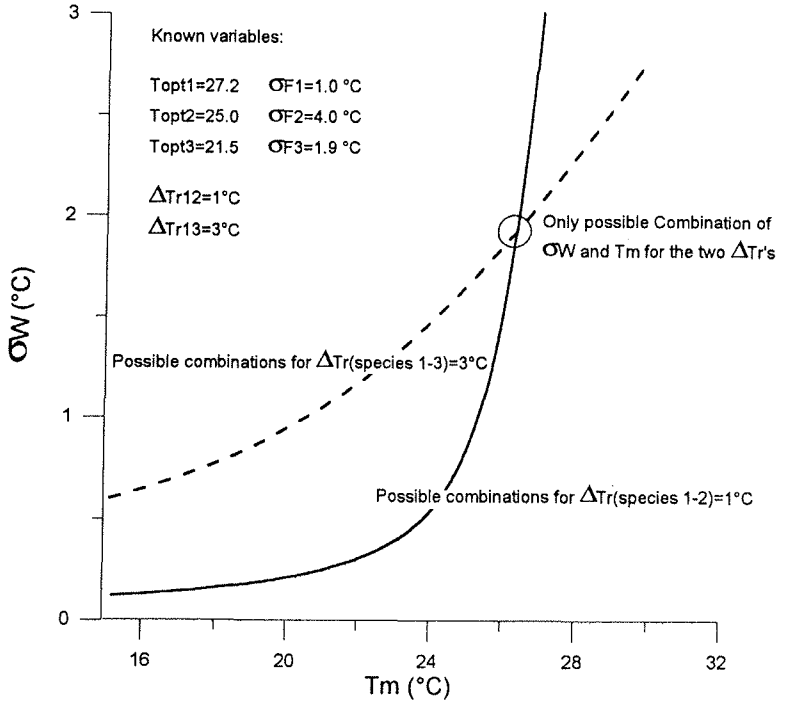

Fig. 15. Illustration of an Isotopic Transfer Function. The graph shows the possible combinations of σ_W and T_m for a given temperature difference between paired species with known optimum temperature (T_{opt}) and known temperature sensitivity (σ_F, see upper left corner). The circle denotes the only possible combination of two known temperature differences (ΔT_r is assumed to be 1°C for species 1 and 2 and 3°C for species 1 and 3, respectively). This point can be calculated using Eq. 10.

and phase of the oxygen-isotope record in the sediment. A simple linear 'calibration' does not account for this distortion, because the slope of the relation between recorded temperature and SST is dependent on both the seasonality and the mean temperature. This makes it difficult to estimate $\delta^{18}O$ values of seawater from core top calibrated $\delta^{18}O$ values for *G. ruber* (pink) and *G. sacculifer*. However, if the temperature sensitivity is known for at least three species, it is theoretically possible to derive a set of equations which allow us to calculate mean and variability of SSTs, and $\delta^{18}O$ of the surface ocean. In the future, the model of Mix should be further refined to reflect more realistic assumptions concerning the distributions of temperature and foraminiferal abundance.

Acknowledgements

This paper was inspired by discussions with A. Mix at the 1994 South Atlantic Symposium in Bremen. We thank H. Thierstein and J. Young for reviews. W.H. Berger and A. Paul provided helpful comments. Thanks to G. Ganssen for sending unpublished data. Stable isotope analyses were run at the University of Bremen by M. Segl and B. Meyer-Schack. Research was funded by the Deutsche Forschungsgemeinschaft (Sonderforschungsbereich 261 at Bremen University, Contribution No. 160).

References

Bijma, J., Faber, W.W., Hemleben, C., 1990. Temperature and salinity limits for growth and survival of some planktonic foraminifers in laboratory cultures. J. Foraminiferal Res. 20, 95–116.

Broecker, W.S., 1986. Oxygen isotope constraints on surface ocean temperatures. Quat. Res. 26, 121–134.

Craig, H., Gordon, L.I., 1965. Deuterium and oxygen-18 variations in the ocean and the marine atmosphere. In: Tongiorgi, E. (Ed.), Stable isotopes in oceanographic studies and paleotemperatures. Spoleto, Pisa Consiglio Nazionale delle Ricerche, Laboratorio di Geologia Nucleare, pp. 9–130.

Deuser, W.G., 1978. Stable-isotope paleoclimatology: A possible

measure of past seasonal contrast from foraminiferal tests. DSIR Bull. 220, 55–60.

Deuser, W.G., Ross, E.H., 1989. Seasonally abundant planktonic foraminifera of the Sagasso Sea: Succession, deep-water fluxes, isotopic compositions and paleoceanographic implications. J. Foraminiferal Res. 19, 268–293.

Duplessy, J.-C., Blanc, J.L., Bé, A.W.H., 1981. Oxygen-18 enrichment of planktonic foraminifera due to gametogenetic calcification below the euphotic zone. Science 213, 1247–1250.

Duplessy, J.-C., Labeyrie, L., Julliet-Leclerc, A., Maitre, F., Duprat, J., Sarnthein, M., 1991. Surface salinity reconstruction of the North Atlantic Ocean during the last glacial maximum. Oceanol. Acta 14, 311–324.

Emiliani, C., 1954. Depth habitats of some species of pelagic foraminifera as indicated by oxygen isotope ratios. Am. J. Sci. 252, 149–158.

Epstein, S., Buchsbaum, H.A., Lowenstam, H.A., Urey, H.C., 1953. Revised carbonate-water isotopic temperature scale. Geol. Soc. Am. Bull. 64, 1315–1326.

Erez, J., Almogi-Labin, A., Avraham, S., 1991. On the live history of planktonic foraminifera: lunar reproduction cycle in *Globigerinoides sacculifer* (Brady). Paleoceanography 6, 295–306.

Fairbanks, R.G., Charles, C.D., Wright, J.D., 1992. Origin of global meltwater pulses. In: Taylor, R.E., Long, A., Kra, R.S. (Eds.), Four Decades of Radiocarbon Studies. Springer, New York, NY, pp. 473–500.

Ganssen, G., 1983. Dokumentation von küstennahem Auftrieb anhand stabiler Isotope. Meteor Forschungs-Ergeb., Reihe C 37, 1–46.

Hemleben, C., Spindler, M., Anderson, O.R., 1989. Modern planktonic foraminifera. Springer, New York, NY, 363 pp.

Hut, G., 1987. Stable isotope reference samples for geochemical and hydrological investigations. Consultants Group Meeting IAEA, Vienna, 16.–18.09.1985, Report to the Director General, IAEA, Vienna, 42 pp.

Imbrie, J., Kipp, N., 1971. A new micropaleontological method for quantitative paleoclimatology: Application to a late Pleistocene Caribbean Core. In: Turekian, K.K. (Ed.), The Late Cenozoic Glacial Ages. Yale Univ. Press, New Haven, pp. 71–181.

Jones, J.I., 1967. Significance of distribution of planktonic foraminifera in the Equatorial Atlantic Undercurrent. Micropaleontology 13, 489–501.

Levitus, S., Boyer, T.B., 1994. World Ocean Atlas 1994, Volume 4: Temperature. NOAA, U.S. Dep. of Commerce, Washington, DC, 117 pp.

Levitus, S., Burgett, R., Boyer, T.B., 1994. World Ocean Atlas 1994, Volume 3: Salinity. NOAA, U.S. Dep. of Commerce, Washington, DC, 99 pp.

Meinecke, G., 1992. Spätquartäre Oberflächenwassertemperaturen im östlichen äquatorialen Atlantik. Ber. Fachbereich Geowiss. Univ. Bremen 29, 181 pp.

Mix, A., 1987. The oxygen-isotope record of glaciation. In: Ruddiman, W.F., Wright, H.E. (Eds.), North America and adjacent oceans during the last deglaciation. (The Geology of North America, Vol. K-3.) Geol. Soc. Am., Boulder CO, pp. 111–135.

Mix, A., 1989. Pleistocene paleoproductivity: evidence from organic carbon and foraminiferal species. In: Berger, W.H., Smetacek, V.S., Wefer, G. (Eds.), Productivity in the Ocean: Present and Past. Wiley, Chichester, pp. 313–340.

Mulitza, S., 1994. Spätquartäre Variationen der oberflächennahen Hydrography im westlichen äquatorialen Atlantik. Ber. Fachbereich Geowiss. Univ. Bremen 57, 97 pp.

Murray, J., 1897. On the distribution of the pelagic foraminifera at the surface and on the floor of the oceans. Nat. Sci. 11, 17–27.

Ottens, J.J., 1991. Planktic foraminifera as North Atlantic water mass indicators. Oceanol. Acta 14, 114–123.

Ravelo, A.C., 1991. Reconstructing the tropical Atlantic seasonal thermocline using planktonic foraminifera. Ph.D. Thesis, Columbia Univ., 168 pp.

Schiffelbein, P., Hills, S., 1984. Direct assessment of stable isotope variability in planktonic foraminifera populations. Palaeogeogr., Palaeoclimatol., Palaeoecol. 48, 197–213.

Shackleton, N., 1974. Attainment of isotopic equilibrium between ocean water and the benthonic foraminifera genus *Uvigerina*: Isotopic changes in the ocean during the last glacial. Colloq. Int. C.N.R.S. 219, 203–209.

Wang, L., Sarnthein, M., Duplessy, J.-C., Erlenkeuser, H., Jung, S., Pflaumann, U., 1995. Paleo sea surface salinities in the low-latitude Atlantic: The $\delta^{18}O$ record of *Globigerinoides ruber* (white). Paleoceanography 10, 749–761.

Wefer, G., Berger, W.H., Bickert, T., Donner, B., Fischer, G., Kemle von Mücke, S., Meinecke, G., Müller, P.J., Mulitza, S., Niebler, H.S., Pätzold, J., Schmidt, H., Schneider, R.R., Segl, M., 1996. Late Quaternary surface circulation of the South Atlantic: The stable Isotope record and implications for heat transport and productivity. In: Wefer, G., Berger, W.H., Siedler, G., Webb, D.J. (Eds.), The South Atlantic: Present and Past Circulation. Springer, Berlin, pp. 461–502.

Williams, D.F., Sommer, M.A., Bender, M.L., 1981. Seasonal stable isotopic variations in living planktonic foraminifera from Bermuda plankton tows. Palaeogeogr., Palaeoclimatol., Palaeoecol. 33, 391–403.

Chapter 4

Oxygen isotopes versus CLIMAP (18 ka) temperatures: A comparison from the tropical Atlantic

Tobias Wolff
Stefan Mulitza
Helge Arz
Jürgen Pätzold
Gerold Wefer

Geology 26 (1998), 675-678

Abstract

Glacial-interglacial differences in $\delta^{18}O$ values of *Globigerinoides sacculifer* have been mapped in the western and central tropical Atlantic using data from surface and core sediments. Glacial-interglacial differences in the western tropical Atlantic, if attributed to temperature changes only, are at odds with temperature reconstructions performed by CLIMAP. In the Ceara Rise region $\Delta\delta^{18}O$ values exceeding 2‰ are recorded. They can only be partly attributed to changes in the precipitation-evaporation regime, i.e., higher salinities and ^{18}O-enriched precipitation. An additional cooling of 1-2 °C as compared to CLIMAP's results is required to balance the $\delta^{18}O$ record. Thus, temperature changes from glacial to modern times amount to 2-3 °C in the tropical Atlantic off the northern coast of Brazil.

Introduction

Oxygen isotope ratios ($\delta^{18}O$) of foraminifera have long been used to assess glacial-interglacial climate changes. The $\delta^{18}O$ values of the foraminiferal calcite tests are related to the temperature and the isotopic composition of the ambient seawater (Emiliani, 1955). During glacial periods both parameters were different from today. Sea-surface temperatures (SSTs) were globally lower in glacial times, although the magnitude of the cooling in tropical regions is debated within the scientific community (see discussion in Broecker, 1996). The seawater was enriched in ^{18}O due to preferential removal of the lighter ^{16}O isotope during evaporation and its storage as ice on land.

The last glacial maximum (LGM) 18 thousand years ago and the present represent end members of climate states. Broecker (1986) used core-top samples and LGM samples from the world oceans to estimate glacial-interglacial temperature changes comparing the $\delta^{18}O$ values of benthic and planktonic foraminifera. He concluded that tropical SSTs were lower by not more than 2 °C at the LGM. During the past 10 years a number of new studies in different regions of the tropical Atlantic significantly improved the oxygen isotope record of planktonic foraminifera for the late Quaternary. The purpose of this study is to bring together these data and shed light on regional differences within the glacial tropical Atlantic concerning the oxygen isotope patterns of the planktonic foraminifer *Globigerinoides sacculifer* . Our results show that in the western tropical Atlantic, low glacial-interglacial SST changes, as reconstructed from foraminiferal census count data (CLIMAP Project Members, 1981), are in contrast to the oxygen isotope record, whereas both records are in good agreement in the other regions. We discuss these patterns and their implications for regional changes in the hydrological cycle and glacial tropical SSTs.

Methods

G. sacculifer is an abundant, surface-dwelling foraminifer of the tropical and subtropical oceans and is assumed to record mixed-layer conditions (e.g., Fairbanks et al., 1982), although some influence of deeper waters due to secondary calcification is reported (Duplessy, 1981). We used $\delta^{18}O$ data of *G. sacculifer* from 43 surface sediment samples taken from the tropical Atlantic between lat 10°S and 10°N and between long 50°W and 0°W (partly published in Mulitza et al., 1997). We exclusively used data from undisturbed sediment samples recovered by multicorer or giant box corer (Fig. 1A). The LGM samples were taken from 13 gravity cores; $\delta^{18}O$ values of these samples were measured in our laboratory (partly published in Dürkoop et al., 1997; Meinecke, 1992; Mulitza, 1994; Wefer et al., 1996). Results of $\delta^{18}O$ measurements of another 17 cores reported in the literature were included (Curry and Crowley, 1987; Curry and Oppo, 1997; Emiliani, 1955; Kähler, 1990; Kassens and Sarnthein, 1989; McIntyre et al., 1989; Mix and Ruddiman, 1985; Sarnthein et al., 1984; Showers et al., 1997; Sikes and Keigwin, 1994)*. We used cores with mean sedimentation rates higher than 2 cm/kyr in order to minimize the effects of bioturbation. In two cases sedimentation rates were ~1.5 cm/kyr. All downcore records of the $\delta^{18}O$ values of *G. sacculifer* were compared with a stacked isotope curve (stack-2, Mix and Ruddiman, 1985). This stack comprises 18 well-dated $\delta^{18}O$ curves of planktonic foraminifera, 13 of which are based on *G. sacculifer*. In all cores we determined the last relative maximum in $\delta^{18}O$ values before the onset of deglaciation and averaged two or more isotope values spanning the relative maximum. Resolution is low in three cores and the LGM seems to be represented by a single value only. In these cases we used this one measurement. Where ^{14}C ages were reported, they were included in the process of determining the LGM.

Data are presented as glacial to interglacial differences in $\delta^{18}O$ values ($\Delta\delta^{18}O$). They were obtained by averaging samples within 10 specific regions where several data points cluster and measurements of LGM samples, as well as surface samples, were available (Fig. 1A). Subsequently, $\Delta\delta^{18}O$ values were compared to glacial-interglacial annual mean temperature differences (CLIMAP Project Members, 1994). Mulitza et al. (1998) demonstrated that SSTs as reconstructed from the $\delta^{18}O$ values of *G. sacculifer* of their surface sediment data set are in good agreement with annual mean temperatures taken from the World Ocean Atlas (Levitus and Boyer, 1994).

Oxygen isotope patterns

Generally, glacial-interglacial differences in $\delta^{18}O$ values range between 1.8‰ and 2.0‰ throughout the study area; the highest values were around 2.1‰ in the Ceara Rise region and in the southeastern part of the study area. Lowest values of roughly 1.6‰ are observed off the Brazilian coast at lat 8°S (Fig. 1B). The precision associated with these values is estimated to be 0.12‰ based on the mean standard deviation of the $\delta^{18}O$ values measured within the 10 boxes.

* Surface sediment and core data are listed in Appendix A.

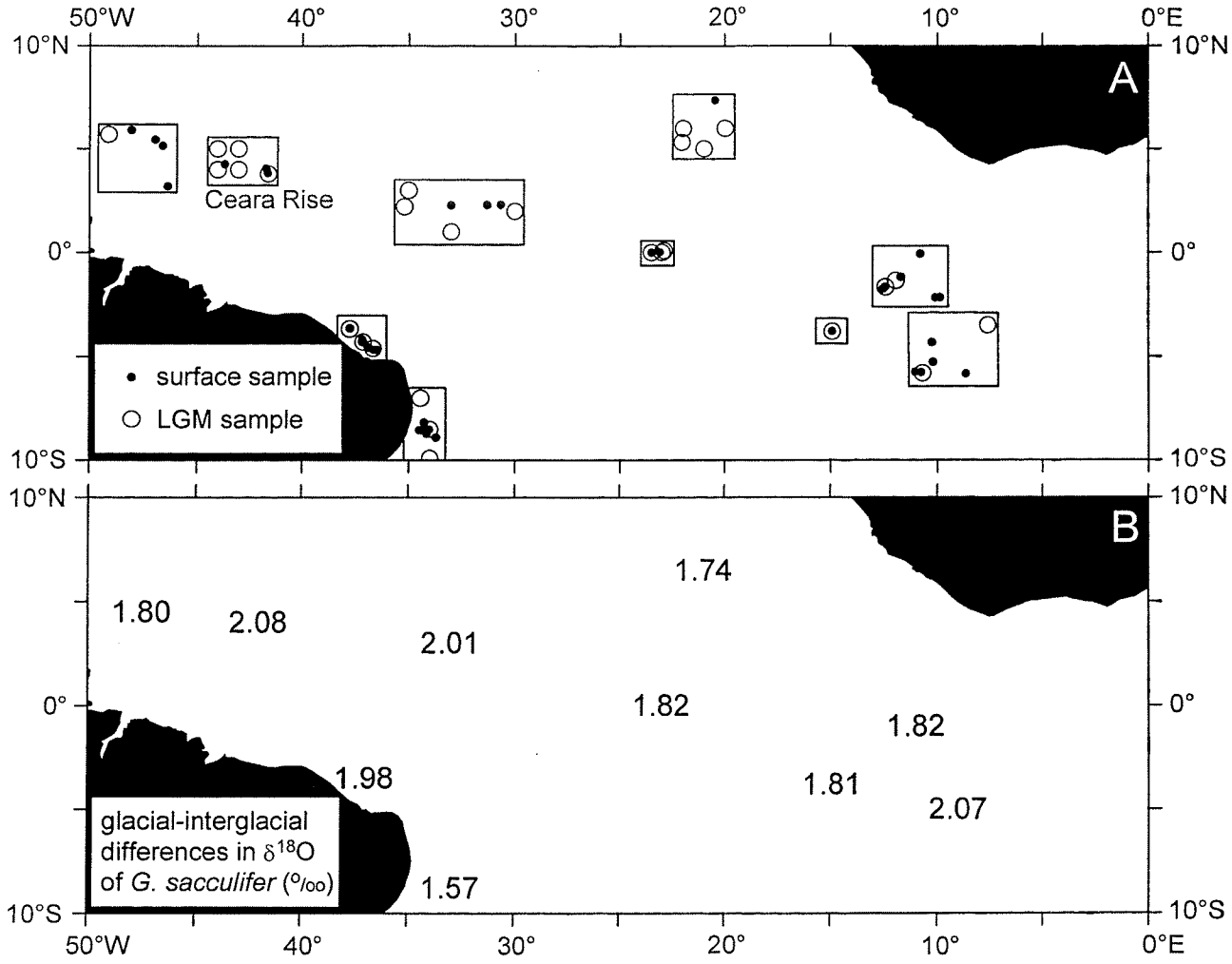

Figure 1: A: Map of region studied. Filled circles mark positions of surface sediment samples, open circles mark sediment core positions. LGM is last glacial maximum. **B:** Glacial to interglacial differences in $\delta^{18}O$ of *G. sacculifer*. Several data points close to each other were averaged in order to reduce noise.

The pattern of $\Delta\delta^{18}O$ values is contrasted by SST differences as reconstructed from relative abundance data of planktonic foraminifera (CLIMAP Project Members, 1994). We averaged CLIMAP's warm- and cold-season temperatures to approximate annual mean temperature differences between the glacial and interglacial (Fig. 2A). To emphasize the discrepancy between the oxygen isotope record and the SST estimates we computed the residual $\Delta\delta^{18}O$: the regional $\Delta\delta^{18}O$ values (Fig. 1B) were modified by subtracting the global glacial-interglacial change in $\delta^{18}O$ of seawater of 1.2‰ (see references in Wefer et al., 1996). The residuals (Fig. 2B) are then compared to theoretical $\Delta\delta^{18}O$ calculated from CLIMAP temperature changes according to the $\delta^{18}O$-temperature relationship of Epstein et al. (1953) for each specific region. Other reported relationships are very similar in the temperature range encountered in the tropics (see discussion in Mix, 1987). For temperatures between 24 °C and

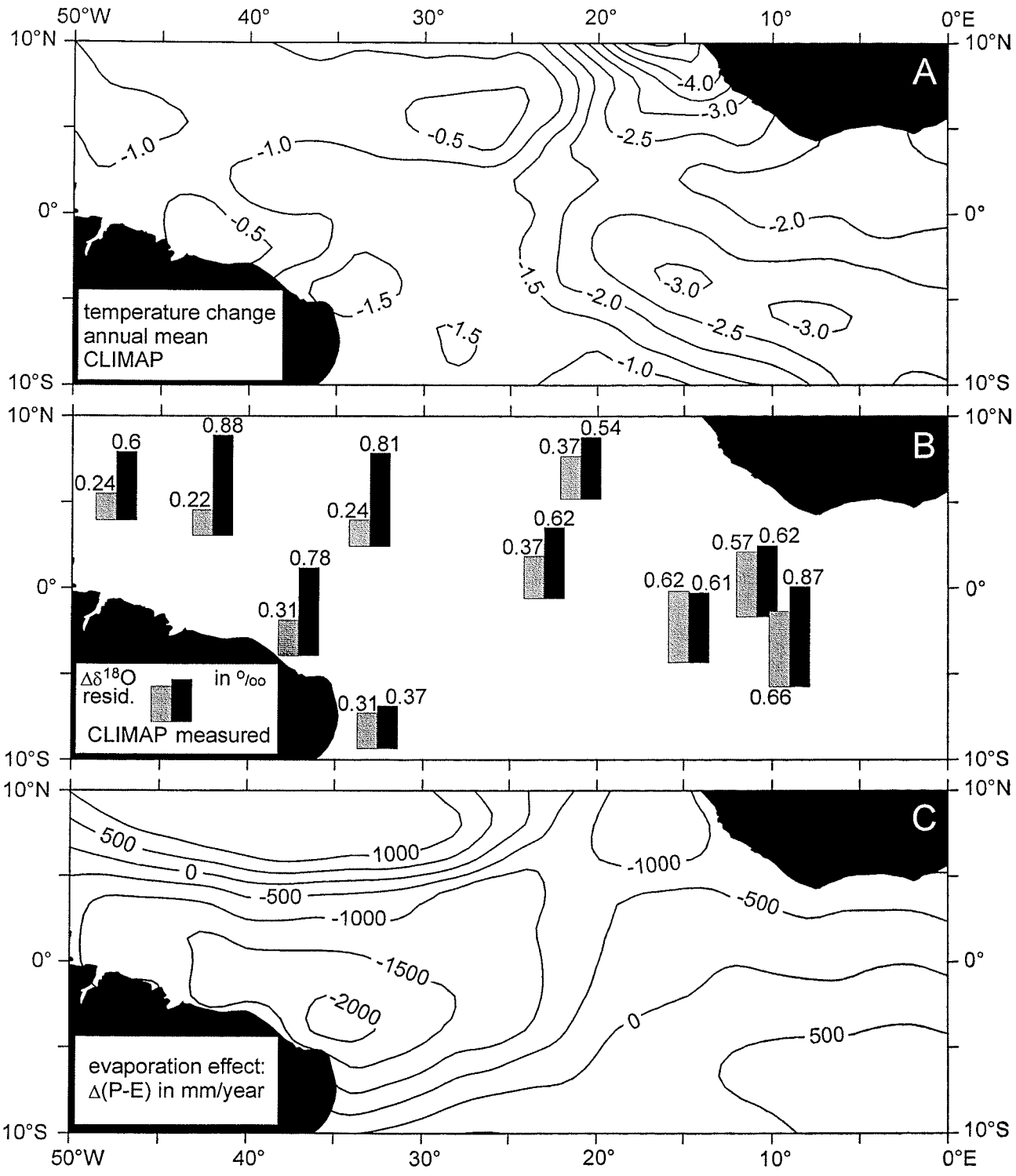

Figure 2: A: Glacial to interglacial differences in annual mean temperatures (we used mean of February and August temperatures) as reported by CLIMAP Project Members (1994). **B:** $\Delta\delta^{18}O$ residuals after subtracting global glacial effect of 1.2‰ (right bar) as opposed to theoretical $\Delta\delta^{18}O$ residuals (left bar) computed from CLIMAP temperature differences of A. Note discrepancy between $\delta^{18}O$ record and CLIMAP temperatures in northwest. **C:** Glacial minus modern P-E (precipitation minus evaporation) from atmospheric model results (Lorenz et al., 1996).

28 °C a change in $\delta^{18}O$ of 0.22‰ is equivalent to a 1 °C temperature change.

In the eastern, northern, and southern parts of the study area oxygen isotope signatures of *G. sacculifer* are in good agreement with temperature estimates of CLIMAP. Differences between isotope and CLIMAP-based data range from 0‰ to 0.2‰. Toward the western part of the study area these differences increase, reaching a maximum of 0.66‰ in Ceara Rise sediments. Here, measured $\Delta\delta^{18}O$ are largest (0.88‰) and would be equivalent to a 4 °C temperature decrease if attributed to temperature alone. Glacial annual mean SSTs according to CLIMAP were only 1 °C lower than today in the same region.

Discussion

How much of the observed high glacial-interglacial differences of $\delta^{18}O$ in the Ceara Rise region can be attributed to changes in $\delta^{18}O$ of seawater ($\delta^{18}O_w$)? Whereas Curry and Oppo (1997) interpreted the $\delta^{18}O$ signature from a Ceara Rise core as a SST decrease alone (> 4 °C), we believe that our data reflect both decreased temperatures and increased $\delta^{18}O_w$ during the LGM. Since the $\delta^{18}O_w$ is related to the sea-surface salinity, the planktonic foraminiferal oxygen isotope signature can also be interpreted in terms of salinity changes (e.g. Keigwin and Boyle, 1989; Duplessy et al., 1991; Rostek et al., 1993). Dürkoop et al. (1997) adopted mean tropical temperature changes of 2 °C (CLIMAP Project Members, 1981) and infered local salinity (evaporation - precipitation) increases amounting to 1.7‰ in addition to the glacial effect by subtracting the temperature effect from their $\delta^{18}O$ record. Our approach is to evaluate the plausibility of changes in $\delta^{18}O_w$ and salinities, and then discuss the consequences for glacial western equatorial SSTs.

Like salinity, the $\delta^{18}O$ of seawater depends on the evaporation-precipitation (E-P) balance. Therefore, in general, there are regionally applying, linear relationships between the two parameters (Craig and Gordon, 1965; Fairbanks et al., 1992). Unlike salinity, the $\delta^{18}O_w$ also depends on the isotopic content of the precipitates. Consequently, the $\delta^{18}O$-salinity relationship has to be reevaluated for the past owing to changes in global glacial effects and regional changes in the isotopic signatures of precipitation.

We assume here that salinity and $\delta^{18}O_w$ are determined by the simple mixing of a fresh-water end member (local precipitation and river runoff) and a salt-water end member (subtropical conditions with maximum salinity). Examination of former reports of regional $\delta^{18}O$-salinity relationships of the Atlantic (Fairbanks et al., 1992; Pierre et al., 1991) reveals that all linear equations are in fact bounded by an upper salinity limit of about 37.2‰ and a maximum $\delta^{18}O_w$ of around 1.3‰.

Evaluation of regional changes in $\delta^{18}O_w$ and salinity (E-P) involves three steps: 1. The salinity in the northwestern equatorial Atlantic is estimated to have been increased by 0.7‰ due to significantly reduced precipitation in addition to the global salinity increase. 2. The $\delta^{18}O$-salinity relationship is corrected for global effects and for increasing $\delta^{18}O$ values of precipitation in the northwestern equatorial Atlantic. 3. The estimated salinity is inserted in the modified $\delta^{18}O$-salinity equation.

Evidence exists from observations and modeling studies that the climate at the LGM might have been drier in the Amazon basin region and off the coast of northeast Brazil (Clapperton, 1993; van der Hammen and Absy, 1994; Lorenz et al., 1996). Clapperton (1993) estimated a reduction in precipitation by roughly 50% for the Amazon basin. Lorenz et al. (1996) performed a LGM run with the atmospheric general circulation model ECHAM3. Figure 2C shows the change in precipitation minus evaporation (P-E) and the significantly lower P-E values off the northeastern coast of Brazil. We assume that the present salinity difference between the subtropical salt-water end member and the Ceara Rise located in the Inter tropical convergence zone is halved during the LGM (0.7‰ as opposed to 1.4‰). The global glacial-interglacial salinity change is estimated to be 1.1‰ (Rostek et al., 1993). As a result the salinity at the Ceara Rise increased by 1.8‰ to approximately 37.6‰ compared to 35.8‰ at present (Table 1). Salinities (and $\delta^{18}O_w$ values) of the northwestern equatorial Atlantic equal or higher than in the subtropics are considered unlikely because the underlying mechanism creating the salinity gradient between the inner tropics and the subtropics is the Hadley circulation. The strength of the Hadley cell may have been reduced (Gates, 1976), but there is no evidence that it vanished during glacial times.

TABLE1. SALINITY AND ISOTOPIC COMPOSITION AT THE SEA SURFACE

Location	Salinity (‰)	$\delta^{18}O$ (‰, SMOW)*	$\Delta\delta^{18}O$ (‰)
Modern situation			
Ceara Rise	35.8†	0.92	-
subtropical maximum	37.2	1.17	-
Glacial situation			
Ceara Rise	37.6	2.32	1.4
subtropical maximum	38.3	2.39	1.2

*SMOW is standard mean ocean water.
†modern salinity value is taken from Levitus et al. (1994)

Secondly, we modified the linear relation between $\delta^{18}O_w$ and salinity (E-P) for today's tropical Atlantic (based on data from GEOSECS Executive Committee, 1987) (Fig. 3). Reduced precipitation in the west would have been accompanied by increased $\delta^{18}O$ values of precipitation in the eastern Amazon basin and off the northern coast of Brazil (Hoffmann, 1995) due to the inverse relationship between the precipitation rate in the tropics and its ^{18}O content (Dansgaard, 1964). Thus we shifted the fresh-water end member by 4‰ on the basis of modeling results by Hoffmann (1995), who incorporated $\delta^{18}O$ in the atmospheric circulation model ECHAM. The salt-water end member was shifted based on global effects only, which are 1.2‰ in $\delta^{18}O_w$ and 1.1‰ in salinity (Rostek et al., 1993).

Inserting today's and the estimated glacial salinity values for the Ceara Rise region into the respective $\delta^{18}O$-salinity equations (Fig. 3) gives $\delta^{18}O_w$ values of 0.92‰ and 2.32‰, respectively. Thus $\delta^{18}O_w$ was increased by 1.4‰ during the LGM (Table 1) which is only 0.2‰ more than the global effect of 1.2‰ already considered in Fig. 2B. As much as 0.68‰ in the Ceara Rise region remains to be explained in terms of temperature amounting to about 3 °C.

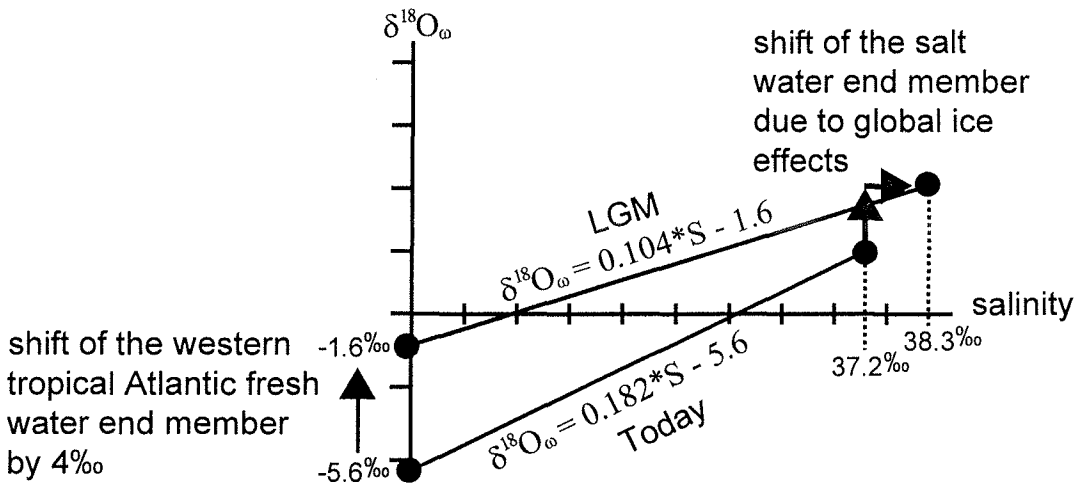

Figure 3: Modification of $\delta^{18}O$-salinity relationship for northwestern equatorial Atlantic as described in text. Today's relation is based on GEOSECS Executive Committee (1987) data from between 30°S and 30°N in Atlantic. It is similar to relationships as reported by Ferronsky and Brezgunov (1989) and Fairbanks et al. (1992).

Implications

Plausible changes in the regional evaporation-precipitation regime of the northwestern equatorial Atlantic as described here can only explain 0.2‰ of the oxygen isotope patterns, as depicted in Figure 2B. The remaining residual $\Delta\delta^{18}O$ of 0.4-0.68‰ in the four northwestern equatorial Atlantic boxes have to be interpreted in terms of temperature changes. We conclude that the oxygen isotope record of *G. sacculifer* is roughly in agreement with temperature estimates by CLIMAP in the central to eastern equatorial Atlantic. After considering plausible changes in salinity and the hydrological cycle an additional cooling of 1-2 °C as compared with CLIMAP is needed in the northwestern equatorial Atlantic amounting to 2-3 °C lower SSTs at the LGM.

Another explanation could be an even further increased salt buildup in the entire Atlantic due to water vapor export to the Pacific, as suggested by Broecker (1989). This would enable us to explain the high $\Delta\delta^{18}O$ values in the west, but would leave us with mismatches in the other regions of the study area, where good agreement (according to Figure 2B) is observed. In view of our data we consider this hypothesis unlikely.

We think that reevaluation of late Quaternary tropical temperatures based on relative abundances of planktonic foraminifera, such as the classic CLIMAP data set, may be necessary. Planktonic foraminifera assemblages in the tropics may be controlled by factors other than temperature (Molfino et al., 1982; Ravelo et al., 1990). Mixed-layer thickness rather than temperature exerts the dominant control on tropical foraminiferal assemblages (Andreasen and Ravelo, 1997).

A temperature change in the northwestern equatorial Atlantic of 2-3 °C as depicted in this study represents an intermediate estimate between the results of CLIMAP (~1 °C) and tropical SST estimates from corals (Guilderson et al., 1994) (~5 °C) and from the South American continental record (e.g., Stute et al., 1995; Thompson et al., 1995) (5-6 °C). Recent results from a coupled ocean-atmosphere model (Ganopolski et al., 1998) also suggest intermediate cooling rates of about 3.3 °C in the tropical Atlantic.

Acknowledgements

We thank M. Segl and B. Meyer-Schack for oxygen isotope measurements. We also thank S. Lorenz and his coworkers for providing their model output data, B. Oelkers for improving the English, and T. Crowley and T. Bralower for their reviews.
Research was funded by the Deutsche Forschungsgemeinschaft (Sonderforschungsbereich 261 at Bremen University, Contribution No. 197).

References

Andreasen, D. J., and A. C. Ravelo (1997). Tropical Pacific Ocean thermocline depth reconstructions for the last glacial maximum. *Paleoceanography 12*, 395-413.

Broecker, W. S. (1986). Oxygen isotope constraints on surface ocean temperatures. *Quaternary Research 26*, 2-14.

Broecker, W. S. (1989). The salinity contrast between the Atlantic and Pacific oceans during glacial time. *Paleoceanography 4*, 207-212.

Broecker, W. S. (1996). Glacial Climate in the Tropics. *Science 272*, 1902-1904.

Clapperton, C. M. (1993). Nature of environmental changes in South America at the last glacial maximum. *Palaeogeography Palaeoclimatology Palaeoecology 101*, 189-208.

CLIMAP, P. M. (1981). Seasonal reconstructions of the Earth's surface at the last glacial maximum. *GSA Map and Chart Ser. MC-36*, 1-18.

CLIMAP, P. M. (1994). Climap 18k Database. *IGBP PAGES/World Data Center-A for Paleoclimatology Data Contribution Series 94-001.*

Craig, H., and L. I. Gordon (1965). Deuterium and oxygen-18 variations in the ocean and marine atmosphere. In E. Tongiorgi (Ed.), *Stable isotopes in oceanic studies and paleotemperatures*, pp. 9-130. Pisa: Consiglio Nazionale Delle Ricerche, Laboratorio di Geologia Nucleare.

Curry, W. B., and T. J. Crowley (1987). The $\delta^{13}C$ of equatorial Atlantic surface water masses: Implications for ice age pCO_2 levels. *Paleoceanography 2*, 489-517.

Curry, W. B., and D. W. Oppo (1997). Synchronous, high-frequency oscillations in the tropical sea surface temperatures and North Atlantic Deep Water production during the last glacial cycle. *Paleoceanography 12*, 1-14.

Dansgaard, W. (1964). Stable isotopes in precipitation. *Tellus 16*, 436-468.

Duplessy, J. C. (1981). Oxygen-18 enrichment of planktonic foraminifera due to gametogenic calcification below the euphotic zone. *Science 213*, 1247-1250.

Duplessy, J. C., L. Labeyrie, A. Juillet-Leclerc, F. Maitre, J. Duprat, and M. Sarnthein (1991). Surface salinity reconstruction of the North Atlantic Ocean during the last glacial maximum. *Oceanologica Acta 14*, 311-324.

Dürkoop, A., W. Hale, S. Mulitza, J. Pätzold, and G. Wefer (1997). Late Quaternary variations of sea surface salinity and temperature in the western tropical Atlantic: Evidence from $\delta^{18}O$ of *Globigerinoides sacculifer*. *Paleoceanography 12*, 764-772.

Emiliani, C. (1955). Pleistocene temperatures. *Journal of Geology 63*, 538-578.

Epstein, S., R. Buchsbaum, H. A. Lowenstam, and H. C. Urey (1953). Revised carbonate-water isotopic temperature scale. *Bull. Geol. Soc. Am. 64*, 1315-1325.

Fairbanks, R. G., C. D. Charles, and J. D. Wright (1992). Origin of global meltwater pulses. In R. E. Taylor (Ed.), *Radiocarbon after four decades*, pp. 473-500. New York: Springer.

Fairbanks, R. G., M. Sverdlove, R. Free, P. H. Wiebe, and A. W. H. Bé (1982). Vertical distribution and isotopic fractionation of living planktonic foraminifera from the Panama Basin. *Nature 298*, 841-844.

Ferronsky, V. I., and V. S. Brezgunov (1989). Stable isotopes and ocean dynamics. In P. Fritz, and J. C. Fontes (Eds.), *The marine environment*, pp. 1-27. Amsterdam: Elsevier.

Ganopolski, A., S. Rahmstorf, V. Petoukhov, and M. Claussen (1998). Simulation of modern and glacial climates with a coupled global model of intermediate complexity. *Nature 391*, 351-356.

Gates, W. L. (1976). The numerical simulation of ice-age climate with a global general circulation model. *J. Atmos. Sci. 33*, 1844-1873.

GEOSECS, Executive, and Committee (1987). GEOSECS Atlantic, Pacific, and Indian Ocean Expeditions, Shorebased Data and Graphics. In H. G. Ostlund, H. Craig, W. S. Broecker, and D. Spencer (Eds.), *International decade of ocean exploration*, 200 pp. Washington D.C.: National Science Foundation.

Guilderson, T. P., R. G. Fairbanks, and J. L. Rubenstone (1994). Tropical Temperature Variations Since 20,000 Years Ago: Modulating Interhemispheric Climate Change. *Science 263*, 663-665.

Hoffmann, G. (1995). *Stabile Wasserisotope im allgemeinen Zirkulationsmodell ECHAM*. Dissertation, Universität Hamburg.

Kähler, G. (1990). *Oberflächentemperatur im Äquatorialen Atlantik während der letzten 330 000 Jahre (Meteor-Kern 16772).* unpublished Diplomarbeit, Kiel University.

Kassens, H., and M. Sarnthein (1989). A link between paleooceanography, early diagenetic cementation, and sheer strength maxima in Late Quaternary deep-sea sediments? *Paleoceanography 4*, 253-269.

Keigwin, L. D., and E. A. Boyle (1989). Late Quaternary paleochemistry of high-latitude surface waters. *Palaeogeography Palaeoclimatology Palaeoecology 73*, 85-106.

Levitus, S., and T. P. Boyer (1994). World Ocean Atlas 1994, Volume 4: Temperature. *NOAA Atlas NESDIS 4*, 117 pp.

Levitus, S., R. Burgett, and T. P. Boyer (1994). World Ocean Atlas 1994, Volume 3: Salinity. *NOAA Atlas NESDIS 3*, 99 pp.

Lorenz, S., B. Grieger, P. Helbig, and K. Herterich (1996). Investigating the sensitivity of the Atmospheric General Circulation Model ECHAM 3 to paleoclimatic boundary conditions. *Geol. Rundschau 85*, 513-524.

McIntyre, A., W. F. Ruddiman, K. Karlin, and A. C. Mix (1989). Surface water response of the equatorial Atlantic Ocean to orbital forcing. *Paleoceanography 4*, 19-55.

Meinecke, G. (1992). Spätquartäre Oberflächenwassertemperaturen im östlichen äquatorialen Atlantik. *Berichte, Fachbereich Geowissenschaften, Universität Bremen 29*, 181 pp.

Mix, A. C. (1987). The oxygen-isotope record of glaciation. In W. F. Ruddiman, and H. E. J. Wright (Eds.), *North America and adjacent oceans during the last deglaciation*, pp. 111-135. Boulder, Colorado: Geol. Soc. Am.

Mix, A. C., and W. F. Ruddiman (1985). Structure and timing of the last deglaciation: Oxygen isotope evidence. *Quaternary Science Reviews 4*, 59-108.

Molfino, B., N. G. Kipp, and J. J. Morley (1982). Comparison of Foraminiferal Coccolithophorid, and Radiolarian Paleotemperature Equations: Assemblage Coherency and Estimate Concordancy. *Quaternary Research 17*, 279-313.

Mulitza, S. (1994). Spätquartäre Variationen der oberflächennahen Hydrographie im westlichen äquatorialen Atlantik. *Berichte, Fachbereich Geowissenschaften, Universität Bremen 57*, 97 pp.

Mulitza, S., A. Dürkoop, W. Hale, G. Wefer, and H. S. Niebler (1997). Planktonic foraminifera as recorders of past surface-water stratification. *Geology 25*, 335-338.

Mulitza, S., T. Wolff, J. Pätzold, W. Hale, and G. Wefer (1998). Temperature sensitivity of planktonic foraminifera and its influence on the oxygen isotope record. *Marine Micropaleontology 33*, 223-240.

Pierre, C., C. Vergnaud-Grazzini, and J. C. Faugeres (1991). Oxygen and carbon stable isotope tracers of the water masses in the Central Brazil Basin. *Deep Sea Research 38*, 597-606.

Ravelo, A. C., R. G. Fairbanks, and S. G. H. Philander (1990). Reconstructing tropical Atlantic hydrography using planktonic foraminifera and an ocean model. *Paleoceanography 5*, 409-431.

Rostek, F., G. Ruhland, F. C. Bassinot, P. J. Müller, L. D. Labeyrie, Y. Lancelot, and E. Bard (1993). Reconstructing sea surface temperature and salinity using $\delta^{18}O$ and alkenone records. *Nature 364*, 319-321.

Sarnthein, M., H. Erlenkeuser, R. v. Grafenstein, and C. Schröder (1984). Stable isotope stratigraphy for the last 750 000 years.-"Meteor" core 13519 from the eastern equatorial Atlantic. *Meteor Forschungsergebnisse CC38*, 9-24.

Showers, W. J., R. Schneider, N. Mikkelson, and M. Maslin (1997). Isotopic stratigraphy of Amazon fan sediments. *Proc. ODP, Sci. Results 155*, 281-303.

Sikes, E. L., and L. D. Keigwin (1994). Equatorial Atlantic sea surface temperature for the last 30 ky: A comparison of U^{k}_{37}, $\delta^{18}O$, and foraminiferal assemblage temperature estimates based analysis on controls of foraminiferal estimates. *Paleoceanography 9*, 31-46.

Stute, M., M. Forster, H. Frischkorn, A. Serejo, J. F. Clark, P. Schlosser, W. S. Broecker, and G. Bonani (1995). Cooling of Tropical Brazil (5°C) During the Last Glacial Maximum. *Science 269*, 379-383.

Thompson, L. G., E. Mosley-Thompson, M. E. Davis, P.-N. Lin, K. A. Henderson, J. Cole-Dai, J. F. Bolzan, and K.-B. Liu (1995). Late Glacial Stage and Holocene Tropical Ice Core Records from Huascarán, Peru. *Science 269*, 46-50.

van der Hammen, T., and M. L. Absy (1994). Amazonia during the last glacial. *Palaeogeography Palaeoclimatology Palaeoecology 109*, 247-261.

Wefer, G., W. H. Berger, T. Bickert, B. Donner, G. Fischer, S. Kemle-von Mücke, G. Meinecke, P. J. Müller, S. Mulitza, H. S. Niebler, J. Pätzold, H. Schmidt, R. R. Schneider, and M. Segl (1996). Late Quaternary Surface Circulation of the South Atlantic: The Stable Isotope Record and Implications for Heat Transport and Productivity. In G. Wefer, W. H. Berger, G. Siedler, and D. J. Webb (Eds.), *The South Atlantic - Present and Past Circulation*, pp. 461-502. Berlin: Springer.

Chapter 5

The tropical Atlantic thermocline seesaw: Surface water response to the South Atlantic trade wind system during the Late Quaternary

Tobias Wolff
Stefan Mulitza
Carsten Rühlemann
Gerold Wefer

submitted to Paleoceanography

Abstract

A Modern Analog Technique using planktonic foraminiferal abundance data was designed in order to reconstruct thermocline depths in three gravity cores from the tropical Atlantic. The method was tested on the reference data set showing a strong dependency of the foraminiferal assemblages on thermocline depth. Application to sediment cores from the eastern and the western equatorial Atlantic shows opposite fluctuations in mixed layer thickness throughout the last 250 000 years. In general, the thermocline deepens in the west and shallows in the east during glacial stages due to stronger zonal trade winds. During interglacials the system relaxes and the thermocline is relatively shallow in the west and relatively deep in the east. While the eastern core shows a pattern characterized by the precession cycle, the western equatorial Atlantic cores as well as an east-west thermocline gradient curve display marked characteristics of southern hemisphere temperature changes. We compare the east-west difference in thermocline depth with tropical-subtropical sea surface temperature differences derived from two South Atlantic gravity cores using alkenone paleotemperature estimates. The similarities of the curves in both shape and timing indicate a major influence of South Atlantic meridional temperature gradients on the southern trade wind system, especially in the western sector.

Introduction

Upper layer characteristics of the tropical oceans are essential in understanding the role of the ocean as an important part of the earth's climate system. Besides sea water properties such as temperature and salinity the structure of the water column is of particular interest. The stability of the water stratification plays an important role in the formation of subsurface water masses. Changes in stratification through time may thus influence global ocean circulation patterns. Getting hands on these changes in the past might improve our understanding of climate changes in both future and past.

Today, the upper equatorial Atlantic is a nearly perfect two layer system, consisting of warm surface water separated from the underlying central waters by a sharp thermocline (Hastenrath and Merle, 1987). The structure of the tropical thermocline is directly related to the wind stress excerted at the sea surface. Seasonally varying SE-trades promote an east-west asymmetry of equatorial mixed layer thickness. In boreal summer, enhanced wind stress induces upwelling in the east and piles up water in the west, progressively deepening the thermocline towards the South American coast (Fig. 1). Water accumulating in this manner at the western boundary escapes in part as eastward flowing under-currents and counter-currents. Also a substantial amount of water is exported into the North Atlantic (Flagg et al., 1986; Johns et al., 1990). This through-flow is the main pathway for the transport of surface and thermocline waters into the North Atlantic, required to balance the southward cross-equatorial transport of North Atlantic Deep Water (Sverdrup et al., 1942). Decreasing wind stress in

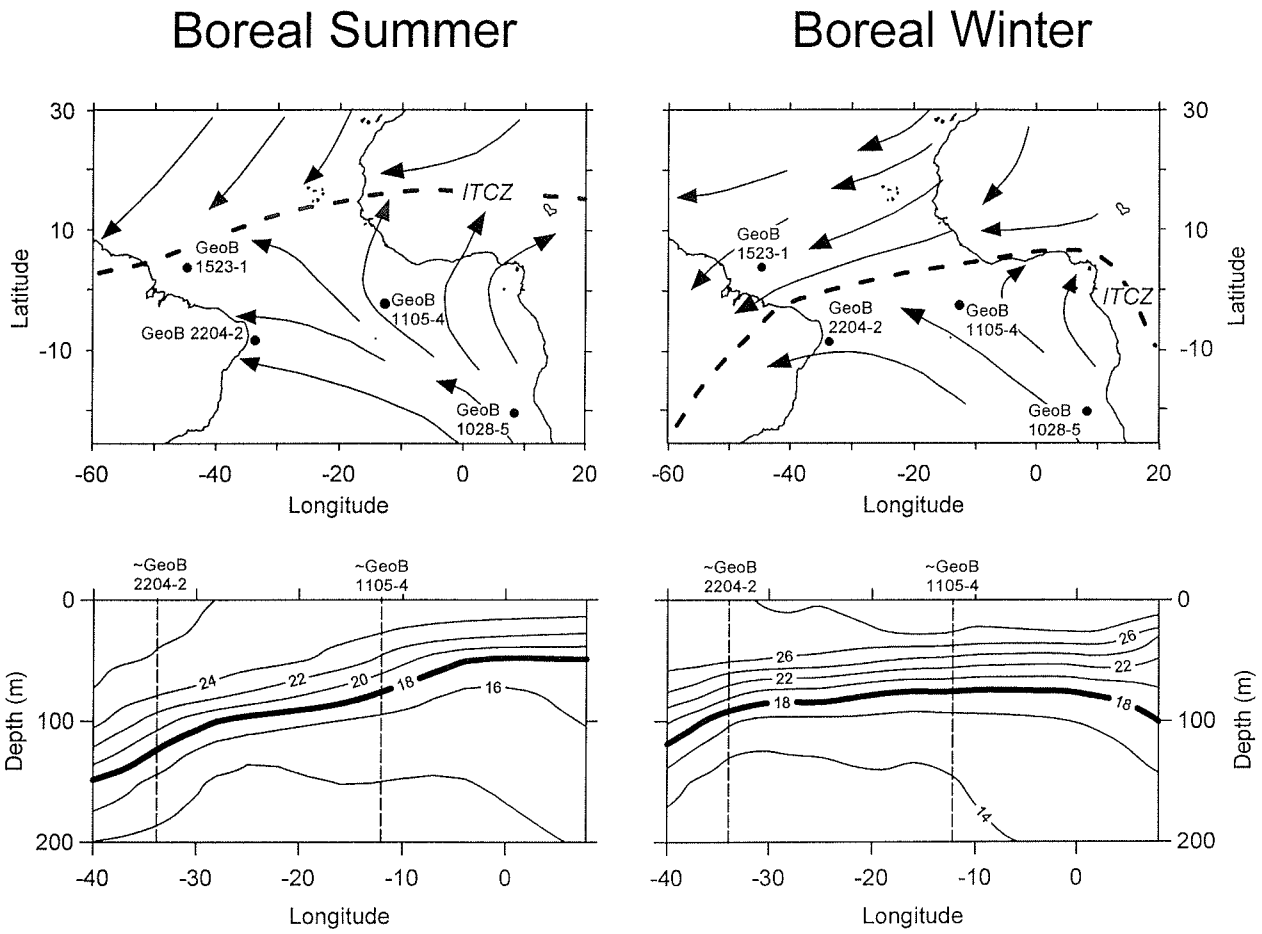

Figure 1: Tropical Atlantic wind system and hydrography. Upper panels: wind direction and location of the ITCZ in boreal summer and winter (after Open University Course Team, 1989). Positions of cores used in this study are marked by filled circles. Lower panels: isotherms of a zonal profile along the equator during the respective seasons (data from Levitus and Boyer, 1994).

boreal winter leads to relaxation of the E-W thermocline gradient.

It has been proposed that the modern seasonal cycle might be an analog for changes of the late Quaternary trade wind system in the tropical Atlantic (McIntyre et al., 1989; Wefer et al., 1996). In a number of studies (Mix et al., 1986; Ravelo et al., 1990; Schneider et al., 1995; Rühlemann et al., 1998) it has been shown that the thermocline shallows in the eastern equatorial Atlantic during glacials due to enhanced zonal trade winds and a reduced African monsoon. Curry and Lohmann (1990) speculated about contemporaneous deepening of the thermocline in the west.

The purpose of this paper is to check whether the thermocline in the western and eastern tropical Atlantic react in opposite ways on late Quaternary changes in trade wind intensity (the tropical Atlantic seesaw). To address this question we use a Modern Analog Technique in

conjunction with foraminiferal census counts in order to reconstruct thermocline depths in three cores in the equatorial Atlantic.

The western equatorial Atlantic cores do in fact show significant deepening of the thermocline at times of thermocline shallowing in the east in analogy to the seasonal cycle. East-west differences display major similarities with global ice volume curves but leading the ice volume signal by several millennia. Our results suggest an important role of South Atlantic meridional temperature gradients as a forcing mechanism on the equatorial trade wind system.

Tropical Atlantic wind system and ocean circulation

Today the Intertropical Convergence Zone (ITCZ) is situated in the Northern Hemisphere for much of the year. During boreal summer, it is located at its northernmost position at about 10°N and strong SE-trades invade the northern hemisphere and accelerate the South Equatorial Current to its maximum strength. Radiative heating of the north African land mass leads to formation of low atmosheric pressure over the continent which causes strong southerly monsoonal winds. Moisture-laden airmasses deliver intense precipitation to Northwest Africa. Simultaneously, the westward wind stress excerted by the SE-trades accelerates the South Equatorial Current which deepens the thermocline in the west and shoals the thermocline in the east (Fig. 1).

The maximum in strength of the SE-trades coincides with a maximum in the zonal component of the SE-trades and with the maximum in tropical-subtropical temperature difference in the South Atlantic (Fig. 2). Flow of the North Brazil Current into the northern hemisphere is also at its seasonal maximum. Sea surface temperatures are lowest in the eastern basin due to divergence and upwelling of cold water (Hastenrath and Merle, 1987; Molinari et al., 1986) and the North Equatorial Counter-Current (NECC) accelerates to its maximum strength.

In boreal winter the ITCZ migrates to its southernmost position at the equator. The NE-trades reach their maximum strength and climate is relatively dry over the Sahara and Sahel. At the equator, the east-west pressure gradient and the thermocline asymmetry relax, the seesaw swings back. Below the unsteady winds at the equator, the NECC is weak or even reverses in spring (Richardson et al., 1991). At this time of the year sea surface temperatures are highest in the eastern basin, owing to the shutdown of trade wind driven equatorial upwelling. Sea surface temperatures in the west are relatively stable throughout the year, while they show large seasonal variations in the east.

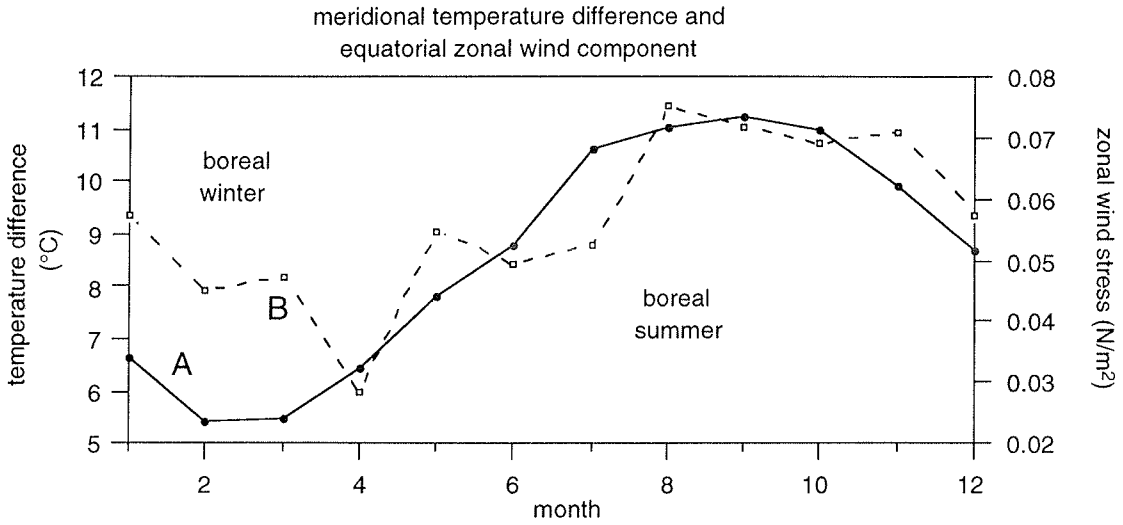

Figure 2: Seasonal cycle of tropical-subtropical temperature gradient and westward windstress along the equator. **A:** temperature gradient between core locations GeoB 1523 (western equatorial Atlantic) and GeoB 1028 (eastern subtropical South Atlantic at Walvis Ridge) as taken from Levitus and Boyer (1994). **B:** zonal wind component (westward wind stress) averaged for the zone between 5°S and 5°N in the tropical Atlantic (data from Picaut et al., 1985).

Materials and methods

Cores and Stratigraphy

We computed the depth of the thermocline for the last 250 kyrs in three tropical Atlantic gravity cores. Core GeoB 1105-4 was recovered from the equatorial divergence east of the mid ocean ridge. Cores GeoB 2204-2 and GeoB 1523-1 were obtained from the western equatorial Atlantic (Fig. 1). Station GeoB 2204 is located on the continental shelf of the Pernambuco Coast off Brazil while GeoB 1523 is located on the Ceara Rise off the northern coast of Brazil. The cores have sedimentation rates between 2.5 (GeoB 1523-1) and 4.5 cm/kyrs (GeoB 1105-4). Foraminiferal census counts were performed on samples taken at 10 cm intervals. The average resolution, therefore, is between 2 and 4 kyrs in our cores. Age scales are based on oxygen isotope stratigraphy using the surface dwelling foraminifer *Globigerinoides sacculifer* (without saclike chamber) in cores GeoB 1523-1 (Mulitza et al., 1998) and GeoB 2204-2 (Dürkoop et al., 1997) and the benthic foraminifer *Cibicoides wuellerstorfi* in core GeoB 1105-4 (Bickert and Wefer, 1996). All downcore oxygen isotope measurements were made at depth intervals of 5 cm. The oxygen isotope curve of GeoB 1105-4 was compared to a second oxygen isotope stratigraphy for core GeoB 1523-1 based on *C. wuellerstorfi* (Mulitza et al., 1998) in order to avoid time lags between age scales based on benthic and planktonic foraminifera. In all cases isotope events were determined by comparison with the SPECMAP time scale (Imbrie et al., 1984). Fig. 3 displays oxygen isotope stratigraphies of the cores used in this study.

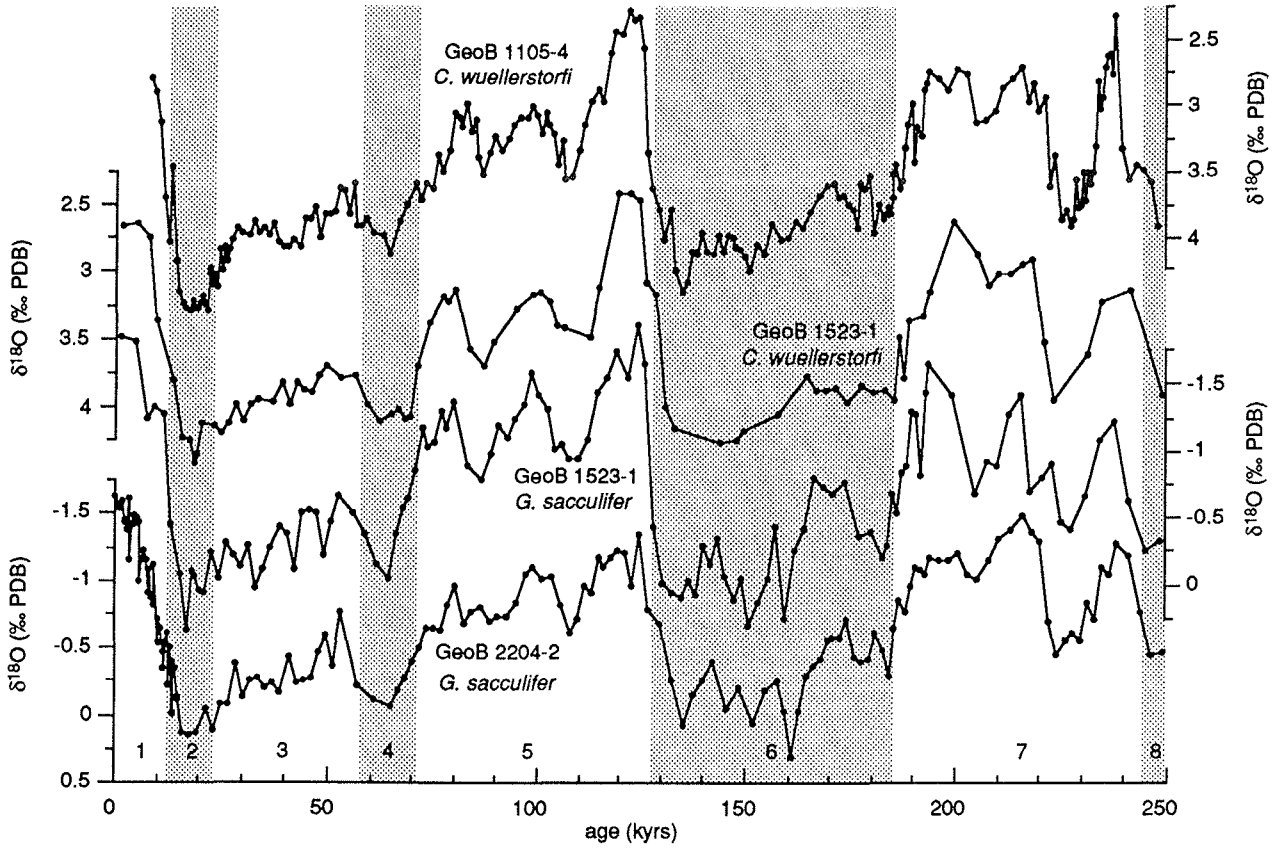

Figure 3: Oxygen isotope stratigraphy of the three cores used for thermocline reconstructions. In core GeoB 1105-4 the benthic foraminifer *C. wuellerstorfi* was used because oxygen isotope curve of the planktonic foraminifer *G. ruber* was difficult to interpret probably due to the position of the core in the equatorial upwelling region. Stratigraphies for cores GeoB 2204-2 and 1523-1 are based on planktonic foraminifer *G. sacculifer*. A second curve for GeoB 1523-1 (*C. wuellerstorfi*) is shown in order to demonstrate that no significant time lag between benthic and planktonic signals exist.

Reconstructing thermocline depth

Foraminiferal census counts have extensively been used for reconstructing sea surface temperatures (CLIMAP, 1976; CLIMAP, 1981; Prell, 1985; Pflaumann et al., 1996). They presume that foraminiferal assemblages are primarily controlled by temperature. Recently there is a growing body of evidence questioning the dominant control of sea surface temperature on planktonic foraminifera in the tropical oceans (Molfino et al., 1982; Ravelo et al., 1990; Andreasen and Ravelo, 1997; Chen and Prell, 1998). In fact, thermocline structure rather than sea-surface temperature (SST) appears to be the most important factor. Andreasen and Ravelo (1997) were the first to use these findings and designed transfer functions to calculate thermocline depths using planktonic foraminiferal census counts. They applied their methods to

Pacific core data and were able to depict a steeper east-west thermocline slope along the equator in the Pacific for the time slice of the Last Glacial Maximum (LGM).

We designed a Modern Analog Technique (MAT) to reconstruct annual mean thermocline depth in the tropical Atlantic. We defined the depth of the tropical thermocline as the depth of the 18°C isotherm which is approximately the depth of maximum temperature change with depth (Houghton, 1991; Andreasen and Ravelo, 1997). When the annual mean sea surface temperature at a location drops below 19°C, the 18°C isotherm does not longer represent a good estimate of the thermocline depth since the point of maximum temperature change moves down towards lower temperatures. In these cases we calculated the depth of the inflection point. Alternatively, the inflection point could be used in all cases, but application of the MAT to the reference samples yielded better agreement between calculated and observed values when the 18°C isotherm was used. Also, results are easier to compare with recent publications using the 18°C isotherm (Chen and Prell, 1998; Andreasen and Ravelo, 1997). In all cases we used annual mean water temperatures from Levitus and Boyer (1994).

The reference data set used comprises planktonic foraminiferal census counts of 206 surface sediment samples from the equatorial Atlantic between 20°S and 20°N. It represents a subset of the SIMMAX core-top data set published by Pflaumann et al. (1996). For this study the original data were reduced to 27 planktonic foraminferal species in both reference data set and in the core data sets.

Our modern analog technique uses the squared chord distance as dissimilarity index. This index was proposed by Ortiz and Mix (1997) as the most reliable which we can confirm by own unpublished results. Andreasen and Ravelo (1997) used this dissimilarity measure for their thermocline reconstructions as well. To get a thermocline depth for each downcore sample, the relative abundance data are presented to each sample of the reference data set and a dissimilarity index is computed. The thermocline depths of the five most similar reference samples are averaged and weighted according to their similarity.

In a first series of computations we applied the method to the surface sediment data set. For each sample a thermocline depth was calculated using the other 205 samples of the data set. Subsequently, we compared the results with the actual thermocline depths as calculated from the World Ocean Atlas (Levitus and Boyer, 1994). In a second step we calculated thermocline depths in the three tropical Atlantic gravity cores. All time series analysis and interpolation procedures in this study were done using AnalySeries (Version 1.0a7; Paillard et al., 1996).

Results

Core-tops

Application of the MAT to our entire core-top data set shows comparable correlation for both temperature and thermocline depth (Fig. 4). In a second calculation we restricted our data set to the inner tropics by allowing SST above 24°C only. On the one hand we get, as expected, a weaker correlation between calculated and measured SST. On the other hand, calculated versus measured annual mean thermocline depths still show a good correlation covering almost

the whole spectrum of existing thermocline depths in today's ocean. Therefore, it is reasonable to argue that in the inner tropics thermocline structure is more important than temperature in determining the overall planktonic foraminiferal assemblages as has previously been stated (Molfino et al., 1982; Ravelo et al., 1990; Andreasen and Ravelo, 1997; Chen and Prell, 1998).

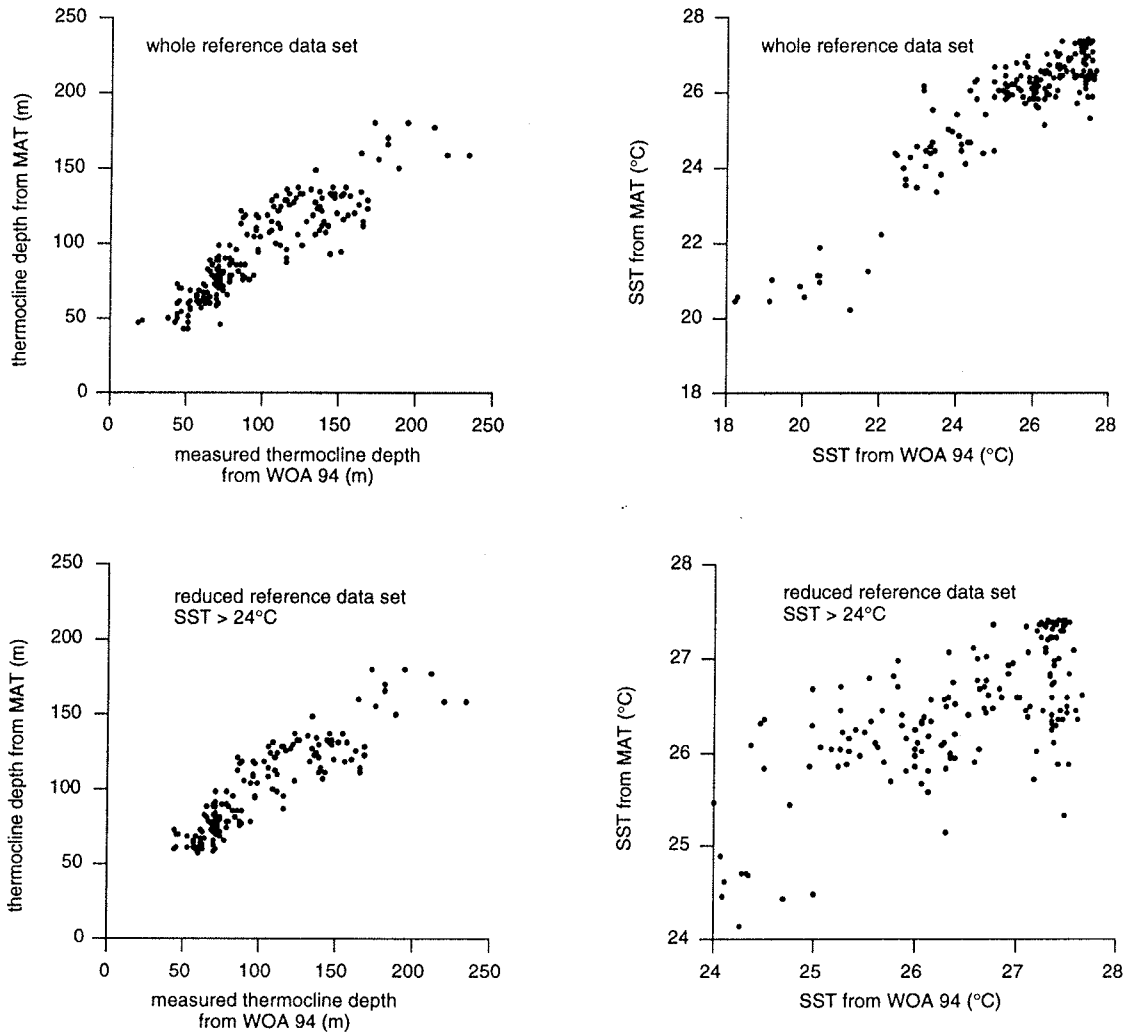

Figure 4: Results of MAT when applied to the reference data set and to a reduced reference data set. Upper left: MAT-derived thermocline depths are plotted against measured thermocline depth as deduced from the World Ocean Atlas (Levitus and Boyer, 1994). Upper right: MAT-temperatures vs. measured temperatures. Lower left and right: The reference data set was reduced so that locations with annual mean temperatures above 24°C were considered only. MAT-temperatures show weaker correlation while thermocline reconstructions are comparable to those achieved with the entire reference data set.

Downcore thermocline reconstructions

Inspection of the time series of thermocline depth calculated for our three tropical cores reveals roughly opposite trends in the west as compared to the east (Fig. 5). When the thermocline deepens in the west, it shoals in the east and vice versa. In general, this pattern can be regarded as a glacial-interglacial feature with increasing contrast in thermocline structure

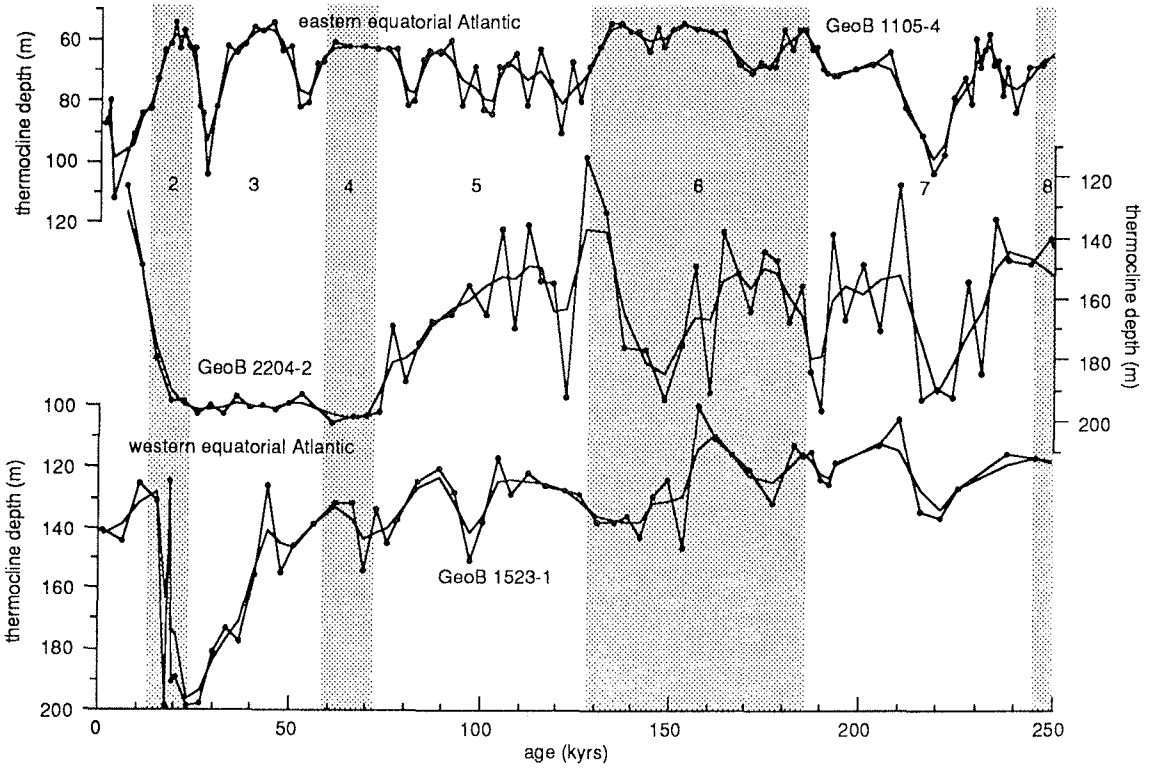

Figure 5: Thermocline reconstructions for cores GeoB 1105-4, 2204-2 and 1523-1. Each curve is represented by a time series of the calculated values (solid line with black dots) and a smoothed time series achieved with a three point running mean (solid line). Note the opposite trends in the eastern (1105-4) and the western (2204-2, 1523-1) equatorial Atlantic.

between the two regions during glacial stages. Especially the early part of isotope stage 2 shows significant deepening of the thermocline in the west contrasted by a shallower thermocline in the east. Cores GeoB 2204-2 and GeoB 1105-4 best document the opposite behaviour of the thermocline in the west in contrast to the east. Today, annual mean thermocline depth is 174 m at GeoB 2204, 144 m at GeoB 1523 and 72 m at GeoB 1105. For cores GeoB 1105-4 and 1523-1 these depths are closely matched by our core-top sample estimates. In core GeoB 2204-2 the upper 14 cm are missing so that our thermocline estimate of the first sample reflects Mid-Holocene rather than today's conditions.

In stage 2 through stage 4 the contrast between the basin parts is at a maximum while the situation during stage 5 is comparable to today. Stage 6 shows a slight deepening of the

thermocline in the west in core GeoB 2204-2, but not in the northern core GeoB 1523-1. During this period, the thermocline shallowed in the east. The strong east-west contrast as recorded for the last glacial stage, however, is not recorded for stage 6. Stage 7 does not show distinctly opposite trends in cores GeoB 2204-2 and GeoB 1105-4.

Comparing core GeoB 1523-1 with GeoB 2204-2 reveals that there are differences between thermocline characteristics in the northern and the southern part of the western equatorial Atlantic. While the more southerly core 2204-2 records a deep thermocline from stage 2 throughout the later part of stage 4, core 1523-1 shows significant lowering of the thermocline only during the later part of stage 3 and the early part of stage 2 suggesting that the governing mechanisms of upper water stratification are different in the Ceara Rise Region as opposed to the tropical Atlantic off the Pernambuco Coast of Brazil.

Generally, amplitudes of thermocline depth fluctuations are higher in the west (100 m) as compared to the east (50 m)(Fig. 5). Interestingly, temperature reconstructions from MAT based on the same data did only show minor fluctuations in core GeoB 2204-2 (own unpublished data). Thus, the species composition of the sediments may record considerable variations in thermocline depth while temperature changes are not reflected in the foraminiferal assemblages.

In order to demonstrate the east-west asymmetry in thermocline depth throughout the last 250 kyrs we calculated differences in thermocline depth between cores GeoB 2204-2 and GeoB 1105-4. The cores were brought on the same time scale by linear interpolation at 500 years intervals before subtraction. The difference curve can be regarded as a measure of the east to west thermocline gradient. In Fig. 6 the time series of the thermocline gradient is plotted together with the SPECMAP curve (Imbrie et al., 1984), the smoothed thermocline depth curves of cores GeoB 2204-2 and Geob 1105-4, and a northern hemisphere summer insolation time series (June through September, 20°N). The latter is taken as a representative curve for the strength of the African monsoon system.

The thermocline depth time series for core GeoB 1105-4 closely matches the northern hemisphere insolation curve suggesting a dominant control of the African monsoon on eastern equatorial Atlantic thermocline characteristics.

The thermocline gradient time series is roughly shaped like the SPECMAP curve suggesting an important influence of either global ice volume or higher latitude SSTs. Moreover, a significant shift between the SPECMAP curve and the thermocline gradient curve exists with the thermocline asymmetry leading the ice volume by several thousand years. This feature is particularly expressed at termination II. The shift associated with stage 2 and termination I is smaller.

The thermocline gradient curve is also compared with alkenone-derived sea surface temperature reconstructions (Fig. 7) of cores GeoB 1523-1 (Rühlemann, 1996) in the western equatorial Atlantic and GeoB 1028-5 (Schneider et al., 1995) in the subtropical southeast Atlantic (Fig. 1). Both cores are considered representative for tropical and subtropical sea surface temperatures. Paleotemperature estimates are based on the calibration of Prahl et al. (1988). Recently, this method has been extensively used in the South Atlantic (Sikes and Keigwin, 1994; Schneider et al., 1995; Müller et al., 1997). Müller et al. (1998) demonstrated

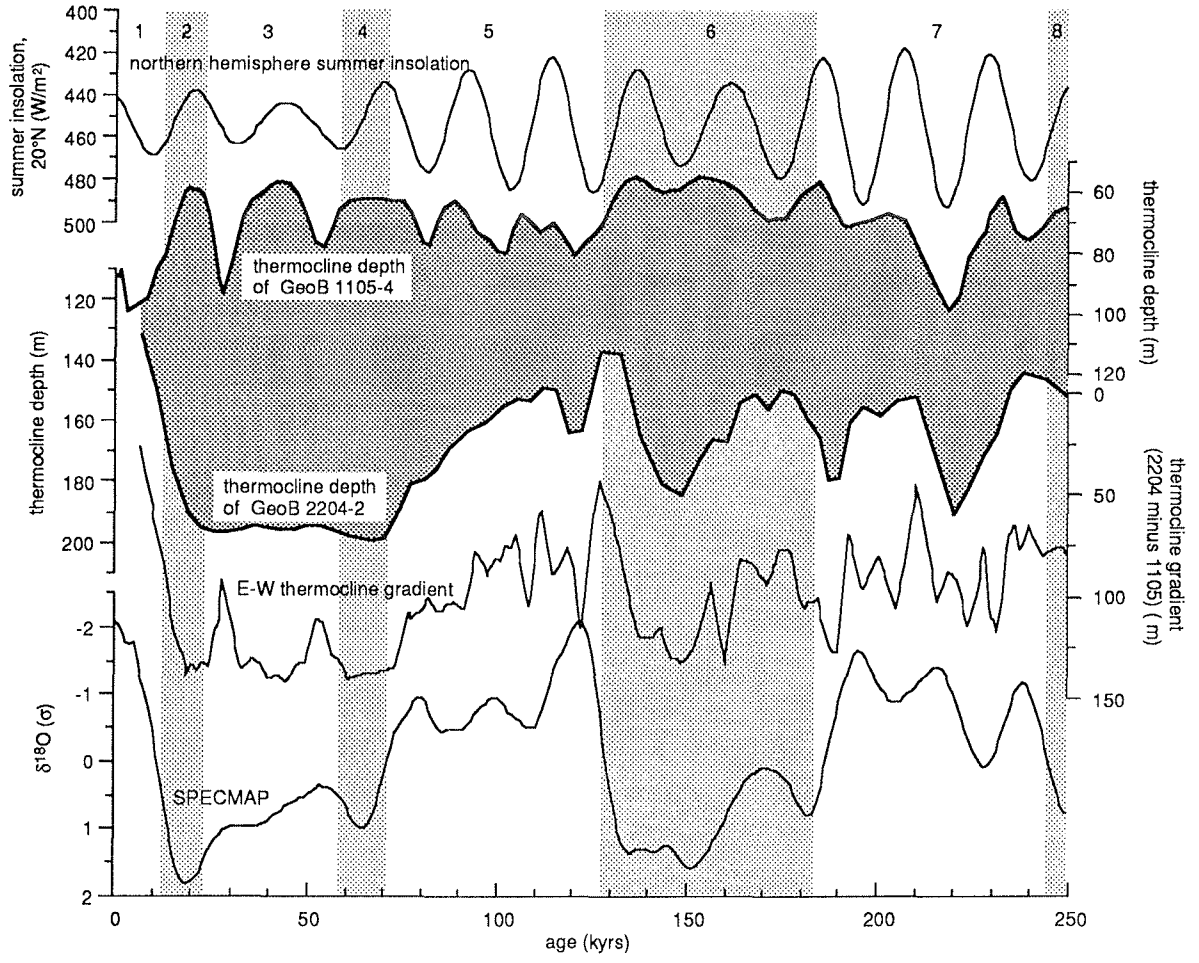

Figure 6: from top to bottom: boreal summer insolation curve (June - September) at 20°N, smoothed thermocline curve of GeoB 1105-4, smoothed thermocline curve of GeoB 2204-2, thermocline gradient curve and SPECMAP curve. Shaded area between the eastern and western equatorial Atlantic cores demonstrates the opposite trends in thermocline depth of both regions. The thermocline difference curve was achieved by subtracting thermocline depth time series of GeoB 1105-4 from thermocline depth values of GeoB 2204-2. Note similarities in shape between thermocline difference curve and SPECMAP curve as well as between the insolation curve and GeoB 1105-4 thermocline depth time series.

that South Atlantic surface sediments confirm the calibration of Prahl et al. (1988) which is valid throughout the last 250 kyrs (Müller et al., 1997).

Temperature estimates in core 1523-1 are only available for the sediments older than 30 kyrs due to very low alkenone concentrations in the younger sediments typical for low production areas in the western tropical Atlantic. The overall pattern in this core is characterized by stable sea surface temperatures between 25 °C and 27 °C. On the contrary, subtropical core GeoB 1028-5 from the Walvis Ridge shows strong temperature fluctuations varying between 16 °C and 23 °C.

In Fig. 8 we show a temperature difference curve computed for both cores. Both records were interpolated at 2 kyrs intervals before subtraction. The temperature difference time series is considered a measure for the tropical-subtropical temperature gradient in the South Atlantic. Subsequently, it is compared to the east-west thermocline gradient curve from Fig. 6. A remarkable similarity between both time series is obvious.

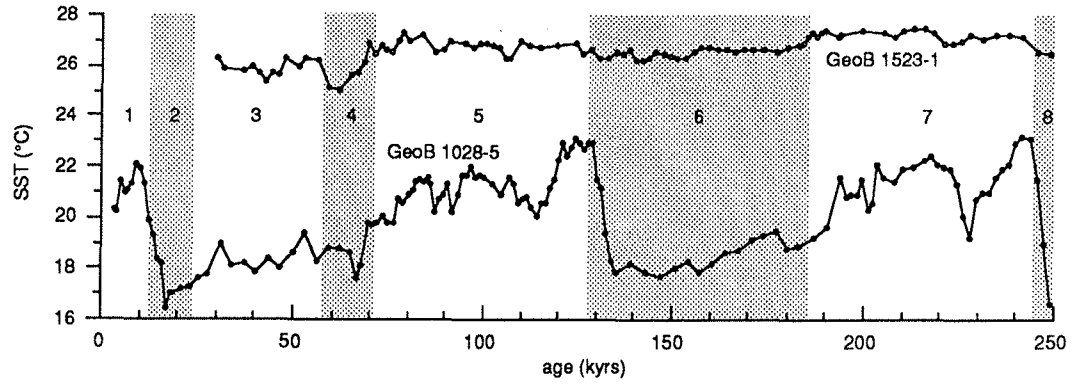

Figure 7: Sea surface temperatures at core locations GeoB 1523-1 and GeoB 1028-5 as reconstructed by the alkenone method.

Discussion

It is generally assumed that the precessional component of insolation is the governing mechanism of the tropical trade wind system (Prell and Kutzbach, 1987; Pokras and Mix, 1987; McIntyre et al., 1989; Schneider et al., 1995). Specifically, during interglacial periods northern hemisphere summer insolation maxima are assumed to promote maximum monsoonal influence coinciding with minimal zonal trade wind activity, minimal equatorial upwelling and maxima in eastern tropical Atlantic thermocline depth (McIntyre et al., 1989). In contrast, glacials are characterized by low northern hemisphere summer insolation resulting in weak monsoons over Africa, strong zonal trade winds and significant decrease in thermocline depth in the east due to increased upwelling. In general, our data from core GeoB 1105-4 confirm these models but evidence from the western equatorial core GeoB 2204-2 emphasizes a significant influence of ice shield extent and/or intermediate latitude SSTs. The good match between the SPECMAP curve and our east-west thermocline asymmetry curve reinforces speculations about further mechanisms determining the tropical wind system and sea surface hydrography. McIntyre et al. (1989) and Mix and Morey (1996) pointed out the importance of southern hemisphere climate change on the equatorial Atlantic. They attributed tropical temperature changes to variations in trade wind velocity and northward advection of heat from high southern latitudes. McIntyre et al. (1989) described the tropical Atlantic hydrography in terms of variations in northern and southern hemisphere insolation as described above plus an important influence of heat advection. The advective term is thought to be at a minimum during

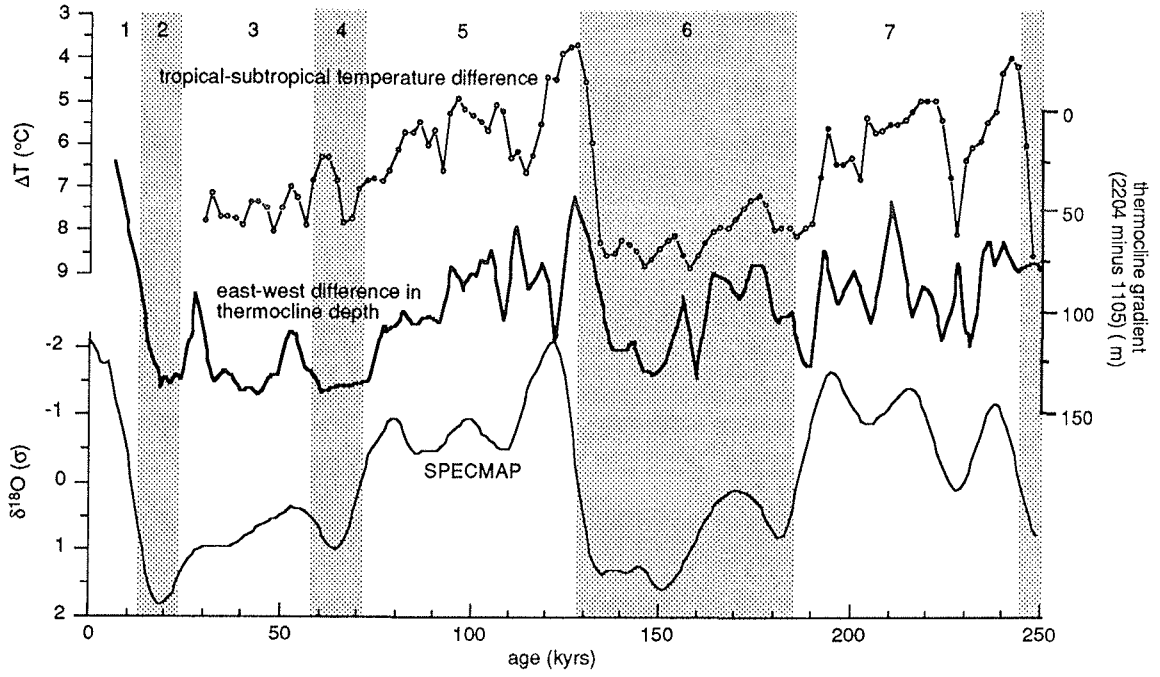

Figure 8: Upper curve: Differences between alkenone temperatures of western tropical Atlantic core GeoB 1523-1 and eastern subtropical South Atlantic core GeoB 1028-5. Middle: East-west difference in thermocline depth as shown in Fig. 6. Lower curve: SPECMAP time series. Note similarities in shape and timing of the two difference curves and the time lag of the SPECMAP curve with respect to the others.

times of high northern hemisphere summer insolation and at a maximum when southern hemisphere summer insolation is high.

Our reconstructions suggest that the higher latitude South Atlantic may play a more important role in the tropical wind system especially with respect to the western tropical Atlantic and the equatorial thermocline gradient. South Atlantic temperature reconstructions generally lead global ice volume by several millennia (Hays et al., 1976; Imbrie et al., 1989; Crowley, 1992). The tropical Atlantic thermocline gradient between east and west as depicted in this study shows a clear leading with respect to global ice volume and synchronity with respect to the tropical-subtropical alkenone temperature difference curve as shown in Fig. 8. We thus assume a major role of the meridional temperature gradient between the tropical Atlantic and the higher latitude South Atlantic as a driving force of the trade wind system. Rind (1998) demonstrated the importance of latitudinal temperature gradients in climate change. His model results showed that increased latitudinal temperature gradients intensify the Hadley circulation leading to stronger surface winds.

At the same time, a positive feedback mechanism may operate: Increasing temperature gradients between intermediate and low latitudes enhance the southern trades as the lower limb

of the Hadley circulation which, in turn, accelerates the SEC. As a result warm water is advected to the northwest and is piled up at the east coast of Brazil, whereas cold water temperatures are achieved in the eastern subtropical South Atlantic by intensified upwelling. Therefore, the temperature contrast is strengthened.

This model can explain why the time series of thermocline depth of core GeoB 2204-2 as well as the east-west difference curve show marked similarities with ice volume and southern hemisphere temperature curves. In contrast, the eastern tropical Atlantic (GeoB 1105-4) is obviously much more influenced by the African monsoon system which is governed by northern hemisphere insolation and, therefore, precessional fluctuations. Here, thermocline depth and upwelling is tightly linked to monsoonal variations.

Core GeoB 1523-1 cannot be interpreted as straight forward as the other two cores. Since it is located at 4°N on the Ceara Rise it is influenced by northern and southern trade winds (Fig. 1). Explaining the downcore record involves the difficulty of differentiation between both parts of the trade wind system. Movements of the ITCZ to the South may enhance the influence of the northern trade winds rendering difficult a simple explanation of the record.

It is well known that oxygen isotope records from Antarctic ice cores and sea surface temperature time series of the southern hemisphere lead global ice volume, oxygen isotope records from Greenland ice cores and northern hemisphere temperature reconstructions (Hays et al., 1976; Imbrie et al., 1989; Crowley, 1992; Sowers and Bender, 1995). In the South Atlantic this is true for records from higher latitudes, subtropics and equatorial regions (Imbrie et al., 1989; Schneider et al., 1995). Evidence from the Indian Ocean, however, suggests that this effect might be restricted to the Atlantic (Bard et al., 1997) because north and south Indian Ocean alkenone temperatures covering the last deglaciation parallel northern hemisphere time series.

Our data add to the evidence that consequences of Antarctic and South Atlantic climate changes leading global and northern hemisphere signals may well extend north into the tropical Atlantic. Changing temperatures in South Atlantic high and mid-latitudes modify the latitudinal temperature gradients which in turn influence the southern trade wind system as well as equatorial Atlantic thermocline characteristics. The reasons for southern hemisphere leading in a global climatic framework, however, remain to be found.

Conclusions

Relative abundances of planktonic foraminifera can be used to reconstruct the depth of the thermocline in the late Quaternary equatorial Atlantic. During glacials the E-W thermocline gradient is strongest. A significant deepening of the thermocline in the west as suggested by Curry and Lohman (1990) is in fact recorded. Contemporaneously, the thermocline shallows in the east as a response to stronger SE-trade winds and reduced monsoonal winds. The South Equatorial Current is accelerated. During interglacials the seesaw swings back and the thermocline shallows in the west and deepens in the east.

In the east the thermocline time series is matched by northern hemisphere summer insolation curves and may thus be explained in terms of a strong monsoonal influence on the mixed layer thickness. The thermocline in the west and the thermocline gradient along the equator are determined by South Atlantic meridional temperature gradients and, therefore, the South Atlantic trade wind system.

References

Andreasen, D. J., and A. C. Ravelo (1997). Tropical Pacific Ocean thermocline depth reconstructions for the last glacial maximum. *Paleoceanography 12*, 395-413.

Bard, E., F. Rostek, and C. Sonzogni (1997). Interhemispheric synchrony of the last deglaciation inferred from alkenone palaeothermometry. *Nature 385*, 707-710.

Bickert, T., and G. Wefer (1996). Late Quaternary deep water circulation in the South Atlantic: Reconstruction from carbonate dissolution and benthic stable isotopes. In G. Wefer, W. H. Berger, G. Siedler, and D. J. Webb (Eds.), *The South Atlantic - Present and Past Circulation*, pp. 599-620. Berlin: Springer.

Chen, M.-T., and W. L. Prell (1998). Faunal distribution patterns of planktonic foraminifers in surface sediments of the low-latitude Pacific. *Palaeogeography, Palaeoclimatology, Palaeoecology 137*, 55-77.

CLIMAP, P. M. (1976). The Surface of the Ice-Age Earth. *Science 191*, 1131-1137.

CLIMAP, P. M. (1981). Seasonal reconstructions of the Earth's surface at the last glacial maximum. *GSA Map and Chart Series MC-36*, 1-18.

Crowley, T. C. (1992). North Atlantic Deep Water cools the southern hemisphere. *Paleoceanography 7*, 489-497.

Curry, W. B., and G. P. Lohmann (1990). Reconstructing past particle fluxes in the tropical Atlantic Ocean. *Paleoceanography 5*, 487-506.

Dürkoop, A., W. Hale, S. Mulitza, J. Pätzold, and G. Wefer (1997). Late Quaternary variations of sea surface salinity and temperature in the western tropical Atlantic: Evidence from $\delta^{18}O$ of *Globigerinoides sacculifer*. *Paleoceanography 12*, 764-772.

Flagg, C. N., R. L. Gordon, and S. McDowell (1986). Hydrographic and current observations on the continental slope and shelf of the western equatorial Atlantic. *Journal of Physical Oceanography 16*, 1412-1429.

Hastenrath, S., and J. Merle (1987). Annual cycle of subsurface thermal structure in the tropical Atlantic Ocean. *Journal of Physical Research 17*, 1518-1538.

Hays, J. D., J. Imbrie, and N. J. Shackleton (1976). Variations in the Earth's orbit: Pacemaker of the ice ages. *Science 194*, 1121- 1132.

Houghton, R. W. (1991). The relationship of sea surface temperature to thermocline depth at annual and interannual time scales in the tropical Atlantic Ocean. *Journal of Geophysical Research 96*, 15173-15185.

Imbrie, J., J. D. Hays, D. G. Martinson, A. McIntyre, A. C. Mix, J. J. Morley, N. G. Pisias, W. L. Prell, and N. J. Shackleton (1984). The orbital theory of Pleistocene climate: support from a revised chronology of the marine $\delta^{18}O$ record. In A. Berger, J. Imbrie, J. Hays, G. Kukla, and B. Saltzman (Eds.), *Milankovitch and climate, Part I*, pp. 269-305. Dordrecht: D. Reidel.

Imbrie, J., A. McIntyre, and A. Mix (1989). Oceanic response to orbital forcing in the late Quaternary: Observational and experimental strategies. In A. Berger (Ed.), *Climate and Geo-Sciences*, pp. 121-164. Kluwer Academic Publishers.

Johns, W. E., T. N. Lee, F. A. Schott, R. J. Zantopp, and R. H. Evans (1990). The North Brazil current retroflection: Seasonal structure and eddy variability. *Journal of Geophysical Research 95*, 22103-22120.

Levitus, S., and T. P. Boyer (1994). *World Ocean Atlas 1994, Volume 4: Temperature.*

McIntyre, A., W. F. Ruddiman, K. Karlin, and A. C. Mix (1989). Surface water response of the equatorial Atlantic Ocean to orbital forcing. *Paleoceanography 4*, 19-55.

Mix, A. C., W. F. Ruddiman, and A. McIntyre (1986). Late Quaternary paleoceanography of the tropical Atlantic, 1: Spatial variability of annual mean sea-surface temperatures, 0-20,000 years B.P. *Paleoceanography 1*, 43-66.

Mix, A. C., and A. E. Morey (1996). Climate feedback and Pleistocene variations in the Atlantic south equatorial current. In G. Wefer, W. H. Berger, G. Siedler, and D. J. Webb (Eds.), *The South Atlantic - Present and Past Circulation*, pp. 503-525. Berlin: Springer.

Molfino, B., N. G. Kipp, and J. J. Morley (1982). Comparison of Foraminiferal Coccolithophorid, and Radiolarian Paleotemperature Equations: Assemblage Coherency and Estimate Concordancy. *Quaternary Research 17*, 279-313.

Molinari, R. L., S. L. Garzoli, E. J. Katz, D. E. Harrison, P. L. Richardson, and G. A. Reverdin (1986). A synthesis of the first GARP global experiment in the equatorial Atlantic Ocean. *Prog. Oceanogr. 16*, 91-112.

Mulitza, S., C. Rühlemann, T. Bickert, W. Hale, J. Pätzold, and G. Wefer (1998). Late Quaternary $\delta^{13}C$ gradients and carbonate accumulation in the western equatorial Atlantic. *Earth and Planetary Science Letters 155*, 237-249.

Müller, P. J., M. Cepek, G. Ruhland, and R. R. Schneider (1997). Alkenone and coccolithophorid species changes in late Quaternary sediments from the Walvis Ridge: Implications for the alkenone paleotemperature method. *Palaeogeography Palaeoclimatology Palaeoecology 135*, 71-96.

Müller, P. J., G. Kirst, R. G., I. von Storch, and A. Rosell-Mele (1998). Calibration of the alkeneone paleotemperature index $U^{k'}_{37}$ based on core-tops from the eastern South Atlantic and the global ocean. *Geochimica et Cosmochimica Acta* , in press.

Open University Course Team (1989). *Ocean Circulation.* Cambridge: Open University/ Pergamon.

Ortiz, J. D., and A. C. Mix (1997). Comparison of Imbrie-Kipp transfer function and modern analog temperature estimates using sediment trap and core top foraminiferal faunas. *Paleoceanography 12*, 175-190.

Paillard, D., L. Labeyrie, and P. Yiou (1996). Macintosh program performs time-series analysis. *Eos Transactions AGU 77*, 379.

Pflaumann, U., J. Duprat, C. Pujol, and L. D. Labeyrie (1996). SIMMAX: A modern analog technique to deduce Atlantic sea surface temperatures from planktonic foraminifera in deep-sea sediments. *Paleoceanography 11*, 15-35.

Picaut, J., P. Servain, M. LeComte, M. Seva, S. Lukas, and G. Rougier (1985). *FOCAL climatic atlas of the tropical Atlantic, wind stress and sea surface temperature 1964-1979.* Brest, France: Université de Bretagne Occidentale.

Pokras, E. M., and A. C. Mix (1987). Earth's precession cycle and Quaternary climatic change in tropical Africa. *Nature 326*, 486-487.

Prahl, F. G., L. A. Muehlhausen, and D. L. Zahnle (1988). Further evaluation of long-chain alkenones as indicators of paleoceanographic conditions. *Geochimica et Cosmochimica Acta 52*, 2303-2310.

Prell, W. L. (1985). *The stability of low-latitude sea surface temperatures: An evaluation of the CLIMAP reconstruction with emphasis on the positive SST anomalies.* Dep. of Energy, Washington D.C.

Prell, W. L., and J. E. Kutzbach (1987). Monsoon variability over the past 150,000 years. *Journal of Geophysical Research 92*, 8411- 8425.

Ravelo, A. C., R. G. Fairbanks, and S. G. H. Philander (1990). Reconstructing tropical Atlantic hydrography using planktonic foraminifera and an ocean model. *Paleoceanography 5*, 409-431.

Richardson, P. L., S. Arnault, S. Garzoli, and J. G. Bruce (1991). Annual cycle of the North Equatorial Countercurrent. *Deep-Sea Research 39*, 997-1014.

Rind, D. (1998). Latitudinal temperature gradients and climate change. *Journal of Geophysical Research 103*, 5943-5971.

Rühlemann, C. (1996). Akkumulation von Carbonat und organischem Kohlenstoff im tropischen Atlantik: Spätquartäre Produktivitäts-Variationen und ihre Steuerungsmechanismen. *Berichte FB Geowissenschaften Universität Bremen 84*, 139 pp.

Rühlemann, C., P. J. Müller, and R. R. Schneider (1998). Organic carbon and carbonate as paleoproductivity proxies: Examples from high and low productivity areas of the tropical Atlantic. In: G. Fischer and G. Wefer (Eds): *Proxies in paleoceanography: Examples from the South Atlantic*, Berlin: Springer, in press.

Schneider, R. R., P. J. Müller, and G. Ruhland (1995). Late Quaternary surface circulation in the east equatorial South Atlantic: Evidence from alkenone sea surface temperatures. *Paleoceanography 10*, 197-219.

Sikes, E. L., and L. D. Keigwin (1994). Equatorial Atlantic sea surface temperature for the last 30 ky: A comparison of $U^{k'}_{37}$, $\delta^{18}O$, and foraminiferal assemblage temperature estimates based analysis on controls of foraminiferal estimates. *Paleoceanography 9*, 31-46.

Sowers, T., and M. Bender (1995). Climate records covering the last deglaciation. *Science 269*, 210-214.

Sverdrup, H. U., M. W. Johnson, and R. H. Fleming (1942). *The oceans: their physics, chemistry and general biology*. Englewood Cliffs: Prentice-Hall.

Wefer, G., W. H. Berger, T. Bickert, B. Donner, G. Fischer, S. Kemle-von Mücke, G. Meinecke, P. J. Müller, S. Mulitza, H. S. Niebler, J. Pätzold, H. Schmidt, R. R. Schneider, and M. Segl (1996). Late Quaternary Surface Circulation of the South Atlantic: The Stable Isotope Record and Implications for Heat Transport and Productivity. In G. Wefer, W. H. Berger, G. Siedler, and D. J. Webb (Eds.), *The South Atlantic - Present and Past Circulation*, pp. 461-502. Berlin: Springer.

Chapter 6

Simulation of oxygen isotopes in a global ocean model

Andre Paul
Stefan Mulitza
Jürgen Pätzold
Tobias Wolff

in: G. Fischer and G. Wefer (eds): Proxies in paleoceanography: Examples from the South Atlantic, Springer, Berlin, in press

Abstract

First a short account on climate modelling in general is given. Then the results of a numerical simulation of oxygen isotopes in the ocean are presented.
The isotopes are added to the Geophysical Fluid Dynamics Laboratory (GFDL) Modular Ocean Model (MOM). The model is forced at the surface by the seasonal cycles of climatological sea surface temperature, sea surface salinity and wind stress. The surface boundary condition on the oxygen isotopes is based on a set of $\delta^{18}O_w$-salinity relationships applied to the seasonal cycle of climatological sea surface salinity.
In present-day oceanography the oxygen isotope composition of seawater $\delta^{18}O_w$ is a tracer much like salinity. In combination with temperature and salinity it may be used to define water masses and differentiate between the effects of local evaporation and precipitation, sea ice formation and decay, river run-off and glacial meltwater. We compare our results with GEOSECS $\delta^{18}O_w$ data and show how model deficiencies are reflected in the representation of Antarctic intermediate and bottom waters.
Using a paleotemperature equation we can also compute the equilibrium fractionation of the oxygen isotope composition of calcite $\delta^{18}O_c$ from the simulated temperature and $\delta^{18}O_w$ fields. This is of particular importance for paleoceanographic studies. In principle we can now check the model circulation against spatial distributions of benthic foraminiferal $\delta^{18}O$. But from oxygen isotope records of benthic foraminifera at a considerable number of core sites we conclude that in praxis the warm bias typical for many ocean models can spoil this check. In order to supply the temperature information missing from the deep sea cores this warm bias must be reduced significantly, possibly by implementing an isopycnal transport parameterization.
Finally we present the isotopic composition of the net surface freshwater flux that can be diagnosed from the model, and we discuss the prospect of simulating oxygen isotopes at the Last Glacial Maximum (LGM).

Introduction

Isotopes in the water molecule (H_2O) are powerful tracers that can be followed through the different stages of the hydrological cycle (Schlotterer et al., 1996). In the geosciences, one radioactive isotope, tritium (^3H), and two stable isotopes, deuterium (^2H) and oxygen-18 (^{18}O), are considered. A water molecule containing either of these isotopes is heavier than a normal water molecule. Therefore, water vapor evaporating from the sea surface is depleted in heavy isotopes relative to ocean water, while rain precipitating from a cloud is enriched relative to the cloud moisture. Whenever a water sample undergoes a phase transition (e.g., evaporation or condensation), isotopic fractionation occurs that is dependent on temperature.

As a result, the isotopic composition of freshwater derived from precipitation shows a large variation with latitude, height and continentality. The variation in the isotopic composition of seawater is comparatively small and mainly determined by freshwater input and mixing between water masses.

So far the stable isotopes deuterium and oxygen-18 have been incorporated into four atmospheric models: the LMD model (Joussaume et al., 1984; Joussaume and Jouzel, 1993), the NASA/GISS model (Jouzel et al., 1987), the ECHAM model (Hoffmann and Heimann, 1993; Hoffmann, 1995) and the GENESIS model (Mathieu, 1996). As these models account for the various fractionation processes that occur at the sea surface and all succeeding stages of the hydrological cycle, they provide a tool for calculating the isotopic content of precipitation δP as well as of evaporation δE (Juillet-Leclerc et al., 1997). Prior to their development there was no way to estimate δE independently (Craig and Gordon, 1965). With respect to oxygen-18, the δ-notation means that the $^{18}O/^{16}O$ ratio is given as the fractional difference between the ratio in the water sample, R_{sample}, to the ratio in Vienna Standard Mean Ocean Water (V-SMOW) or some other standard, $R_{standard}$, expressed in permil: $\delta = (R_{sample} - R_{standard})/R_{standard} \times 1000$.

The distributions of both salinity S and oxygen isotope composition of seawater $\delta^{18}O_w$ or simply δ_w are mainly controlled by the same two processes precipitation P and evaporation E. Locally, S and δ_w of surface waters are linearly related. However, the slope of the δ_w-S relationship varies between 0.1 for tropical surface waters and 0.6 for high-latitude surface waters. This reflects the so-called temperature effect: in high latitudes, precipitation occurs at lower temperatures and is more enriched in oxygen-18 than in low latitudes, which leads to a strong depletion of the remaining cloud moisture. Furthermore, salinity is influenced by freezing of sea ice, but δ_w is almost not. Thus surface waters of the Southern Ocean show a wide range of salinities although $\delta_w \sim 0.3$ is nearly constant. Finally freshwater input from rivers or ice sheets can also modify the δ_w-S relationship. Hence S and δ_w label the surface waters in different ways. Mixing of water masses that originate from the sea surface creates the characteristic vertical sections known from GEOSECS (Birchfield, 1987; Östlund et al., 1987).

In present-day oceanography δ_w allows to distinguish between different freshwater sources. Thus it is possible to investigate the influence of local P-E, sea ice formation and decay, river-runoff and glacial meltwater on a water mass of interest (Weiss et al., 1979; Jacobs et al., 1993; Bauch, 1995; Toggweiler and Samuels, 1995).
Paleoceanographic applications rest on the isotope content preserved in benthic and planktonic foraminifera. For example, Broecker (1986; 1989) uses benthic and planktonic foraminifera to constrain tropical SSTs and to determine the salinity contrast between tropical Atlantic and Pacific, and Duplessy et al. (1991) present a reconstruction of Last Glacial Maximum (LGM) sea surface salinities (SSS) derived from planktonic foraminifera. A number of studies address the vertical structure of the ice-age ocean (e.g., Birchfield, 1987; Zahn and Mix, 1991; Labeyrie et al., 1992).

In a paleoceanographic setting in which there is no direct proxy for salinity, the oxygen isotope composition of seawater δ_w and temperature T can be combined to characterize different water masses. If a global ocean model is used to simulate δ_w and T, the equilibrium

fractionation of the oxygen isotope composition of calcite $\delta^{18}O_c$ or simply δ_c can be uniquely determined from a paleotemperature equation and compared with benthic foraminiferal $\delta^{18}O$. Here we test these ideas and apply them to the present-day situation. We incorporate δ_w into an ocean model and find that it can indeed serve to trace the formation and spreading of deep and bottom waters. But in order to compute δ_c a warm bias that is a widespread problem in ocean modelling must be reduced.

Short account on climate modelling

In the following we want to give a short account on the basis and mechanisms of climate models. More complete but still very readable accounts on climate modelling in general are the books by Washington and Parkinson (1986) and McGuffie and Henderson-Sellers (1996). Although somewhat more technical, the articles on ocean modelling in particular by Cane (1986) and Semtner (1986) are also quite useful.
A climate model is an attempt to simulate all processes that determine the real climate. It can improve our understanding of these processes, as well as of the interactions among them. Furthermore it can be used for forecasting future conditions or, in a paleoceanographic setting, 'hindcasting' past conditions. This is accomplished by solving numerically the fundamental equations that govern the motions of the atmosphere, oceans and sea ice.
These fundamental equations are derived from the basic laws of physics, particularly the conservation laws for momentum, mass and energy.

Conservation of momentum

Applied to the atmosphere or ocean, the law of conservation of momentum asserts that the net force exerted on an air or water parcel equals the time rate of change of its momentum, which is the product of its mass and velocity. The major forces acting on an air or water parcel are the frictional forces, the gravitational force, the pressure gradient force and the forces resulting from the Earth's rotation.

Conservation of mass

The law of conservation of mass states that the mass transports entering or leaving a volume of air or water must balance in such a way that mass is conserved. This law is often referred to as the equation of continuity.

Conservation of energy

The temperature of an air or water parcel is a measure for its internal energy. The law of conservation of internal energy is called the first law of thermodynamics which equates the time rate of change of internal energy to the work done on an air or water parcel by compression or expansion of its volume and the net heat gain or loss from external forces.

Equation of state

In addition to the three conservation laws, atmospheric or ocean models require an equation of state which relates several of the variables in the other equations to each other. For the atmosphere, the equation of state is called the ideal gas law. It expresses a relationship between the density, pressure, temperature and humidity of air. For the ocean, the equation of state relates seawater density to pressure, temperature and salinity. The ocean model to be described in the next section employs the equation of state as it has been defined by the Joint Panel on Oceanographic Tables and Standards (UNESCO, 1981).

Prediction equations for active and passive tracers

In addition to the variables velocity, temperature and pressure, atmospheric models contain a humidity variable and ocean models contain a salinity variable. Since they enter the equation of state and cause density differences which drive atmospheric or ocean circulations, they are called active tracers. Further variables that do not influence circulations are called passive tracers. For each tracer a prediction equation is required which is obtained from a conservation law, in anology to the conservation of mass.

Approximations

Several standard approximations are used to simplify the fundamental equations. On the large scale, ocean motions are shallow and slow, and the gravitational force and the vertical gradient of pressure are balanced very well. This means that the time rate of change of vertical velocity is negligible compared to other terms in the conservation of momentum (Cane, 1986). Therefore, in the hydrostatic approximation, it is dropped.

Since seawater is nearly incompressible, the time rate of change of density is neglected in the equation of continuity, but density variations are generally included as far as buoyancy effects are concerned. This is called the Boussinesq approximation (Washington and Parkinson, 1986). Furthermore, in the conservation of energy the work done on a water parcel by compression or expansion of its volume can be ignored, and the net heat gain or loss from external sources now explicitly includes the vertical and horizontal eddy diffusions of heat.
In many ocean models the surface is assumed to be a horizontal rigid lid, whereby no vertical motion is allowed at the top of the ocean. This boundary condition suppresses high frequency external gravity waves and allows a longer time step.

Discretization

The first step in solving the model equations is to discretize them. Some atmospheric models and most ocean models compute the temporal evolution of the variables velocity, temperature, humidity or salinity on a three-dimensional grid spanning the domain of interest. Usually this grid is obtained by dividing the atmosphere or ocean into a number of boxes. A set of coupled non-linear finite difference equations results which then is solved by various numerical techniques, using a timestep approach.

Initial and boundary conditions

The fundamental equations for the atmosphere and oceans involve spatial as well as temporal derivatives. In order to step these equations through time, values for all variables must be specified in space at some starting instant. This set of starting values in three-dimensional space is the set of initial conditions. Furthermore a set of boundary conditions must also be specified at the upper and lower boundaries as well as the lateral boundaries of the domain. For example, at the ocean bottom the flow is required to parallel the slope.

A note of caution

Numerical modeling studies shed light on modeled phenomena, but extrapolations from model results to the corresponding geophysical phenomena should not be done without caution (Washington and Parkinson, 1986). This is because the controlled nature of modeling experiments allows far more precise conclusions to be stated about modeled phenomena than are possible regarding the corresponding phenomena in the real world.

Ocean model

The governing equations of the ocean model used in the present study are the primitive equations in spherical coordinates. The primitive equations differ from the fundamental equations in that the hydrostatic, Boussinesq and rigid-lid approximations are applied (see above). The ocean model is based on the Modular Ocean Model (MOM) 2.2 of the Geophysical Fluid Dynamics Laboratory (GFDL) (Pacanowski, 1996). Additional features are the ability to taper the horizontal viscosity and diffusivity coefficents in order to satisfy the viscous stability criterion (Weaver and Hughes, 1996; NCAR Oceanography Section, 1996) and the inclusion of extra metric terms in the momentum equations in order to preserve solid body rotation (Wajsowicz, 1993).

The model resolution, land-sea mask and bathymetry are the same as in the coarse-resolution ocean model of Large et al. (1997). The only exception is that two deep vertical levels are added, such that the maximum model depth is now 5900 m, and that there are 27 vertical levels in total, monotonically increasing in thickness from 12 m near the surface to 450 m near the bottom. The longitudinal resolution is 3.6°. The latitudinal resolution is 1.8° near the Equator (to better resolve the Equatorial currents), increases away from the Equator to a maximum of 3.4°, then decreases in the mid-latitudes as the cosine of latitude (to maintain horizontally isotropic arid boxes) and is finally kept constant at 1.8° polewerd of 60° (to prevent any further restrictions on the model time step).

The continental outlines of the model are shown in Figure 1. While the 9.4°-wide Drake Passage closely matches its actual width, the Indonesian Channel, the Florida Straits and the connections to the Sea of Japan are much wider than in reality. Furthermore the Bering and Gibraltar Straits and the Red Sea outflow are closed.

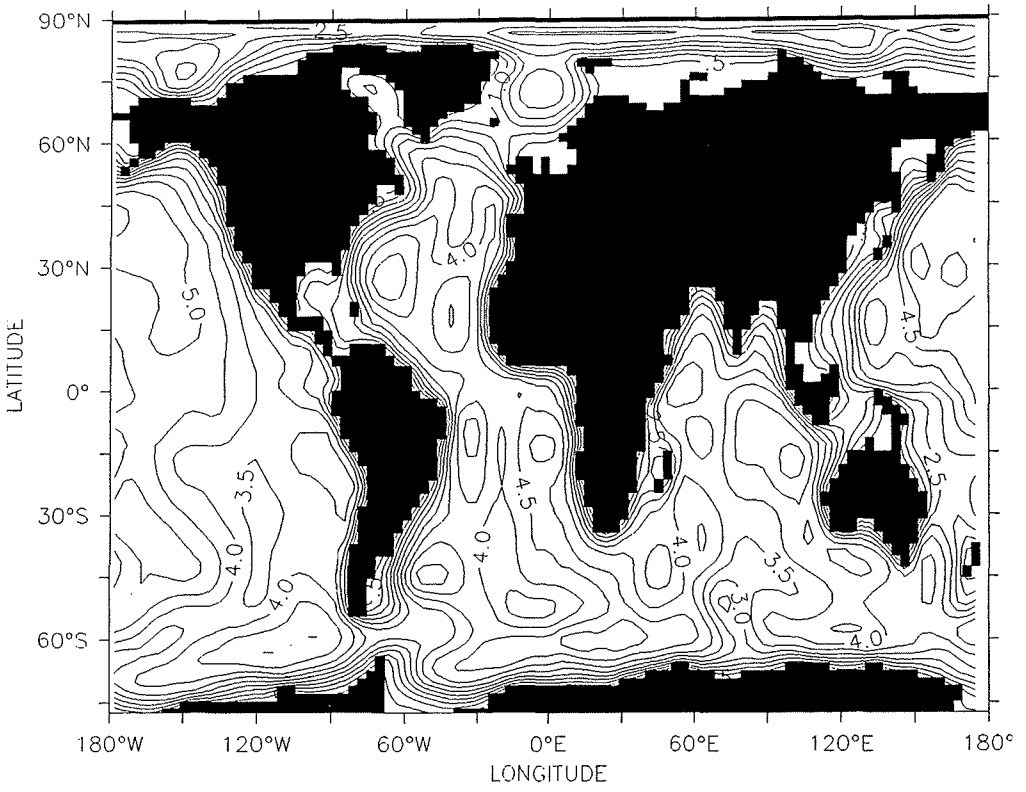

Figure 1: Continental outlines and bathymetry of the model. Contour interval is 0.5 km.

The bathymetry used in the present study is derived from the bathymetry used by Large et al. (1997), which in turn is based on the data from the NOAA National Geophysical Data Center (Sloss, 1988). This bathymetry is fairly realistic, e.g., the maximum depths of the Denmark Strait and Faroe-Iceland ridge are 734 m and 903 m. Regions deeper than 5000 m are filled in from the ETOPO5 topography data (NCAR Data Support Section, 1986).

Since the horizontal resolution is coarser than the Rossby radius of deformation at all latitudes, the effects of mesoscale eddies are only parameterized in terms of enhanced viscosity and diffusion. The horizontal viscosity is $A_{MH} = 2.5 \times 10^5$ m^2 s^{-1}. The vertical viscosity is $A_{MV} = 16.7 \times 10^{-4}$ m^2 s^{-1}. Following Bryan and Lewis (1979), depth-dependent horizontal and vertical diffusivities are employed. Hence

$$A_{\tau H}(z) = A_{BH} + (A_{SH}-A_{BH}) \exp(-z/500\text{m}), \quad (1)$$

such that the horizontal eddy diffusion $A_{\tau H}$ decreases from $A_{SH} = 0.8 \times 10^6$ m^2 s^{-1} in the top layer to $A_{BH} = 0.4 \times 10^6$ m^2 s^{-1} in the bottom layer. Furthermore

$$A_{\tau H}(z) = A^* + C_r/\pi \ \arctan [\lambda(z-z^*]\,, \quad (2)$$

where $A^* = 0.6 \times 10^{-4}$ m^2 s^{-1}, $C_r = 1.0 \times 10^{-4}$ m^2 s^{-1}, $\lambda = $ m^{-1} and $z^* = 1000$ m (Weaver and Hughes, 1996), such that the vertical viscosity $A_{\tau H}$ is about 0.1×10^{-4} m^2 s^{-1} at the surface and

1.1×10^{-4} m^2 s^{-1} in the deep ocean. To increase the permissible time step, the flow variables are Fourier filtered north of 75° N, and the horizontal viscosity A_{MH} is tapered north of 81.9° N.

The oxygen isotope composition of seawater δ_w is introduced as a third tracer. It is passive in the sense that it does not influence the ocean circulation.

In the control experiment (Experiment A), the acceleration technique of Bryan (1984) is used to accelerate the approach to equilibrium in the deep ocean. Thus, in the first stage, the tracer time step is ten times larger in the deep ocean than at the surface. Furthermore the surface tracer time step is ten times larger than the time step of 3504 s for the momentum and barotropic streamfunction equations. In the second stage, the integration is continued with equal time steps of 3504 s for all equations at all depths. The length of the accelerated phase is 96 momentum years, 960 surface tracer years and 9600 deep tracer years, as in the experiments of Large et al. (1997). The length of the synchronous phase is 15 years, which is the minimum length recommended by Danabasoglu et al. (1996). In the sensitivity experiment (Experiment B), the length of the accelerated phase is 20 momentum years, 200 surface tracer years and 2000 deep tracer years, and the length of the synchronous phase is 15 years.

Experiment A is started from a set of initial conditions that corresponds to a state of rest with January-mean distributions of potential temperature and salinity from Levitus (1982). The converged state at the end of the accelerated phase of Experiment A is then used as the set of initial conditions for Experiment B.

The set of boundary conditions at the ocean surface consists of mid-month fields of the zonal and meridional wind stress components, the sea surface temperature, the sea surface salinity and the sea surface oxygen isotope composition. The surface wind stress fields are obtained from the NCEP reanalysis data covering the four years 1985 through 1988 (Kalnay et al., 1996), and the surface temperature and salinity fields are derived from the climatologies of Shea et al. (1990) and Levitus (1982), as described by Large et al. (1997).

The surface δ_w forcing field is computed from the mid-month fields of the sea surface salinity using a set of seven δ_w-salinity relationships, in a manner similar to Fairbanks et al. (1992). The δ_w and salinity data are taken from GEOSECS (Östlund et al., 1987), Mackensen et al. (1996), Bauch (1995) and Vetshteyn et al. (1974). The set of δ_w-salinity relationships is depicted in Figure 2 and summarized in Table 1.

All tracer equations are linearly restored to the surface forcing fields with a 50-day time constant relative to the upper 50 m. The fraction of a grid cell covered by sea ice is diagnosed from the climatology and subject to a strong restoring in temperature only, with a 6-day time constant relative to the upper 50 m (Large et al., 1997)

Two different experiments are performed: In Experiment A, a slope of 1.030 and an abscissa of -35.80 is used to compute the isotopic composition of Antarctic Surface Water (AASW). In Experiment B, a constant value of -0.31‰ is used. This latter experiment takes into account that in polar regions salinity is influenced by freezing of sea ice, but $\delta^{18}O_w$ is almost not.

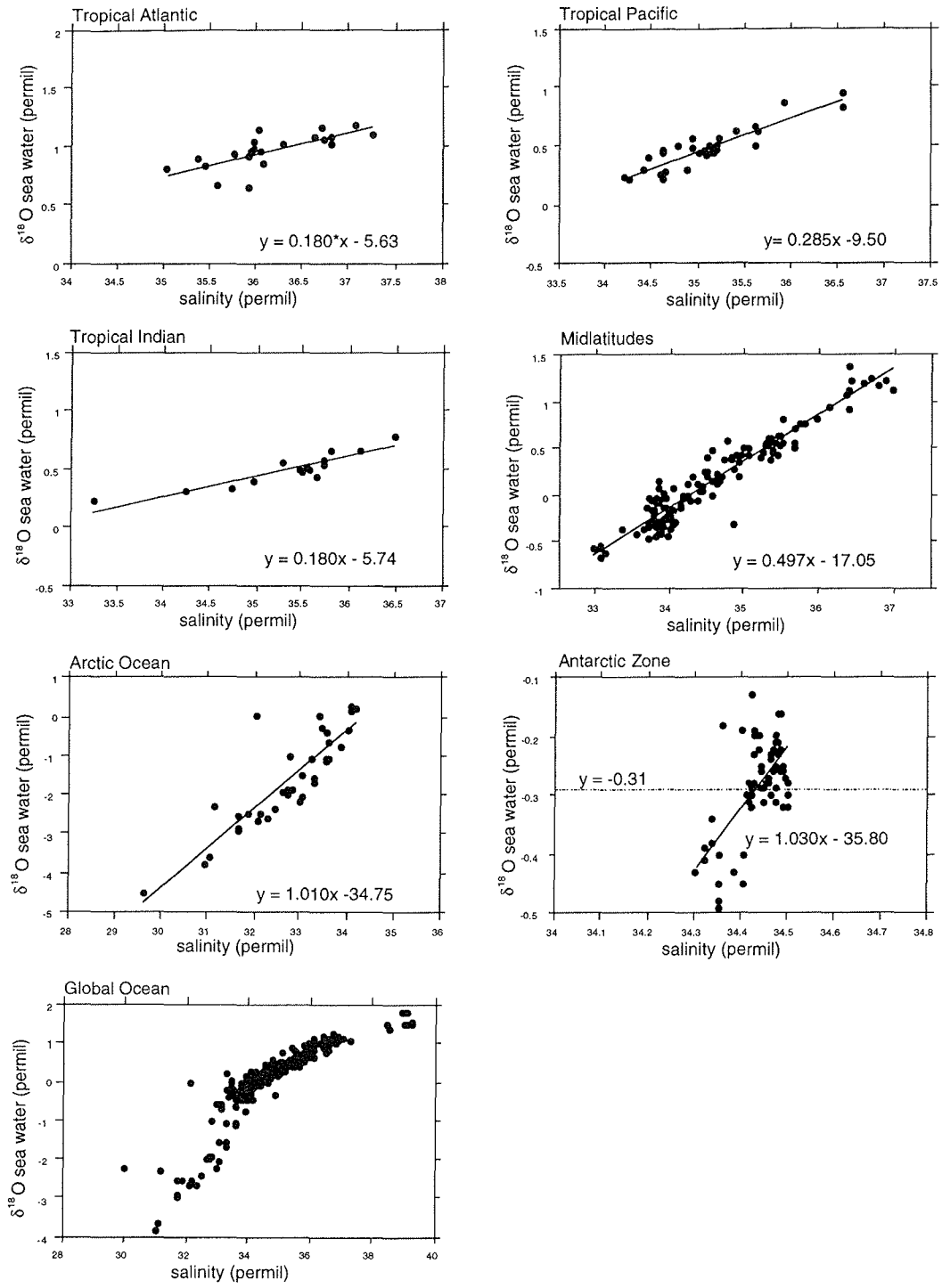

Figure 2: δ_w-salinity relationships for various regions of the global ocean,based on the GEOSECS data. The Tropics extend from 25° S to 25° N. The Arctic Ocean includes the North Atlantic Ocean north of 60° N. The term Antarctic Zone is used to describe the Southern Ocean surface waters south of the 2° C-isotherme. The δ_w-salinity relationship for the Midlatitudes is applied to the remaining regions of the global ocean.

Region	Slope	Abscissa	Note	Reference
Arctic Ocean	1.010	-34.75		Vetshteyn et al., 1974 Bauch, 1995
Tropical Atlantic	0.180	-5.63		GEOSECS
Tropical Pacific	0.285	-9.50		GEOSECS
Tropical Indian	0.180	-5.74		GEOSECS
Midlatitudes	0.497	-17.05		GEOSECS
Antarctic Zone	1.030	-35.80	Experiment A	Mackensen et al. 1996
	0.000	-0.31	Experiment B	

Table 1: Slopes and abscissas of δ_w-S relationship

Results

Barotropic streamfunction

The vertically integrated volume transport is presented in Figure 3. Here we use a streamfunction map rather than a vector map because on a global scale a streamfunction map is easier to visualize. The flow is directed along the streamlines, with the sense of rotation clockwise for positive values and anti-clockwise for negative values of the streamfunction. The flow rate through any line intersecting two adjacent streamlines is given by the contour interval.

The spatial features of the vertically integrated mass transport are determined by the wind forcing and the bathymetry. Because of the identical winds and the almost identical bathymetry, all gyre patterns and transport magnitudes are very similar to the solutions of Large et al. (1997). The major currents and passage throughflows are reproduced reasonably well.

In the Northern Hemisphere, the maximum transport in the Gulf Stream is 21 Sv. This is lower than that observed, which is about 40 Sv at 30° N, upstream of the recirculation regime (Knauss, 1969), or 32.2±3.2 Sv for the Florida Current alone (Larsen, 1992). The maximum transport in the Kuroshio is low, too. The Atlantic inflow into the Nordic Seas is 4 Sv, about half the observational estimate by Gould et al. (1985).

In the Southern Hemisphere, we obtain for the Agulhas Current a maximum transport of 62 Sv. This is in good agreement with the estimates of Gordon et al. (1987) and Stramma and Lutjeharms (1996). The 25 Sv-flow through the Mozambique Channel is significantly stronger than the 5 Sv observed by Stramma and Lutjeharms (1996). The flow in the Benguela Current is 12 Sv. According to Garzoli and Gordon (1996), the observed transport at 30° S in the upper kilometer of the ocean is 13 Sv, with considerable seasonal variations. The maximum Brazil Current transport amounts to 30 Sv, on the high side of the estimate of Peterson and Stramma (1991).

A distinct feature of the vertically integrated mass transport is the Antarctic Circumpolar Current (ACC). The flow through Drake Passage is 225 Sv. An observational estimate for this flow is 130±20 Sv (Whitworth and Peterson, 1985). Thus it is clearly overestimated in our model. As demonstrated by Danabasoglu and McWilliams (1995), the ACC flow through the

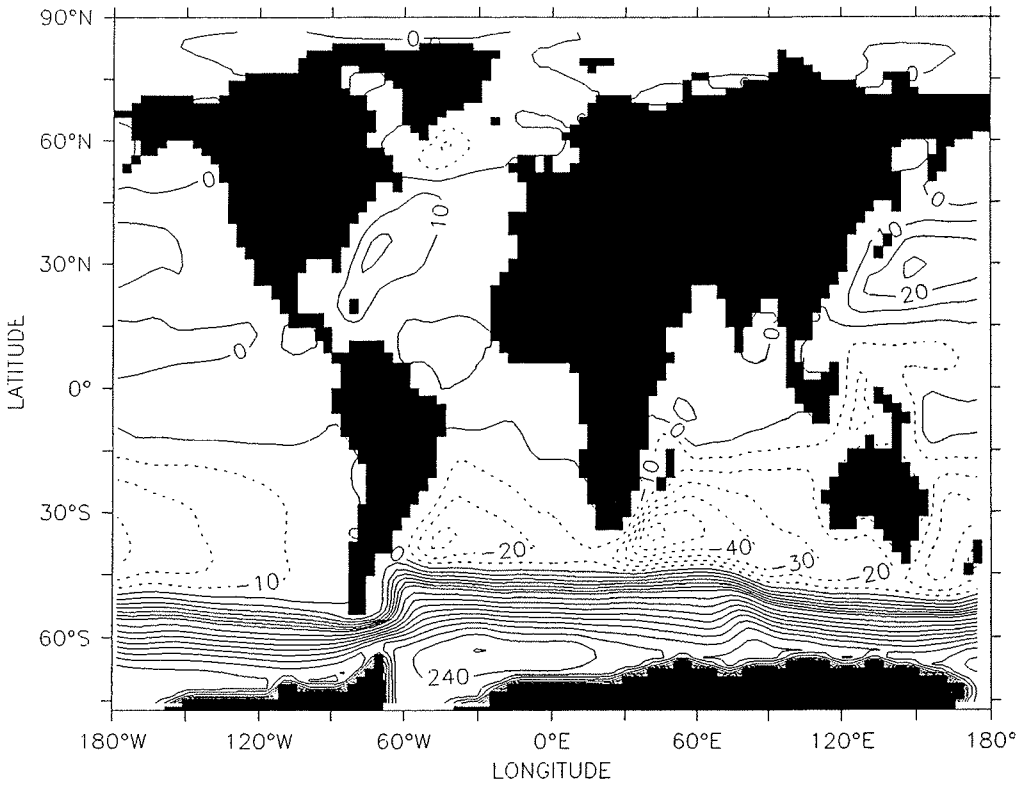

Figure 3: Annual-mean barotropic streamfunction. Contour interval is 10 Sv below a vertically integrated volume transport of 60 Sv and 20 Sv above. The dashed lines represent negative contour levels and indicate anti-clockwise circulation.

Drake Passage depends on the diffusion coefficients, showing an enhancement in transport with decreased diffusivity. Furthermore the ACC transport is larger in the case of horizontal diffusion than in the case of isopycnal diffusion. In our model the vertically averaged horizontal diffusivity is 0.43×10^3 m^2 s^{-1}. Extrapolating from the two solutions of Danabasoglu and McWilliams (1995) with horizontal diffusion we find a flow of about 250 Sv. From the studies of Danabasoglu and McWilliams (1995) and Large et al. (1997) we conclude that we can obtain a lower and more realistic ACC transport by turning to an isopycnal diffusion parameterization.

Meridional overturning streamfunction

The zonally integrated meridional overturning streamfunction is presented in Figure 4a-c. Figure 4a shows the total transport of all the ocean basins in one section, whereas Figures 4b and c show the total transport broken down among the Atlantic and Indo-Pacific basins, restricted to those latitudes where the ocean basins are limited zonally by continental boundaries. The sections that represent the meridional overturning streamfunction are read in the same way as the barotropic streamfunction map (Figure 3).

The mode of ocean circulation most important for ventilating the deep sea is the vertical overturning (Toggweiler et al., 1989). It is usually thought of as a manifestation of the thermohaline circulation, although in the upper ocean the upwelling and downwelling induced

by the surface wind stress are the dominant processes. In Figure 4a two shallow cells are depicted that straddle the Equator. These cells are driven by the divergence of the Ekman transport under the easterly trade winds. Figures 4a and b also indicate downwelling in mid-latitudes that produce another set of overturning cells, which is linked to wind-induced divergences in the subpolar regions. The overturning cell in the Northern Hemisphere is much weaker and shallower than the so-called Deacon cell in the Southern Hemisphere. This is due to a partial cancellation between the northern cell and the thermohaline circulation (Toggweiler et al., 1989).

Between 1500 m and 3500 m the meridional overturning is dominated by the southward flow of North Atlantic Deep Water (NADW), which is produced at a rate of 21 Sv. As much as 7 Sv of this transport upwells north of the Equator, only 14 Sv of it is exported into the Southern Ocean. An estimate for the total southward transport of NADW at 24° N is 17 ± 4 Sv (Roemmich and Wunsch, 1985), which is somewhat larger than the 15-Sv flow in the model.

There is a northward flow of Antarctic Bottom Water (AABW) in all three ocean basins, compensated by a return flow above 4000 m depth. In the Atlantic, the deep inflow at the bottom amounts to 3 Sv.

Potential temperature and salinity distributions

The annual and zonal mean distributions of potential temperature and salinity for the Atlantic Ocean are presented in Figure 5. Figure 6a depicts the corresponding deviation of potential temperature from the climatology of Levitus et al. (1994). All water masses are up to 4° C warmer than the observations, except for the AABW that is colder than the observations by 0.5°-1.0° C. The warm bias is largest in the thermocline, which therefore is more diffuse than observed. A warm bias and a diffuse thermocline are two widespread problems in ocean modelling (Danabasoglu and McWilliams, 1995).

Figure 6b illustrates the deviation of salinity from the climatology of Levitus and Boyer (1994) for the Atlantic Ocean. It reveals that the tongue of Antarctic Intermediate Water (AAIW) is rather broad and much too salty in the model ocean. The AABW is too fresh by 0.30-0.35 psu.

Seawater oxygen isotope composition and benthic foraminiferal $\delta^{18}O$

In Figure 7 the GEOSECS δ_w along a cross section in the Atlantic Ocean is compared with the annual and zonal mean δ_w from Experiments A and B. Experiment A yields a very heavy δ_w of AABW, whereas in Experiment B the δ_w of AABW is close to the GEOSECS data. Both experiments result in the broad tongue of AAIW that is also evident from the salinity distribution. The δ_w of AAIW is heavier than observed by 0.1-0.2‰. Figure 8 extends the comparison of the GEOSECS and the Experiment B δ_w to the Pacific Ocean. In the upper 3000 m the agreement is reasonably good. The δ_w of AABW is too light by about 0.1‰. Unfortunately, there is no GEOSECS δ_w data between 30° S and 15° N.

Anticipating an application of the global ocean model in a paleoceanographic setting, Figure 9 presents core-top benthic foraminiferal $\delta^{18}O$ compiled from 169 Atlantic core sites. To facilitate a comparison with the model ocean, the equilibrium fractionation of $\delta^{18}O_c$ is

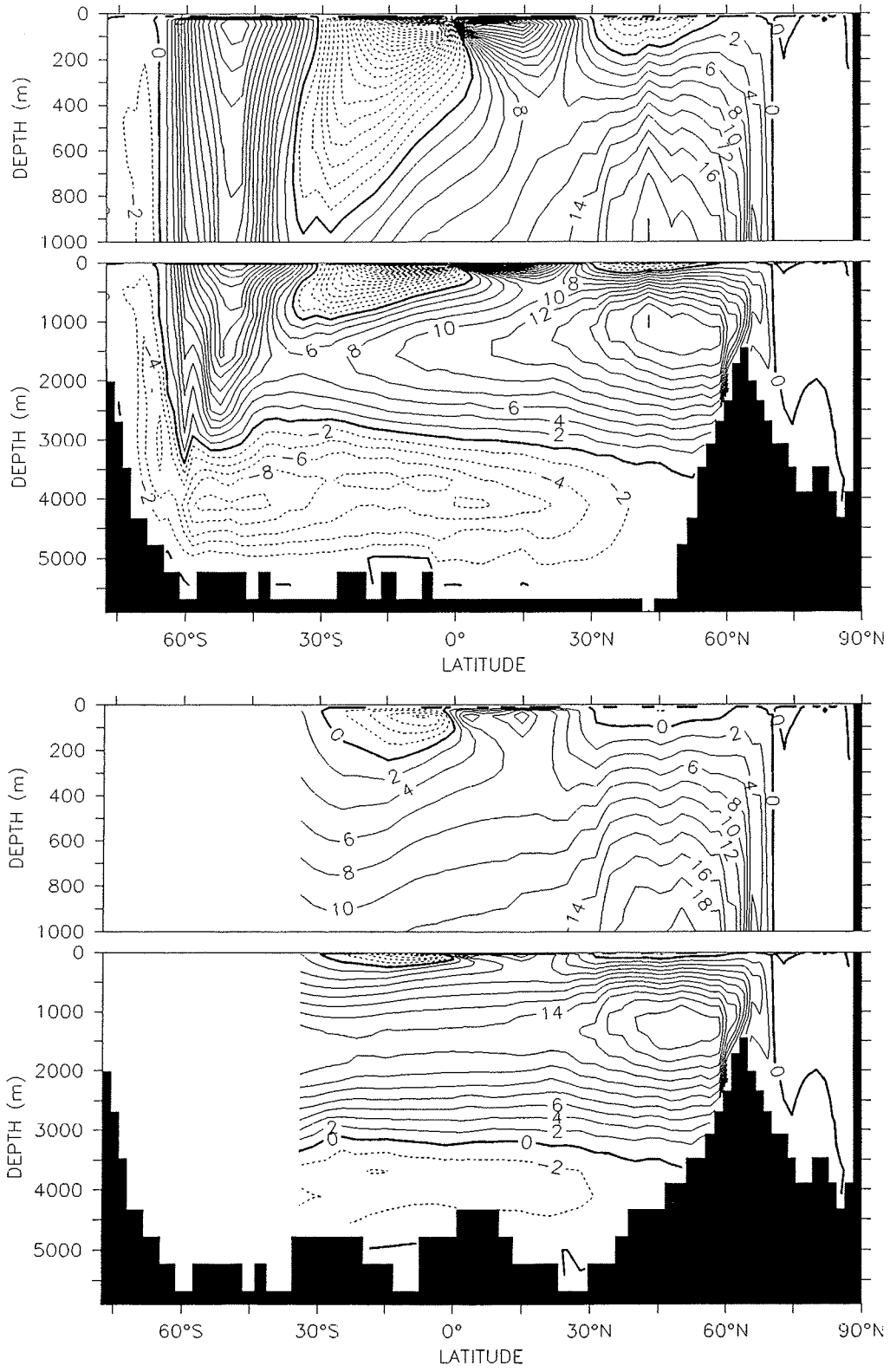

Figure 4: Annual-mean meridional overturning streamfunction. Contour interval is 2 Sv except for the Atlantic where it is 1 Sv for negative levels. Negative contour levels are represented by dashed lines that indicate anti-clockwise circulation. Upper panel (4a): global; lower panel (4b): Atlantic; next page (4c): Indo-Pacific.

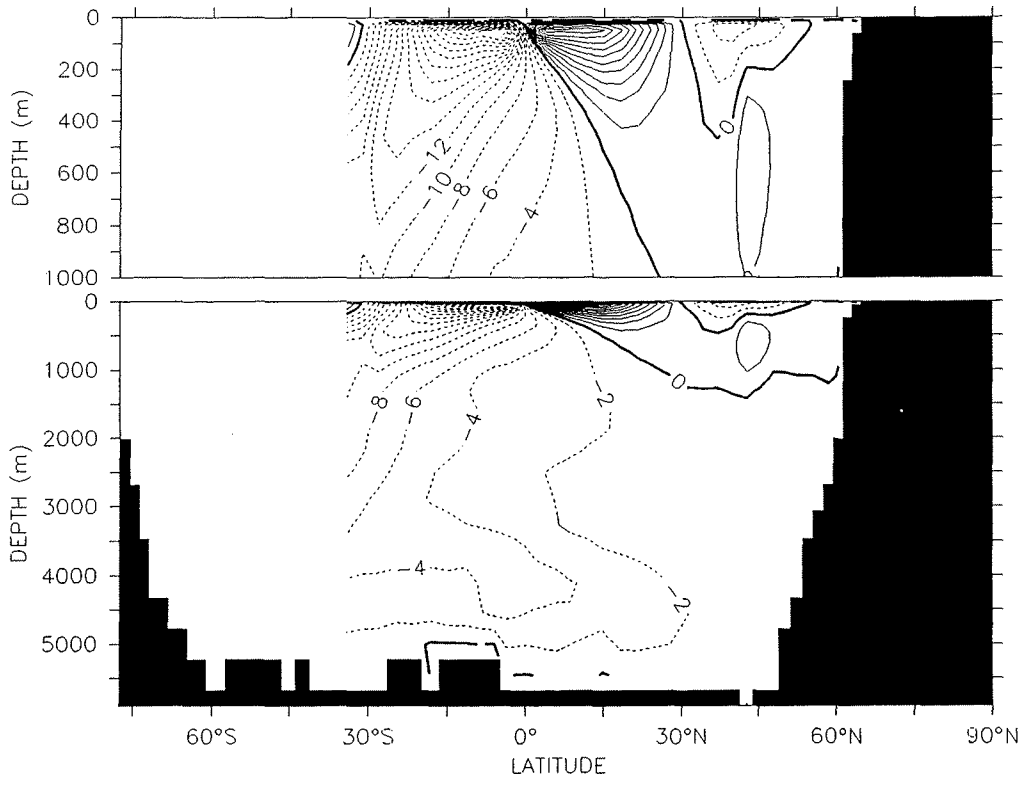

Figure 4 (continued)

computed for Experiment B. Two cases are studied: In the first case (Figure 10a) the model temperature is inserted into the paleotemperature equation of Erez and Luz (1983). In the second case (Figure 10b) the climatologic temperature of Levitus et al. (1994) is used. In the latter case the decrease of $\delta^{18}O_w$ with depth is correctly offset by a similar decrease of temperature. Therefore, NADW and AABW can be seen in $\delta^{18}O_w$, but cannot be distinguished in $\delta^{18}O_c$. Below about 2000 m water depth a roughly constant level of about 3‰ is reached. This is also suggested by the Atlantic core-top benthic foraminiferal $\delta^{18}O$ shown in Figure 9 (Zahn and Mix, 1991). The warm bias in the model temperature introduces an artifical vertical gradient into the $\delta^{18}O_c$ distribution that is evident in Figure 10a.

Net surface $\delta^{18}O$ flux

Figure 11 shows the net surface $\delta^{18}O$ flux for the present Atlantic and Pacific oceans, as diagnosed from the global ocean model. This flux can be compared with the output of an atmospheric model that includes the stable water isotope cycles (e.g., Juillet-Leclerc et al., 1997). A local minimum occurs in the equatorial zone between 10° S and 10° N where precipitation dominates over evaporation. Local maxima are found in the subtropics of each hemisphere where there is a deficit of precipitation.

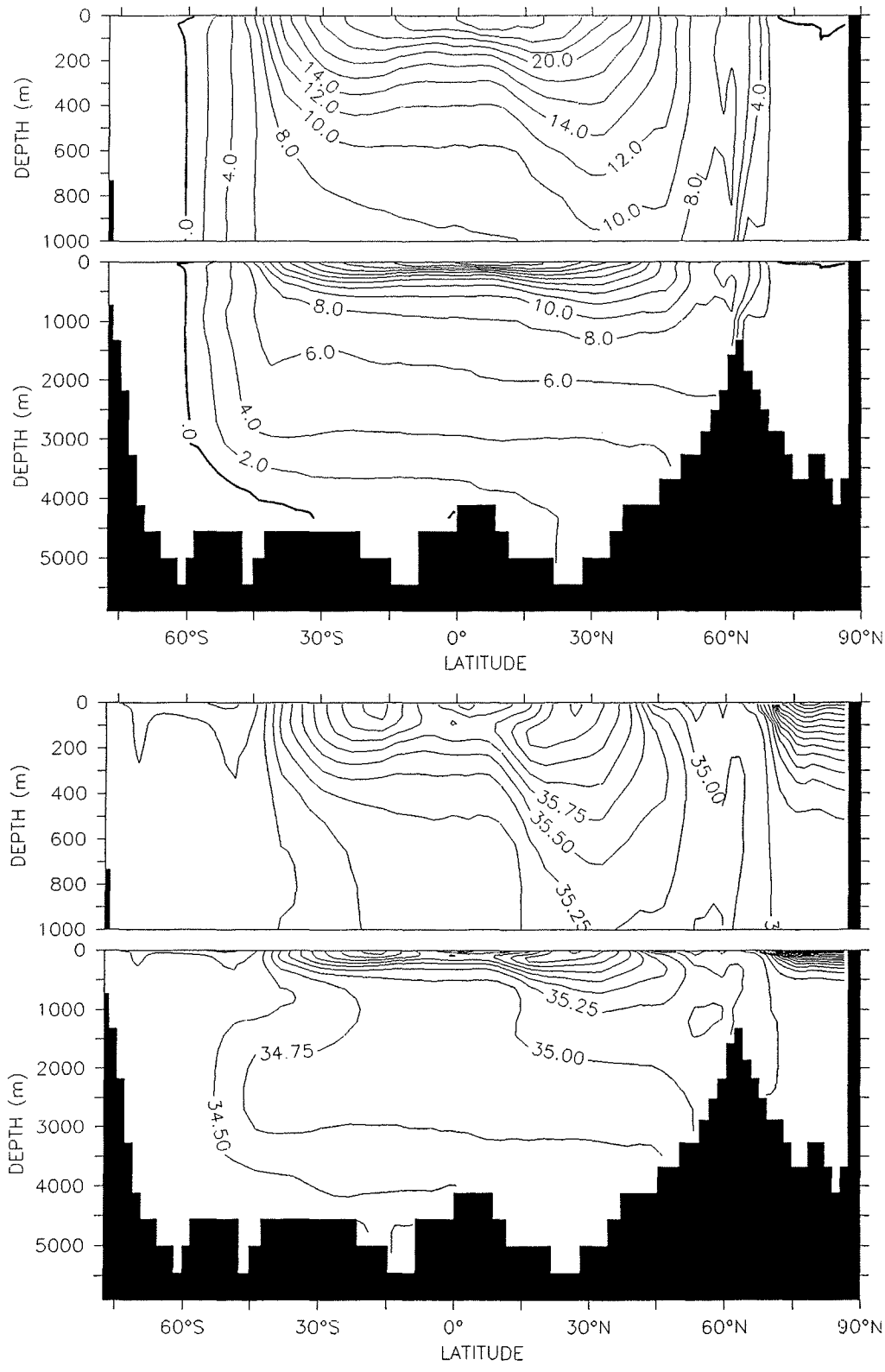

Figure 5: Annual and zonal mean tracer distributions for the present Atlantic Ocean. Upper panel (5a): Potential temperature. Contour interval is 2° C. Lower panel (5b): Salinity. Contour interval is 0.25 psu.

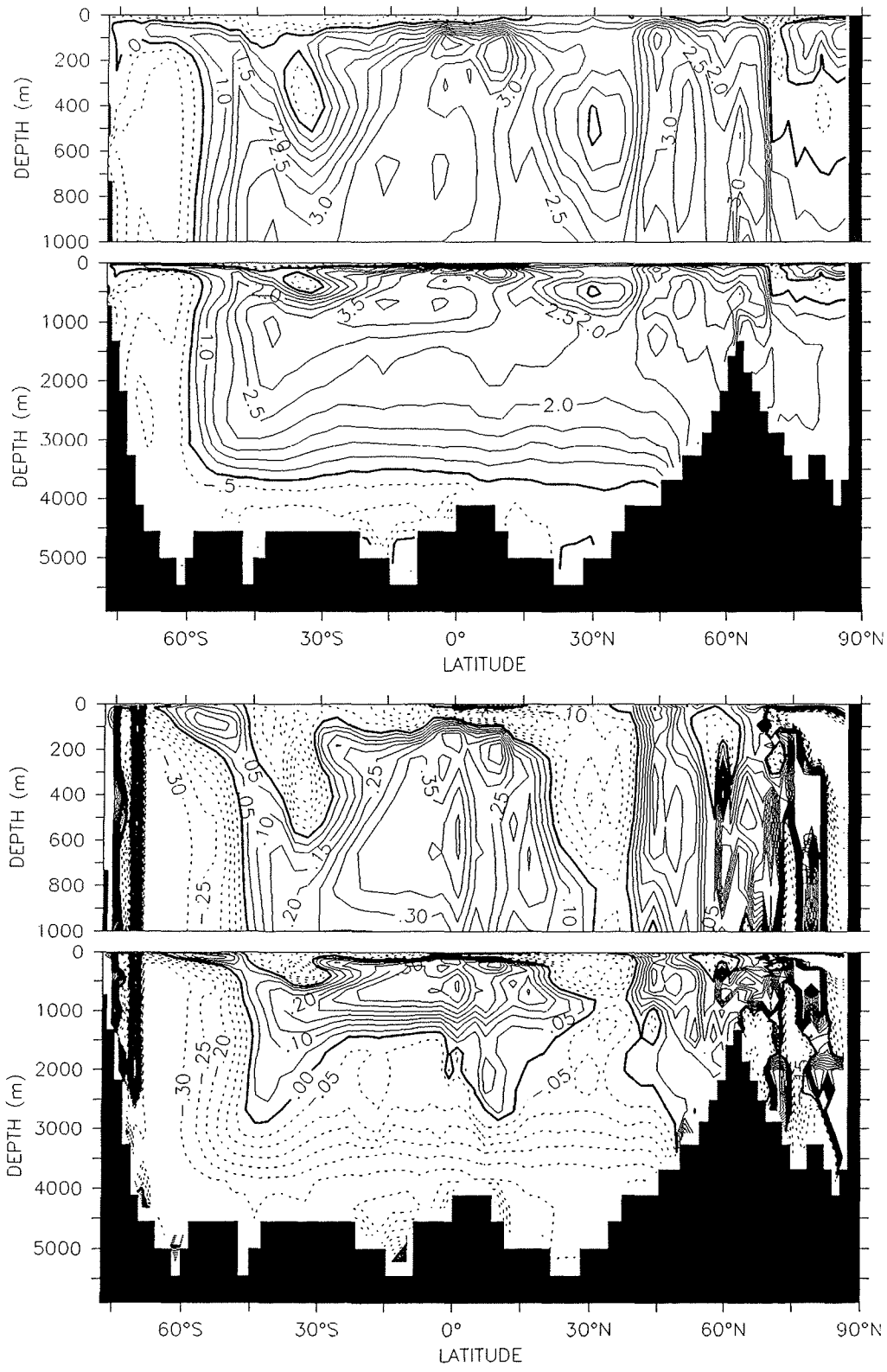

Figure 6: Annual and zonal mean tracer distributions for the present Atlantic Ocean. Difference between simulation and climatology. Upper panel (6a): Potential temperature. Contour interval is 0.5° C. Lower panel (6b): Salinity. Contour interval is 0.05 psu.

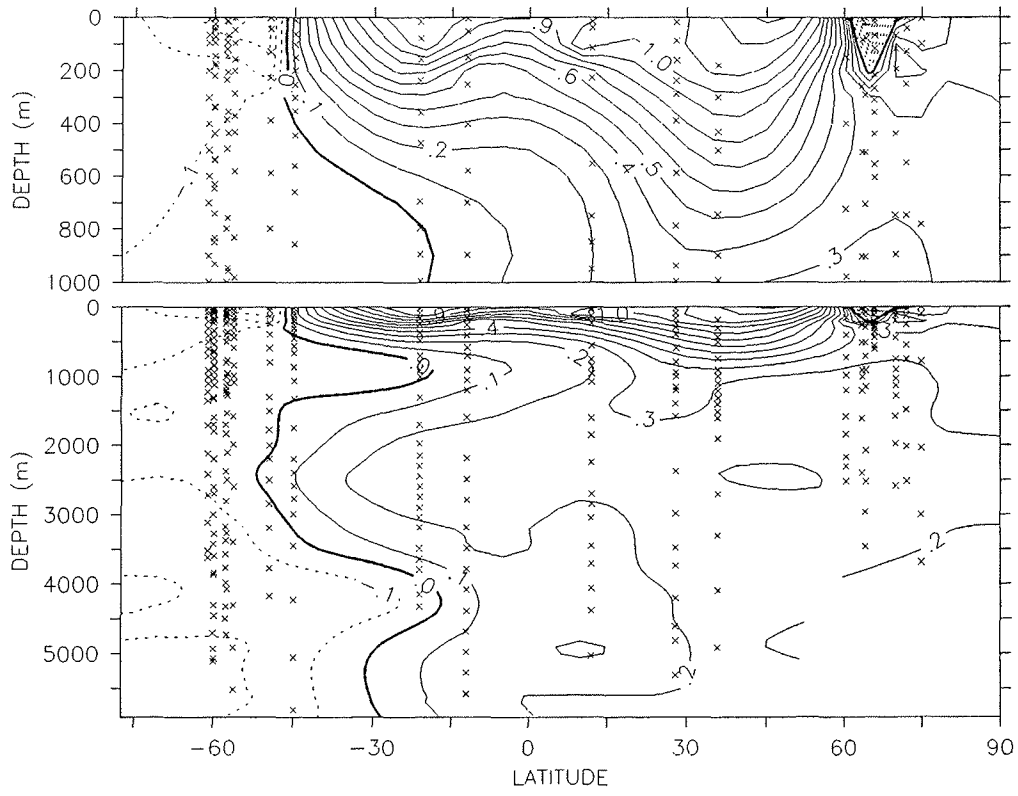

Figure 7a: Seawater oxygen isotope composition for the present Atlantic Ocean in units of parts per mil versus SMOW. Contour interval is 0.1 ‰. GEOSECS δ_w along a cross section in the Atlantic Ocean. Crosses indicate data points.

Water depth (km)	Temperature (°C)		Salinity (psu)		δ_w (‰ SMOW)	
	Model	Data	Model	Data	Model	Data
			North Atlantic			
> 1	4.95		34.87	34.93	0.28	0.24
2-4	4.66	2.9	34.86	34.92	0.29	0.26
> 4	1.99	2.4	34.60	34.89	0.07	0.21
			Pacific			
2-4	2.75	1.7	34.44	34.67	-0.04	0.00
> 4	1.08	1.1	34.41	34.70	-0.07	-0.01
			Globe			
Whole-basin mean	5.34		34.59	34.74	0.08	0.08

Table 2: Hydrography of present-day water masses. The observed temperature, salinity and δ_w are taken from GEOSECS as given in Zahn and Mix (1991) and Labeyrie et al. (1992).

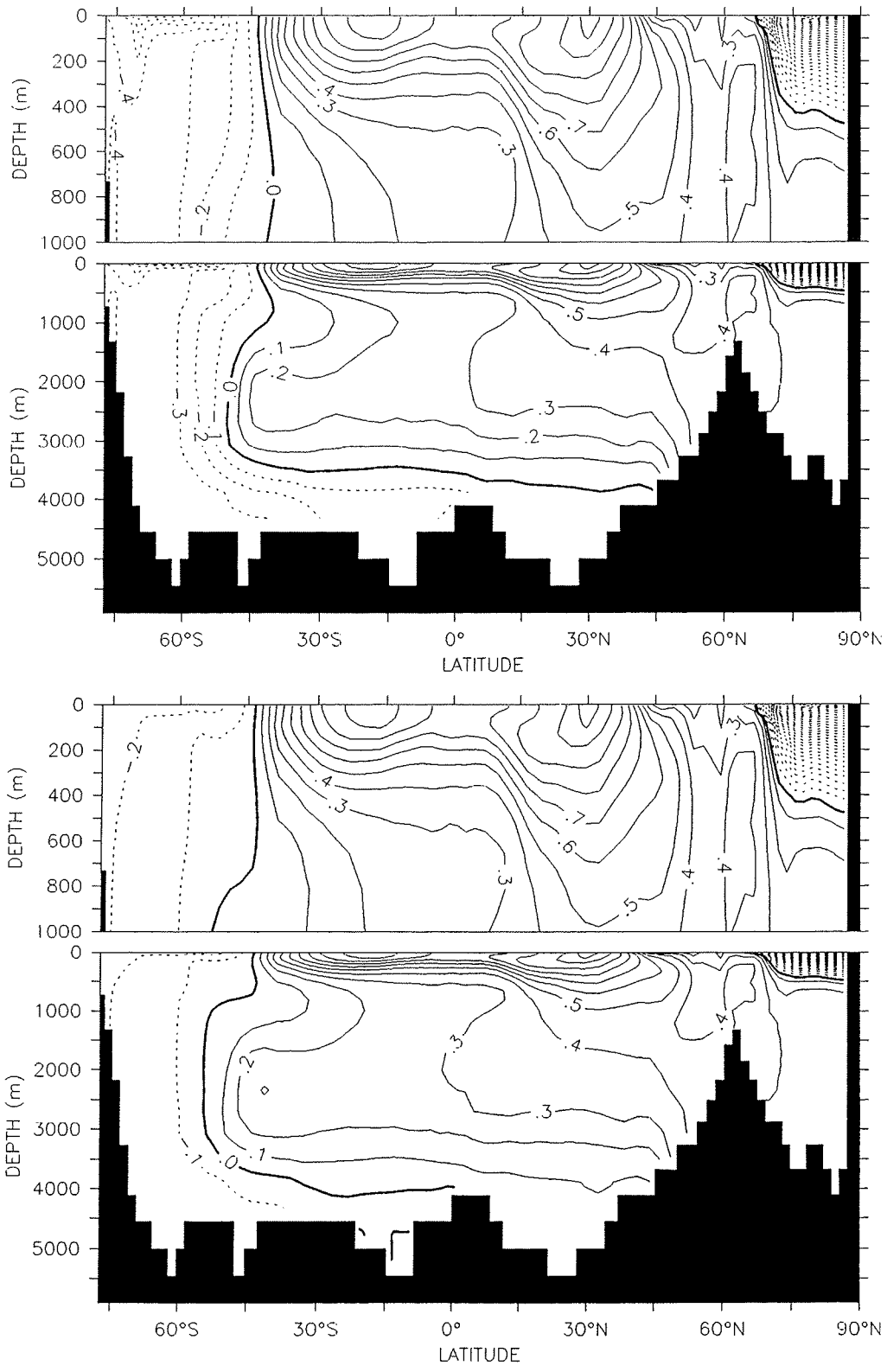

Figure 7bc: Seawater oxygen isotope composition for the present Atlantic Ocean in units of parts per mil versus SMOW. Contour interval is 0.1 ‰. Upper panel (7b) Annual and zonal mean δ_w from Experiment A. Lower panel (7c): Annual and zonal mean δ_w from Experiment B.

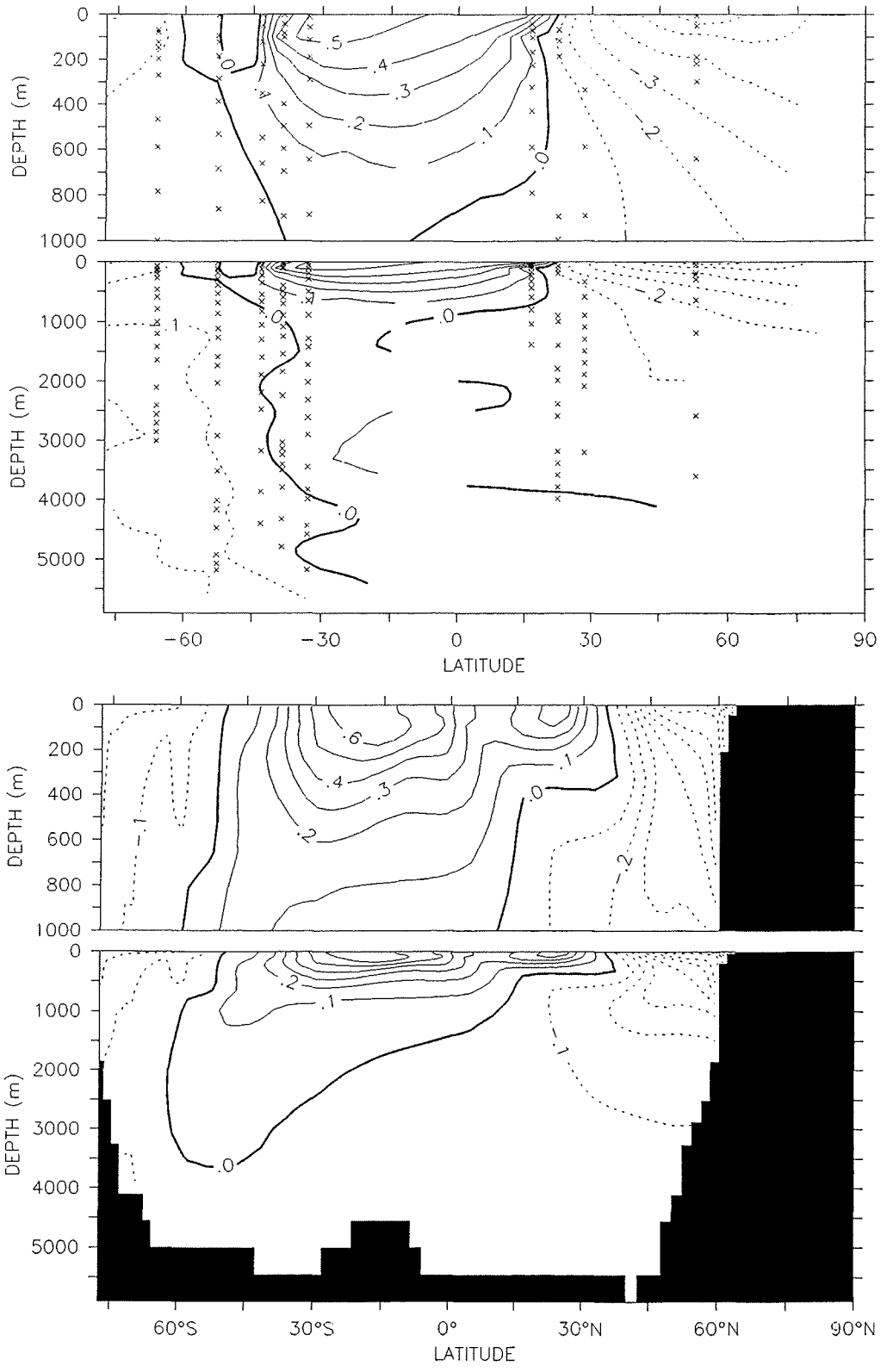

Figure 8: Seawater oxygen isotope composition for the present Pacific Ocean in units of parts per mil versus SMOW. Contour interval is 0.1 ‰. Upper panel (8a): GEOSECS δ_w along a cross section in the Pacific Ocean. Crosses indicate data points. Lower panel (8b): Annual and zonal mean δ_w from Experiment B.

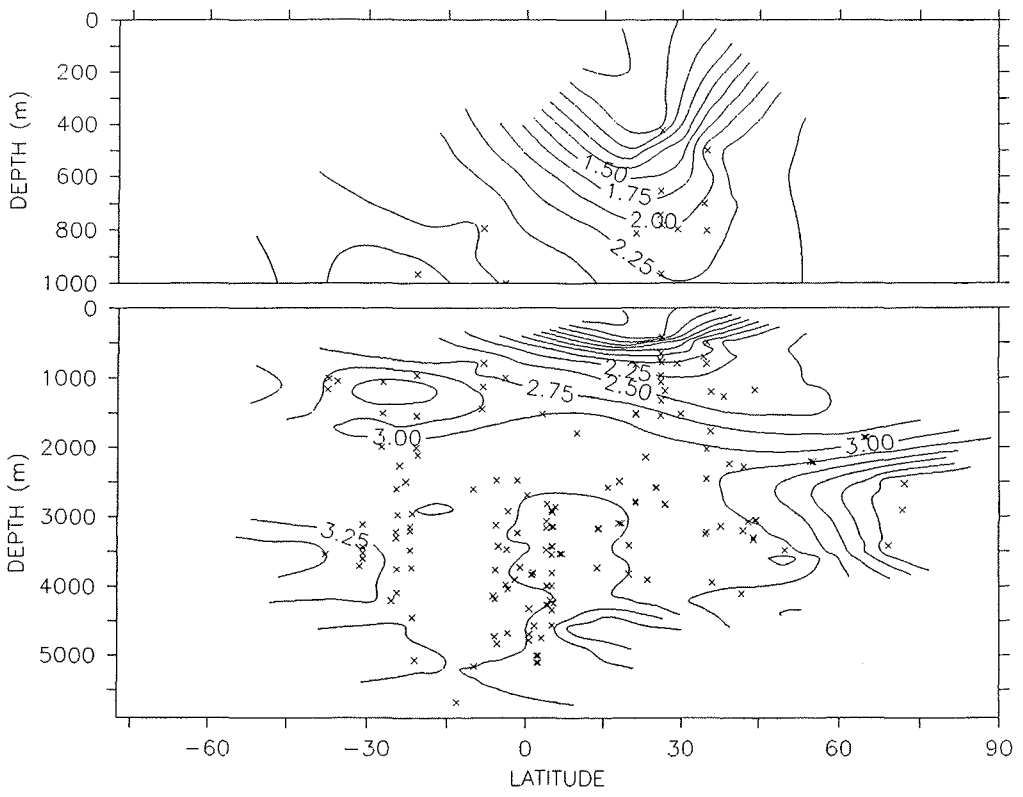

Figure 9: Benthic foraminiferal oxygen isotope composition for the present Atlantic Ocean in units of parts per mil versus PDB (normalized to *Uvigerina).* Contour interval is 0.25 ‰. The δ_c data are compiled from 169 core sites. Some data are unpublished, but most of them are taken from the literature (Broecker, 1986; Birchfield, 1987; Curry et al., 1988; Zahn and Mix, 1991; Labeyrie et al., 1992; Bickert, 1992; McCorkle and Keigwin, 1994).

Discussion

Table 2 summarizes the hydrography of the present-day water masses. The regional means yield the same results as the zonal mean distributions shown in Figure 5a and Figure 6a: The simulated temperature is warmer than the observations except for the AABW. As far as salinity and $\delta^{18}O_w$ are concerned, the model is too fresh and light. The deviations are small except for the bottom North Atlantic Ocean where the AABW influence is too strong.

We find that a surface $\delta^{18}O_w$ forcing field can be generated such that a global ocean model reproduces the GEOSECS $\delta^{18}O_w$ data fairly well, both along cross sections in the Atlantic and Pacific oceans and in terms of regional means. However, in order to simulate the benthic foraminiferal $\delta^{18}O$ data successfully, the bias towards warm temperatures must be reduced significantly.

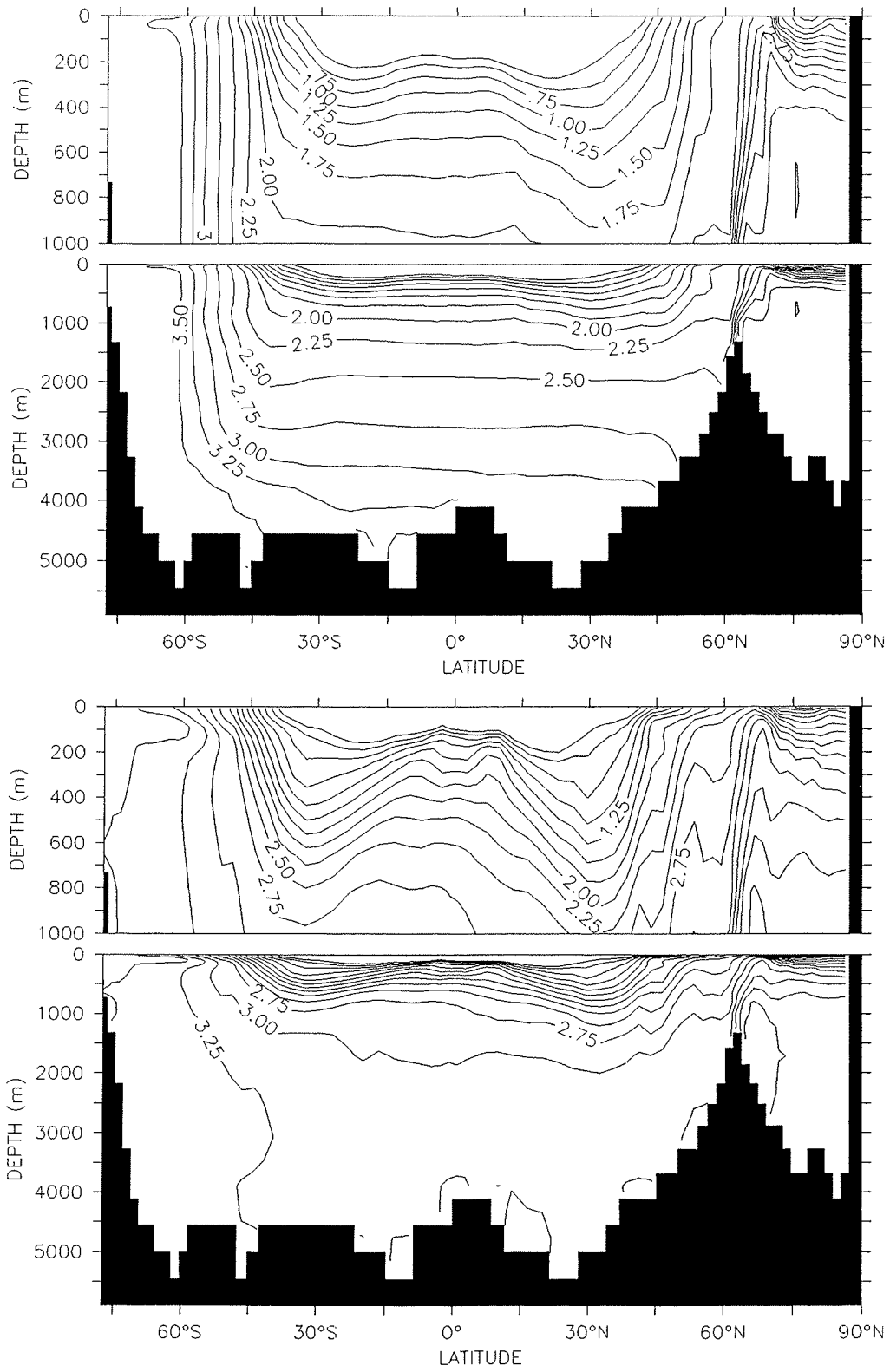

Figure 10: Equilibrium fractionation δ_c computed from the paleotemperature equation of Erez and Luz (1983). Upper panel (10a): Temperature taken from Experiment B. Lower panel (10b): Temperature taken from climatology. Contour interval is 0.25 ‰.

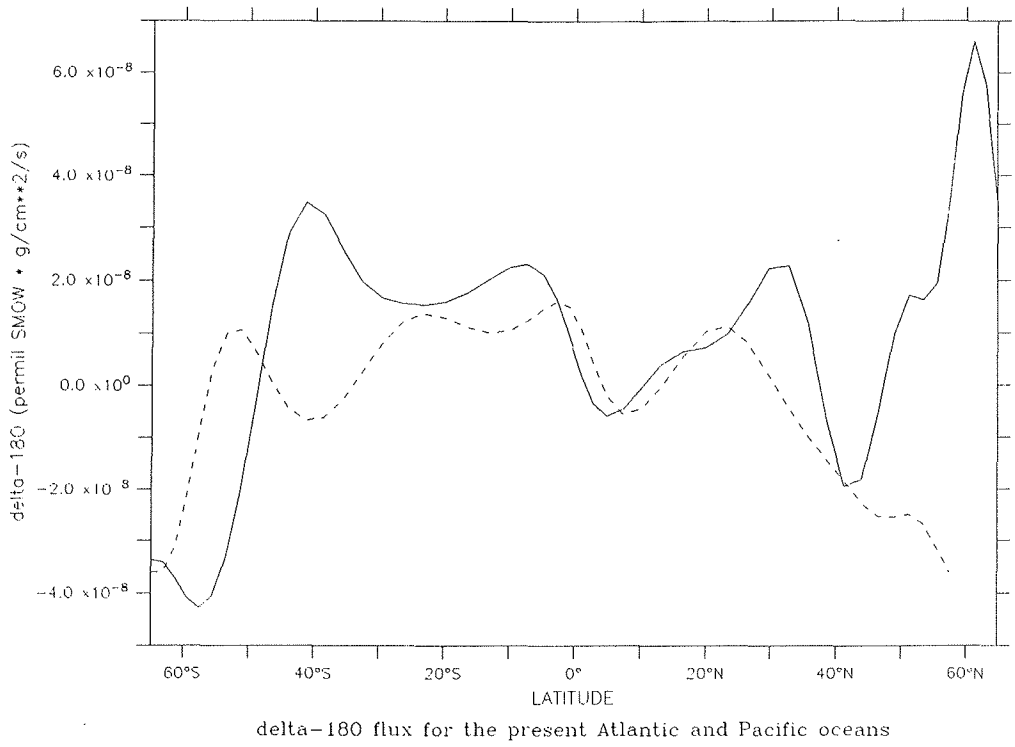

Figure 11: Annual and zonal mean net surface $\delta^{18}O_w$ flux. Solid line: For the present Atlantic Ocean. Dashed fine: For the present Pacific Ocean.

A warm bias and diffuse thermocline are two widespread problems in ocean modelling, which can probably be overcome by using diffusion of tracers along isopycnals rather than the physically unjustifiable horizontal diffusion of tracers (Danabasoglu and McWilliams, 1995). Furthermore, the formulation of Gent and McWilliams (1990) includes an additional tracer transport by mesoscale eddies, which largely eliminates the effect of the Deacon cell on tracers. Finally, the ACC transport through the Drake Passage can probably take a more realistic value due to the isopycnal form stress that supports more drag with weaker flow.

The improved fit of Experiment B as compared to Experiment A to the GEOSECS $\delta^{18}O_w$ of AABW in the Atlantic Ocean illustrates that sea-ice freezing and melting have a strong effect on salinity, but a very weak effect on $\delta^{18}O_w$. This opens up the possibility to constrain the role of sea-ice in past and present AABW formation.

If there had been no information on the salinity distribution in the ocean model, the misrepresentation of AAIW (too broad and salty) and AABW (too fresh) could have been anticipated from the $\delta^{18}O_w$ distribution. Having paleoceanographic applications in mind, this is an encouraging result. Admittedly, the equilibrium fractionation of the oxygen isotope composition of calcite $\delta^{18}O_c$ cannot be used to separate NADW and AABW in the present Atlantic Ocean. But this may have been different during colder periods of the past. Still, it would be desirable to incorporate an additional tracer into the ocean model that could better resolve the vertical structure of the deep ocean.

In the present North Atlantic Ocean, water masses deeper than 1 km have considerably higher salinity and δ_w than in the global ocean. This salinity and δ_w excess may have persisted during glacial times although NADW was probaly produced at a lower rate (Labeyrie et al., 1992). Zahn and Mix (1991) found that benthic foraminiferal $\delta^{18}O$ data from the bottom Atlantic Ocean (deeper than 4 km) and deep Pacific Ocean (2-4 km water depth) are 0.1-0.2‰ lower than from the deep Atlantic Ocean (2-4 km water depth) at the LGM. If the measured gradients were taken at face value, and if the slope of the δ_w-S relationship were assumed to be larger at the LGM than at present, then Atlantic bottom waters and Pacific deep waters may have had a common source in the Southern Ocean.

The required surface forcing fields for the LGM can be generated from a combination of SST reconstructions, planktonic foraminiferal $\delta^{18}O$ data and atmospheric model output (e.g., Herterich et al., this volume). The simulated equilibrium fractionation of the oxygen isotope composition of calcite $\delta^{18}O_c$ can be directly compared with the benthic foraminiferal $\delta^{18}O$ data for the LGM. Thus the simulation of oxygen isotopes in an ocean model has the potential to investigate and validate circulation regimes very different from the present one.

Conclusions

In conclusion,

• a surface $\delta^{18}O_w$ forcing field can be generated such that a global ocean model reproduces the GEOSECS $\delta^{18}O_w$ data fairly well, along cross sections in the Atlantic and Pacific oceans and in terms of regional means,

• a successful simulation of benthic foraminiferal $\delta^{18}O$ however requires a reduction of the warm bias typical for many ocean models, possibly by using an isopycnal transport parameterization,

• $\delta^{18}O_w$ turns out to be a good water mass tracer that has the potential to be applied in a paleoceanographic setting,

• $\delta^{18}O_c$ taken by itself cannot be used to distinguish between NADW and AABW in the present Atlantic Ocean, but maybe it can be used to do so at the LGM.

Acknowledgements

We would like to thank Dr. G. Edward Birchfield and Dr. Christopher D. Charles for their help during the early stages of this work. We are grateful to Dr. Harmon Craig for providing us with the GEOSECS δ_w data. We would also like to thank Dr. Martina Pätzold for supplying her unpublished δ_w data.

References

Bauch, D. (1995). The distribution of $\delta^{18}O$ in the Arctic Ocean: Implications for the freshwater balance of the halocline and the sources of deep and bottom waters. *Berichte zur Polarforschung 159,* 144 pp. Alfred Wegener Institut.

Bickert, T. (1992). Rekonstruktion der spätquartären Bodenwasserzirkulation im östlichen Südatlantik über stabile Isotope benthischer Foraminiferen. *Berichte FB Geowissenschaften Universität Bremen 27,* 205 pp.

Birchfield, G. E. (1987). Changes in deep-ocean water $\delta^{18}O$ and temperature from the last glacial maximum to the present. *Paleoceanography 2,* 431-442.

Broecker, W. S. (1986). Oxygen isotope constraints on surface ocean temperatures. *Quaternary Research 26,* 121-134.

Broecker, W. S. (1989). The salinity contrast between the Atlantic and Pacfic oceans during glacial time. *Paleoceanography 4,* 207-212.

Bryan, K. (1984). Accelerating the convergence to equilibrium of ocean climate models. *Journal of Physical Oceanography 14,* 666-673.

Bryan, K. and L. J. Lewis (1979). A water mass model of the world ocean circulation. *Journal of Geophysical Research 84,* 2503-2517.

Cane, M. A. (1986). Introduction to ocean modeling. In J. J. O'Brien (Ed.), *Advanced Physical Oceanographic Modelling,* NATO Advanced Science Institutes Series C: Mathematical and Physical Sciences 186, pp. 5-21. Dordrecht, Netherlands: D. Reidel Publishing Company.

Craig, H. and L. I. Gordon (1965). Isotopic oceanography: Deuterium and oxygen 18 variations in the ocean and the marine atmosphere. In E. Tongiorgi (Ed.), *Proceedings of the Third Spoleto Conference,* pp. 9-130. Consiglio Nazionale Delle Ricerche.

Curry, W. B., J. C. Duplessy, L. D. Labeyrie, and N. J. Shackleton (1988). Changes in the distribution of $\delta^{13}C$ of deep water ΣCO_2 between the last glaciation and the Holocene. *Paleoceanography 3,* 317-341.

Danabasoglu, G. and J. C. McWilliams (1995). Sensitivity of the global ocean circulation to parameterizations of mesoscale tracer transports. *Journal of Climate 8,* 2967-2987.

Danabasoglu, G., J. C. McWilliams, and W. G. Large (1996). Approach to equilibrium in accelerated global oceanic models. *Journal of Climate 9,* 1092-1110.

Duplessy, J.-C., L. Labeyrie, A. Juillet-Leclerc, F. Maitre, J. Duprat, and M. Sarnthein (1991). Surface salinity reconstruction of the North Atlantic Ocean during the last glacial maximum. *Oceanologica Acta 14,* 311-324.

Erez, J. and B. Luz (1983). Experimental paleotemperature equation for planktonic foraminifera. *Geochimica et Cosmochimica Acta 47,* 1025-1031.

Fairbanks, R. G., C. D. Charles, and J. D. Wright (1992). Origin of global meltwater pulses. In R. E. Taylor (Ed.), *Radiocarbon after four decades,* pp. 473-500. Springer-Verlag.

Garzoli, S. L. and A. L. Gordon (1996). Origins and variability of the Benguela Current. *Journal of Geophysical Research 101,* 897-906.

Gent, P. R. and J. C. McWilliams (1990). Isopycnal mixing in ocean circulation models. *Journal of Physical Oceanography 20,* 150-155.

Gordon, A. L., J. R. E. Lutjeharms, and M. L. Gründlingh (1987). Stratification and circulation at the Agulhas Retroflection. *Deep Sea Research 34,* 565-599.

Gould, W. J., J. Loynes, and J. Backhaus (1985). Seasonality in slope current transports northwest of Shetland. Technical Report 7, ICES, Hydrography Commitee.

Hoffmann, G. (1995). *Stabile Wasserisotope im allgemeinen Zirkulationsmodell ECHAM.* Dissertation, Universität Hamburg.

Hoffmann, G. and M. Heimann (1993). Water tracers in the ECHAM general circulation model. In International Atomic Energy Agency (Ed.), *Isotope techniques in the study of past and current environmental changes in the hydrosphere and the atmosphere.*

Jacobs, S. S., R. G. Fairbanks, and Y. Horibe (1993). Origin and evolution of water masses near the antarctic continental margin. In: *Oceanology of the Antarctic Continental Shelf, Antarctic Research Series 43,* 59-85.

Joussaume, S., R. Sadourny, and J. Jouzel (1984). A general circulation model of water isotope cycles in the atmosphere. *Nature 311,* 24-29.

Joussaume, S. and J. Jouzel (1993). Paleoclimatic tracers: an investigaton using an Atmospheric General Circulation Model under Ice-Age conditions. 2. Water isotopes. *Journal of Geophysical Research 98,* 2807-2830.

Jouzel, J., G. L. Russel, R. J. Suozzo, R. D. Koster, J. W. C. White, and W. S. Broecker (1987). Simulations of the HDO and $H_2{}^{18}O$ atmospheric cycles using the NASA GISS General Circulation Model: the seasonal cycle for present-day conditions. *Journal of Geophysical Research 92,* 14,739-14,760.

Juillet-Leclerc, A., J. Jouzel, L. Labeyrie, and S. Joussaume (1997). Modern and last glacial maximum sea surface $\delta^{18}O$ derived from an Atmospheric General Circulation Model. *Earth and Planetary Science Letters 146,* 591605.

Kalnay, E., M. Kanamitsu, R. Kistler, W. Collins, D. Deaven, L. Gandin, M. Iredell, S. Saha, G. White, J. Woolen, Y. Zhu, M. Chelliah, W. Ebisuzaki, W. Higgins, J. Janowiak, K. C. Mo, C. Ropelewski, L. A. R. Reynolds, and R. Jenne (1996). The NCEP/NCAR reanalysis project. *Bulletin of the American Meteorological Society 77,* 437-471.

Knauss, J. (1969). A note on the transport of the Gulf Stream. *Deep Sea Research 16,* suppl., 117-124.

Labeyrie, L. D., J.-C. Duplessy, J. Duprat, A. Juillet-Leclerc, J. Moyes, E. Michel, N. Kallel, and N. J. Shackleton (1992). Changes in the vertical structure of the North Atlantic ocean between glacial and modern times. *Quaternary Science Reviews 11,* 401-413.

Large, W. G., G. Danabasoglu, J. C. Doney, and S. C. McWilliams (1997). Sensitivity to surface forcing and boundary layer mixing in a global ocean model: Annual-man climatology. *Journal of Physical Oceanography 27,* 2418-2447.

Larsen, J. C. (1992). Transport and heat flux of the Florida Current at 27° N derived from cross-stream voltages and profiling data: Theory and observations. *Philosophical Transactions of the Royal Society of London A 338,* 169-236.

Levitus, S. (1982). Climatological atlas of the World Ocean. *NOAA Prof. Paper No. 13,* 173 pp.

Levitus, S., and T. P. Boyer (1994). World Ocean Atlas 1994, Volume 4: Temperature. *NOAA Atlas NESDIS 4*, 117 pp.

Levitus, S., R. Burgett, and T. P. Boyer (1994). World Ocean Atlas 1994, Volume 3: Salinity. *NOAA Atlas NESDIS 3*, 99 pp.

Mackensen, A., H.-W. Hubberten, N. Scheele, and R. Schlitzer (1996). Decoupling of $\delta^{13}C_{\Sigma CO2}$ and phosphate in recent Weddell Sea deep and bottom water: Implications for glacial Southern Ocean paleoceanography.*Paleoceanography 11* 203-215.

Mathieu, R. (1996). GENESISΣ. A Water Molecule Stable Isotopes and Tracers Version of the GENESIS Global Climate Model Version 2.0. Model Description, Interdisciplinary Climate System Section, Climate and Global Dynamics Division, National Center for Atmospheric Research. Institute of Alpine and Arctic Research.

McCorkle, D. C. and L. D. Keigwin (1994). Depth profiles of $\delta^{13}C$ in bottom water and core top C. *wuellerstorfi* on the Ontong Java Plateau and Emperor Seamounts. *Paleoceanography 9,* 197-208.

McGuffie, K. and A. Henderson-Sellers (1996). *A Climate Modelling Primer* . Chichester: John Wiley & Sons.

NCAR Data Support Section (1986). NGDC ETOPO5 global ocean depth & fand elevation, 5-min. Data Set 759.1, National Center for Atmospheric Research, Boulder, Colorado.

NCAR Oceanography Section (1996). The NCAR CSM ocean model. NCAR Technical Note NCAR/TN-423+STR, National Center for Atmospheric Research, Boulder, Colorado.

Östlund, H., H. Craig, W. S. Broecker, and D. Spencer (1987). GEOSECS Atlantic, Pacific, and Indian Ocean expeditions. Shorebased data and graphics. GEOSECS Atlas Series Volume 7, U. S. Government Printing Office, Washington, D. C.

Pacanowski, R. C. E. (1996). MOM 2. Documentation, User's Guide and Reference Manual. Technical Report 3.2, GFDL Ocean Group, GFDL, Princeton, New Jersey.

Peterson, R. G. and L. Stramma (1991). Upper-level circulation in the South Atlantic Ocean. *Progress in Oceanography 26,* 1-73.

Roemmich, D. and C. Wunsch (1985). Two transatlantic sections: Meridional circulation and heat flux in the subtropical North Atlantic Ocean. *Deep-Sea Research 32,* 619-664.

Schlotterer, U., F. Oldfield, and K. Frölich (1996). Global network for isotopes in precipitation. Technical report, IAEA, Vienna.

Semtner, A. (1986). Finite-difference formulation of a World Ocean model. In J. J. O'Brien (Ed.), *Advanced Physical Oceanographic Modelling,* NATO Advanced Science Institutes Series C: Mathematical and Physical Sciences 186, pp. 187-202. Dordrecht, Netherlands: D. Reidel Publishing Company.

Shea, D. J., K. E. Trenberth, and R. W. Reynolds (1990). A global monthly sea surface temperature climatology. NCAR Technical Note NCAR/TN 345, National Center for Atmospheric Research, Boulder, Colorado.

Sloss, P. W. (1988). Digital relief of the surface of the Earth. Data Announcement 88-MGG-02, NOAA, National Geophysical Data Center, Boulder, Colorado.

Stramma, L. and J. R. E. Lutjeharms (1996). The flow field of the subtropical gyre of the South Indian Ocean. *Journal of Geophysical Research 102,* 5513.

Toggweiler, J., K. Dixon, and K. Bryan (1989). Simulations of radiocarbon in a coarse-resolution World Ocean model. 1. Steady state prebomb distributions. *Journal of Geophysical Research 94,* 8217-8242.

Toggweiler, J. R. and B. Samuels (1995). Effect of sea ice on the salinity of Antarctic Bottom Waters. *Journal of Physical Oceanography 25,* 1980-1997.

UNESCO (1981). Tenth report of the joint panel of oceanographic tables and standards. UNESCO Technical Papers in Marine Sciences No. 36, UNESCO, Paris.

Veshteyn, V. Y., G. A. Malyuk, and V. P. Rusanov (1974). Oxygen-18 distribution in the Central Arctic Basin. *Oceanology 14,* 514-519.

Wajsowicz, R. C. (1993). A consistent formulation of the anisotropic stress tensor for use in models of the large scale ocean circulation. *Journal of Computational Physics 105,* 333-338.

Washington, W. M. and C. L. Parkinson (1986). *An Introduction to Three Dimensional Climate Modeling.* Mill Valley, California: University Science Books.

Weaver, A. J. and T. M. C. Hughes (1996). On the incompatibility of ocean and atmosphere models and the need for flux adjustments. *Climate Dynamics 12,* 141-170.

Weiss, R. F., H. G. Östlund, and H. Craig (1979). Geochemical studies of the Weddell Sea. *Deep-Sea Research 26A,* 1093-1120.

Whitworth, T., I. and R. G. Peterson (1985). Volume transport of the Antarctic Circumpolar Current from bottom pressure measurements. *Journal of Physical Oceanography 15,* 810-816.

Zahn, R. and A. C. Mix (1991). Benthic foraminiferal $\delta^{18}O$ in the ocean's temperature-salinity-density field: constraints on the ice age thermohaline circulation. *Paleoceanography 6,* 1-20.

Chapter 7

Conclusions

Principle results of research papers

- Paleosalinity reconstructions using $\delta^{18}O$ of planktonic foraminifera are constrained by the accuracy of the independent temperature estimate and the regional $\delta^{18}O$-salinity relationship (chapter 2). In the tropical Atlantic, errors associated with the paleosalinity estimates exceed 1‰. Paleosalinity reconstructions based on relative abundances of planktonic foraminifera give unrealistic results due to a predominant response of the fauna to temperature.

- Planktonic foraminiferal species are characterized by optimum temperatures and specific temperature sensitivities. While *G. sacculifer* shows a weak temperature sensitivity and an optimum temperature around 22°C, *G. ruber* (pink) is characterized by a pronounced temperature sensitivity and optimum conditions around 27°C. If the temperatures at the sea surface change through time the temperature sensitivites may influence phase and amplitude of the oxygen isotope record (chapter 3).

- The western equatorial Atlantic is characterized by large glacial-to-modern changes in $\delta^{18}O$ of the planktonic foraminifera *G. sacculifer* (chapters 2 and 4). These changes are interpreted in terms of increased salinities, ^{18}O-enriched precipitation and a glacial cooling of the SST of 2-3°C. These oxygen-isotope based estimates of the western equatorial SST at the LGM are intermediate between the reconstructions of CLIMAP (1 °C) and the evidence from corals and the South American continental record (5-6 °C) (chapter 4).

- Planktonic foraminiferal species counts can be used to reconstruct thermocline depths in the tropical oceans (chapter 5). During glacials the thermocline was shallow in the eastern equatorial Atlantic and it was deep in the west. The SE-trade winds were increased, the African monsoon was weak, and the South Equatorial Current was accelerated. The east-to-west thermocline gradient was at a maximum. During interglacials the system relaxed due to weakened SE-trades and intensification of the monsoon. The equatorial thermocline gradient was at a minimum. In the east the thermocline signal is dominated by monsoon related periodicities. The thermocline structure in the west and the equatorial thermocline gradient appear to be dominantly controlled by South Atlantic meridional temperature gradients which lead global ice volume.

- Oxygen isotopes can be incorporated into ocean general circulation models. When a sea surface $\delta^{18}O_w$ forcing field based on regional applying $\delta^{18}O$-salinity relationships is defined, cross sections of measured $\delta^{18}O_w$ through the ocean basins are reasonably well reproduced. Benthic foraminiferal $\delta^{18}O$ are not matched by the simulated $\delta^{18}O$ due to the warm bias of the ocean model. However, the $\delta^{18}O_w$ is a promising indicator of different water masses and a tracer that can be directly compared with the geological record.

The equatorial Atlantic during the last glacial maximum

What is the paleoceanographic and paleoclimatic picture of the equatorial Atlantic at the last glacial maximum as depicted from these results?

Sea surface temperatures are generally lowered by 2-3 °C. In the western equatorial Atlantic an increase in sea surface salinity is likely, probably due to a glacial reduction in precipitation. Reduced precipitation rates are accompanied by ^{18}O-enrichment of the precipitation, leading to a modification of the $\delta^{18}O_w$-salinity characteristics of western equatorial Atlantic surface waters in addition to the global glacial effects.

The structure of the surface water mass is markedly different from today. In the western equatorial Atlantic the thermocline is deeper than today while it shallows in the east where upwelling is intensified. These changes in thermocline depth are directly linked to the surface wind fields. Due to a greater meridional temperature gradient in the South Atlantic region the SE-trade winds are stronger than today. At the equator the zonal component of the SE-trade winds is enhanced. The South Equatorial Current is accelerated leading to the pronounced E-W thermocline gradient.

Increased salinities in the western equatorial Atlantic may be interpreted in terms of either a reduction in the intensity of the South Atlantic Hadley circulation or reduced atmospheric moisture contents in the tropics. The latter explanation is favored here, because a stronger glacial thermocline gradient along the equator and increased trade wind intensity suggest enhanced Hadley circulation. The atmospheric water vapor content may have been reduced due to lower air and sea surface temperatures, especially in the eastern subtropical South Atlantic where the SE-trade winds originate.

Future research

The reconstruction of paleosalinities from $\delta^{18}O$ in the tropics may be improved if the errors of the independent temperature estimates can be minimized and past $\delta^{18}O_w$-salinity relationships will be better understood. Further $\delta^{18}O_w$ and salinity measurements of today's surface ocean waters and the addition of oxygen isotopes to atmospheric and ocean circulation models as well as to coupled models may help to solve this problem.

The question of tropical sea surface temperatures at the last glacial maximum has still to be answered. Reevaluation of temperature reconstructions from planktonic foraminiferal

assemblages should be undertaken. Research should focus on the sensitivities of planktonic foraminiferal species on different environmental parameters. Foraminiferal species counts from sediment trap samples may help in this context. Knowledge about the sensitivities of foraminifera will also further improve our understanding of the foraminiferal oxygen isotope record.

A promising tool in conjunction with planktonic foraminiferal species counts may be artificial neural networks. In contrast to transfer functions they can relate foraminiferal abundance data to several parameters simultaneously which appears to be more appropriate with respect to the complexity of the system.

Improvement of the tools may then further improve the knowledge about the late Quaternary equatorial Atlantic. The reconstruction of thermocline depths and sea surface temperatures in sediment cores from all parts of the equatorial Atlantic may help in answering the questions about the role of the late Quaternary tropical Atlantic in delivering heat to the northern hemisphere.

Appendix

Explanations:

Appendix A: Data from Chapter 2.

$\delta^{18}O$ of *G.sacculifer:*	Data from Dürkoop et al. (1997)
Twin (MacMAT):	winter temperature from MacMAT
Tsum (MacMAT):	summer temperature from MacMAT
Sal (T from MacMAT):	salinity from oxygen isotope method using Tsum from MacMAT
Sal (T from SIMMAX):	salinity from oxygen isotope method using Tsum from SIMMAX (Hale and Pflaumann, 1998)
Sal ($\delta^{18}O$-Sal tropics):	salinity from oxygen isotope method using Tsum from MacMAT and $\delta^{18}O$-salinity relationship for the tropical Atlantic
Sal (ANN):	salinity derived from Artificial Neural Network
Sal (MacMAT):	salinity derived from MacMAT

Appendix B: Data from Chapter 4

$\delta^{18}O$ of *G.sacculifer*	average of values covering the LGM
values averag	number of values averaged for the LGM
sed. rate	sedimentation rate in cm/kyrs

Appendix C: Data from Chapter 5

thermocline depth in m	thermocline depth as reconstructed from planktonic foraminiferal assemblages using MAT

Appendix A

GeoB 1523-1:

depth	age	$\delta^{18}O$	Twin	Tsum	Sal	Sal	Sal	Sal	Sal
		saccul.	MacMAT	MacMAT	T from MacMAT	T from SIMMAX	$\delta^{18}O$-Sal tropics	ANN	MacMAT
(cm)	(kyrs)	(‰)	(°C)	(°C)	(‰)	(‰)	(‰)	(‰)	(‰)
3	2	-1.85	25.2	26.9	35.4	35.8	34.1	35.5	36.1
13	8	-1.24	25.4	27.3	36.7	36.8	37.3	35.5	35.8
23	12	-1.27	24.7	26.9	36.1	36.4	35.3	35.5	35.8
33	16	-0.08	22.1	25.0	37.0	38.1	36.2	36.2	36.4
43	19	-0.10	25.5	27.0	37.9	38.1	39.0	36.6	35.9
53	21	0.04	24.3	26.4	37.9	38.3	38.8	36.5	36.0
63	23	-0.23	24.1	26.4	37.6	37.9	38.3	36.7	36.2
73	27	-0.31	22.2	25.5	37.2	38.0	37.9	36.6	36.3
83	30	-0.13	22.4	26.3	37.9	38.3	39.5	36.7	36.8
93	34	0.02	22.2	25.9	38.0	38.7	40.0	36.5	36.4
103	37	-0.28	19.0	22.7	36.2	37.8	35.0	36.5	36.5
113	41	-0.37	20.4	24.2	36.5	37.9	35.8	36.2	36.6
123	44	-0.55	25.7	27.2	37.4	37.6	38.3	36.4	35.7
133	48	-0.54	21.4	25.0	36.6	37.5	36.1	36.2	36.1
143	51	-0.47	22.4	25.4	37.1	37.8	37.9	36.6	36.2
153	56	-0.53	21.0	25.5	36.8	37.6	36.7	36.1	36.6
163	62	-0.16	22.0	24.6	37.3	38.5	38.3	36.6	36.5
173	67	-0.38	18.1	22.5	35.8	37.9	33.8	36.7	36.2
183	70	-0.65	22.6	26.2	37.0	37.3	37.3	36.8	36.3
193	73	-1.18	22.1	25.6	35.8	36.6	34.2	36.4	36.7
203	76	-1.07	25.3	27.0	36.6	36.7	36.5	35.6	36.2
213	79	-1.18	23.5	26.2	36.4	36.9	36.5	36.1	36.1
223	84	-0.89	25.2	26.9	37.2	37.5	38.9	35.9	36.1
233	89	-0.99	23.7	25.9	36.3	37.0	35.8	36.5	36.1
243	93	-1.11	23.7	25.8	36.1	36.9	35.3	36.1	36.2
253	97	-1.35	23.7	25.9	35.9	36.7	35.2	35.9	36.1
263	101	-1.41	25.9	27.7	36.4	36.4	36.4	36.4	36.0
273	105	-1.02	24.9	26.7	36.5	36.8	36.0	35.8	35.9
283	108	-0.95	24.2	26.6	36.6	36.9	36.5	36.5	36.1
293	112	-1.08	24.5	26.8	36.4	36.7	35.8	36.7	35.9
303	117	-1.55	22.9	25.8	35.3	36.1	33.4	36.0	36.0
313	122	-1.54	25.5	27.2	36.3	36.4	36.7	36.0	35.8
323	126	-1.65	24.6	27.0	35.8	36.1	35.2	36.3	35.4
333	131	-0.01	20.8	24.0	37.2	38.6	37.7	36.2	36.1
343	135	0.09	20.1	23.9	36.9	36.9	36.1	36.1	36.3
353	139	0.08	22.2	25.0	37.4	37.2	37.5	36.2	36.5

depth	age	$\delta^{18}O$	Twin	Tsum	Sal	Sal	Sal	Sal	Sal
		saccul.	MacMAT	MacMAT	T from MacMAT	T from SIMMAX	$\delta^{18}O$-Sal tropics	ANN	MacMAT
(cm)	(kyrs)	(‰)	(°C)	(°C)	(‰)	(‰)	(‰)	(‰)	(‰)
363	142	-0.16	21.0	25.0	37.0	37.1	36.6	36.4	36.1
373	146	-0.07	23.4	25.8	37.6	37.4	38.2	36.2	36.5
383	149	-0.05	22.9	26.3	37.8	38.2	38.8	36.3	36.4
393	153	0.13	21.5	24.7	37.5	38.1	38.3	36.5	36.2
403	158	-0.43	24.0	26.4	37.4	37.8	38.4	36.1	36.1
413	162	-0.26	23.7	25.7	37.5	38.1	38.4	36.3	36.1
423	167	-0.80	21.6	24.6	35.9	37.2	34.4	36.3	36.1
433	171	-0.68	25.0	26.9	37.3	37.6	38.3	35.8	35.9
443	177	-0.36	23.7	25.9	37.2	37.9	37.7	36.3	36.1
453	183	-0.21	22.2	25.3	37.2	38.2	37.6	36.2	36.2
463	185	-0.68	22.4	25.0	36.2	37.2	34.7	36.5	36.3
473	187	-0.84	25.6	27.1	37.1	37.3	37.8	36.4	35.8
483	190	-1.29	24.4	26.4	36.1	36.6	35.5	36.5	36.0
493	192	-0.82	26.0	27.5	37.5	37.6	39.3	35.9	35.9
503	194	-1.65	25.5	27.2	35.8	36.0	34.8	36.1	35.9
513	205	-0.68	25.0	26.8	37.6	37.9	39.7	36.3	36.0
523	211	-0.89	24.7	26.9	37.2	37.6	38.7	36.1	35.8
533	216	-1.41	25.8	27.4	36.3	36.4	36.2	36.0	35.8
543	221	-0.80	25.6	27.6	38.0	37.9	41.4	35.6	35.8
553	226	-0.47	23.0	25.4	37.1	38.0	38.0	36.7	36.1
563	231	-0.67	23.7	26.0	37.0	37.6	37.8	36.8	35.9
573	238	-1.23	24.4	26.6	36.3	36.7	36.0	35.9	35.6
583	245	-0.26	23.9	26.6	38.0	38.4	40.4	36.1	35.9
593	252	-0.25	23.3	25.6	37.3	37.8	38.0	36.3	36.3
603	259	-0.45	20.8	24.0	36.7	38.0	36.9	36.2	36.6
613	266	-0.36	22.7	25.9	37.2	37.7	37.6	36.3	36.1
623	274	-0.38	24.9	27.0	37.9	38.4	39.8	36.9	35.9
633	283	-0.95	24.1	26.6	36.4	36.9	35.8	36.1	35.8
643	292	-0.32	24.0	26.5	38.0	38.6	40.5	36.2	35.9
653	301	-0.84	25.5	27.1	37.1	37.3	38.1	36.9	36.0
663	310	-0.79	22.7	25.5	36.7	37.7	36.9	36.9	36.1
673	320	-1.14	23.8	26.3	36.4	37.0	36.5	35.9	36.0
683	331	-1.82	24.9	26.9	35.6	35.7	34.7	35.9	35.8
693	346	-0.85	23.2	25.7	36.1	36.7	34.5	36.8	36.2
703	355	-0.22	23.8	25.9	37.5	38.2	38.1	36.6	36.4

RC 12-294:

depth	age	salinity	Twin	Tsum	salinity
		MacMAT	MacMAT	MacMAT	ANN
(cm)	(kyrs)	(‰)	(°C)	(°C)	(‰)
0	0.0	35.2	12.4	16.6	34.7
5	2.2	34.9	12.4	16.0	34.5
10	4.3	34.9	11.3	14.7	34.4
15	6.5	35.1	13.0	17.1	34.9
20	8.7	34.9	13.3	17.3	35.1
30	12.7	35.2	14.0	18.2	35.2
40	15.9	35.2	10.5	14.5	35.3
45	17.4	34.8	10.7	14.3	35.0
50	19.0	34.8	10.7	14.3	35.3
55	20.8	34.5	8.2	12.1	35.1
60	22.6	34.1	5.9	9.5	35.0
70	26.2	34.7	9.8	13.4	34.9
80	31.1	34.2	6.2	9.5	34.8
90	37.4	34.4	5.3	8.3	34.7
100	43.6	34.3	6.0	8.6	35.1
110	49.9	34.9	7.5	10.9	35.2
120	56.0	34.8	10.7	14.3	35.1
130	62.0	34.8	10.9	14.6	35.3
140	66.2	34.1	4.9	8.4	34.9
150	68.5	35.0	11.6	15.6	34.8
160	70.8	34.2	4.6	7.3	34.9
170	76.8	34.9	9.8	13.4	35.2
180	83.5	35.4	11.8	16.3	35.0
190	90.0	34.8	10.7	14.3	35.2
200	96.0	34.9	10.9	14.7	34.7
210	100.6	35.0	13.1	17.1	35.2
220	103.8	34.5	7.9	11.1	35.1
230	107.0	34.9	13.3	17.5	35.2
232	107.6	34.4	7.9	11.0	35.3
234	108.3	34.7	10.6	14.1	35.2
236	108.9	35.1	10.9	14.5	35.0
238	109.5	34.9	11.6	15.5	35.3
240	110.1	34.9	13.2	17.3	35.7
242	110.8	35.0	13.5	17.6	35.6
244	111.4	34.9	12.4	16.0	35.4
246	112.0	35.1	12.7	16.8	35.7
248	112.6	34.9	13.3	17.5	35.9
250	113.3	35.5	15.8	20.2	36.3
252	113.9	35.3	13.4	18.0	36.1
254	114.5	35.0	13.2	17.2	35.4
256	115.1	35.1	12.1	16.3	35.3
258	115.8	34.8	12.9	16.9	35.7
260	116.4	35.3	12.2	16.7	35.7
262	117.0	35.3	13.4	18.0	35.3
264	117.6	35.0	12.5	16.7	34.9
266	118.3	35.2	13.5	17.8	35.2
268	118.9	35.5	13.5	18.4	35.4
270	119.5	35.4	14.6	19.3	35.5
272	120.1	34.8	12.6	16.4	35.3
274	120.8	35.1	13.6	18.1	35.6

depth	age	salinity	Twin	Tsum	salinity
		MacMAT	MacMAT	MacMAT	ANN
(cm)	(kyrs)	(‰)	(°C)	(°C)	(‰)
276	121.4	35.0	12.5	16.7	36.3
278	122.0	34.9	11.2	15.0	36.5
280	122.7	35.3	13.6	18.2	36.4
282	123.5	35.3	12.7	17.4	36.7
284	124.2	35.5	13.7	18.6	36.7
286	124.9	35.6	14.9	19.8	36.8
288	125.7	35.4	14.6	19.3	36.7
290	126.4	35.7	15.4	20.1	36.9
292	127.1	35.4	14.9	19.5	36.5
294	127.9	35.4	13.0	17.9	36.2
296	128.9	35.3	14.0	18.5	35.9
298	129.9	35.2	13.1	17.6	36.2
300	130.9	35.0	13.6	17.7	36.3
302	131.9	34.8	12.9	16.9	35.5
304	133.0	34.1	4.7	8.3	35.2
306	134.0	34.3	7.1	11.7	35.4
308	135.0	34.2	5.2	9.3	35.3
310	135.4	34.3	5.8	10.3	35.0
315	136.4	34.7	10.5	14.0	34.9
320	137.3	34.1	5.1	9.6	35.1
325	138.3	34.1	4.7	8.3	35.2
330	139.3	34.3	6.1	10.2	35.1
335	140.2	34.1	5.2	9.7	34.8
340	141.2	34.1	4.7	8.3	35.1
345	142.1	34.1	4.7	8.3	35.1
350	143.1	34.3	6.2	11.1	35.2
355	144.1	34.7	7.7	10.9	34.9
360	145.0	35.0	10.0	13.7	34.8
365	146.0	34.2	5.1	7.6	35.0
370	148.5	34.1	5.2	9.7	34.7
375	151.0	34.2	5.1	7.6	34.9
380	153.1	34.2	4.6	7.3	34.9
385	155.2	34.1	4.7	8.3	34.9
390	157.3	34.5	7.6	10.9	34.9
395	159.4	34.2	4.6	7.3	35.0
400	161.5	34.5	7.6	10.9	35.2
405	163.6	34.1	4.5	7.2	35.0
410	165.7	34.2	4.6	7.3	35.2
415	167.8	34.2	5.0	8.7	34.8
420	170.0	34.2	4.8	7.0	33.6
425	171.7	34.2	4.6	7.3	34.8
430	173.1	34.5	7.7	11.2	35.0
435	174.5	34.0	5.2	9.6	34.8
440	175.9	34.3	7.1	10.4	35.1
445	177.4	34.6	9.6	13.2	34.9
450	178.8	34.1	5.2	9.7	34.6
455	180.2	34.5	7.6	10.9	34.8
460	181.6	34.0	4.7	8.2	34.9
465	183.0	34.5	7.8	11.1	34.7
470	184.0	34.0	4.7	8.2	34.8

depth	age	salinity	Twin	Tsum	salinity
		MacMAT	MacMAT	MacMAT	ANN
(cm)	(kyrs)	(‰)	(°C)	(°C)	(‰)
490	191.3	34.9	12.1	16.0	34.7
495	194.0	35.1	11.3	15.4	33.6
500	197.7	35.3	14.3	18.7	34.7
505	201.3	35.5	12.6	17.2	33.7
510	205.0	35.0	11.6	15.9	34.4
515	210.5	34.8	11.2	14.7	34.5
520	216.0	34.3	6.3	8.9	32.3
525	219.0	34.6	8.6	12.8	34.3
530	222.0	34.3	6.5	9.6	34.3
535	225.0	35.0	9.9	13.6	34.4
540	228.0	34.8	10.0	13.7	34.6
545	230.5	34.9	9.1	12.7	34.2
550	233.0	34.7	10.5	14.1	34.0
555	235.5	35.2	12.6	16.9	34.9
560	238.0	35.0	12.5	16.7	34.2
565	241.7	35.7	14.0	18.3	35.1
570	245.3	35.1	13.4	17.9	35.8
575	249.0	35.1	13.4	17.9	35.5
580	254.0	35.5	13.0	17.7	35.1
585	259.0	34.1	4.7	8.3	34.7
590	264.0	34.1	4.5	7.2	34.2
595	269.0	34.8	11.2	14.7	34.9
600	270.4	34.1	4.5	7.2	34.3
605	271.8	34.1	4.7	8.3	34.5
610	273.2	35.1	12.8	16.9	35.0
615	274.5	34.1	4.6	7.7	34.2
620	275.9	34.0	4.3	8.1	34.3
625	277.3	34.0	4.9	8.4	34.8
630	278.7	34.1	4.6	8.2	34.4
635	280.1	34.1	5.2	8.5	34.4
640	281.5	34.3	6.4	9.3	33.9
645	282.9	34.7	9.7	13.9	34.9
650	284.2	34.5	9.5	12.5	34.8
655	285.6	34.8	10.0	13.7	34.9
660	287.0	34.9	13.3	17.5	35.2
665	291.0	34.4	6.7	10.8	34.9
670	295.0	34.3	7.0	9.9	34.5
675	299.0	34.1	5.1	8.6	34.6
680	299.9	34.1	4.7	8.3	34.7
685	300.8	34.1	4.7	8.3	34.9
690	301.8	34.8	8.8	12.1	34.8
695	302.7	34.2	5.1	7.6	35.0
700	303.6	34.2	4.6	7.4	34.6
705	304.5	34.4	6.3	9.5	34.9
710	305.4	34.7	9.7	14.0	34.6
715	306.3	35.0	10.4	14.3	34.5
720	307.3	34.7	8.5	11.6	34.4
725	308.2	34.7	10.4	13.6	35.0
730	309.1	34.8	9.3	12.9	34.8
735	310.0	34.6	8.6	12.3	34.5

depth	age	salinity	Twin	Tsum	salinity
		MacMAT	MacMAT	MacMAT	ANN
(cm)	(kyrs)	(‰)	(°C)	(°C)	(‰)
740	320.0	35.2	10.5	14.7	34.1
745	323.7	34.8	12.6	16.4	35.5
750	327.3	35.5	13.0	17.7	35.8
755	331.0	35.6	11.8	16.6	36.3
760	334.3	35.5	12.4	17.4	36.3
765	337.7	34.9	11.7	15.5	34.4
770	341.0	34.3	6.0	9.1	34.3
775	342.3	35.0	11.6	15.9	34.6
780	343.7	34.0	4.8	8.7	34.1
785	345.0	34.6	8.8	12.3	34.0
790	346.3	34.0	4.6	7.6	34.2
795	347.7	34.0	4.6	7.6	34.3
800	349.0	34.4	7.2	10.3	34.7
805	349.2	35.2	11.0	14.9	34.8
810	349.4	34.9	10.4	13.8	34.6
815	349.6	34.1	4.7	8.8	34.3
820	349.9	34.3	5.8	9.3	34.8
825	350.1	34.1	4.6	8.2	34.5
830	350.3	34.1	4.7	8.8	34.3
835	350.5	34.1	4.7	8.3	34.7
840	350.7	34.5	7.8	11.1	34.6
845	350.9	34.8	9.2	12.7	34.7
850	351.1	34.3	6.4	10.2	34.3
855	351.4	34.1	4.4	7.1	34.9
860	351.6	34.1	3.9	6.9	34.6
865	351.8	34.3	6.3	8.8	34.7
870	352.0	34.7	10.2	14.0	34.9
875	352.9	34.2	6.4	9.6	34.7
880	353.8	34.3	5.9	9.4	34.9
885	354.7	34.3	6.0	9.2	34.1
890	355.6	34.3	6.4	9.7	34.0
895	356.6	34.1	4.3	8.2	34.4
900	357.5	34.3	6.2	9.7	34.6
905	358.4	34.1	4.6	7.7	34.2
910	359.3	34.1	4.7	7.3	34.3
915	360.2	34.0	4.6	7.6	33.9
920	361.1	34.1	4.1	7.0	34.3
925	362.0	34.0	4.6	7.6	34.0

Appendix B

LGM data $\delta^{18}O$ *G. sacculifer*

Core	Lat	Lon	$\delta^{18}O$ *G. sacc.*	Author	depth (m)	values averag	sed. rate
M 13519	6	-20	0.4	Sarnthein et al. (1984)	2862	3	2
V30-40	0	-23	0.51	McIntyre et al. (1989)	3706	3	3.5
V25-59	1	-33	0.27	Mix and Ruddiman (1985)	3824	3	3
KNR110-43PC	5	-44	0.21	Curry and Crowley (1987)	3435	2	5
EN66-38	5	-21	0.27	Curry and Crowley (1987)	2931	2	1.5
V25-60	3	-35	0.15	Mix and Ruddiman (1985)	3749	3	2.5
KNR110-82	4	-43	0.21	Curry and Crowley (1987)	2816	3	2.3
V30-41	0	-23	0.45	Mix and Ruddiman (1985)	3874	3	2
RC13-189	2	-30	0.26	Mix and Ruddiman (1985)	3233	8	4
A180-73	0	-23	0.51	Emiliani (1955)	3749	1	2
234A	6	-22	0.06	Emiliani (1955)	3577	2	1.5
ODP Site 942	5.7	-49.1	0.18	Showers et al. (1997)	3400	3	30
V22-38	-10	-34	0.03	Mix and Ruddiman (1985)	3797	4	2
EW9209-1	5	-43	0.41	Curry and Oppo (1997)	4056	2	2.5
12PC51	0.1	-22.9	0.61	Sikes and Keigwin (1994)	3870	2	2
M16458	5.33	-22.05	0.69	Kassens and Sarnthein (1989)	3518	1	2
M16772	-1.35	-11.96	0.75	Kähler (1990)	3913	2	3
GeoB1112	-5.8	-10.7	0.62	Meinecke (1992)	3125	3	3.5
GeoB2204	-8.5	-34	0.14	Dürkoop et al. (1997)	2072	3	2.5
GeoB3176	-7	-34.44	0.29	this study; data in Arz (1998)	1385	3	30
GeoB3117	-4.29	-37.1	0.36	this study; data in Arz (1998)	800	6	18
GeoB3129	-4.6	-36.63	0.27	this study; data in Arz (1998)	830	3	50
GeoB3104	-3.66	-37.72	0.44	this study; data in Arz (1998)	767	2	10
GeoB1506	2.21	-35.18	0.31	this study	4310	2	2.3
GeoB1105	-1.67	-12.43	0.85	this study	3225	3	4
GeoB1041	-3.48	-7.6	0.84	this study	4033	2	3.5
GeoB1117	-3.8	-14.9	0.76	this study	3984	4	4
GeoB2215	0	-23.5	0.58	this study	3711	3	3
GeoB1515	4	-44	0.26	Mulitza (1994)	3129	2	3.5
GeoB1523	3.8	-41.6	0.1	Wefer et al. (1996)	3292	1	2

Surface Sediment Data			$\delta^{18}O$ *G. saccul.*
GeoB-station	Lat.	Long.	$\delta^{18}O$ *G. sacc.*
1046	7.34	-20.47	-1.39
1105	-1.67	-12.43	-1.03
1106	-1.76	-12.55	-1.05
1108	-2.17	-9.87	-0.85
1111	-5.84	-8.65	-1.57
1112	-5.77	-10.75	-1.16
1113	-5.75	-11.04	-1.63
1114	-5.28	-10.2	-1.18
1117	-3.82	-14.9	-1.06
1402	-2.18	-10.07	-1.09
1403	-1.2	-11.71	-0.97
1404	-0.08	-10.78	-1.16
1407	-4.33	-10.25	-1.18
1503	2.31	-30.65	-1.95
1504	2.29	-31.29	-1.58
1505	2.27	-33.01	-1.85
1505	2.27	-33.01	-1.67
1511	3.18	-46.34	-1.67
1512	5.9	-48.04	-1.57
1513	5.43	-46.93	-1.66
1514	5.14	-46.58	-1.53
1515	4.24	-43.67	-1.88
1522	4.03	-41.68	-1.81
1523	3.82	-41.62	-1.84
2202	-8.2	-34.26	-1.43
2204	-8.53	-34.02	-1.55
2205	-8.57	-34.35	-1.45
2206	-8.56	-34.48	-1.46
2207	-8.74	-34.14	-1.28
2208	-8.92	-33.7	-1.29
2215	-0.01	-23.49	-1.3
2216	0	-23.1	-1.28
3103	-3.65	-37.7	-1.4
3108	-4.18	-37.13	-1.62
3116	-4.31	-37.14	-1.49
3117	-4.3	-37.09	-1.63
3118	-4.56	-36.86	-1.9
3119	-4.57	-36.82	-1.6
3127	-4.57	-36.86	-1.67
3137	-4.67	-36.58	-1.92
3138	-4.67	-36.45	-1.51
3911	-4.67	-36.58	-1.7
3912	-3.65	-37.7	-1.33

Core Data $\delta^{18}O$ *G. sacculifer*

Core	depth cm	$\delta^{13}C$ PDB	$\delta^{18}O$ PDB
GeoB 1506-2	3	1.67	-1.59
	8	1.73	-1.36
	13	1.46	-1.24
	18	1.29	-0.74
	23	1.07	-0.87
	28	1.13	-0.61
	33	0.98	0.31
	38	1.18	0.31
	43	1.18	0.10
	48	1.01	0.10
	53	1.09	0.13
	58	1.21	0.33
	63	1.09	0.31
	68	0.89	-0.25
	73	0.78	-0.26
	78	0.73	-0.04
	83	0.85	-0.13
	88	1.07	-0.26
	93	0.96	-0.22
	98	0.98	-0.15
GeoB 1105-4	23	1.33	-0.63
	28	1.75	-1.16
original	33	1.07	-0.39
stratigraphy	38	0.70	0.12
Meinecke,	43	0.88	0.47
1992	48	0.72	0.39
G. ruber pink	53	0.79	0.40
	58	0.66	0.05
	63	0.67	0.77
	68	0.49	0.91
	73	1.11	0.87
	78	0.71	0.54
	83	0.76	0.48
	88	0.63	0.41
	93	0.68	0.66
	98	0.88	0.58
GeoB 1041-3	38	0.73	0.29
	43	0.85	0.54
original	48	0.62	0.56
stratigraphy	53	0.82	0.85
Meinecke,	58	1.04	0.83
1992	63	0.75	0.19
G. ruber pink	68	0.88	0.51
	73	1.10	0.71

Core	depth cm	$\delta^{13}C$ PDB	$\delta^{18}O$ PDB
GeoB 1117-2	38	1.12	-0.26
	43	0.95	0.12
original	48	0.85	0.20
stratigraphy	53	0.93	0.67
Meinecke,	58	0.92	0.34
1992	63	1.00	0.71
G. ruber pink	68	1.06	0.74
	73	1.01	0.83
	78	1.14	0.78
	83	1.00	0.63
GeoB 2215-10	3	1.53	-1.24
	8	1.39	-1.32
	13	1.31	-1.21
	18	1.26	-0.81
	23	0.96	-0.53
	28	0.90	-0.20
	33	0.90	-0.01
	38	0.78	0.17
	43	0.80	0.62
	48	0.99	0.51
	53	0.85	0.61
	58	0.78	0.54
	63	0.81	0.56
	68	0.92	0.59
	73	0.82	0.52
	78	0.89	0.49
	83	0.81	0.46
	88	0.98	0.38
	93	0.80	0.32
	98	0.76	0.28
	103	0.92	0.33
	108	0.88	0.15
	113	0.91	0.17
	118	0.80	0.10
	123	0.95	0.15
	128	0.98	0.27
	133	0.72	-0.09
	138	0.91	0.04
	143	0.98	0.19
	148	1.03	0.19
	153	0.99	0.13
	158	1.03	0.13
	163	0.92	0.15
	168	1.06	-0.05
	173	0.94	0.08
	178	1.05	0.06
	183	1.01	-0.11
	188	0.95	-0.01
	193	0.96	-0.17
	198	0.83	-0.03

Appendix C

Core	depth (cm)	age (kyrs.)	thermocline depth (m)
GeoB 1523-1	3	1.4	141
	13	6.1	145
	23	10.8	125
	33	15.5	131
	38	17.8	198
	43	18.7	125
	48	19.6	191
	53	20.5	189
	63	23.2	199
	73	26.7	198
	83	30.2	181
	93	33.7	173
	103	37.2	178
	113	40.7	155
	123	44.2	126
	133	47.7	155
	143	51.2	146
	153	56.0	139
	163	62.0	131
	173	66.5	132
	183	69.5	154
	193	72.5	133
	203	75.5	145
	213	78.5	137
	223	83.5	125
	233	89.0	120
	243	93.0	128
	253	97.0	150
	263	100.8	138
	273	104.5	117
	283	108.2	129
	293	112.4	122
	303	117.2	126
	313	122.0	127
	323	126.3	129
	333	130.7	138
	343	135.0	138
	353	138.6	136
	363	142.1	143
	373	145.7	130
	383	149.2	124
	393	153.2	147
	403	157.7	100
	413	162.1	110
	423	166.6	115
	433	171.0	121
	443	177.0	132
	453	183.0	113
	463	185.2	116
	473	187.4	115
	483	189.6	124
	493	191.8	125
	503	194.0	118
	513	205.0	113
	523	210.5	104
	533	216.0	135
	543	220.8	137
	553	225.6	127
	573	238.0	116
	583	245.3	117
	593	252.3	119

Core	depth (cm)	age (kyrs.)	thermocline depth (m)
GeoB 2204-2	17	6.9	124
	27	10.9	149
	37	15.0	180
	47	19.0	194
	57	22.4	194
	67	25.8	198
	77	29.2	195
	87	32.6	198
	97	36.0	193
	107	39.4	196
	117	42.8	196
	127	46.2	197
	137	49.6	194
	147	53.0	192
	157	61.0	201
	167	66.7	199
	177	70.0	199
	187	73.3	198
	197	76.7	169
	207	80.0	188
	217	83.5	175
	227	87.0	168
	237	91.8	166
	247	96.6	155
	257	101.0	166
	267	105.0	137
	277	108.7	170
	287	112.0	136
	297	115.3	155
	307	118.7	155
	317	122.0	192
	327	127.2	113
	337	132.4	132
	347	137.7	176
	357	143.0	177
	367	148.3	193
	377	152.8	175
	387	156.5	150
	397	160.1	191
	407	163.7	138
	417	167.4	151
	427	171.0	164
	437	174.4	145
	447	177.9	147
	457	181.3	168
	467	184.4	156
	477	187.1	184
	487	189.9	197
	497	192.6	139
	507	196.2	167
	517	200.6	149
	527	205.0	171
	537	210.5	123
	547	216.0	193
	557	220.0	190
	567	224.0	192
	577	228.0	154
	587	231.3	185
	597	234.7	134
	607	238.0	147
	617	243.5	149
	627	249.0	140

core	depth (cm)	age (kyrs.)	thermocline depth (m)
GeoB 1105-4	1	1.0	88
	4	1.6	86
	7	2.3	80
	13	3.5	112
	38	8.8	91
	48	10.9	84
	58	12.9	82
	68	14.6	73
	78	16.3	64
	88	18.0	61
	98	19.1	54
	108	20.2	62
	118	21.3	57
	128	22.4	62
	138	23.6	63
	148	24.7	63
	158	25.8	82
	168	26.9	84
	178	28.0	104
	188	30.4	82
	198	32.8	62
	208	35.1	64
	218	37.5	62
	228	39.9	56
	238	42.3	57
	248	44.7	54
	258	47.0	63
	268	49.4	62
	278	51.8	82
	288	54.0	80
	298	56.0	68
	308	58.0	67
	318	61.0	61
	328	65.0	62
	338	69.0	62
	348	72.3	63
	358	74.9	63
	368	77.4	62
	378	80.0	81
	388	82.0	80
	398	84.0	66
	408	86.0	64
	418	88.5	64
	428	91.5	60
	438	94.5	81
	448	97.5	68
	458	100.0	83
	468	102.0	84
	478	104.0	69
	488	106.0	68
	498	108.5	64
	508	111.5	81
	518	114.5	63
	528	117.5	73
	538	120.5	90
	548	123.2	67
	558	125.6	79
	568	128.0	69
	578	130.8	62
	588	133.6	54
	598	136.2	54
	608	138.7	57
	618	141.1	57
	628	143.6	63
	638	146.0	56
	648	148.0	62
	658	150.0	56
	668	152.8	54
	678	156.5	57
	688	160.1	57
	698	163.7	57
	708	167.4	68
	718	171.0	71
	728	173.2	67
	738	175.4	68
	748	177.5	69
	758	179.7	56
	768	181.9	63
	778	183.5	56
	788	184.5	56
	798	185.5	57
	808	186.7	62
	818	188.2	62
	828	189.6	69
	838	191.1	71
	848	192.5	71
	858	194.0	71
	868	198.4	69
	878	202.8	68
	888	207.2	63
	898	211.6	82
	908	216.0	91
	918	218.7	104
	928	221.3	97
	938	224.0	78
	948	226.7	72
	958	228.6	80
	968	229.7	59
	978	230.8	68
	988	231.9	63
	998	233.0	58
	1008	234.1	68
	1018	235.2	66
	1028	236.3	78
	1038	237.4	68
	1048	239.8	83
	1058	243.3	68
	1068	246.8	67
	1078	250.3	63